

國立交通大學

電子工程學系電子研究所

博士論文

雙載子異質接面電晶體的熱穩定最佳化設計

Thermally Stable Optimum Design of Power
Heterojunction Bipolar Transistors

研究生：廖志豪

指導教授：李建平

中華民國九十四年十月

雙載子異質接面電晶體的熱穩定最佳化
設計

Thermally Stable Optimum Design of Power
Heterojunction Bipolar Transistors

研究生：廖志豪

Student: Chih-Hao Liao

指導教授：李建平 博士

Advisor: Dr. Chien-Ping Lee



A Dissertation
Submitted to Department of Electronics Engineering
& Institute of Electronics
College of Electrical and Computer Engineering
National Chiao Tung University
in Partial Fulfillment of the Requirements
for the Degree of
Doctor of Philosophy
in
Electronics Engineering
October 2005
Hsinchu, Taiwan, Republic of China

中華民國九十四年十月

雙載子異質接面電晶體的熱穩定最佳化 設計

研究生：廖志豪

指導教授：李建平 博士

國 立 交 通 大 學

電子工程學系電子研究所



本論文的研究目標為多指電晶體的熱穩定壓艙電阻設計，當在高功率操作時，元件因為熱耦合效應的影響將會變的不穩定，壓艙電阻通常會被用來避免多指電晶體發生熱不定的情形，如何設計壓艙電阻是元件熱穩定的主要議題。熱阻是熱問題最主要的參數，論文中討論了熱阻的理論計算以及熱阻與元件幾何形狀之間的關係，並解釋溫度相依的基板熱導對熱流方程式及熱阻所造成的影響，熱耦合現象的發生可由耦合電流電壓方程式的推導來解釋，可使用線性化的能隙溫度關係來簡化熱電迴授係數及耦合電流電壓方程式，

我們並發展使用牛頓法求解耦合電流電壓方程式的程序。

使用簡單模型來分析使用非均勻壓艙電阻的多指電晶體，可得到熱穩定最佳化壓艙電阻分佈的解析公式，與傳統均勻壓艙電阻設計作比較，新的最佳非均勻設計可以大幅增加元件穩定操作時的電流大小，使用此理想壓艙電阻分佈，可經由求解特徵方程式得到絕對穩定的最佳壓艙電阻值，第二大的正特徵值就是此最佳壓艙電阻值。多指電晶體熱穩定分析可由簡單模型拓展至準確模型，並可將溫度相依的基板熱導效應一併考慮，如此可以得到兩個熱穩定最佳化壓艙電阻分佈的設計流程，分別為均勻電流設計與均勻溫度設計，我們可以利用此兩設計流程在設定的電流或溫度之下設計最佳的熱穩定壓艙電阻值。



Thermally Stable Optimum Design of Power Heterojunction Bipolar Transistors

Student: Chih-Hao Liao

Advisor: Dr. Chien-Ping Lee

Department of Electronics Engineering and Institute of Electronics,

National Chiao Tung University



In this dissertation, the design of ballasting resistors for thermally stable operation of multi-finger transistors was investigated. When the devices are operated at high powers, devices will become unstable due to the phenomenon of the thermal coupling effect. To prevent the thermal instability of multi-finger transistors, ballasting resistors are often used. How to design the ballasting resistors is key issue of the thermal stability. The thermal resistance is the most importance parameter of thermal problem. Theoretical calculation of the thermal resistance was shown and the properties of the thermal resistance dependent on device geometry were discussed. The effect of temperature dependent thermal conductivity on the heat flow equation and the thermal resistance were also explained. The coupled current-voltage equations were derived and discussed to explain the origin of the thermal coupling effect. A linearized temperature dependent band-gap energy expression is used to simplify the definition of the thermal-electrical feedback coefficient and the coupled current-voltage equations. The procedure utilized

to solve the coupled current-voltage equations by using the Newton-Raphson method was developed.

Multi-finger transistors with nonuniform distribution of ballasting resistance have been analyzed by using the simple model. Analytical formulas for the best ballasting resistance distribution for optimum thermal stability operation were derived. Comparing to conventional method of using uniform ballasting resistance, the new schemes with optimized design could result in a significant increase in the device current under stable operation. With the ideal ballasting resistance distribution, the optimum ballasting resistance for absolutely stable operation was obtained by solving an eigenvalue equation. The second largest real positive eigenvalue of this eigenvalue equation is the optimum ballasting resistance. A design procedure for the thermally stable optimum design was developed. By extending the works on the multiple-finger transistor thermal stability from the simple thermal-electrical feedback equations to the accurate model equations and taking the temperature dependence of the thermal conductivity into account, two design flows, uniform current design and uniform temperature design, of the best ballasting resistance distribution for optimum thermal stability operation were developed. Using these design flows, we could design the best ballasting resistance needed for thermally stable operation under the specified current level or junction temperature.

Acknowledgments

I would like to express my sincere appreciation to my advisor, Dr. Chien-Ping Lee, for his great help and guidance during the more than six years period in Chiao-Tung University. He gave me tremendous freedom in pursuing my research work. Although there were some difficult days during these years, the unforgettable experience of doing research under Dr. Lee's supervision is delighted and substantial. His academic style is the most valuable training and worthy to be imitated. I really learned a lot from Dr. Lee's instruction.

I would also like to thank Dr. Chung-Er Huang, the senior of Dr. Lee's group, for his guidance of measurement skill and providing the device samples of this work. His suggestions and the discussions with him were very valuable and constructive for me to accomplish this work.

Then, I want to deeply appreciate my parents. They are the most important support behind me and also the largest pressure for me to carry their hope. Now, I could tell them loudly that I got my Ph.D. degree.

Finally, I want to give my special thank to my fiancée, Ya-Ting, the most lovely girl for me. Without her support and patience, this work might have more delay and even could not be accomplished. I really thank her for endless love and care.

Contents

Abstract (in Chinese)	i
Abstract	iii
Acknowledgments	v
Contents	viii
List of Tables	ix
List of Figures	xv
1 Introduction	1
1.1 Background	1
1.2 Motivation	2
1.3 Overview and Outline	3
2 The Thermal Resistance	6
2.1 Thermal Conductivity of GaAs and InGaP	7
2.2 Theoretical Calculation	8
2.2.1 The Heat Flow Equation	9
2.2.2 Theoretical Thermal Resistance	12
2.2.3 Properties of Thermal Resistance	18
2.3 DC Measurement	23



2.3.1	The Equal Sensing Variables Method	24
2.3.2	The Derivatives of Sensing Variables Method	27
2.4	Summary	29
3	The Coupled Current-Voltage Equations	32
3.1	The Current-Voltage Equation with Self-Heating	33
3.2	The Coupled Current-Voltage Equations	40
3.3	Solving of The Coupled Current-Voltage Equations	45
3.4	The Phenomenon of The Thermal Coupling Effect	48
3.5	Summary	52
4	Thermally Stable Optimum Design of Multifinger HBTs in Simple Model	54
4.1	Ideal Emitter Ballasting Resistance Distribution: Nonuniform Ballasting Resistors	55
4.2	The Optimum Emitter Ballasting Resistance for Absolutely Thermal Stable Operation	64
4.3	N-Finger Transistors: The General Case	71
4.4	The Effect of Finger Separation	76
4.5	Summary	83
5	Thermally Stable Optimum Design of Multifinger HBTs in Accurate Model	84
5.1	The Accurate Model	85
5.2	The Uniform Current Design	90
5.2.1	With Temperature Dependent Thermal Conductivity	96
5.2.2	With Constant Thermal Conductivity	104
5.3	The Uniform Temperature Design	111
5.3.1	With Temperature Dependent Thermal Conductivity	117
5.3.2	With Constant Thermal Conductivity	121
5.4	The General N-Finger Case	125

Contents

5.4.1	The Uniform Current Design	126
5.4.2	The Uniform Temperature Design	130
5.5	Summary	134
6	Conclusion	135
6.1	Summary	135
6.2	Future Work	137
	References	138
	A Program Code for Solving The Coupled I_C-V_{BE} Equations	143
	B Elementary Constants	154
	Vita	155
	Publication List	156



List of Tables

2.1	The thermal conductivity of GaAs, InGaP, Si and gold.	7
B.1	The important elementary constants.	154



List of Figures

2.1	Schematic diagram of a 3-finger device.	10
2.2	The size effect of finger area for aspect ratio $r = l/w$ fixed at 1, 5, 10, 25, and 50.	19
2.3	Thermal resistance as a function of finger width for finger area fixed at 100, 50, and 25 μm^2	21
2.4	Thermal resistance as a function of substrate thickness for devices of 2.8 $\mu\text{m} \times 12 \mu\text{m}$, 3 $\mu\text{m} \times 40 \mu\text{m}$, and 2 $\mu\text{m} \times 20 \mu\text{m}$ finger size.	21
2.5	Thermal resistance as a function of chip size for a 10 $\mu\text{m} \times 10 \mu\text{m}$ finger device.	22
2.6	Thermal resistance as a function of finger separation for devices of 2.8 $\mu\text{m} \times 12 \mu\text{m}$, 3 $\mu\text{m} \times 40 \mu\text{m}$, and 10 $\mu\text{m} \times 10 \mu\text{m}$ finger size.	22
2.7	Measured $I-V$ curves of a 2 \times 20 InGaP/GaAs HBT for $I_B = 1$ mA at heat plate temperature changing from 300 K to 450 K with 30 K step.	25
2.8	Linear fit of dissipated power with respect to heat plate temperature for different specified collector current by using Marsh's method.	26
2.9	Thermal resistance extracted by Marsh's method as a function of fitted junction temperature.	26
2.10	Measured curves of current gain β versus dissipated power of a 2 \times 20 InGaP/GaAs HBT for $I_B = 1$ mA at heat plate temperature changing from 300 K to 450 K with 30 K step.	30

List of Figures

2.11	Extracted thermal resistances for different dissipated power and heat plate temperature by using Bovolon’s method.	30
3.1	The fit of the Gummel data of a 2×20 InGaP/GaAs HBT to (3.11) which measured at heat plate temperature changing from 300 K to 450 K with 30 K step.	36
3.2	The linear fit of (3.18) in the temperature range 250 K to 700 K.	39
3.3	The measured $I_E - V_{BE}$ curves of a two-separated-fingers InGaP/GaAs HBT.	49
3.4	The measured $I_E - V_{CE}$ curves of a two-separated-fingers InGaP/GaAs HBT under constant I_B bias.	50
3.5	The comparison of measured and simulated $I_E - V_{BE}$ curves of the two-separated-fingers InGaP/GaAs HBT at $V_{CE} = 6$ V.	51
4.1	The simulation results of a 3f 3x40 s40 HBT with $R_{E_{13}} = R_{E_2} = 3 \Omega$	59
4.2	The simulation results of a 3f 3x40 s40 HBT with $R_{E_{13}} = 3 \Omega$ and $R_{E_2} = R_{E_{2,ideal}} = 3.26 \Omega$	60
4.3	The simulation results of a 3f 3x40 s40 HBT with $R_{E_{13}} = R_{E_2} = 3.4 \Omega$	61
4.4	The simulation results of a 3f 3x40 s40 HBT with $R_{E_{13}} = 4 \Omega$ and $R_{E_2} = R_{E_{2,ideal}} = 4.26 \Omega$	62
4.5	The simulation results of a 3f 3x40 s40 HBT with the absolutely stable condition, $R_{E_{13}} = R_{E_{13,opt}} = 4.66 \Omega$ and $R_{E_2} = R_{E_{2,ideal}} = 4.92 \Omega$, and with the no bend-over condition, $R_{E_{13}} = R_{E_{13,no-bend}} = 5.34 \Omega$ and $R_{E_2} = R_{E_{2,ideal}} = 5.60 \Omega$	69
4.6	The simulation results of the total current versus V_{BE} curves collected from Fig. 4.1-Fig. 4.5 for the 3f 3x40 s40 HBT.	70
4.7	The simulation results of a 5f 3x40 s40 HBT with $R_{E_{15}} = 3 \Omega$ and $R_{E_{2/3/4}} = R_{E_{ideal}} = 3.37/3.45/3.37 \Omega$	74

List of Figures

4.8	The simulation results of a 3f 3x40 s15 HBT with $R_{E_{13}} = R_{E_2} = 3 \Omega$ compared with the results of the 3f 3x40 s40 HBT in Fig. 4.1.	77
4.9	The simulation results of a 3f 3x40 s15 HBT with $R_{E_{13}} = 3 \Omega$ and $R_{E_2} = R_{E_{2,ideal}} = 3.55 \Omega$ compared with the results of the 3f 3x40 s40 HBT in Fig. 4.2.	78
4.10	The simulation results of a 3f 3x40 s15 HBT with the absolutely stable condition, $R_{E_{13}} = R_{E_{13,opt}} = 4.23 \Omega$ and $R_{E_2} = R_{E_{2,ideal}} = 4.78 \Omega$, and with the no bend-over condition, $R_{E_{13}} = R_{E_{13,no-bend}} = 6.48 \Omega$ and $R_{E_2} = R_{E_{2,ideal}} = 7.03 \Omega$ compared with the results of Fig. 4.5.	79
4.11	The simulation results of the total current versus V_{BE} curves collected from Fig. 4.1-Fig. 4.2 for the 3f 3x40 s40 HBT and Fig. 4.8-Fig. 4.9 for the 3f 3x40 s15 HBT.	81
4.12	The simulation results of a 5f 3x40 s15 HBT with $R_{E_{15}} = 3 \Omega$ and $R_{E_{2/3/4}} = R_{E_{ideal}} = 3.37/3.45/3.37 \Omega$	82
5.1	The simulation result of T_{2SI} as a function of $I_{C_{SI}}$ for a 3f 3x40 s40 and a 3f 3x40 s15 HBT with temperature dependent and constant thermal conductivity.	92
5.2	The simulation result of ϕ_{2SI} as a function of $I_{C_{SI}}$ for a 3f 3x40 s40 and a 3f 3x40 s15 HBT with temperature dependent and constant thermal conductivity.	92
5.3	The simulation result of $\Delta R_{E_{2,SI}}$ as a function of $I_{C_{SI}}$ for a 3f 3x40 s40 and a 3f 3x40 s15 HBT with temperature dependent and constant thermal conductivity.	94
5.4	The simulation result of $R_{E_{13,SI}}$ as a function of $I_{C_{SI}}$ for a 3f 3x40 s40 and a 3f 3x40 s15 HBT with temperature dependent and constant thermal conductivity.	95
5.5	The simulation results of a 3f 3x40 s15 HBT with $R_{E_{13}} = R_{E_2} = 3 \Omega$ in the accurate model with temperature dependent thermal conductivity. . .	98

List of Figures

5.6 The simulation results of a 3f 3x40 s15 HBT with $R_{E_{13}} = 3 \Omega$ and $R_{E_2} = R_{E_{13}} + \Delta R_{E_2,SI} = 4.17 \Omega$ as $I_{C_{SI}} = 24$ mA in the accurate model with temperature dependent thermal conductivity. 99

5.7 The simulation results of a 3f 3x40 s15 HBT with $R_{E_{13}} = 5 \Omega$ and $R_{E_2} = R_{E_{13}} + \Delta R_{E_2,SI} = 6.17 \Omega$ as $I_{C_{SI}} = 24$ mA in the accurate model with temperature dependent thermal conductivity compared with the results of $R_{E_{13}} = 3 \Omega$ and $R_{E_2} = 4.17 \Omega$ in Fig. 5.6. 100

5.8 The simulation results of a 3f 3x40 s15 HBT with $R_{E_{13}} = R_{E_{13,SI}} = 6.79 \Omega$ and $R_{E_2} = R_{E_2,SI} = 7.96 \Omega$ as $I_{C_{SI}} = 24$ mA in the accurate model with temperature dependent thermal conductivity. 101

5.9 The simulation results of a 3f 3x40 s15 HBT with $R_{E_{13}} = R_{E_{13,SI}} = 12.02 \Omega$ and $R_{E_2} = R_{E_2,SI} = 13.92 \Omega$ as $I_{C_{SI}} = 36$ mA in the accurate model with temperature dependent thermal conductivity. 102

5.10 The simulation results of a 3f 3x40 s40 HBT with $R_{E_{13}} = R_{E_{13,SI}} = 6.38 \Omega$ and $R_{E_2} = R_{E_2,SI} = 6.84 \Omega$ as $I_{C_{SI}} = 24$ mA in the accurate model with temperature dependent thermal conductivity compared with the results of the 3f 3x40 s15 HBT in Fig. 5.8. 103

5.11 The simulation results of a 3f 3x40 s15 HBT with $R_{E_{13}} = R_{E_2} = 3 \Omega$ in the accurate model with constant thermal conductivity. 105

5.12 The simulation results of a 3f 3x40 s15 HBT with $R_{E_{13}} = 3 \Omega$ and $R_{E_2} = R_{E_{13}} + \Delta R_{E_2,SI} = 3.54 \Omega$ as $I_{C_{SI}} = 24$ mA in the accurate model with constant thermal conductivity. 106

5.13 The simulation results of a 3f 3x40 s15 HBT with $R_{E_{13}} = R_{E_{13,SI}} = 2.48 \Omega$ and $R_{E_2} = R_{E_2,SI} = 3.02 \Omega$ as $I_{C_{SI}} = 24$ mA in the accurate model with constant thermal conductivity. 108

5.14 The simulation results of a 3f 3x40 s15 HBT with $R_{E_{13}} = R_{E_{13,SI}} = 2.94 \Omega$ and $R_{E_2} = R_{E_2,SI} = 3.49 \Omega$ as $I_{C_{SI}} = 36$ mA in the accurate model with constant thermal conductivity. 109

List of Figures

5.15 The simulation results of a 3f 3x40 s40 HBT with $R_{E_{13}} = R_{E_{13,SI}} = 2.89 \Omega$ and $R_{E_2} = R_{E_{2,SI}} = 3.14 \Omega$ as $I_{C_{SI}} = 24 \text{ mA}$ in the accurate model with constant thermal conductivity compared with the results of the 3f 3x40 s15 HBT in Fig. 5.13. 110

5.16 The simulation results of $I_{C_{2,ST}}$ as a function of T_{ST} for a 3f 3x40 s40 and a 3f 3x40 s15 HBT with temperature dependent and constant thermal conductivity. 114

5.17 The simulation results of ϕ_{2ST} as a function of T_{ST} for a 3f 3x40 s40 and a 3f 3x40 s15 HBT with temperature dependent and constant thermal conductivity. 114

5.18 The simulation results of $\Delta R_{E_{2,ST}}$ as a function of T_{ST} for a 3f 3x40 s40 and a 3f 3x40 s15 HBT with temperature dependent and constant thermal conductivity. 115

5.19 The simulation results of $R_{E_{13,ST}}$ as a function of T_{ST} for a 3f 3x40 s40 and a 3f 3x40 s15 HBT with temperature dependent and constant thermal conductivity. 117

5.20 The simulation results of a 3f 3x40 s15 HBT with $R_{E_{13}} = R_{E_{13,ST}} = 5.41 \Omega$ and $R_{E_2} = R_{E_{2,ST}} = 6.73 \Omega$ as $T_{ST} = 470 \text{ K}$ in the accurate model with temperature dependent thermal conductivity. 118

5.21 The simulation results of a 3f 3x40 s15 HBT with $R_{E_{13}} = R_{E_{13,ST}} = 7.55 \Omega$ and $R_{E_2} = R_{E_{2,ST}} = 9.20 \Omega$ as $T_{ST} = 550 \text{ K}$ in the accurate model with temperature dependent thermal conductivity. 119

5.22 The simulation results of a 3f 3x40 s40 HBT with $R_{E_{13}} = R_{E_{13,ST}} = 6.35 \Omega$ and $R_{E_2} = R_{E_{2,ST}} = 6.86 \Omega$ as $T_{ST} = 470 \text{ K}$ in the accurate model with temperature dependent thermal conductivity compared with the results of the 3f 3x40 s15 HBT in Fig. 5.20. 120

List of Figures

5.23 The simulation results of a 3f 3x40 s15 HBT with $R_{E_{13}} = R_{E_{13,ST}} = 2.62 \Omega$ and $R_{E_2} = R_{E_{2,ST}} = 3.36 \Omega$ as $T_{ST} = 470 \text{ K}$ in the accurate model with constant thermal conductivity. 122

5.24 The simulation results of a 3f 3x40 s15 HBT with $R_{E_{13}} = R_{E_{13,ST}} = 3.03 \Omega$ and $R_{E_2} = R_{E_{2,ST}} = 3.78 \Omega$ as $T_{ST} = 550 \text{ K}$ in the accurate model with constant thermal conductivity. 123

5.25 The simulation results of a 3f 3x40 s40 HBT with $R_{E_{13}} = R_{E_{13,ST}} = 3.20 \Omega$ and $R_{E_2} = R_{E_{2,ST}} = 3.49 \Omega$ as $T_{ST} = 470 \text{ K}$ in the accurate model with constant thermal conductivity compared with the results of the 3f 3x40 s15 HBT in Fig. 5.23. 124

5.26 The contour plot of the optimum ballasting resistance $R_{E_{1,SI}}$ of a 10-finger device varied with the finger width w and the finger separation s for the specified current $I_{CSI} = 20 \text{ mA}$ and the finger area fixed at $100 \mu\text{m}^2$ 128

5.27 The contour plot of the optimum resistance distribution difference of finger 2, $\Delta R_{E_{2,SI}}$, and finger 5, $\Delta R_{E_{5,SI}}$, of a 10-finger device varied with the finger width w and the finger separation s for the specified current $I_{CSI} = 20 \text{ mA}$ and the finger area fixed at $100 \mu\text{m}^2$ 129

5.28 The contour plot of the optimum ballasting resistance $R_{E_{1,ST}}$ of a 10-finger device varied with the finger width w and the finger separation s for the specified current $T_{ST} = 550 \text{ K}$ and the finger area fixed at $100 \mu\text{m}^2$. 132

5.29 The contour plot of the optimum resistance distribution difference of finger 2, $\Delta R_{E_{2,ST}}$, and finger 5, $\Delta R_{E_{5,ST}}$, of a 10-finger device varied with the finger width w and the finger separation s for the specified current $T_{ST} = 550 \text{ K}$ and the finger area fixed at $100 \mu\text{m}^2$ 133

Chapter 1

Introduction

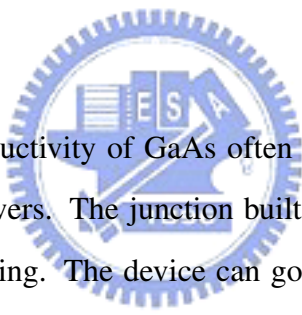
Bipolar transistors are useful for power amplifications. With the advances in fiber communications, wireless and satellite communications, there is a strong demand on the power transistors in microwave and millimeter frequencies. GaAs based heterojunction bipolar transistors (HBTs), because of their excellent performance of high-speed, high gain, high power density, high power-added efficiency (PAE), and superior linearity, have become the dominant devices used in these applications [1]. In recent year, they dominate the application of cellular-handset power stages and become the excellent candidate of base stations for third-generation (3G) cellular networks and Universal Mobile Telecommunication System (UMTS) mobile networks which require high-power and extremely linear power amplifiers.

1.1 Background

Transistors used for power applications often have multiple fingers to spread out current and dissipated heat. However, because of the heat generated and the nonuniform heat distribution, transistors will become unstable at high power operation seriously limiting the power handling capability of transistors. The equation that describes the current-voltage behavior of a multi-finger transistor device is not just to multiply one

finger equation to the total number of fingers. This simple scaling is only correct when the transistor is operated at low power bias. As the power increases, the temperature of each finger is not the same anymore. Usually, the fingers at the center of transistor will be hotter than the fingers at the side. Because that each finger temperature will be affected by the dissipated powers of other fingers, the current-voltage behavior of each finger will also be affected by the other finger. It is the phenomenon of the thermal coupling effect and is the reason that transistors will become unstable. When this happens, thermal runaway is observed for Si BJTs and current collapse is observed for GaAs based HBTs [2]-[5]. The discussions in this work are concentrated on InGaP/GaAs HBTs. And the conclusion is also applicable to any material based HBTs.

1.2 Motivation



The poor thermal conductivity of GaAs often causes the devices to be self-heated when operated at high powers. The junction built-in voltage decreases as the temperature rises due to self-heating. The device can go into a negative resistance region as a result of this phenomenon. When this happens, the device easily becomes unstable because a same voltage bias can result in two different currents. The instability can cause one or several fingers to suck up all the current while others become not functional. This is the phenomenon of the current collapse. The mechanism of the current collapse phenomenon is like that as the dissipated power increases the hotter finger will conduct more current because of the nature of the current-voltage behavior of HBTs. The higher finger current will result in hotter finger as well. This is a positive feedback loop and eventually only the hottest finger can conduct current. For a power transistor, only one finger conducting the total current of device means that the device must be burned out. In order to have sufficient power output, the finger number of transistors needs to increase largely to reduce the average power handled per finger to avoid the thermal unstable effect. It will result in inefficient chip area usage when designing a

large power device.

To prevent the thermal instability of multi-finger transistors, ballasting resistors are often used. The voltage drop across these resistors compensates the build-in voltage change due to temperature rise caused by self-heating and as a result the thermal stability is improved. Traditionally, the fingers and the ballasting resistors connected to the fingers are usually identical to one another. However, because of the nonuniform heat dissipation, it has been realized that the uniform layout commonly used for the fingers of power transistor is not ideal for thermal stability. A non-optimized design can easily over correct the problem and even make the problem worse. If we over design the ballasting resistors, the performance of the device will suffer. For this reason, an optimal design of ballasting resistors is very important. We need to know an minimal value of ballasting resistors to just make the device stable. In this work, we tried to find the optimum values of the ballasting resistors for each finger. And the optimum design procedure for thermally stable multi-finger transistor was developed.

1.3 Overview and Outline

In Chapter 2, we first discuss the thermal resistance which is the origin of the thermal feedback phenomenon of semiconductor devices. Although it is usually treated as a fitting parameter and without any explanation, it has more physical significance than just a fitting parameter and is derivable from the fundamental heat flow equation. The analysis of this work is based on the assumption that the thermal resistance matrix is already known. This chapter will talk about the methods to obtain the thermal resistance and discuss its properties. Both of the theoretical and experimental methods to determine the thermal resistance will be investigated and compared. Based on the results, some useful remarks about the chip layout design to reduce the thermal resistance will be given. Additionally, when the temperature dependent thermal conductivity is taken into account, by the help of Kirchoff transform, the thermal resistance obtained

by solving the temperature independent k_{th} heat flow equation can be used to rewrite the temperature equation of a device from a linear function of the dissipated power to a nonlinear one. The theoretical background of the extraction methods will be explained by the temperature dependent thermal conductivity effect.

In Chapter 3, the temperature dependence of the current-voltage equation is taken into account. This interaction between current and temperature is called self-heating because the device temperature usually becomes higher than that without this effect. The self-heating effect will make the current-voltage equation nonlinear and couple the current-voltage behavior of each finger together. Because of the thermal coupling effect, the finger temperature and the finger current will affect each other. The coupled current-voltage expressions of each finger are functions of other finger currents. The coupled current-voltage equations in simple model and accurate model was defined and derived in this chapter. The method to solve the coupled current and temperature simultaneously was also discussed. The MATLAB[®] [6] program code used to solve the coupled current-voltage equations was listed in Appendix A.

In Chapter 4, we solved the basic coupled current-voltage equations in simple model. We found that there is an ideal distribution for the ballasting resistance. Significant improvement in thermal stability can be obtained when the ideal distributions are used. Simple analytical formulas for the ideal distributions of the emitter ballasting resistance to achieve the highest stable operation current are derived by using the concept of cancellation of positive and negative feedback. With the ideal distribution, we have also found an optimum emitter ballasting resistance for absolutely thermal stable operation condition that the device never becomes unstable. Base on the above results, a design procedure for multi-finger transistors is developed [7].

In Chapter 5, we extended our model to the accurate model and take the temperature dependence of thermal conductivity into account. A more physical model will give us a more practical result. By this manipulation, although the behavior of the current-voltage curves are quit different from the simple model, the basic concept of the ideal ballasting

1.3 Overview and Outline

resistance distribution and the absolutely stable condition are still similar and only need small modification. We could use the same derivation procedure to derive the ballasting resistance equations for the accurate model. Two practical design procedures based on uniform current and uniform temperature consideration were obtained and described from the accurate model [8]. The results with the temperature dependent and constant thermal conductivity were also compared.



Chapter 2

The Thermal Resistance

The thermal resistance is the central parameter to describe the thermal behaviors of semiconductor devices. This important parameter, which is usually treated as a fitting parameter and without any explanation, is the origin of the thermal feedback phenomenon of devices. It has more physical significance than just a fitting parameter and is derivable from the fundamental heat flow equation. The analysis of this work is based on the assumption that the thermal resistance matrix \mathbf{R}_{th} is already known. Therefore, this chapter will discuss the thermal resistance further in advance, including the methods to obtain it and its properties. There are two main categories of methods to determine the thermal resistance R_{th} , theoretically and experimentally. Both of these two methods will be investigated and compared in this work. The theoretical result will show that R_{th} is a function of device geometry and inverse proportional to the thermal conductivity k_{th} of substrate wafers. Based on this result, some useful remarks about the chip layout design to reduce R_{th} will be given.

Additionally, when the temperature dependent thermal conductivity is taken into account, by the help of Kirchoff transform, the thermal resistance obtained by solving the temperature independent k_{th} heat flow equation still served as an essential parameter. The only change needed in this case is that one has to rewrite the temperature equation of a device from a linear function of the dissipated power to a nonlinear one. Of course,

this change will affect device thermal behavior substantially but it will not increase too much mathematical efforts. The following discussion will include this temperature dependent thermal conductivity effect to understand the theoretical background of the extraction methods.

2.1 Thermal Conductivity of GaAs and InGaP

The thermal conductivity is a basic material parameter. It is the key factor of thermal behaviors of all devices. Although the temperature dependent property of GaAs has been revealed for decades, a large discrepancy of data between literatures is still a problem. Anholt has collected several expressions and values of the GaAs thermal conductivity from different references (Table 4.1 in [9]). The deviations of parameters used by different authors are remarkably. The physical preferable temperature dependence expression could be written as [10], [11]

$$k_{th}(T) = k_{th0} \left(\frac{T}{300} \right)^{-b} \quad (2.1)$$

This expression has the mathematical advantages of integration and differentiation with respect to temperature. Table 2.1 summarizes the values used in this work and the values of silicon [12] and gold for reference. The experiment data which could be used to determine the parameters in this expression can be found in [13]-[16]. Because that HBT devices are always fabricated on semi-insulating substrate wafers, Blanc's

	k_{th0} (W/cm-°C)	b
GaAs	0.45	1.25
InGaP	0.05	0
Si	1.56	1.31
Au	3.17	-

Table 2.1. The thermal conductivity of GaAs, InGaP, Si and gold.

[16] measurement result of high-resistivity sample is used in this work, i.e. $k_{th0} = 0.45 \text{ W/cm}^\circ\text{C}$. The temperature dependence is taken from Amith's [14] work on lattice thermal conductivity at high temperature, i.e. $b = 1.25$, under the assumption that the difference between total thermal conductivity and lattice thermal conductivity is small for GaAs.

The thermal conductivity of InGaP is another thermal parameter in the InGaP/GaAs material system. The parameters of InGaP are listed and discussed here for reference. In author's knowledge, there is no direct measurement data of InGaP has been published. Adachi's [17] interpolation method is another way to obtain the InGaP value and is used in this work. According to [17], the thermal resistivity of InP, W_{InP} , is $1.47 \text{ cm}^\circ\text{C/W}$ and GaP, W_{GaP} , is $1.30 \text{ cm}^\circ\text{C/W}$. With the assumption of the alloy-disorder bowing factor $C_{\text{In-Ga}} = 72 \text{ cm}^\circ\text{C/W}$, the thermal resistivity of InGaP, W_{InGaP} , can be computed by substituted these three values into the interpolation formula

$$W_{\text{InGaP}}(x = 0.51) = xW_{\text{GaP}} + (1 - x)W_{\text{InP}} + C_{\text{In-Ga}}x(1 - x).$$

The final value of the thermal conductivity of InGaP is $0.05 \text{ W/cm}^\circ\text{C}$. Since there is no reliable temperature dependent data for InGaP, a temperature independent k_{th} is assumed for simplicity.

2.2 Theoretical Calculation

In order to obtain the thermal resistance R_{th} theoretically, the fundamental heat flow equation must be solved for the 3D temperature distribution inside the whole chip. For most semiconductor devices, the heating source, the fingers in our case, can be treated as a zero thickness surface source at the top of the wafer because the thickness of the active region of devices is usually much smaller than the substrate. With this configuration, the solved temperature distribution function can be used to define R_{th} . The property of R_{th} and the effect of temperature dependent thermal conductivity will be discussed in the

following subsections.

2.2.1 The Heat Flow Equation

The steady state heat flow equation is

$$\nabla \cdot [k_{th}(T)\nabla T] = 0. \quad (2.2)$$

When the thermal conductivity k_{th} is a constant, this equation will reduce to

$$\nabla^2 T = 0 \quad (2.3)$$

or

$$\frac{\partial^2 T}{\partial x^2} + \frac{\partial^2 T}{\partial y^2} + \frac{\partial^2 T}{\partial z^2} = 0. \quad (2.4)$$

The boundary conditions of the problem at hand are

$$\left. \frac{\partial T}{\partial x} \right|_{x=0,a} = 0 \quad (2.5)$$

$$\left. \frac{\partial T}{\partial y} \right|_{y=0,b} = 0 \quad (2.6)$$

$$\left. \frac{\partial T}{\partial z} \right|_{z=0} = -\frac{p_i}{k_{th}} \quad (2.7)$$

$$T|_{z=c} = T_A. \quad (2.8)$$

where p_i is the dissipated power density of finger i and i is the finger index. Furthermore, it is reasonable in most case to assume that the fingers will dissipate power uniformly across the whole finger area of each finger. In other words, p_i is constant for each finger as a uniform heat source at the top of the chip. Fig. 2.1 is the schematic diagram of the problem and boundary conditions that one needs to deal with. The physical meaning of these boundary conditions are that the bottom of the chip is held on ambient or heat plate temperature T_A , only the finger area is the power source, and other surfaces are adiabatic.

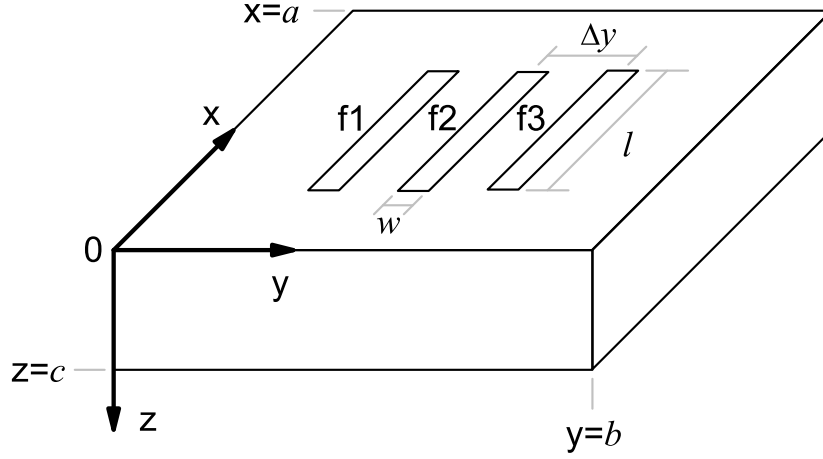


Fig. 2.1. Schematic diagram of a 3-finger device. f1, f2, and f3 are the finger labels.

The heat flow equation (2.4) and its boundary conditions (2.5)-(2.8) can be solved by the standard mathematical procedure and the result will be shown in Section 2.2.2. The commonly used definition of thermal resistance is that the thermal resistance R_{th} is equal to the temperature rising $T - T_A$ divided by the dissipated power P , which can be rewritten as

$$T = T_A + R_{th}P. \quad (2.9)$$

It is the result of constant thermal conductivity and only correct to the first order. In other words, a constant R_{th} must come from constant k_{th} and a temperature dependent R_{th} means k_{th} must be temperature dependent. As it will be shown in Section 2.2.2, because that R_{th} is inverse proportional to k_{th} , the temperature dependence of the thermal resistance is

$$R_{th}(T) = R_{th0} \left(\frac{T}{300} \right)^b \quad (2.10)$$

where R_{th0} is the thermal resistance of devices at 300 K. In the temperature dependent k_{th} case, (2.9) is not valid and a nonlinear equation of temperature is needed.

As taking the temperature dependent k_{th} into account, the general heat flow equation

(2.2) must be used. This equation can be solved by using the Kirchoff transform [18] through defining a linearized temperature $U(x, y, z)$ as

$$U(x, y, z) = T_A + \frac{1}{k_{th}(T_A)} \int_{T_A}^{T(x,y,z)} k_{th}(T) dT. \quad (2.11)$$

Then, the heat flow equation (2.2) can be linearized to the same form as the temperature independent case, which is

$$\nabla^2 U = 0. \quad (2.12)$$

And the boundary conditions (2.5)-(2.8) are still unchanged in this problem except that k_{th} of (2.8) becomes $k_{th}(T_A)$. As a result of the same form of differential equation and boundary conditions, the solution of (2.12) will be the same as the solution of (2.3) by letting $k_{th} = k_{th}(T_A)$ and $R_{th} = R_{th}(T_A)$, and (2.9) is also valid for U as

$$U = T_A + R_{th}(T_A)P. \quad (2.13)$$

Substituting (2.1) into (2.11), one can obtain

$$U = T_A - \left(\frac{T_A}{300}\right)^b \frac{300}{b-1} \left[\left(\frac{T}{300}\right)^{-(b-1)} - \left(\frac{T_A}{300}\right)^{-(b-1)} \right]. \quad (2.14)$$

By using (2.10), the real temperature T can be obtained from (2.14) as

$$\begin{aligned} T &= T_A \left[1 - \frac{b-1}{T_A} (U - T_A) \right]^{\frac{-1}{b-1}} \\ &= T_A \left[1 - \frac{b-1}{T_A} R_{th0} \left(\frac{T_A}{300}\right)^b P \right]^{\frac{-1}{b-1}}. \end{aligned} \quad (2.15)$$

From the above derivation, it can be found that the thermal resistance calculated by the constant k_{th} condition is also a parameter of the temperature dependent k_{th} case. The only change of the new cases is that one needs to compute the real temperature T from the linearized temperature U by using (2.15). Therefore, R_{th0} can be treated as a

universal parameter of thermal problems.

2.2.2 Theoretical Thermal Resistance

Many authors have solved the heat flow equation (2.4) by using the Fourier series expansion to analyze the thermal properties of HBT devices [19], [20]. A detail derivation can be found in Chapter 5 of [21]. In the following paragraph, the result of [21] will be used and simplified. Following the long derivation in Chapter 5 of [21], the temperature distribution at every point inside the chip can be solved. But we are usually interested only in the temperature distribution at the top surface, $z = 0$, where the fingers are located. That is

$$\begin{aligned}
 T(x, y, 0) = T_A &+ \frac{clw}{ab} \sum_{i=1}^N \frac{p_i}{k_{th}} \\
 &+ \frac{2w}{ab} \sum_{m=1}^{\infty} \frac{\tanh(\beta_m c)}{\beta_m^2} \cos(\beta_m x) \sum_{i=1}^N \frac{p_i}{k_{th}} F_i \\
 &+ \frac{2l}{ab} \sum_{n=1}^{\infty} \frac{\tanh(\nu_n c)}{\nu_n^2} \cos(\nu_n y) \sum_{i=1}^N \frac{p_i}{k_{th}} G_i \\
 &+ \frac{4}{ab} \sum_{m=1}^{\infty} \sum_{n=1}^{\infty} \frac{\tanh(\gamma_{mn} c)}{\beta_m \nu_n \gamma_{mn}} \cos(\beta_m x) \cos(\nu_n y) \sum_{i=1}^N \frac{p_i}{k_{th}} F_i G_i
 \end{aligned} \tag{2.16}$$

where

$$\begin{aligned}
 F_i &= 2 \cos(\beta_m x_i) \sin(\beta_m \frac{l}{2}) \\
 G_i &= 2 \cos(\nu_n y_i) \sin(\nu_n \frac{w}{2}) \\
 \beta_m &= \frac{m\pi}{a} \\
 \nu_n &= \frac{n\pi}{b} \\
 \gamma_{mn} &= \sqrt{\beta_m^2 + \nu_n^2},
 \end{aligned}$$

a is the x-direction dimension of the chip, b is the y-direction dimension of the chip, c is the thickness of the substrate, w is the finger width, l is the finger length, i is the finger index, and N is the total number of fingers. The schematic diagram of this problem is

Fig. 2.1. Although (2.16) is valid for every points at the top surface, we only concern about the highest temperature of a finger that is the temperature at the center of each finger. Therefore, this problem becomes only need to simply consider the relationship between two highest temperature points at the chip surface, the center point of finger i and the center point of finger j . It can be concluded from the observation on (2.16) that the finger temperature can be written as

$$T_i = T_A + \sum_{j=1}^N R_{thij} P_j \quad (2.17)$$

where $P_j = wlp_j$ is the dissipated power of finger j and R_{thij} is the thermal resistance between finger i and finger j . It can be found that T_i is a function of dissipated power of all fingers and coupled with other fingers through the parameter R_{thij} . From (2.17) and (2.16), the definition of thermal resistance can be expressed as

$$\begin{aligned} R_{thij} &= \frac{c}{abk_{th}} \\ &+ \frac{2}{abk_{th}l} \sum_{m=1}^{\infty} \frac{\tanh(\beta_m c)}{\beta_m^2} \cos(\beta_m x_i) F_j \\ &+ \frac{2}{abk_{th}w} \sum_{n=1}^{\infty} \frac{\tanh(\nu_n c)}{\nu_n^2} \cos(\nu_n y_i) G_j \\ &+ \frac{4}{abk_{th}lw} \sum_{m=1}^{\infty} \sum_{n=1}^{\infty} \frac{\tanh(\gamma_{mn} c)}{\beta_m \nu_n \gamma_{mn}} \cos(\beta_m x_i) \cos(\nu_n y_i) F_j G_j \\ &= \frac{c}{abk_{th}} \\ &+ \frac{4a^2}{abk_{th}l\pi^2} \sum_{m=1}^{\infty} \frac{1}{m^2} \tanh\left(\frac{m\pi c}{a}\right) \cos\left(\frac{m\pi x_i}{a}\right) \cos\left(\frac{m\pi x_j}{a}\right) \sin\left(\frac{m\pi l}{2a}\right) \\ &+ \frac{4b^2}{abk_{th}w\pi^2} \sum_{n=1}^{\infty} \frac{1}{n^2} \tanh\left(\frac{n\pi c}{b}\right) \cos\left(\frac{n\pi y_i}{b}\right) \cos\left(\frac{n\pi y_j}{b}\right) \sin\left(\frac{n\pi w}{2b}\right) \\ &+ \frac{16ab}{abk_{th}wl\pi^3} \sum_{m=1}^{\infty} \sum_{n=1}^{\infty} \frac{\tanh(r_{mn}\pi c)}{mnr_{mn}} \left[\cos\left(\frac{m\pi x_i}{a}\right) \cos\left(\frac{m\pi x_j}{a}\right) \sin\left(\frac{m\pi l}{2a}\right) \right. \\ &\quad \left. \cos\left(\frac{n\pi y_i}{b}\right) \cos\left(\frac{n\pi y_j}{b}\right) \sin\left(\frac{n\pi w}{2b}\right) \right] \end{aligned} \quad (2.18)$$

2.2 Theoretical Calculation

where

$$r_{mn} = \sqrt{\left(\frac{m}{a}\right)^2 + \left(\frac{n}{b}\right)^2}.$$

If $i = j$, (2.18) gives the self-thermal resistance of fingers. If $i \neq j$, (2.18) gives the coupling thermal resistance between fingers. For simplicity, it is reasonable to assume that the first finger, the finger i , is located at center of chip and the second finger, the finger j , is shifted along the y -axis by a finger separation Δy . These assumptions can be written as

$$\begin{aligned} x_i &= x_j = \frac{a}{2} \\ y_i &= \frac{b}{2} \\ y_j &= \frac{b}{2} + \Delta y. \end{aligned}$$

Now, the thermal resistance between finger i and finger j is

$$\begin{aligned} R_{th_{ij}} &= \frac{c}{abk_{th}} \\ &+ \frac{4a^2}{abk_{th}l\pi^2} \sum_{m=1}^{\infty} \frac{1}{m^2} \tanh\left(\frac{m\pi c}{a}\right) \cos\left(\frac{m\pi}{2}\right) \cos\left(\frac{m\pi}{2}\right) \sin\left(\frac{m\pi l}{2a}\right) \\ &+ \frac{4b^2}{abk_{th}w\pi^2} \sum_{n=1}^{\infty} \frac{1}{n^2} \tanh\left(\frac{n\pi c}{b}\right) \cos\left(\frac{n\pi}{2}\right) \cos\left(\frac{n\pi y_j}{b}\right) \sin\left(\frac{n\pi w}{2b}\right) \\ &+ \frac{16ab}{abk_{th}wl\pi^3} \sum_{m=1}^{\infty} \sum_{n=1}^{\infty} \frac{\tanh(r_{mn}\pi c)}{mnr_{mn}} \left[\cos\left(\frac{m\pi}{2}\right) \cos\left(\frac{m\pi}{2}\right) \sin\left(\frac{m\pi l}{2a}\right) \right. \\ &\quad \left. \cos\left(\frac{n\pi}{2}\right) \cos\left(\frac{n\pi y_j}{b}\right) \sin\left(\frac{n\pi w}{2b}\right) \right]. \end{aligned} \tag{2.19}$$

By using the properties of the cosine function

$$\cos\left(\frac{n\pi}{2}\right) = \begin{cases} 0 & n = \text{odd} \\ -1 & n = 2, 6, 10, \dots \\ 1 & n = 4, 8, 12, \dots \end{cases}$$

and

$$\begin{aligned}\cos\left(\frac{2n\pi y_j}{b}\right) &= \cos\left(n\pi + \frac{2n\pi\Delta y}{b}\right) \\ &= (-1)^n \cos\left(\frac{2n\pi\Delta y}{b}\right),\end{aligned}$$

and replacing the summation indices m and n by $2m$ and $2n$, (2.19) can be rewritten more concisely as

$$\begin{aligned}R_{thij} &= \frac{c}{abk_{th}} \\ &+ \frac{a^2}{abk_{th}l\pi^2} \sum_{m=1}^{\infty} \frac{1}{m^2} \tanh\left(\frac{2m\pi c}{a}\right) \sin\left(\frac{m\pi l}{a}\right) \\ &+ \frac{b^2}{abk_{th}w\pi^2} \sum_{n=1}^{\infty} \frac{1}{n^2} \tanh\left(\frac{2n\pi c}{b}\right) \sin\left(\frac{n\pi w}{b}\right) \cos\left(\frac{2n\pi\Delta y}{b}\right) \\ &+ \frac{2ab}{abk_{th}wl\pi^3} \sum_{m=1}^{\infty} \sum_{n=1}^{\infty} \frac{\tanh(2r_{mn}\pi c)}{mnr_{mn}} \sin\left(\frac{m\pi l}{a}\right) \sin\left(\frac{n\pi w}{b}\right) \cos\left(\frac{2n\pi\Delta y}{b}\right).\end{aligned}\tag{2.20}$$

Finally, in most case, we will prefer a square chip, i.e. $a = b$, because of the efficiency of wafer area usage. Under this assumption, the result can be simplified further as

$$\begin{aligned}R_{thij} &= \frac{c}{a^2k_{th}} \\ &+ \frac{1}{k_{th}l\pi^2} \sum_{m=1}^{\infty} \frac{1}{m^2} \tanh\left(\frac{2m\pi c}{a}\right) \sin\left(\frac{m\pi l}{a}\right) \\ &+ \frac{1}{k_{th}w\pi^2} \sum_{n=1}^{\infty} \frac{1}{n^2} \tanh\left(\frac{2n\pi c}{a}\right) \sin\left(\frac{n\pi w}{a}\right) \cos\left(\frac{2n\pi\Delta y}{a}\right) \\ &+ \frac{2a}{k_{th}wl\pi^3} \sum_{m=1}^{\infty} \sum_{n=1}^{\infty} \frac{\tanh\left(\frac{2\pi c}{a}\sqrt{m^2+n^2}\right)}{mn\sqrt{m^2+n^2}} \sin\left(\frac{m\pi l}{a}\right) \sin\left(\frac{n\pi w}{a}\right) \cos\left(\frac{2n\pi\Delta y}{a}\right).\end{aligned}\tag{2.21}$$

This equation is easy to implement into computer program code but it is time consuming. Especially, the convergence of this equation will become very slow when the finger is much smaller than the chip. The most valuable advantage of (2.21) is its ability of calculating the coupling thermal resistance. There is an important property of (2.21) that R_{th} is inversely proportional to k_{th} . If measured R_{th} is different from the theoretical

result, it is straightforward to define an effective thermal conductivity to meet the measurement data. The reason is that a real thermal environment is more complicated than Fig. 2.1 shown. Adjusting k_{th} to fit the measurement results is an easy way to include other heat flow path effect. In this work, (2.21) will be used to calculate the theoretical thermal resistance and to analyze the properties of thermal resistance dependent on device geometry. The infinite summations in (2.21) are replaced by finite summations terminated at a large number of summation order. If without any mention, the results using (2.21) will be obtained by summing the series up to order 30,000.

There is a closed-form analytical formula that provides an easy and fast way to calculate the self-thermal resistance which is derived by Rinaldi [22]-[23]. He uses the method of image, which is usually used in electrostatics problems, to solve the boundary value problem of heat flow equation. Because of the feature of the method of image, Rinaldi's formula assumes an infinitely large chip in $x-y$ plane. It means that the chip size effect is not included. And he also uses the assumption $c > w+l$ to cut the recursion formula into closed form in z direction. Therefore, when the chip thickness becomes small, his formula will become incorrect and not a closed-form analytical one. Although there are these disadvantages, the advantage of his formula is taking the thickness and the depth of the heat source into account. Two of his formulas will be used in this work. The formula for a heat source of depth $h/2$ and thickness h extending from the top

surface is

$$\begin{aligned}
 R_{th_{ii}}(h) = \frac{1}{2\pi k_{th}} \frac{1}{wh} \left\{ \right. & -\frac{w^2}{2} \arctan \left[\frac{2hl}{w\sqrt{w^2 + l^2 + 4h^2}} \right] \\
 & -\frac{l^2}{2} \arctan \left[\frac{2hw}{l\sqrt{w^2 + l^2 + 4h^2}} \right] \\
 & -2h^2 \arctan \left[\frac{wl}{2h\sqrt{w^2 + l^2 + 4h^2}} \right] \\
 & + wl \ln \left[\frac{\sqrt{w^2 + l^2}}{-2h + \sqrt{w^2 + l^2 + 4h^2}} \right] \\
 & + wh \ln \left[\frac{l + \sqrt{w^2 + l^2 + 4h^2}}{-l + \sqrt{w^2 + l^2 + 4h^2}} \right] \\
 & \left. + lh \ln \left[\frac{w + \sqrt{w^2 + l^2 + 4h^2}}{-w + \sqrt{w^2 + l^2 + 4h^2}} \right] \right\} \\
 & - \frac{1}{2\pi k_{th}} \frac{\ln 2}{c}
 \end{aligned} \tag{2.22}$$

and the formula for a zero thickness heat source at the top surface is

$$\begin{aligned}
 R_{th_{ii}} = \frac{1}{2\pi k_{th}} \left[\frac{1}{l} \ln \left(\frac{l + \sqrt{w^2 + l^2}}{-l + \sqrt{w^2 + l^2}} \right) + \frac{1}{w} \ln \left(\frac{w + \sqrt{w^2 + l^2}}{-w + \sqrt{w^2 + l^2}} \right) \right] \\
 - \frac{1}{2\pi k_{th}} \frac{\ln 2}{c}.
 \end{aligned} \tag{2.23}$$

A comparison between (2.21)-(2.22) was shown in Fig. 2.3-2.4. It will be found that the solutions of (2.22) are always smaller than (2.23) because that a zero thickness heat source is the worst case of this problem [22]. As the heat source becomes thicker the thermal resistance and the finger temperature rise will decrease. But for HBTs, which commonly are mesa structure, the heat source is more close to the zero thickness case because the generated heat only could conduct through the bottom of the mesa to the substrate and than the heat sink. The contribution of heat conduction from the sidewall of the mesa could be neglected since the air surrounding the mesa will block the heat conduction. The heat source will look like a surface source at the top of the substrate and its area size not larger than the mesa area size. We usually use the emitter finger

size, not the mesa size, as the heat source area size. It is because in normal operation, the electric field inside the collector is very high and the electron from the emitter into the collector will be accelerated straightly through to the sub-collector. As a result, the collector current will be confined inside the region under the emitter and generate heat here. Using emitter size is more suitable than mesa size.

2.2.3 Properties of Thermal Resistance

Fig. 2.2(a) and (b) shows the effect of finger area size A . The finger width w and finger length l are controlled by the aspect ratio $r = l/w$. There are five aspect ratios r used in (2.23) and two in (2.18) to compute the R_{th} . As the finger area A becomes smaller (2.18) needs more terms to get a converged solution. In this case, we use order 100,000 to get the solutions. Fig. 2.2(b) shows thermal resistance increases as finger area decreases. The reason is quite straightforward to understand. When we feed the same power into two fingers of different area, the small one will have higher temperature rise. It is because the definition of thermal resistance is temperature rise divided by input power, not power density. Since power density is the real operation constrain of a device, a quantity of thermal resistance times finger area is more meaningful to describe the thermal behavior of devices. Fig. 2.2(b) shows this quantity. From this figure, we know that a small finger will have less temperature rise when two devices conduct the same current density and bias voltage. The benefit of scaling down is very obviously in thermal consideration.

Fig. 2.3 shows the effect of finger shape. There are three devices of different finger area A whose finger width w and finger length l will be changed accordingly to keep the finger area constant. The curves in Fig. 2.3 are symmetric with respect to the vertical line at $w = \sqrt{A}$ and only the left half part of the curves are shown. The result that the solutions of (2.21) and (2.23) are very close to each other confirms the validity of (2.23) as the chip size a large enough. From Fig. 2.3, two observations will be obtained. First, the thermal resistance will reach its maximum value when the finger is square, i.e. $w =$

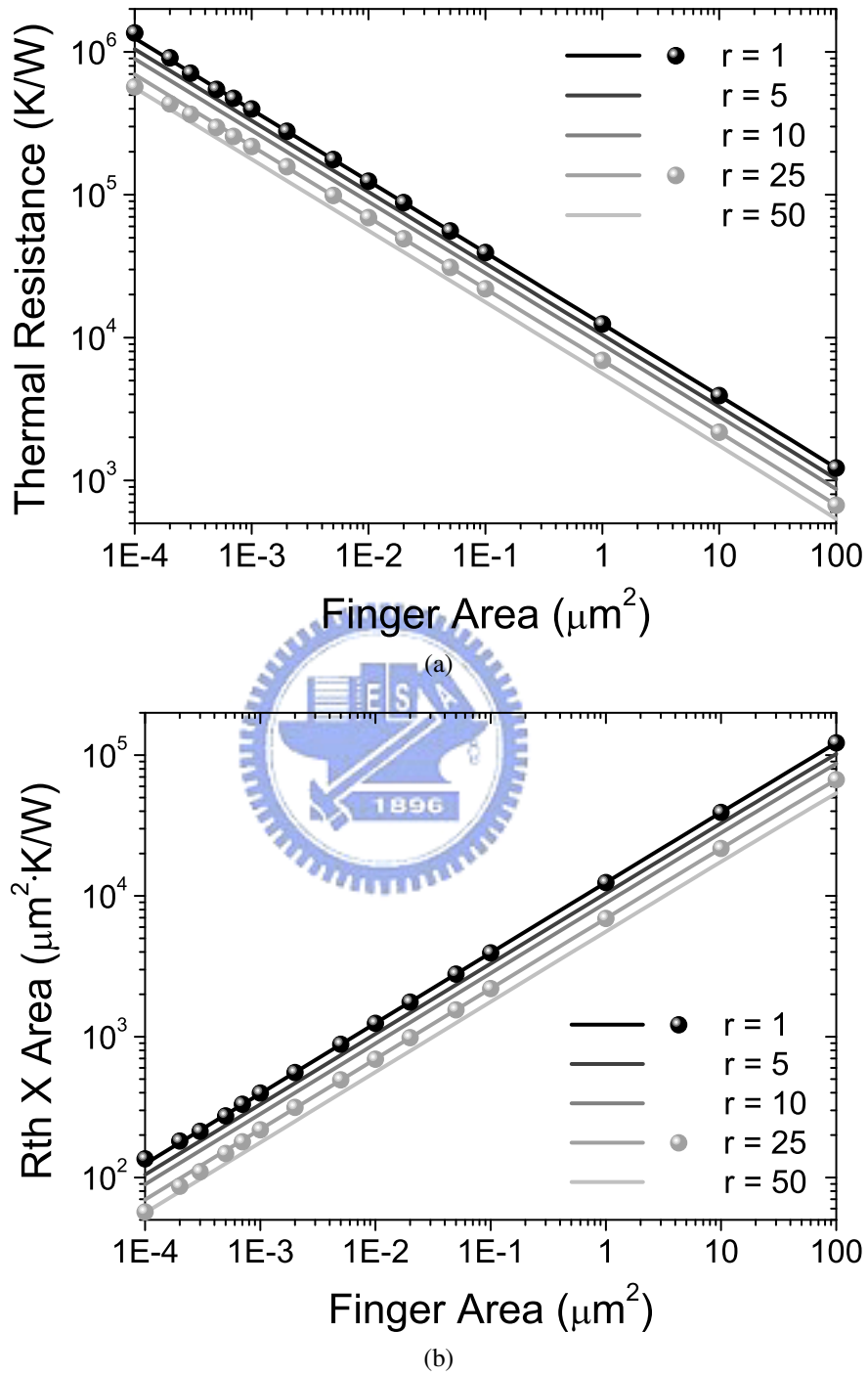


Fig. 2.2. The size effect of finger area for aspect ratio $r = l/w$ fixed at 1, 5, 10, 25, and 50. (a) Thermal resistance as a function of finger area. (b) The quantity of thermal resistance times finger area as a function of finger area. Symbols were calculated by (2.21) and lines by (2.23). The other parameters that hold constant are $a = 1000 \mu\text{m}$, $c = 100 \mu\text{m}$, and $\Delta y = 0 \mu\text{m}$.

l . Second, the larger finger area is the smaller thermal resistance. The first observation implies that a long and narrow finger is preferred in the thermal consideration. But the second does not say we need a large finger. The reason has been explained in the previous paragraph.

Fig. 2.4 shows the effect of substrate thickness c . Because of the derivation of (2.23) using the assumption $c > w + l$, which had mentioned in Section 2.2.2, as the thickness shrink the solutions of (2.23) and (2.22) will deviate from the solutions of (2.21). From Fig. 2.4, we can find that thinning the substrate is not an effective way to reduce thermal resistance. When the substrate thickness thinning from $700 \mu\text{m}$ to $50 \mu\text{m}$ the thermal resistance is only reduced by 2.7 percent for $2.8 \mu\text{m} \times 12 \mu\text{m}$ device and 6.6 percent for $3 \mu\text{m} \times 40 \mu\text{m}$ device. It can be found that the decreasing is faster for large thermal resistance device. Although thinning the substrate is not an effective way, the improvement may be obvious when the original thermal resistance is very large.

Fig. 2.5 shows the effect of chip size a . Thermal resistance will increase quickly when the chip size a shrinks to be smaller than $100 \mu\text{m}$. It is because the conducted heat starts to be confined in x-y direction and the heat density inside the substrate will be higher. This result can be used to explain how large chip size a is enough when applying (2.23). The thermal resistance will stay in a rather constant value when chip size increases to be larger than $200 \mu\text{m}$. Actually, the key parameter is the distance between finger edge and chip edge, not the chip size. It is more correctly to say that $200 \mu\text{m}$ is the minimum distance between finger edge and chip edge that (2.23) is valid.

Fig. 2.6 shows the effect of finger separation Δy . Coupling thermal resistance decreases as finger separation increases. Even the coupling thermal resistance when the separation is less than half of finger width can be defined. It represents the temperature rise inside the finger itself. We can find that the coupling thermal resistance decreases slowly as the separation smaller than $w/2$ but decrease rapidly as the separation larger than $w/2$. The coupling thermal resistance inside a finger is more or less constant. From this result, it is reasonable to use the center point temperature of a finger to represent the

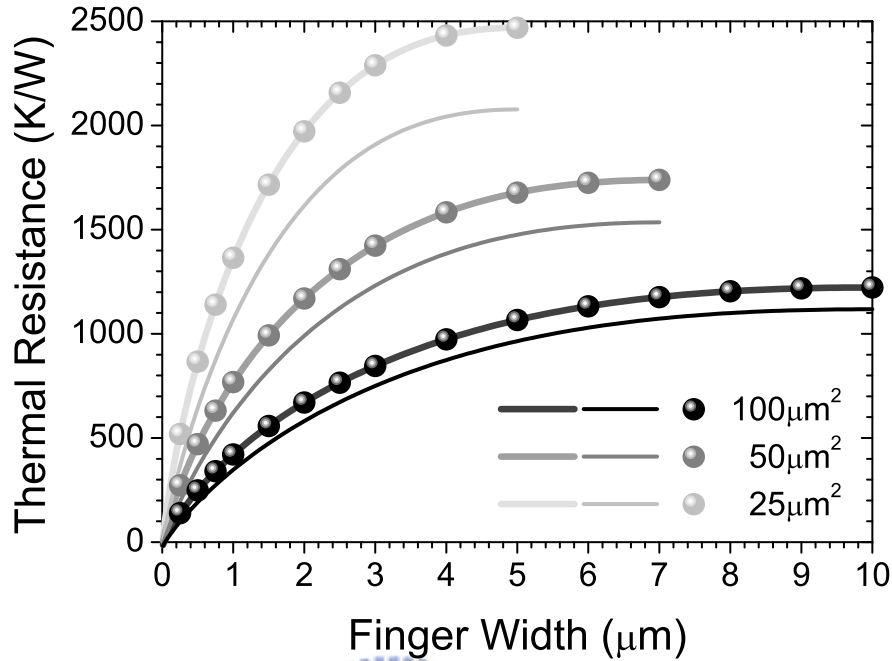


Fig. 2.3. Thermal resistance as a function of finger width for finger area fixed at 100, 50, and 25 μm^2 . Symbols were calculated by (2.21), thick lines by (2.23) with, and thin lines by (2.22). The other parameters that hold constant are $a = 1000 \mu\text{m}$, $c = 100 \mu\text{m}$, $\Delta y = 0 \mu\text{m}$, and $h = 1 \mu\text{m}$.

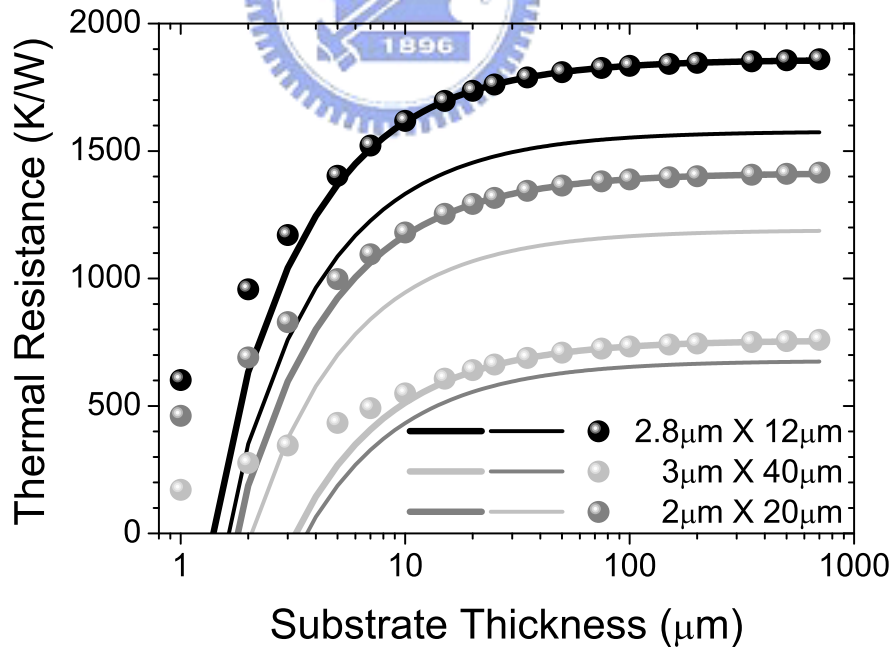


Fig. 2.4. Thermal resistance as a function of substrate thickness for devices of $2.8 \mu\text{m} \times 12 \mu\text{m}$, $3 \mu\text{m} \times 40 \mu\text{m}$, and $2 \mu\text{m} \times 20 \mu\text{m}$ finger size. Symbols were calculated by (2.21), thick lines by (2.23), and thin lines by (2.22). The other parameters that hold constant are $a = 1000 \mu\text{m}$, $\Delta y = 0 \mu\text{m}$, and $h = 1 \mu\text{m}$.

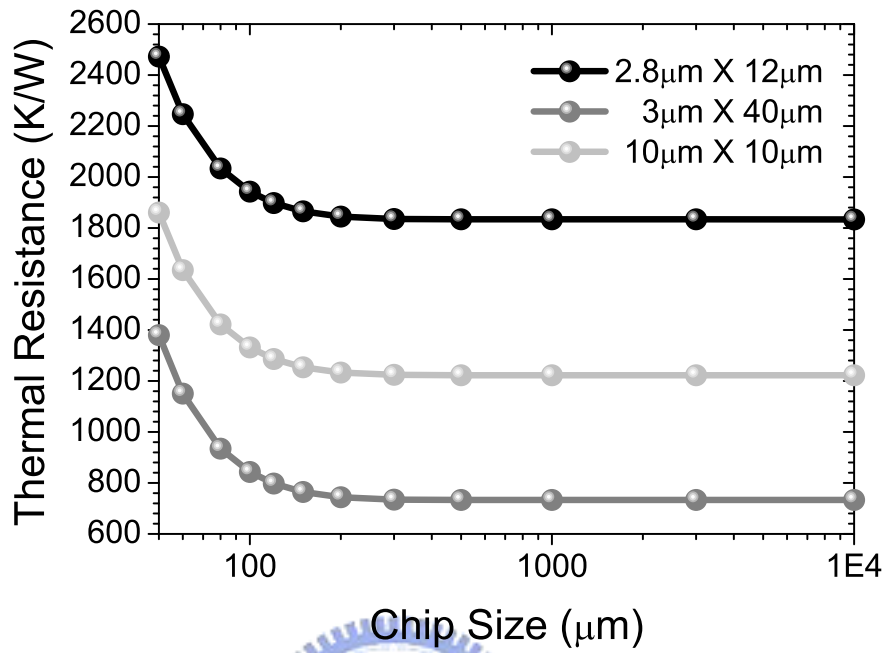


Fig. 2.5. Thermal resistance as a function of chip size for a $10 \mu\text{m} \times 10 \mu\text{m}$ finger device. Data were calculated by (2.21). The other parameters that hold constant are $c = 100 \mu\text{m}$ and $\Delta y = 0 \mu\text{m}$.

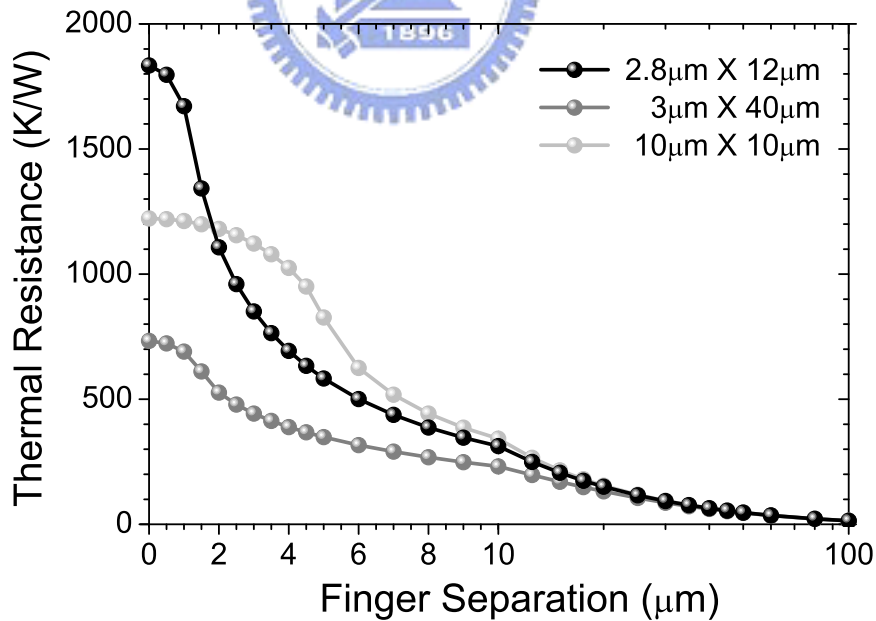


Fig. 2.6. Thermal resistance as a function of finger separation for devices of $2.8 \mu\text{m} \times 12 \mu\text{m}$, $3 \mu\text{m} \times 40 \mu\text{m}$, and $10 \mu\text{m} \times 10 \mu\text{m}$ finger size. The x-axis is linear scale as finger separation smaller than $10 \mu\text{m}$ and log scale as finger separation larger than $10 \mu\text{m}$. Data were calculated by (2.21). The other parameters that hold constant are $a = 1000 \mu\text{m}$ and $c = 100 \mu\text{m}$.

whole finger temperature.

2.3 DC Measurement

There are many experimental methods in literature to measure the thermal resistance of devices. Scott [24] has compared these methods systematically and completely. These methods could be divided into two major groups, including pulsed $I-V$ [25] and DC measurement [26]-[29]. Although pulsed $I-V$ method is more directly from the physical point of view, this method needs more complicated instrument setup because the pulse width must be less than $1 \mu s$. It means this method is difficult to obtain satisfactory results and needs advanced measurement skill. In this work, the subjects will be concentrated on DC measurement method and two measurement methods, Marsh's [29] method and Bovolon's [28] method, will be applied to the experimental data of a 2×20 InGaP/GaAs HBT to extract the thermal resistance.

The DC method could be also classified into two major kinds by their theoretical foundations. To explain their difference, two types of variables must be defined first. The first is the sensing variable and the second is the controlling variable. The sensing variable could be the current gain β or the base-emitter voltage V_{BE} that is monitored during the measurement. The controlling variable could be the dissipated power P or the heat plate temperature T_A that is controlled to drive the measurement. Changing sensing variable from one to another is theoretically equivalent. In this work, β will be used as the only sensing variable for the sake of brevity. Now, the difference of these two methods can be defined as follows: The first kind of the DC method uses the assumption to extract R_{th} that the junction temperature T_j with different controlling variables but equal sensing variables will be the same. Otherwise, the second kind uses the ratio of the derivatives of sensing variables with respect to the controlling variables as R_{th} . Liu's [27] method and Marsh's [29] method are the first kind. Dawson's [26] method and Bovolon's [28] method are the second kind. The reasons will be described

in the following subsections.

2.3.1 The Equal Sensing Variables Method

Liu [27] supposes that the intercept points of measurement curves under different controlling variables in the I_C-V_{BE} plane will have the same T_j and T_j will approach heat plate temperature T_A as the dissipated power P is small. Therefore, he measure the regressive I_C-V_{BE} curves at constant T_A with varied high collector voltage V_C and linear I_C-V_{BE} curves at low V_C with different T_A . The low V_C curves serve as temperature probes to determine T_j of the regressive curves and then extract the thermal resistance R_{th} . Liu's method has a shortcoming that it is difficult to measure the junction temperature of a device under high biasing current operation. Because of the existence of knee voltage, collector voltage cannot decrease low enough to keep both low power requirement and normal operation requirement at the same time. Besides, as the current becomes large the emitter resistance will distort the I_C-V_{BE} curves at low V_C bias from linear and make the task more difficult. For this reason, Liu's method is only suitable for the low current condition.

Marsh [29] supposes β is only the function of T_j and I_C . Consequently, he measures I_C-V_C curves at constant I_B with varied T_A and then intercepts each curve with a specified horizontal constant I_C line to extract the linear dissipated power versus heat plate temperature $P-T_A$ curves. Because of each (I_C, V_C) pair have the same β and I_C , the last variable T_j should be also the same. Therefore, every points on the $P-T_A$ line under the same I_C will have the same T_j . Then, the slope of $P-T_A$ line can be used to extract R_{th} . Now, we use Marsh's method to measure the thermal resistance of a 2×20 InGaP/GaAs HBT whose substrate had been thinned to $100 \mu\text{m}$ thick. The theoretical R_{th} of this device assuming $a = 1000 \mu\text{m}$ as shown in Fig. 2.4 is $1389 \text{ }^\circ\text{C/W}$. Fig. 2.7 shows the measured I_C-V_C curves at six different heat plate temperature and constant base current $I_B = 1 \text{ mA}$. The intercept points of eight specified currents and I_C-V_C curves are shown as $P-T_A$ curves in Fig. 2.8. The linear relationship (2.9) between

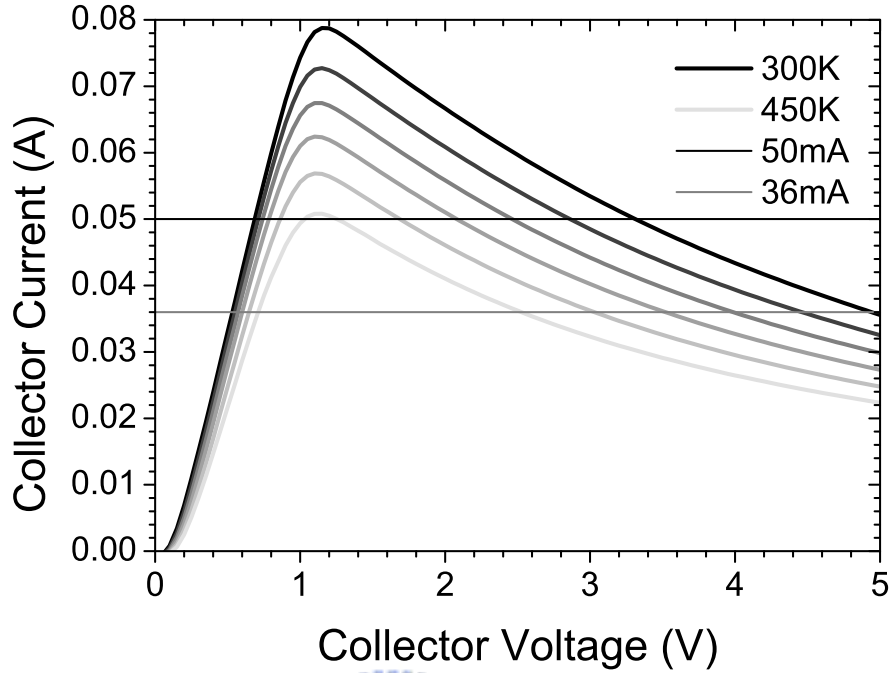


Fig. 2.7. Measured $I-V$ curves of a 2×20 InGaP/GaAs HBT for $I_B = 1$ mA at heat plate temperature changing from 300 K to 450 K with 30 K step. The specified collector current increases from 36 mA to 50 mA with 2 mA step to interpolate the linear dissipated power versus heat plate temperature $P-T_A$ data of Fig. 2.8.

temperature and power can be rewritten as

$$P = \frac{T - T_A}{R_{th}}. \quad (2.24)$$

By using this equation, we can apply linear fit to these eight lines of different specified current to extract R_{th} and T_j . The fitted results are also shown in Fig. 2.8. We can find that the fitted thermal resistance is still a function of junction temperature. Fig. 2.9 shows the results that the extracted thermal resistances of Fig. 2.8 are fitted by (2.10). Although it seems reasonable that $R_{th0} = 650$ °C/W and $b = 1.37$ are obtained, there is a theoretical contradiction that (2.9) and (2.24) are based on the assumption of temperature independent thermal conductivity which implies a temperature independent R_{th} . Unless the dissipated power of devices is small enough to make the first order expansion of (2.15) applicable, the assumption of Marsh's method that the same β and I_C implies

2.3 DC Measurement

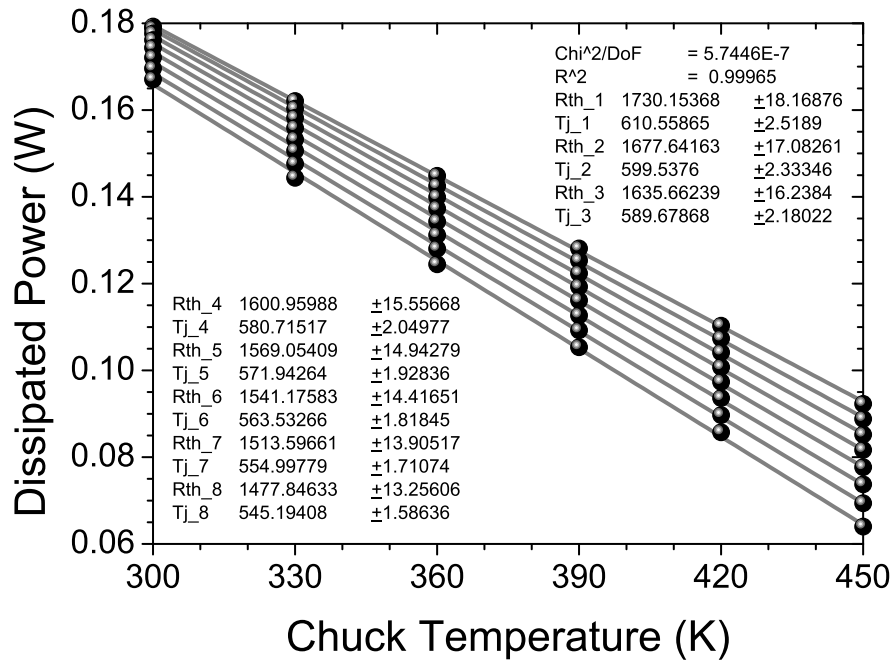


Fig. 2.8. Linear fit of dissipated power with respect to heat plate temperature for different specified collector current by using Marsh's method. Symbols are measured data and lines are fitted lines. The fitted parameters and variances of parameters are listed in the figure. "Chi²/DoF" is the reduced chi-square. "R²" is the R-square or the square of correlation coefficient.

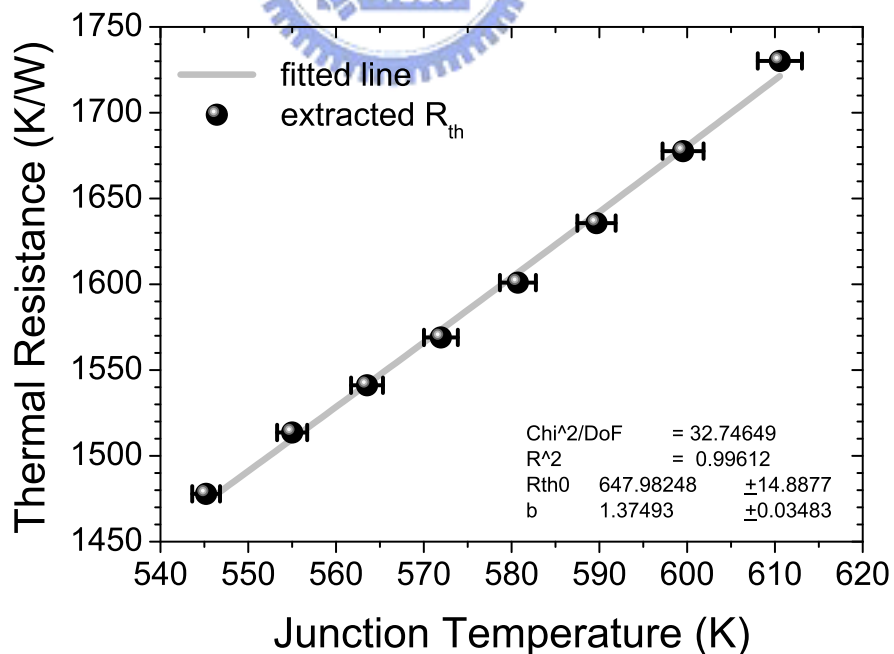


Fig. 2.9. Thermal resistance extract by Marsh's method as a function of fitted junction temperature. The fitting equation is (2.10). The fitted parameters and variances of parameters are listed in the figure. The error bars represent the values of variances in Fig. 2.8. "Chi²/DoF" is the reduced chi-square. "R²" is the R-square or the square of correlation coefficient.

the same T_j obviously is not quit correct. The junction temperature T_j of the high power part of the curves in Fig. 2.8 should be higher than the extracted value. For this reason, Marsh's method is only suitable for low power condition.

2.3.2 The Derivatives of Sensing Variables Method

Dawson [26] measures the slope of linear I_C-P curves at constant I_B and T_A , and the slope of linear I_C-T_A curves at constant I_B and P . The ratio of these two slopes is R_{th} . The reason will be explained in the following paragraph. Here, I_C is equivalent to β because the I_B is held constant. Therefore, changing I_C to another sensing variable V_{BE} is theoretically equivalent. One drawback of Dawson's method is that the validity of his method is restricted to low T_j region because of the nonlinearity of the sensing variables. This drawback can be improved by Bovolon's [28] method. His method is almost the same as Dawson's beside the concept of differential thermal resistance at operating points. Bovolon measures the derivative of I_C with respect to P at constant T_A and the derivative of I_C with respect to T_A at constant P . Similarly, the ratio of these two derivatives is R_{th} . Because that Bovolon's measurement is with respect to small perturbation of controlling variables, not the wide range slopes, his method is mathematically correct and free from the nonlinear error of sensing variables. Scott [24] categorizes Dawson's method as the first kind, the equal sensing variables method. But we thought Dawson's method should be the second kind, the derivatives of sensing variables method. It is because this method measures the slope of β or V_{BE} versus P and T_A to calculate R_{th} without equalizing the sensing variables.

The theoretical foundation of this method will be explained, now. We relist (2.15) here for convenient.

$$T = T_A \left[1 - \frac{b-1}{T_A} R_{th0} \left(\frac{T_A}{300} \right)^b P \right]^{\frac{-1}{b-1}}$$

This nonlinear relationship can be rewritten as

$$P = \frac{-1}{b-1} \frac{300}{R_{th0}} \left[\left(\frac{T}{300} \right)^{-(b-1)} - \left(\frac{T_A}{300} \right)^{-(b-1)} \right]. \quad (2.25)$$

By using (2.15) and (2.25), the following relations of partial derivatives between these three variables, T , P , and T_A , will be obtained.

$$\left. \frac{\partial T}{\partial P} \right|_{T_A=\text{const.}} = \left(\left. \frac{\partial P}{\partial T} \right|_{T_A=\text{const.}} \right)^{-1} = R_{th0} \left(\frac{T}{300} \right)^b \quad (2.26)$$

$$\left. \frac{\partial T}{\partial T_A} \right|_{P=\text{const.}} = \left(\left. \frac{\partial T_A}{\partial T} \right|_{P=\text{const.}} \right)^{-1} = \left(\frac{T}{T_A} \right)^b \quad (2.27)$$

$$\left. \frac{\partial T_A}{\partial P} \right|_{T=\text{const.}} = \left(\left. \frac{\partial P}{\partial T_A} \right|_{T=\text{const.}} \right)^{-1} = -R_{th0} \left(\frac{T_A}{300} \right)^b \quad (2.28)$$

These three equations (2.26)-(2.28) are the foundations of the derivatives of sensing variables method. There are many combinations of the ratio of derivatives corresponding to different measurement methods that can be used to determine R_{th} . The most common one of them is to divide (2.26) by (2.27).

$$\frac{\left. \frac{\partial T}{\partial P} \right|_{T_A=\text{const.}}}{\left. \frac{\partial T}{\partial T_A} \right|_{P=\text{const.}}} = \frac{\left. \frac{\partial T}{\partial \beta} \frac{\partial \beta}{\partial P} \right|_{T_A=\text{const.}}}{\left. \frac{\partial T}{\partial \beta} \frac{\partial \beta}{\partial T_A} \right|_{P=\text{const.}}} = R_{th0} \left(\frac{T_A}{300} \right)^b \quad (2.29)$$

It is because that β is an explicit function of T . The $\partial T/\partial \beta$ terms in the denominator and numerator of (2.29) are equal and can be canceled out. The final result is

$$\frac{\left. \frac{\partial \beta}{\partial P} \right|_{T_A=\text{const.}}}{\left. \frac{\partial \beta}{\partial T_A} \right|_{P=\text{const.}}} = R_{th0} \left(\frac{T_A}{300} \right)^b. \quad (2.30)$$

This equation is the kernel of the derivatives of sensing variables method. In a linear

model, such as Dawson's and Bovolon's, because of $b = 0$, the ratio of these two derivatives gives the constant thermal resistance. Equation (2.30) is more general to be able to include the temperature dependent effect of thermal resistance.

Now, we use Bovolon's method and (2.30) to measure the thermal resistance of the same 2×20 InGaP/GaAs HBT device in Section 2.3.1. The measured data we need is the same $I_C - V_C$ curves in Fig. 2.7 as Marsh's method. And then, we convert these curves to current gain versus dissipated power $\beta - P$ curves as shown in Fig. 2.10. By using the data of Fig. 2.10, we can calculate these two derivatives we need. The derivatives are taken by averaging the slopes of two adjacent data points. The slopes are calculated by the forward difference, i.e. $slope = (y_{i+1} - y_i)/(x_{i+1} - x_i)$. The first and last points of each data sequence will vanish after differentiating. Careful measurement is needed when applying Bovolon's method because of the use of derivatives by which any small fluctuation will be amplified and cause large error. The measured R_{th} and the fitted lines by using (2.30) are shown in Fig. 2.11. The measured R_{th} for each temperature almost lay on the same level as (2.30) expected. It is a good proof that Bovolon's method is theoretically correct and better than Marsh' method. The fitted parameters $R_{th0} = 1100 \text{ }^\circ\text{C/W}$ and $b = 1.15$ are obtained.

2.4 Summary

The values of the thermal conductivity and its temperature dependence of GaAs and InGaP in literature had been reviewed. The values used in this work are given in Table 2.1. The effect of temperature dependent thermal conductivity on the heat flow equation and the thermal resistance was also explained. Theoretical calculation of the thermal resistance was shown and the properties of the thermal resistance dependent on device geometry were discussed. A small, long and narrow finger is better for the sake of reducing thermal resistance. Thinning the substrate is not an effective way to reduce thermal resistance. Two methods of DC measurement were investigated and had been

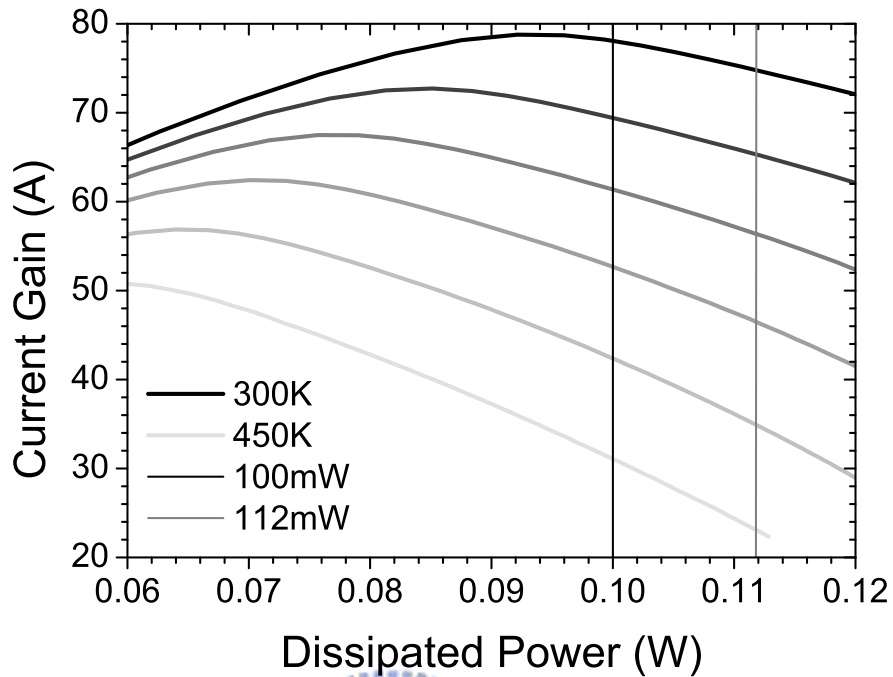


Fig. 2.10. Measured curves of current gain β versus dissipated power of a 2×20 InGaP/GaAs HBT for $I_B = 1$ mA at heat plate temperature changing from 300 K to 450 K with 30 K step. The specified dissipated power increases from 100 mW to 112 mW with 1 mW step to extract the thermal resistance data of Fig. 2.11.

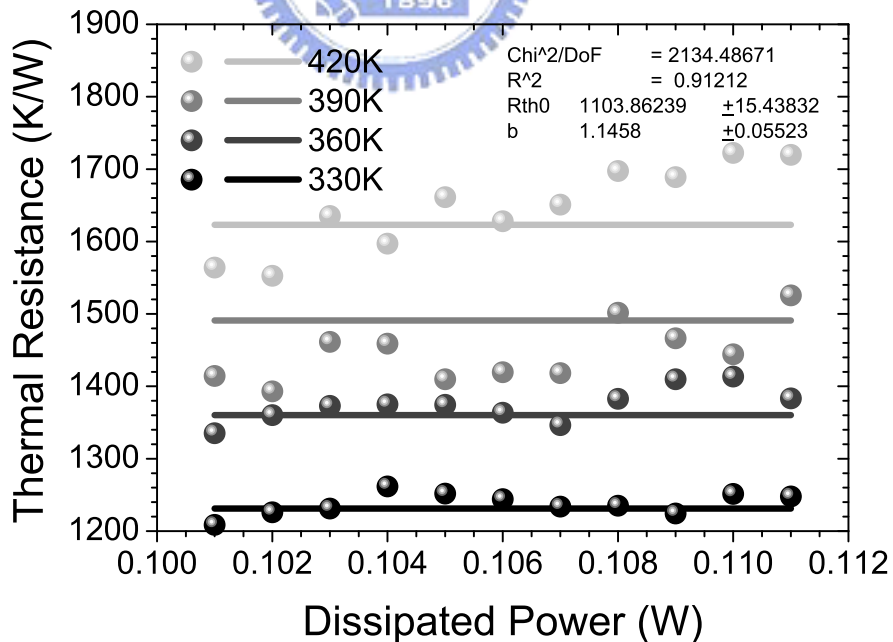


Fig. 2.11. Extracted thermal resistances for different dissipated power and heat plate temperature by using Bovolon's method. Symbols are measured data and lines are fitted lines. The fitting equation is (2.10). The fitted parameters and variances of parameters are listed in the figure. "Chi²/DoF" is the reduced chi-square. "R²" is the R-square or the square of correlation coefficient.

2.4 Summary

applied to a 2×20 InGaP/GaAs HBT. It was found that Marsh's method is only suitable in low power operation and Bovolon's method is preferred.



Chapter 3

The Coupled Current-Voltage

Equations

When the temperature dependence of the current-voltage equation is taken into account, the device current will be affected by the device temperature and in turn the device temperature will be changed by the device current. This interaction between current and temperature is called self-heating because the device temperature usually becomes higher than that without this effect. The self-heating effect will make the current-voltage equation nonlinear and a method to solve current and temperature simultaneously is needed. The current-voltage equations we need to solve will be defined first in this chapter.

For a multi-finger transistor, the equation that describes the current-voltage behavior of the whole device is not just to multiply one finger equation to the total number of fingers. This simple scaling is only correct when the device is operated under low power condition. As the power increases, the temperature of each finger is not the same anymore. Usually, the fingers at the center of transistor will be hotter than the fingers near the edge. Because that each finger temperature will be affected by the dissipated power of other fingers, the current-voltage behavior of each finger will also be affected by the other fingers and the current of each finger will not be the same. It is the phenomenon

of the thermal coupling effect. When this coupling effect happens, a single expression cannot describe the current-voltage behavior of the whole device. We need a set of separated coupled current-voltage expressions for each finger and the current of each finger is a function of other finger currents. In this chapter, the coupled I_C-V_{BE} equations will be derived and the method to solve them will also be discussed. The equations and the solving method will be used in the following chapters to design a thermally stable multi-finger transistor.

3.1 The Current-Voltage Equation with Self-Heating

The classical Ebers-Moll expression of collector current versus emitter-base voltage equation, I_C-V_{BE} equation, is [19]

$$I_C = I_S \left[\exp\left(\frac{qV_{BEj}}{kT}\right) - 1 \right] \quad (3.1)$$

where I_S is the temperature dependent reverse saturation current and V_{BEj} is the base-emitter junction voltage given by

$$\begin{aligned} V_{BEj} &= V_{BE} - (I_C + I_B)(R_{E0} + R_{Eb}) - I_B(R_B + R_{Bb}) \\ &= V_{BE} - I_C R_E \end{aligned} \quad (3.2)$$

where R_{E0} and R_B are the emitter and base resistance, R_{Eb} and R_{Bb} are the ballasting resistors for emitter ballasting and for base ballasting, and R_E is the total resistance seen into the emitter and given by

$$R_E = \left(1 + \frac{1}{\beta}\right) (R_{E0} + R_{Eb}) + \frac{1}{\beta}(R_B + R_{Bb}) \quad (3.3)$$

where β is the current gain. In most case, R_E can be treated as a constant because that R_{E0} , R_B , R_{Eb} , and R_{Bb} are almost temperature independent and the temperature

3.1 The Current-Voltage Equation with Self-Heating

dependence of β is small, especially true for InGaP/GaAs HBT. The ballasting resistors will be discussed in the following chapters.

There are two expressions of I_S depending on its origin of physics. For drift-diffusion limited devices, I_S is

$$I_S = \frac{qAD_nN_CN_V}{W_BN_B} \exp\left(-\frac{q}{kT}E_g\right) \quad (3.4)$$

where A is the device area, D_n is the diffusion constant, N_C is the conduction band density of states, N_V is the valence band density of states, W_B is the base width, N_B is the base doping, and E_g is the band-gap voltage of the base layer material. We know N_C and N_V have the temperature dependence $\sim T^{1.5}$. If we substitute the Einstein relation $D_n = (kT/q)\mu_n$, where μ_n is the mobility, into (3.4) and assume the temperature dependence of mobility as $\mu_n \sim T^{-x}$ where $x > 0$, the temperature dependent reverse saturation current I_S of (3.4) can be obtained as

$$I_S \sim T^{4-x} \exp\left[-\frac{q}{kT}E_g(T)\right]. \quad (3.5)$$

For thermionic emission limited devices, I_S is [30]

$$I_S = AA^*T^2 \exp\left[\frac{q}{kT}(-E_g - V_p - \Delta E_C)\right]. \quad (3.6)$$

where A^* is the effective Richardson constant, V_p is the energy difference between the valence band edge and the hole quasi-Fermi level E_{fp} of the base layer, i.e. $E_V - E_{fp}$, and ΔE_C is the conduction band discontinuity at base-emitter junction. Here, we neglect the voltage drop of the base depletion region because that the base doping is very high in modern HBT devices. It implies that the base depletion region is negligible small and the voltage drop on it is also small. In order to eliminate the variable V_p in (3.6), we substitute the relation $N_B = p = N_V \exp(qV_p/kT)$ into (3.6). Although this relation is derived from the Boltzmann statistics which is valid for non-degenerate semiconductor,

3.1 The Current-Voltage Equation with Self-Heating

it still could give us a qualitative analysis of the temperature dependence of I_S . After substituting this relation, (3.6) becomes

$$I_S = AA^*T^2 \frac{N_V}{N_B} \exp \left[-\frac{q}{kT} (E_g + \Delta E_C) \right].$$

If we assume the effect of ΔE_C can be written as

$$\exp \left(-\frac{q}{kT} \Delta E_C \right) \sim T^y,$$

the temperature dependent reverse saturation current I_S of (3.6) can be obtained as

$$I_S \sim T^{3.5+y} \exp \left[-\frac{q}{kT} E_g(T) \right] \quad (3.7)$$

where $y > 0$ because of the fact that ΔE_C is almost temperature independent and results in as the temperature increasing the exponential term will also increasing. As the results of (3.4) and (3.6), we know that no matter the dominated effect of device current is drift-diffusion limited or thermionic emission limited, I_S has a general form as

$$I_S = I_{S0} \left(\frac{T}{300} \right)^\gamma \exp \left[-\frac{q}{kT} E_g(T) \right] \quad (3.8)$$

where I_{S0} is the temperature independent reverse saturation current or the reverse saturation current at 300 K, and the exponent γ is a constant. From (3.5) and (3.7), we know that if $\gamma > 4$, the current is thermionic emission dominated and if $\gamma < 3.5$, the current is drift-diffusion dominated. In the range $3.5 < \gamma < 4$, these two mechanisms are both possible.

In this work, because we only concern about the normal operation of devices, i.e. the base-emitter junction forward biased, the second term in the square brackets of (3.1), -1 , can be neglected safely. Combining (3.2) and (3.8), we have the general expression

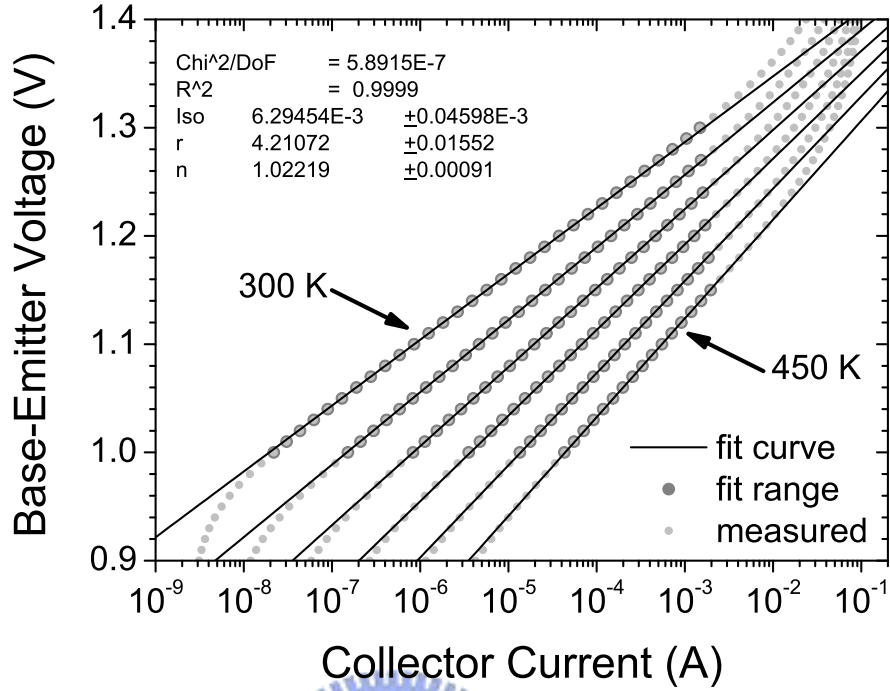


Fig. 3.1. The fit of the Gummel data of a 2×20 InGaP/GaAs HBT to (3.11) which measured at heat plate temperature changing from 300 K to 450 K with 30 K step. The fit range is limited to the low power data which is selected from $V_{BE} \geq 1.0$ V to $I_C \leq 2$ mA. Small symbols are measured data, large symbols are the measured data used in fit, and the line is the fit curve of (3.17). The fitted parameters and variances of parameters are listed in the figure. “Chi²/DoF” is the reduced chi-square. “R²” is the R-square or the square of correlation coefficient.

of the $I_C - V_{BE}$ equation as

$$I_C = I_{S0} \left(\frac{T}{300} \right)^\gamma \exp \left\{ \frac{q}{kT} [V_{BE} - E_g(T) - I_C R_E] \right\} \quad (3.9)$$

and take the logarithm of both sides of (3.9) as

$$V_{BE} = \frac{kT}{q} \left(\ln \frac{I_C}{I_{S0}} - \gamma \ln \frac{T}{300} \right) + E_g(T) + I_C R_E. \quad (3.10)$$

Fig. 3.1 shows the fit of the varied temperature Gummel data, which are the $I_C - V_{BE}$ curves measured with collector and base shorted, of a 2×20 InGaP/GaAs HBT. The

fitting equation is

$$V_{BE} = \frac{nkT_A}{q} \left(\ln \frac{I_C}{I_{S0}} - \gamma \ln \frac{T_A}{300} \right) + E_g(T_A) \quad (3.11)$$

where n is the ideal factor which is close to one, $n = 1.022$ for our device, and will set to unity in the following discussions for simplicity. We use the equation (3.17), which will be discussed later, for $E_g(T_A)$ and take the band-gap narrowing effect into account. We use Harmon's [31] equation for GaAs to compute the band-gap narrowing value of the base material, i.e.

$$\Delta E_g = 2.55 \times 10^{-8} N_B^{\frac{1}{3}} \text{ V} \quad (3.12)$$

where N_B is the base doping level. For our devices, $N_B = 4 \times 10^{19} \text{ cm}^{-3}$ and the corresponding $\Delta E_g = 87.2 \text{ mV}$. The extracted γ is about 4.21 which implies that our device is most possibly thermionic emission dominated. It is a common property of HBTs. But the value of fitted γ is still close to the largest possible value of the drift-diffusion dominated case. And we cannot exclude this possibility completely. It may be because that the conduction band discontinuity ΔE_C between InGaP and GaAs is small, electrons could pass through the base-emitter junction with little blocking.

From the definition of the thermal-electrical feedback coefficient ϕ and (3.10), we can obtain an expression as [32]

$$\phi = - \left. \frac{\partial V_{BE}}{\partial T} \right|_{I_C = \text{const.}} = - \frac{k}{q} \left(\ln \frac{I_C}{I_{S0}} - \gamma \ln \frac{T}{300} - \gamma \right) - \frac{\partial E_g}{\partial T}. \quad (3.13)$$

The negative sign in the definition is to make ϕ positive because that V_{BE} decreases as T increases. We can see that the thermal-electrical feedback coefficient $\phi = \phi(I_C, T)$ is actually a function of collector current and temperature even though it is usually treated as a constant because of the slow variations of $\ln I_C$ and $\ln T$. Although (3.9) and (3.10) are the more accurate equations, we often want a simplified formula in practice to look inside the physics of the thermal feedback effect. We use the Taylor series to expand

3.1 The Current-Voltage Equation with Self-Heating

$V_{BE}(I_C, T)$ in (3.10) about $T = T_A$ to the first order.

$$\begin{aligned} V_{BE}(I_C, T) &= V_{BE}(I_C, T_A) + \frac{\partial V_{BE}}{\partial T}(T - T_A) \\ &= \frac{kT_A}{q} \left(\ln \frac{I_C}{I_{S0}} - \gamma \ln \frac{T_A}{300} \right) + E_g(T_A) + I_C R_E \\ &\quad - \phi(I_C, T_A)(T - T_A) \end{aligned} \quad (3.14)$$

From (3.14), if we set $\phi(I_C, T_A)$ to be a constant, we can get the commonly used thermal feedback I_C-V_{BE} equation [2].

$$I_C = I_O \exp \left\{ \frac{q}{kT_A} [V_{BE} + \phi(T - T_A) - I_C R_E] \right\} \quad (3.15)$$

where I_O is given by

$$I_O = I_{S0} \left(\frac{T_A}{300} \right)^\gamma \exp \left[-\frac{qE_g(T_A)}{kT_A} \right]. \quad (3.16)$$

We will call (3.15) the simplified I_C-V_{BE} equation. In this equation, it is very clear that the contribution of the self-heating effect on collector current is opposite to the effect from the emitter resistance. The emitter resistance acts as a negative feedback element but the self-heating effect acts as a positive feedback element. In order to achieve a thermal stable transistor, we can utilize the negative feedback effect of emitter resistance to compensate the positive feedback effect of self-heating. This is the original ideal of this work.

The last parameter we have mentioned but not discussed in I_C-V_{BE} equation is the band-gap voltage E_g which is an important factor to affect the thermal behavior of devices. The temperature dependence of band-gap voltage E_g can be represented by the well-known Varshni's empirical formula [33].

$$E_g(T) = E_{g0} - \frac{\alpha T^2}{T + T_\beta} \quad (3.17)$$

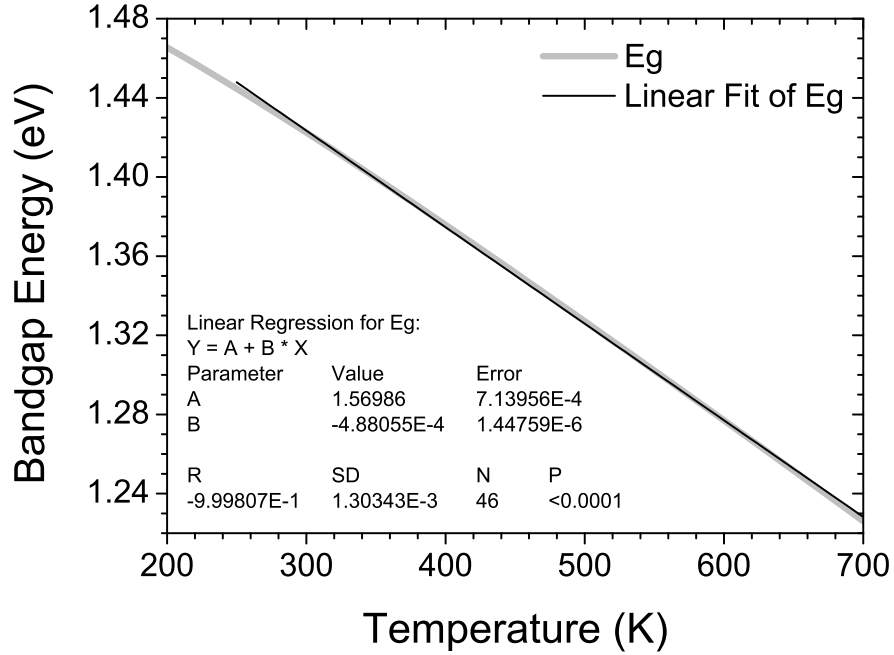


Fig. 3.2. The linear fit of (3.18) in the temperature range from 250 K to 700 K. The thick line is the curve of (3.17), and the thin line is the fitted line (3.20). The fitting equation and the fitted parameters are listed in the figure. “R” is the correlation coefficient. “SD” is the standard deviation of the fit.

For GaAs, that is

$$E_{g,GaAs}(T) = 1.519 - 5.405 \times 10^{-4} \frac{T^2}{T + 204} \quad \text{V.} \quad (3.18)$$

Sometimes, it is more convenient to represent E_g as a linear function of temperature. We use the linear fit of (3.18) in the temperature range from 250 K to 700 K as the linear expression of E_g , i.e.

$$E_{g,GaAs}(T) = 1.570 - 4.88 \times 10^{-4} T \quad \text{V.} \quad (3.19)$$

Fig 3.2 is a comparison between (3.18) and (3.19) and shows that two curves fit very closely. The maximum deviation in the fitted temperature range is about 3.3 mV and in the temperature range from 290 K to 670 K is less than 1.5 mV. The validity of (3.19) in this temperature range is confirmed. We still need to take the band-gap narrowing effect into account to obtain our final expression of the band-gap voltage by subtract

ΔE_g from $E_{g,GaAs}(T)$. Combining (3.12) and (3.19), we have

$$\begin{aligned} E_{g,GaAs,bgn}(T) &= E_{g0}^* - \alpha^*T \\ &= 1.483 - 4.88 \times 10^{-4}T \quad \text{V}. \end{aligned} \quad (3.20)$$

This linear expression of E_g will simplify the whole problem largely but with small error. It is the reason why we use (3.20) in the following thermal stable problems. By substituting (3.20) into (3.13), the thermal-electrical feedback coefficient ϕ is obtained as

$$\phi(I_C, T) = -\frac{k}{q} \left(\ln \frac{I_C}{I_{S0}} - \gamma \ln \frac{T}{300} \right) + \gamma \frac{k}{q} + \alpha^*. \quad (3.21)$$

With (3.21), we can simplify (3.10) as

$$\begin{aligned} V_{BE} &= \frac{kT}{q} \left(\ln \frac{I_C}{I_{S0}} - \gamma \ln \frac{T}{300} \right) + E_{g0}^* - \alpha^*T + I_C R_E \\ &= E_{g0}^* - \phi T + \gamma \frac{k}{q} T + I_C R_E. \end{aligned} \quad (3.22)$$

Define a new variable ϕ^* ,

$$\phi^* \equiv \phi - \gamma \frac{k}{q} \quad (3.23)$$

then, (3.22) becomes

$$V_{BE} = E_{g0}^* - \phi^*T + I_C R_E. \quad (3.24)$$

We will call (3.24) the accurate I_C-V_{BE} equation. In this work, both the accurate and simplified I_C-V_{BE} equations will be solved and used to derive the thermal stable design of ballasting resistors.

3.2 The Coupled Current-Voltage Equations

Although the simplified I_C-V_{BE} equation (3.15) and the accurate I_C-V_{BE} equation (3.24) are both only functions of finger temperature T_i and current I_{C_i} apparently, from the discussion of Section 2.2 and (2.17), it can be found that the finger temperature is a

3.2 The Coupled Current-Voltage Equations

function of all finger powers P_j . The finger temperature T_i will be affected by the power of other fingers and then change the behavior of the finger current I_{C_i} . The amount of the influence of the power of other fingers on the finger temperature T_i is determined by the values of coupling thermal resistance. Therefore, the coupling effect is originated from the finger temperature coupling dependence on the power of other fingers through the coupling thermal resistances.

For a multi-finger transistor, the fingers usually mean emitter fingers. Although the emitter fingers are separated in device structure, they are electrically connected by metal line to the contact pads. The voltage bias of all fingers is the same. We will assume V_C and V_{BE} are the same for all fingers in the following analysis. The dissipate power P_i for each finger is

$$\begin{aligned}
 P_i &= I_{C_i}V_C + I_{B_i}V_{BE} \\
 &= I_{C_i}V_C + \frac{I_{C_i}}{\beta}V_{BE} \\
 &\cong I_{C_i}V_C.
 \end{aligned} \tag{3.25}$$

Here, we neglect the power contribution of I_{B_i} and V_{BE} . It is because that β is quit large and base-emitter voltage is several times smaller than collector-emitter voltage under normal operation. Therefore, the finger temperature can be simplified as just a function of collector currents of all fingers, i.e. $T_i = T_i(I_{C_1}, I_{C_2}, I_{C_3}, \dots, I_{C_N})$. Then, we can combine (2.15) and (2.17) to obtain the coupled temperature equation of the finger temperature T_i as a function of the finger current I_{C_j} and the derivative of T_i with respect to the finger current I_{C_j} . For the constant thermal conductivity case, they are

$$T_i = T_A + V_C \sum_{j=1}^N R_{th_{ij}} I_{C_j} \tag{3.26}$$

$$\frac{\partial T_i}{\partial I_{C_j}} = V_C R_{th_{ij}}. \tag{3.27}$$

3.2 The Coupled Current-Voltage Equations

For the temperature dependent thermal conductivity case, they are

$$T_i = T_A \left[1 - \frac{b-1}{T_A} V_C \sum_{j=1}^N R_{thij} I_{C_j} \right]^{\frac{-1}{b-1}} \quad (3.28)$$

$$\frac{\partial T_i}{\partial I_{C_j}} = \left(\frac{T_i}{T_A} \right)^b V_C R_{thij} \quad (3.29)$$

where

$$R_{thij} = R_{th0ij} \left(\frac{T_A}{300} \right)^b .$$

The calculation of the derivative of T_i with respect to the finger current I_{C_j} is necessary when solving the coupled I_C-V_{BE} equations by using the Newton-Raphson method which will be discussed in Section 3.3.

From the simplified I_C-V_{BE} equation (3.15) and the accurate I_C-V_{BE} equation (3.24), we found that both of them can be expressed as

$$V_{BE} = V_{BE}(I_{C_i}, T_i) \quad i = 1, 2, 3 \dots N \quad (3.30)$$

for a N -finger device. Because that the finger temperature is a function of currents of all fingers, the expression of (3.30) is a set of coupled functions of currents of all fingers. We subtract the equation of each finger in (3.30) by the equation of selected finger r , whose current is assumed constant, and define the goal function $g_{ir} = g_{ir}(I_{C_1}, I_{C_2}, I_{C_3}, \dots, I_{C_{r-1}}, I_{C_{r+1}}, \dots, I_{C_N})$ as the voltage difference $V_{be_i} - V_{be_r}$, where $i = 1, 2, 3 \dots N$ but $i \neq r$.

$$g_{ir} = V_{BE}(I_{C_i}, T_i) - V_{BE}(I_{C_r}, T_r) \quad i \neq r \quad (3.31)$$

We call finger r as the reference finger. There are N sets of goal functions corresponding to the N fingers to be the reference finger in turn. The rank of the problem at hand is reduced by one, from N coupled equations to $N - 1$ goal functions. When solving the

3.2 The Coupled Current-Voltage Equations

coupled equations, we will set I_{C_r} as a known constant and only need to solve the other $N - 1$ unknowns $I_{C_i, i \neq r}$ actually. It has some advantages when solving large problems. In order to achieve our goal to solve the coupled $I_C - V_{BE}$ equation, we theoretically just need to find out a solution of $I_{C_i, i \neq r}$ to make the goal functions zero. In Section 3.3, the method to find out the solution of $g_{ir}(I_{C_i, i \neq r}) = 0$ will be discussed.

In this work, we will use three models to calculate the $I_C - V_{BE}$ curves. The models include the simple model, the accurate model with constant thermal conductivity, and the accurate model with temperature dependent thermal conductivity. For the simple model, using the simplified $I_C - V_{BE}$ equation (3.15), we can write down the coupled equations as

$$I_{C_i} = I_O \exp \left\{ \frac{q}{kT_A} [V_{BE} + \phi(T_i - T_A) - I_{C_i} R_{E_i}] \right\} \quad (3.32)$$

Because that (3.15) is already a first order approximation, it is unnecessary to use high order equation (3.28) for T_i . Therefore, substituting the constant thermal conductivity case equation (3.26) into T_i , we can write down the coupled equations and the goal function for a N -finger device as

$$V_{BE} = \frac{kT_A}{q} \ln \frac{I_{C_i}}{I_O} - \phi V_C \sum_{j=1}^N R_{th_{ij}} I_{C_j} + I_{C_i} R_{E_i} \quad i = 1, 2, 3 \dots N \quad (3.33)$$

$$g_{ir} = \frac{kT_A}{q} \ln \frac{I_{C_i}}{I_{C_r}} - \phi V_C \sum_{j=1}^N (R_{th_{ij}} - R_{th_{rj}}) I_{C_j} + (I_{C_i} R_{E_i} - I_{C_r} R_{E_r}) \quad i \neq r. \quad (3.34)$$

From (3.34) and using (3.27), the derivative of g_{ir} with respect to the finger current I_{C_j} is

$$\frac{\partial g_{ir}}{\partial I_{C_j}} = \left(\frac{kT_A}{q} \frac{1}{I_{C_i}} + R_{E_i} \right) \delta_{ij} - \phi V_C (R_{th_{ij}} - R_{th_{rj}}) \quad (3.35)$$

where δ_{ij} is the Kronecker delta which is defined by

$$\delta_{ij} \equiv \begin{cases} 0 & \text{for } i \neq j \\ 1 & \text{for } i = j \end{cases} .$$

3.2 The Coupled Current-Voltage Equations

The derivative of the goal function will be used in Section 3.3 to solve the coupled I_C-V_{BE} equations.

For the accurate model, using the accurate I_C-V_{BE} equation (3.24), we can write down the coupled equations and the goal function for a N -finger device as

$$V_{BE} = E_{g0}^* - \phi_i^* T_i + R_{Ei} I_{C_i} \quad i = 1, 2, 3 \dots N \quad (3.36)$$

$$g_{ir} = -(\phi_i^* T_i - \phi_r^* T_r) + (R_{Ei} I_{C_i} - R_{Er} I_{C_r}) \quad i \neq r \quad (3.37)$$

where

$$\phi_i^* = -\frac{k}{q} \left(\ln \frac{I_{C_i}}{I_{S0}} - \gamma \ln \frac{T_i}{300} \right) + \alpha^*. \quad (3.38)$$

From (3.38), the derivative of ϕ_i^* with respect to the finger current I_{C_j} is

$$\frac{\partial \phi_i^*}{\partial I_{C_j}} = -\frac{k}{q} \frac{1}{I_{C_i}} \delta_{ij} + \gamma \frac{k}{q} \frac{1}{T_i} \frac{\partial T_i}{\partial I_{C_j}}. \quad (3.39)$$

From (3.37) and using (3.39), the derivative of g_{ir} with respect to the finger current I_{C_j} is

$$\begin{aligned} \frac{\partial g_{ir}}{\partial I_{C_j}} &= \left(\frac{k}{q} \frac{T_i}{I_{C_i}} + R_{Ei} \right) \delta_{ij} - \left(\gamma \frac{k}{q} + \phi_i^* \right) \frac{\partial T_i}{\partial I_{C_j}} + \left(\gamma \frac{k}{q} + \phi_r^* \right) \frac{\partial T_r}{\partial I_{C_j}} \\ &= \left(\frac{k}{q} \frac{T_i}{I_{C_i}} + R_{Ei} \right) \delta_{ij} - \phi_i \frac{\partial T_i}{\partial I_{C_j}} + \phi_r \frac{\partial T_r}{\partial I_{C_j}}. \end{aligned} \quad (3.40)$$

With constant thermal conductivity, substituting (3.27) into (3.40), we obtain

$$\frac{\partial g_{ir}}{\partial I_{C_j}} = \left(\frac{k}{q} \frac{T_i}{I_{C_i}} + R_{Ei} \right) \delta_{ij} - \phi_i V_C R_{thij} + \phi_r V_C R_{thrj}. \quad (3.41)$$

With temperature dependent thermal conductivity, substituting (3.29) into (3.40), we obtain

$$\frac{\partial g_{ir}}{\partial I_{C_j}} = \left(\frac{k}{q} \frac{T_i}{I_{C_i}} + R_{Ei} \right) \delta_{ij} - \phi_i \left(\frac{T_i}{T_A} \right)^b V_C R_{thij} + \phi_r \left(\frac{T_r}{T_A} \right)^b V_C R_{thrj}. \quad (3.42)$$

For the accurate model, both with constant thermal conductivity and with temperature dependent thermal conductivity are use (3.37) as their goal function. The only difference is that (3.41) is used for the constant thermal conductivity case and (3.42) is used for the temperature dependent thermal conductivity case. All of them will be used in Section 3.3 to solve the coupled I_C-V_{BE} equations.

3.3 Solving of The Coupled Current-Voltage Equations

From the discussion of Section 3.2, we found that both the coupled I_C-V_{BE} equations (3.33) and (3.36) are very nonlinear. In order to solve these nonlinear equations, the Newton-Raphson method [21] are usually used. The simulation results of Chapter 4 and Chapter 5 are all obtained by using this method to solve the coupled I_C-V_{BE} equations. It is important to describe this method in detail. We will derive the solving procedure and the working equations of different models in this section.

We firstly define two new variables, the reduced collector current vector $\tilde{\mathbf{I}}_C$ and the reduced collector current step vector $\Delta\tilde{\mathbf{I}}_C$, as

$$\begin{aligned}\tilde{\mathbf{I}}_C &= (I_{C_1} \ I_{C_2} \ I_{C_3} \ \cdots \ I_{C_{r-1}} \ I_{C_{r+1}} \ \cdots \ I_{C_N})^T \\ \Delta\tilde{\mathbf{I}}_C &= (\Delta I_{C_1} \ \Delta I_{C_2} \ \Delta I_{C_3} \ \cdots \ \Delta I_{C_{r-1}} \ \Delta I_{C_{r+1}} \ \cdots \ \Delta I_{C_N})^T.\end{aligned}$$

Then, we can express $g_{ir} = g_{ir}(\tilde{\mathbf{I}}_C)$ and the set of goal functions of finger r , which is composed by $N - 1$ equations of $g_{ir}(\tilde{\mathbf{I}}_C)$, can be obtained as

$$\mathbf{g}_r(\tilde{\mathbf{I}}_C) = \left[g_{1r}(\tilde{\mathbf{I}}_C) \ g_{2r}(\tilde{\mathbf{I}}_C) \ g_{3r}(\tilde{\mathbf{I}}_C) \ \cdots \ g_{r-1,r}(\tilde{\mathbf{I}}_C) \ g_{r+1,r}(\tilde{\mathbf{I}}_C) \ \cdots \ g_{Nr}(\tilde{\mathbf{I}}_C) \right]^T. \quad (3.43)$$

We expand (3.31) by using the Taylor expansion to the first order.

$$g_{ir}(\tilde{\mathbf{I}}_C + \Delta\tilde{\mathbf{I}}_C) = g_{ir}(\tilde{\mathbf{I}}_C) + \sum_{j=1, j \neq r}^N \frac{\partial g_{ir}}{\partial I_{C_j}} \Delta I_{C_j} \quad i \neq r \quad (3.44)$$

3.3 Solving of The Coupled Current-Voltage Equations

Each row of (3.43) can be expanded by using (3.44). By using the notation of matrix, the expansion of goal functions set $\mathbf{g}_r(\tilde{\mathbf{I}}_C)$ can be written as

$$\mathbf{g}_r(\tilde{\mathbf{I}}_C + \Delta\tilde{\mathbf{I}}_C) = \mathbf{g}_r(\tilde{\mathbf{I}}_C) + \mathbf{d}\mathbf{g}_r\Delta\tilde{\mathbf{I}}_C \quad (3.45)$$

where

$$\mathbf{d}\mathbf{g}_r = \begin{pmatrix} \frac{\partial g_{1r}}{\partial I_{C_1}} & \frac{\partial g_{1r}}{\partial I_{C_2}} & \cdots & \frac{\partial g_{1r}}{\partial I_{C_{r-1}}} & \frac{\partial g_{1r}}{\partial I_{C_{r+1}}} & \cdots & \frac{\partial g_{1r}}{\partial I_{C_N}} \\ \frac{\partial g_{2r}}{\partial I_{C_1}} & \frac{\partial g_{2r}}{\partial I_{C_2}} & \cdots & \frac{\partial g_{2r}}{\partial I_{C_{r-1}}} & \frac{\partial g_{2r}}{\partial I_{C_{r+1}}} & \cdots & \frac{\partial g_{2r}}{\partial I_{C_N}} \\ \vdots & \vdots & & \vdots & \vdots & & \vdots \\ \frac{\partial g_{r-1,r}}{\partial I_{C_1}} & \frac{\partial g_{r-1,r}}{\partial I_{C_2}} & \cdots & \frac{\partial g_{r-1,r}}{\partial I_{C_{r-1}}} & \frac{\partial g_{r-1,r}}{\partial I_{C_{r+1}}} & \cdots & \frac{\partial g_{r-1,r}}{\partial I_{C_N}} \\ \frac{\partial g_{r+1,r}}{\partial I_{C_1}} & \frac{\partial g_{r+1,r}}{\partial I_{C_2}} & \cdots & \frac{\partial g_{r+1,r}}{\partial I_{C_{r-1}}} & \frac{\partial g_{r+1,r}}{\partial I_{C_{r+1}}} & \cdots & \frac{\partial g_{r+1,r}}{\partial I_{C_N}} \\ \vdots & \vdots & & \vdots & \vdots & & \vdots \\ \frac{\partial g_{Nr}}{\partial I_{C_1}} & \frac{\partial g_{Nr}}{\partial I_{C_2}} & \cdots & \frac{\partial g_{Nr}}{\partial I_{C_{r-1}}} & \frac{\partial g_{Nr}}{\partial I_{C_{r+1}}} & \cdots & \frac{\partial g_{Nr}}{\partial I_{C_N}} \end{pmatrix}. \quad (3.46)$$

The key ideal of the Newton-Raphson method is that we want to find the step $\Delta\tilde{\mathbf{I}}_C$ from one starting guess $\tilde{\mathbf{I}}_C$ to be such that $\mathbf{g}_r(\tilde{\mathbf{I}}_C + \Delta\tilde{\mathbf{I}}_C)$ is zero. Therefore, if we set the left hand side of (3.45) to be zero, we found that the step $\Delta\tilde{\mathbf{I}}_C$ can be solved as

$$\Delta\tilde{\mathbf{I}}_C = -(\mathbf{d}\mathbf{g}_r)^{-1}\mathbf{g}_r(\tilde{\mathbf{I}}_C). \quad (3.47)$$

In general, the Newton-Raphson method works like that once the k -th guess $\tilde{\mathbf{I}}_{C_k}$ is known, the Newton-Raphson method uses (3.47) to give us the information of the next guess $\tilde{\mathbf{I}}_{C_k} + \Delta\tilde{\mathbf{I}}_{C_k}$. If $\mathbf{g}_r(\tilde{\mathbf{I}}_{C_k} + \Delta\tilde{\mathbf{I}}_{C_k})$ is not zero, we will use $\tilde{\mathbf{I}}_{C_{k+1}} = \tilde{\mathbf{I}}_{C_k} + \Delta\tilde{\mathbf{I}}_{C_k}$ as the new guess and use (3.47) again to calculate the new next guess $\tilde{\mathbf{I}}_{C_{k+1}} + \Delta\tilde{\mathbf{I}}_{C_{k+1}}$. This is an iterative process that the whole procedure will be repeated until a satisfactory

result is obtained.

The solving procedure we used in this work is described here. First, we select finger 1 as the reference finger and the goal function set \mathbf{g}_1 is determined. Then, we need to decide the initial guess of $\tilde{\mathbf{I}}_C$ as $\tilde{\mathbf{I}}_{C_0}$ and the current of the reference finger I_{C_r} , which will keep constant during the solving process, to start the Newton-Raphson solving procedure. It is because the coupled $I_C - V_{BE}$ equations are nonlinear, one value of I_{C_r} may have several solutions by using different initial guess of $\tilde{\mathbf{I}}_{C_0}$. In this work, a combination of a large enough high current initial guess and a small enough low current initial guess for each finger will be used. For the three fingers device example, there are eight possibilities of initial guesses, e.g. high high high, high high low, high low high, ... etc. Some initial guesses will inevitably have the same solutions. Although trying all initial guesses is redundant and wasted, it is the easiest way to solve all solutions. Sometimes, it is necessary to do “try and error” task to find out all the solutions.

Once I_{C_r} and the proper initial guess $\tilde{\mathbf{I}}_{C_0}$ are determined, the solving process is that $\tilde{\mathbf{I}}_{C_0}$ is substituted into (3.47) to find out the value of $\Delta\tilde{\mathbf{I}}_{C_0}$. The new guess of the solutions becomes $\tilde{\mathbf{I}}_{C_1} = \tilde{\mathbf{I}}_{C_0} + \Delta\tilde{\mathbf{I}}_{C_0}$. If the absolute value of all elements of $\Delta\tilde{\mathbf{I}}_{C_0}$ are smaller than convergence criterion, we get the solution. If not, we substitute $\tilde{\mathbf{I}}_{C_1}$ into (3.47) to find out the next step value $\Delta\tilde{\mathbf{I}}_{C_1}$ and check the convergence criteria again. This process can be done iteratively until a satisfactory result is obtained. After solving the solution of $\tilde{\mathbf{I}}_C$ for the selected I_{C_r} and $\tilde{\mathbf{I}}_{C_0}$, the next initial guess will be used to repeat the solving process. When all initial guesses have been tried, we will increase I_{C_r} if it starts from low start value or decrease if it starts from high start value. And then, we repeat process that change different initial guesses and solve the solution iteratively. The whole $I_C - V_{BE}$ curve will be traced by sweeping I_{C_r} from predetermined start value to stop value with the accompanied solving procedure. After sweeping I_{C_r} , the next finger is selected as the reference finger and the whole procedure is repeated until all fingers are selected. If the device is symmetric, only half of the fingers need to be the reference finger.

The MATLAB® [6] program code used in this work with the above mentioned procedure could be found in Appendix A. We arrange the solving procedure used in the program as follows:

- 1) Select finger r as the reference finger, where $r = 1, 2, 3, \dots, N$. And then, the goal function set \mathbf{g}_r is build.
- 2) Select one combination of initial guess. There are 2^N combinations of the initial guess of $\tilde{\mathbf{I}}_{\mathbf{C}}$. Each combination will determine the start value of finger r , I_{C_r} , and the initial guess $\tilde{\mathbf{I}}_{\mathbf{C}_0}$. Use $\tilde{\mathbf{I}}_{\mathbf{C}_0}$ as the first guess.
- 3) Set the value of I_{C_r} . Sweep I_{C_r} from the start value to stop value to get he whole $I_{\mathbf{C}}-V_{BE}$ curve.
- 4) Substitute the guess $\tilde{\mathbf{I}}_{\mathbf{C}_k}$ into (3.43) and (3.46) to calculate $\mathbf{g}_r(\tilde{\mathbf{I}}_{\mathbf{C}_k})$ and $d\mathbf{g}_r(\tilde{\mathbf{I}}_{\mathbf{C}_k})$. And then, $\Delta\tilde{\mathbf{I}}_{\mathbf{C}_k}$ is obtained by using (3.47).
- 5) Check if the absolute value of all elements of $\Delta\tilde{\mathbf{I}}_{\mathbf{C}_k}$ are smaller than convergence criteria. If the convergence criteria is not met, use $\tilde{\mathbf{I}}_{\mathbf{C}_{k+1}} = \tilde{\mathbf{I}}_{\mathbf{C}_k} + \Delta\tilde{\mathbf{I}}_{\mathbf{C}_k}$ as the new guess and go back to 4).
- 6) Check if the sweep of I_{C_r} is done. If it is done, go to 2). If not, go back to 3).
- 7) Check if all combinations of initial guess are used. If all are used, go to 1). If not, go back to 2).
- 8) Check if all fingers are used as the reference finger. If all are used, the problem is solved. If not, go back to 1)

For the simple model, (3.43) is substituted by (3.34) and (3.46) is substituted by (3.35). For the accurate model with constant thermal conductivity, (3.43) is substituted by (3.37) and (3.46) is substituted by (3.41). For the accurate model with temperature dependent thermal conductivity, (3.43) is substituted by (3.37) and (3.46) is substituted by (3.42).

3.4 The Phenomenon of The Thermal Coupling Effect

Transistors used for power applications often have multiple fingers to spread out device output current and generated heat. Under the same collector current, the base-emitter voltage V_{BE} decrease as the device temperature increase. When transistors are

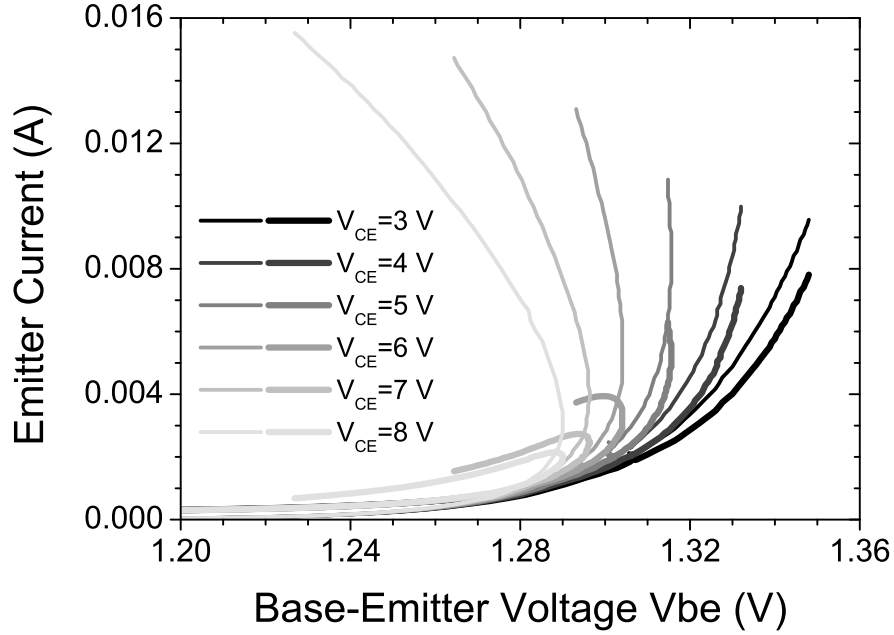


Fig. 3.3. The measured I_E-V_{BE} curves of a two-separated-fingers InGaP/GaAs HBT. The values of collector voltage biased for each curve are varied from 3 V to 8 V with 1 V step.

thermally unstable, thermal runaway is observed for constant V_{BE} bias and current collapse is observed for constant I_B bias. The most important phenomenon of the thermal coupling effect is the current collapse in multi-finger transistors. It is originated from the uneven temperature distribution between fingers when the output power is large makes the current distribution between fingers non-uniform. Eventually, all device current will only conduct through the hottest finger and kill the device. When this happens, we call the transistor is thermally unstable. The drawback of this phenomenon is that the scaling of the device output power by increasing fingers becomes ineffective. Ballasting resistors are often used to prevent the thermal instability of multi-finger transistors. The mechanism is that the negative feedback provided by ballasting resistors cancels the thermal positive feedback and stabilizes the device. As over-cancellation by resistors is unwanted, the values of ballasting resistors need to be optimized. The optimization of the ballasting resistors is the ultimate goal of this work.

Fig. 3.3 shows the measured I_E-V_{BE} curves of a two-separated-fingers InGaP/GaAs HBT under varied V_{CE} . The finger size is $2.8 \mu\text{m} \times 12 \mu\text{m}$ per single finger and the

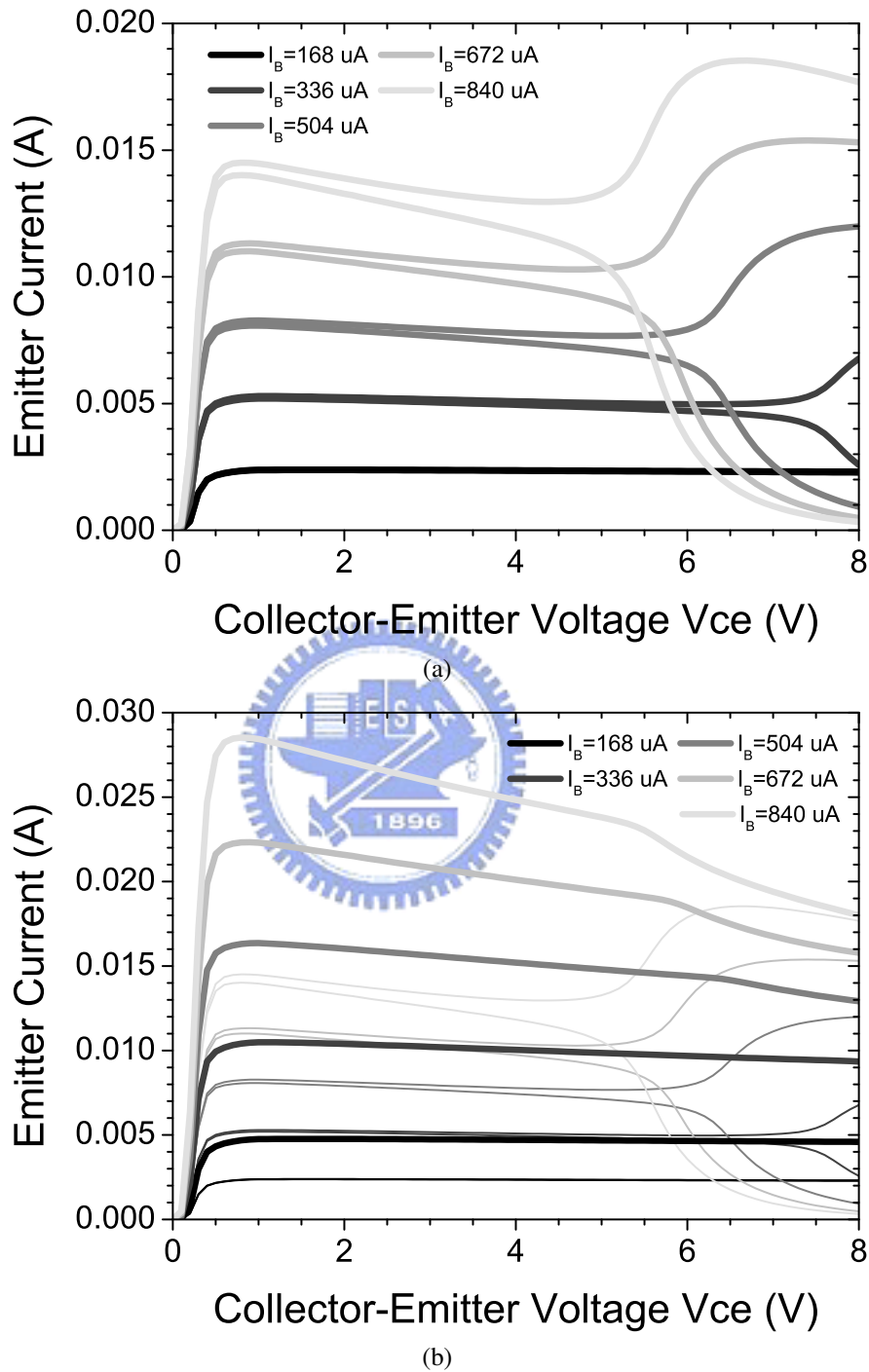


Fig. 3.4. The measured I_E-V_{CE} curves of a two-separated-fingers InGaP/GaAs HBT under constant I_B bias. (a) I_E-V_{CE} curves for each finger and (b) the total current (thick lines) and the current for each finger (thin lines). The finger size is $2.8 \mu\text{m} \times 12 \mu\text{m}$ per single finger and the spacing between fingers is $17.8 \mu\text{m}$. The values of base current biased for each curve are varied from $168 \mu\text{A}$ to $840 \mu\text{A}$ with $168 \mu\text{A}$ step.

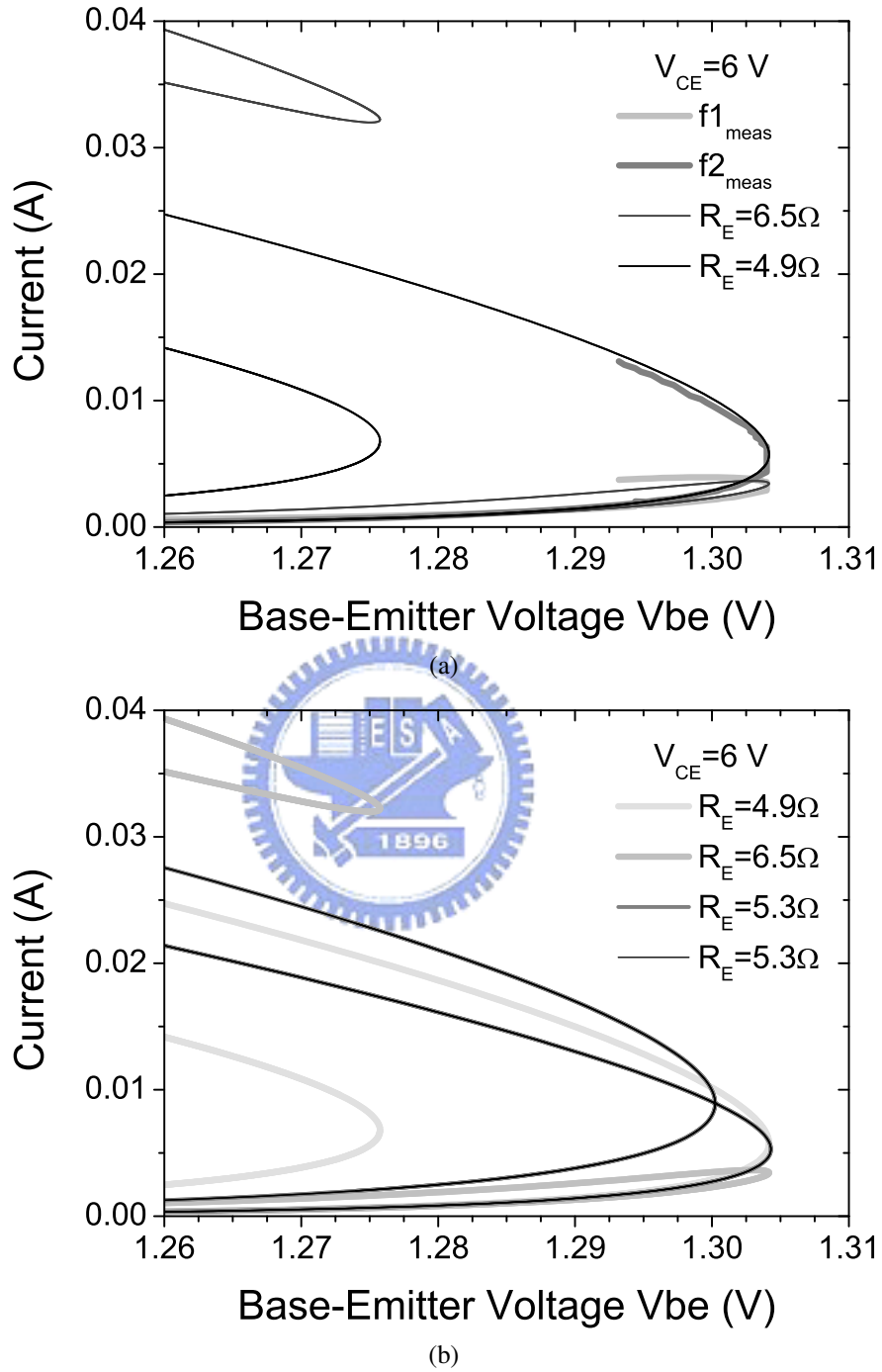


Fig. 3.5. The comparison of measured and simulated I_E-V_{BE} curves of the two-separated-fingers In-GaP/GaAs HBT at $V_{CE} = 6$ V. (a) the measured curves and the simulated curves with $R_{E1} = 6.5 \Omega$ and $R_{E2} = 4.9 \Omega$ and (b) the simulated curves with $R_{E1} = 6.5 \Omega$ and $R_{E2} = 4.9 \Omega$ case and with $R_{E1} = R_{E2} = 5.3 \Omega$ case. The model used is the accurate model with constant thermal conductivity. Parameters used are $I_O = 2.1 \times 10^{-25}$ A, $E_{g0}^* = 1.483$ V, $\alpha^* = 4.88 \times 10^{-4}$ V/K, $\gamma = 4.21$, $k_{th,eff} = 0.45$ W/cm- $^\circ$ C, $b = 0$, $V_C = 6$ V, $R_{th1} = 1834$ $^\circ$ C/W, and $R_{th2} = 174$ $^\circ$ C/W.

spacing between fingers is $17.8 \mu\text{m}$. It is obviously that as the dissipated power increase the curves will be bent more seriously, and only one finger still turn on and another one will be turned off. Fig. 3.4(a) and (b) also shows similar behaviors of the measured I_E-V_{CE} curves under constant I_B bias of the same device. The fingers will separated as a hot finger and a cold finger. The total current curves in Fig. 3.4(b) show degradation started at about $V_{CE} = 5.5 \text{ V}$ for $I_B = 840 \mu\text{A}$ curve, $V_{CE} = 6.0 \text{ V}$ for $I_B = 672 \mu\text{A}$ curve, and $V_{CE} = 6.5 \text{ V}$ for $I_B = 504 \mu\text{A}$ curve. It is because that when the degradation happens, the two-finger device acts as an one-finger device. The degradation is the current collapse effect. It is an evidence of the ineffectiveness of increasing finger number to increase power.

Fig. 3.5(a) and (b) shows the comparison of measured and simulated I_E-V_{BE} curves of the two-separated-fingers InGaP/GaAs HBT at $V_{CE} = 6 \text{ V}$. The model used in simulation is the accurate model with constant thermal conductivity. The parameters used are listed in the figure caption. Although the layouts of these two fingers are identical, the measured curves of these two fingers are still quit different. It might be due to the process deviation. Therefore, we had to add different emitter resistance for each finger to get a better fit. In Fig. 3.5(a), there are two solutions for simulated curves. In Fig. 3.5(b), the solutions are merged together for the identical R_E case. The intercept point is the unstable point of this case. It means that even these two fingers are identical, the current collapse phenomenon will still happen at the unstable point. It is the property of this coupled physical system. There are always many sets of solutions and many unstable, or intercept, points in this system. The reason will be explained in the following chapters.

3.5 Summary

The coupled current-voltage equations were derived and discussed. A linearized temperature dependent band-gap voltage expression is used to simplify the definition

3.5 Summary

of the thermal-electrical feedback coefficient and the coupled I_C-V_{BE} equations. The goal function is defined and used to solve the thermal coupling problems. There are three models that need to be solved, including the simple model, the accurate model with constant thermal conductivity, and the accurate model with temperature dependent thermal conductivity. The Newton-Raphson method is discussed and the equations needed to solve the coupled I_C-V_{BE} equations of the three models are derived. The procedure utilized to solve the coupled I_C-V_{BE} equations by using the Newton-Raphson method was developed.



Chapter 4

Thermally Stable Optimum Design of Multifinger HBTs in Simple Model

Transistors used for power applications often have multiple fingers to spread out current and dissipated heat. However, because of the heat generated and the uneven heat distribution, transistors can become unstable at high power and seriously limit the power handling capability of transistors. When this happens, thermal runaway is observed for Si BJTs and current collapse is observed for GaAs based HBTs. To prevent the thermal instability of multi-finger transistors, ballasting resistors are often used. The voltage drop across these resistors compensates the build-in voltage change due to temperature rise caused by self-heating and as a result the thermal stability is improved. This compensation is a mechanism of the cancellation of positive feedback and negative feedback [34]-[35]. Many papers have devoted to the thermal modeling of transistors and the design of ballasting resistors [36]-[40]. In real device implementation, each finger of the transistor is connected in series to a ballasting resistor, which can be either a part of the transistor made from epilayers or an external thin-film resistor. The fingers and the ballasting resistors connected to the fingers are usually identical to one another. However, because of the nonuniform heat dissipation, it has been realized that the uniform layout traditionally used for the fingers is not ideal for thermal stability. Instead,

4.1 Ideal Emitter Ballasting Resistance Distribution: Nonuniform Ballasting Resistors

the use of a nonuniform distribution in the ballasting resistors [41], the emitter finger sizes [19], the spacing between fingers [20], [42] and both finger size and spacing [43] has been proposed to improve the thermal stability. But the remaining question is: what are the optimum distributions for the ballasting resistors? A non-optimized design can easily over correct the problem and even make the problem worse.

In this chapter, we solved the basic coupled I_C-V_{BE} equations. We found that there is an ideal distribution for the ballasting resistors. Significant improvement in thermal stability can be obtained when the ideal distributions are used. Simple analytical formulas for the ideal distributions of the emitter ballasting resistors to achieve the highest stable operation current are derived. With the ideal distribution, we have also found an optimum emitter ballasting resistance for absolutely thermal stable operation condition that the device never becomes unstable. Base on the above results, a design procedure for multi-finger transistors is developed [7].

4.1 Ideal Emitter Ballasting Resistance Distribution: Nonuniform Ballasting Resistors

In a multi-finger transistor, the fingers are thermally coupled, which results in a nonuniform temperature distribution with the fingers near the center hotter than the fingers on the sides even before the transistors become unstable. To examine the thermal behavior of those fingers, we first use a three-finger configuration for analysis because the coupled equations can be solved easily and it can illustrate the nonuniform temperature distribution for multiple fingers. The behavior of transistors with number of fingers greater than three will be discussed later. Liu et. al. have solved a two-finger problem [32], but it cannot reflect the uneven distribution of current and temperature of multifingers due to thermal coupling.

The coupled I_C-V_{BE} equations for the three identical fingers when self heated are

4.1 Ideal Emitter Ballasting Resistance Distribution:
Nonuniform Ballasting Resistors

[2]

$$\begin{aligned}
 I_{C_1} &= I_O \exp \left\{ \frac{q}{kT_A} [V_{BE} + \phi(T_1 - T_A) - R_{E_{13}} I_{C_1}] \right\} \\
 I_{C_2} &= I_O \exp \left\{ \frac{q}{kT_A} [V_{BE} + \phi(T_2 - T_A) - R_{E_2} I_{C_2}] \right\} \\
 I_{C_3} &= I_O \exp \left\{ \frac{q}{kT_A} [V_{BE} + \phi(T_3 - T_A) - R_{E_{13}} I_{C_3}] \right\}
 \end{aligned} \tag{4.1}$$

where I_{C_1} and I_{C_3} are the current flowing through the two side fingers and I_{C_2} is the current of the center finger, T_1 and T_3 are the temperature of the two side fingers and T_2 is the temperature of the center finger, V_{BE} is the applied base-emitter voltage, ϕ is the emitter junction build-in potential change per unit temperature rise, T_A is the ambient temperature or the heat plate temperature that is 300 K in our simulation. This is a three fingers case of (3.32) as had been discussed in Section 3.2. $R_{E_{13}}$ and R_{E_2} are the emitter resistances of the side fingers and the center finger, respectively. Here we have assumed a symmetric structure that R_E is the same for the two side fingers. Notice that the ideality factor in the I_C - V_{BE} equations is set to unity for simplicity. The junction temperature rises for the three fingers are related to the power consumption of each finger by

$$\begin{aligned}
 T_1 &= T_A + V_C (R_{th_1} I_{C_1} + R_{th_2} I_{C_2} + R_{th_3} I_{C_3}) \\
 T_2 &= T_A + V_C (R_{th_2} I_{C_1} + R_{th_1} I_{C_2} + R_{th_2} I_{C_3}) \\
 T_3 &= T_A + V_C (R_{th_3} I_{C_1} + R_{th_2} I_{C_2} + R_{th_1} I_{C_3})
 \end{aligned} \tag{4.2}$$

as a three fingers case of (3.26) in Section 3.2. Here, for a symmetric structure device, R_{th_1} is the thermal resistance of each finger, and R_{th_2} is the coupling thermal resistances between two adjacent fingers, and R_{th_3} is the coupling thermal resistances between two fingers separated by one finger. V_C is the collector voltage.

Because the current of all fingers must be the same under the stable operation condition, we can obtain a relation between $R_{E_{13}}$ and R_{E_2} from (4.1) and (4.2) by setting the currents of all fingers identical, i.e. $I_{C_1} = I_{C_2} = I_{C_3} = I$, and dividing the first equation

4.1 Ideal Emitter Ballasting Resistance Distribution: Nonuniform Ballasting Resistors

of (4.1) by the second equation of (4.1) after substituting (4.2) into (4.1). That is

$$\begin{aligned} R_{E_2,ideal} &= R_{E_{13}} + R_{th_2}^* - R_{th_3}^* \\ &= R_{E_{13}} + \Delta R_{E_2,ideal} \end{aligned} \quad (4.3)$$

where we define the effective thermal resistance R_{th_i} as

$$R_{th_i}^* = \phi V_C R_{th_i} \quad (4.4)$$

for conciseness. This relation gives the ideal emitter ballasting resistance distribution of a three-identical-finger transistor. In order to get the stable operation condition, the difference between the emitter resistances of the center finger and the side fingers should be $\Delta R_{E_{ideal}} = R_{th_2}^* - R_{th_3}^*$. This is the necessary condition for achieving identical currents in all three fingers. Otherwise, the current of each finger is decided by the total effect of the positive feedback term of ΔT 's and the negative feedback term of R_E 's, and the currents of the fingers will never be the same. The basic idea of ideal distribution is to design a proper R_{E_2} to compensate the additional thermal coupling resistance between the center finger and the side fingers.

Now, we show the simulation result of a three-finger transistor with each finger having the following parameters: $I_O = 6 \times 10^{-25}$ A, $R_{th_1} = 800$ °C/W, $(1+1/\beta)R_{E0} + R_B/\beta = 0.9$ Ω, $\phi = 1$ mV/°C. Those numbers are experimentally determined from a 3×40 InGaP/GaAs HBT by fitting the measured $I_C - V_{BE}$ of a single-finger transistor with (4.1). The current gain β is assumed to be independent of temperature, which is a valid assumption for InGaP/GaAs transistors. With those numbers, we then solved the steady state heat flow equation [19], [20] with proper boundary conditions as had mentioned in Section 2.2.1 to obtain the coupling thermal resistance. The finger size used is $3 \mu\text{m} \times 40 \mu\text{m}$ and the spacing between fingers is $40 \mu\text{m}$. The chip dimension used in simulation is $1000 \mu\text{m} \times 1000 \mu\text{m}$ and the substrate thickness is $100 \mu\text{m}$. The calculated coupling thermal resistances are $R_{th_2} = 66.9$ °C/W, $R_{th_3} = 23.5$ °C/W,

4.1 Ideal Emitter Ballasting Resistance Distribution: Nonuniform Ballasting Resistors

$R_{th4} = 10.2 \text{ }^\circ\text{C/W}$, and $R_{th5} = 4.7 \text{ }^\circ\text{C/W}$ with the effective thermal conductivity $k_{th,eff} = 0.4124 \text{ W/cm-}^\circ\text{C}$, which is computed from the theoretical result of $R_{th1} = 733 \text{ }^\circ\text{C/W}$ calculated by $k_{th} = 0.45 \text{ W/cm-}^\circ\text{C}$ as shown in Fig. 2.6 and the fitting result $R_{th1} = 800 \text{ }^\circ\text{C/W}$. And the collector voltage V_C is taken to be 6 V in the simulation. We will call this three finger transistor used for simulation as a 3f 3x40 s40 HBT for short where 3f means three-finger, and 3x40 means the finger size is $3 \mu\text{m} \times 40 \mu\text{m}$, s40 means the finger separation is $40 \mu\text{m}$.

Let's first consider a case that each finger has a total R_E of 3Ω , or a ballasting resistance of 2.1Ω for this device. Fig. 4.1(a) and (b) show the calculated I_C-V_{BE} curves and the temperature of each finger as a function of the total current. There are totally four sets of solutions for (4.1). Three sets of solutions are shown in the figure. The solution with $I_{C3} > I_{C2} > I_{C1}$ is not shown because the behavior is identical to the case with $I_{C1} > I_{C2} > I_{C3}$ due to the layout symmetry. The first set shows that the currents in the fingers are nearly the same before they reach the unstable point which we define as the highest current of the side fingers, i.e. about 11.1 mA in the case. At the unstable point, the currents in the side fingers drops while that of the center finger continue to increase. The temperatures also start to deviate from each other after the unstable point. The other sets of solutions, however, show that one or both of the side finger current is always much larger than the center finger current in all the voltage range, and the curves are separated from those of the first set of solutions. In other words, it is almost impossible to go into these situations if the transistor is powered up from zero bias.

Now we increase the emitter resistance of the center finger to the ideal value of $R_{E2,ideal} = 3.26 \Omega$ or $\Delta R_{E2,ideal} = 0.26 \Omega$, calculated by (4.3), but keep that of the side fingers at 3Ω . In other words, the ballasting resistance for the center finger is 2.36Ω while that for the side fingers is 2.1Ω . The I_C-V_{BE} curves and the temperature distribution become those shown in Fig. 4.2(a) and (b). We can see that there is a set of solution that has $I_{C1} = I_{C2} = I_{C3}$ in all voltage range. However other solutions

4.1 Ideal Emitter Ballasting Resistance Distribution:
Nonuniform Ballasting Resistors

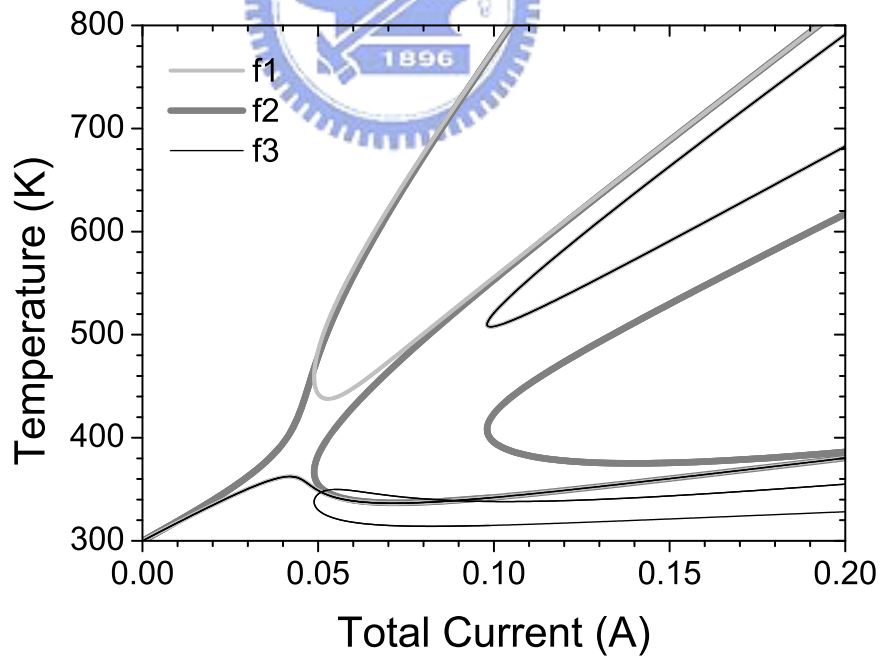
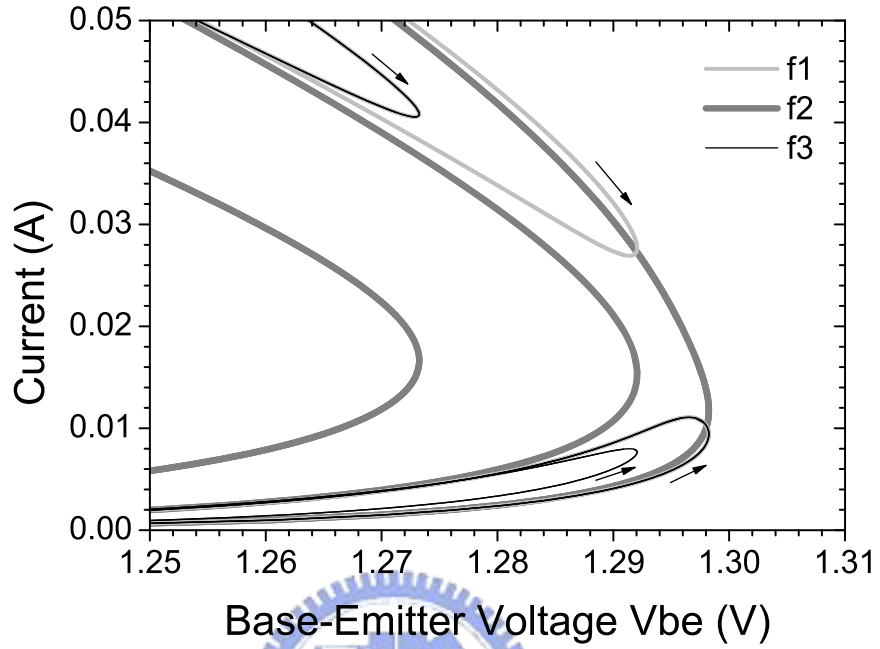


Fig. 4.1. The simulation results of a 3f 3x40 s40 HBT with $R_{E_{13}} = R_{E_2} = 3 \Omega$. (a) $I_C - V_{BE}$ curves and (b) the finger temperature as a function of the total current. The arrows mark the direction of current sweep of the side fingers as the current of the center finger increasing from low to high for the three sets of solutions. f2 is the center finger. f1 and f3 are the side fingers.

4.1 Ideal Emitter Ballasting Resistance Distribution:
Nonuniform Ballasting Resistors

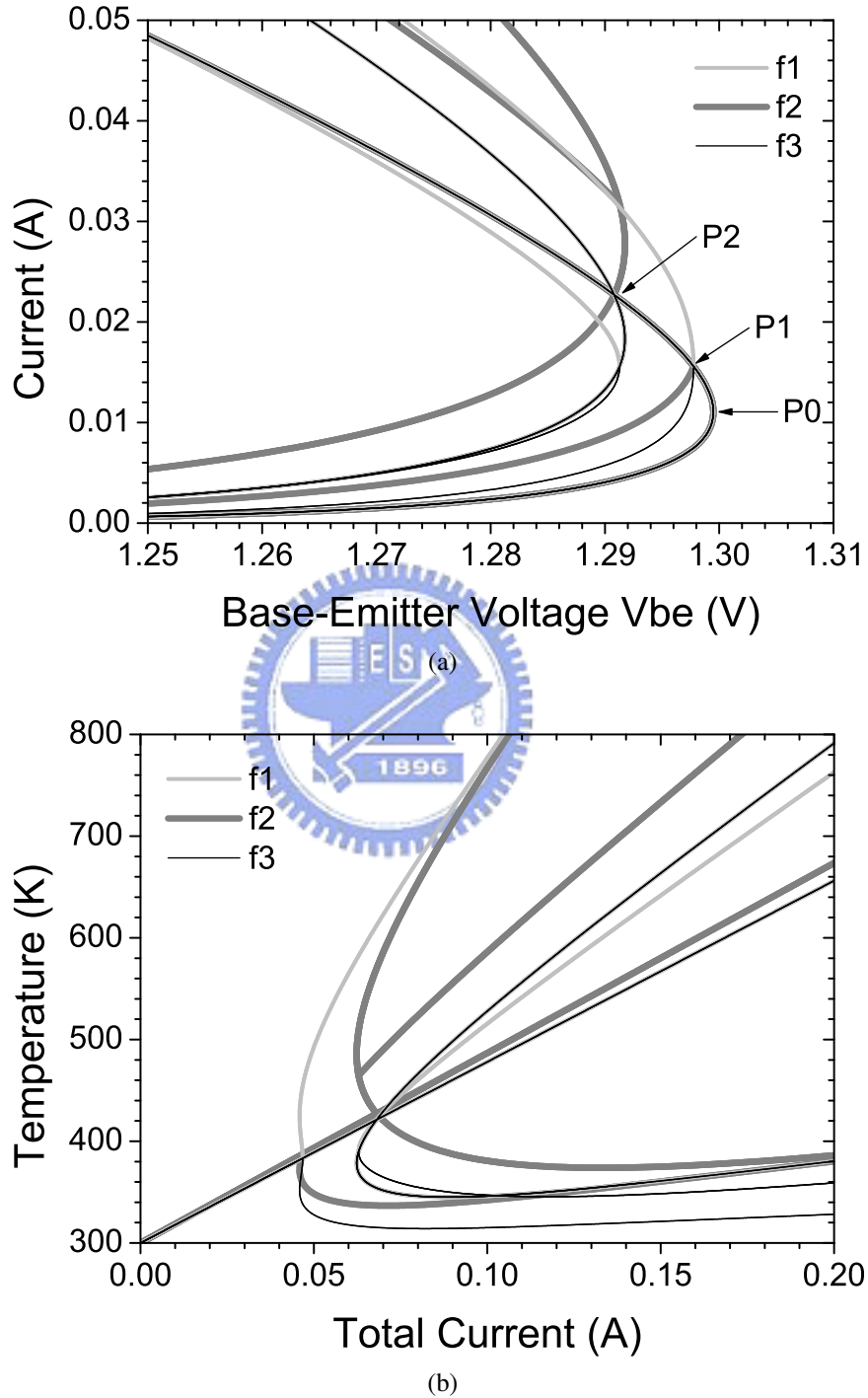


Fig. 4.2. The simulation results of a 3f 3x40 s40 HBT with $R_{E_{13}} = 3 \Omega$ and $R_{E_2} = R_{E_{2,ideal}} = 3.26 \Omega$. (a) $I_C - V_{BE}$ curves and (b) the finger temperature as a function of the total current. P0 marks the bend-over point, P1 marks the first unstable point, and P2 marks the second unstable point. f2 is the center finger. f1 and f3 are the side fingers.

4.1 Ideal Emitter Ballasting Resistance Distribution:
Nonuniform Ballasting Resistors

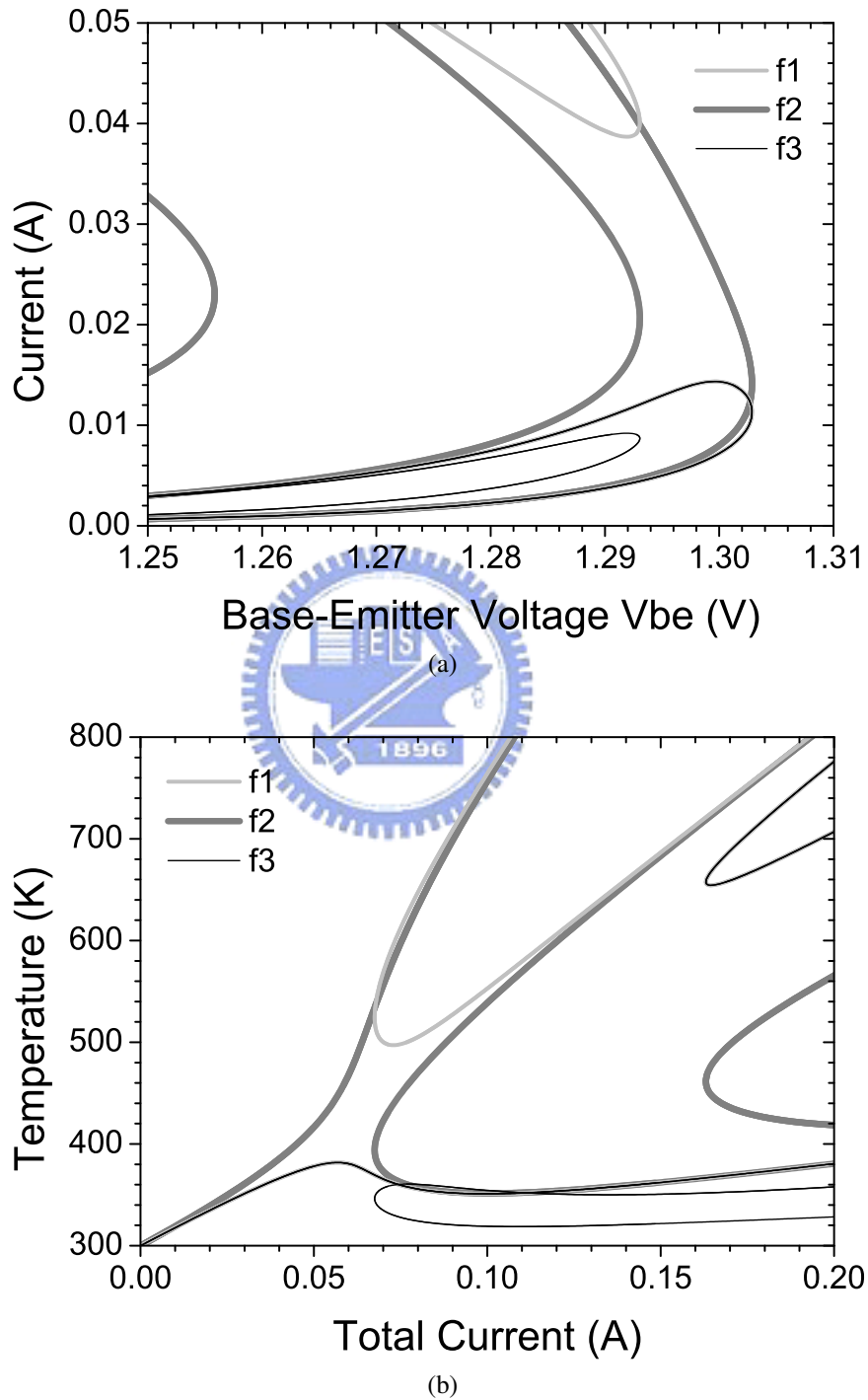


Fig. 4.3. The simulation results of a 3f 3x40 s40 HBT with $R_{E_{13}} = R_{E_2} = 3.4 \Omega$. (a) $I_C - V_{BE}$ curves and (b) the finger temperature as a function of the total current. f2 is the center finger. f1 and f3 are the side fingers.

4.1 Ideal Emitter Ballasting Resistance Distribution:
Nonuniform Ballasting Resistors

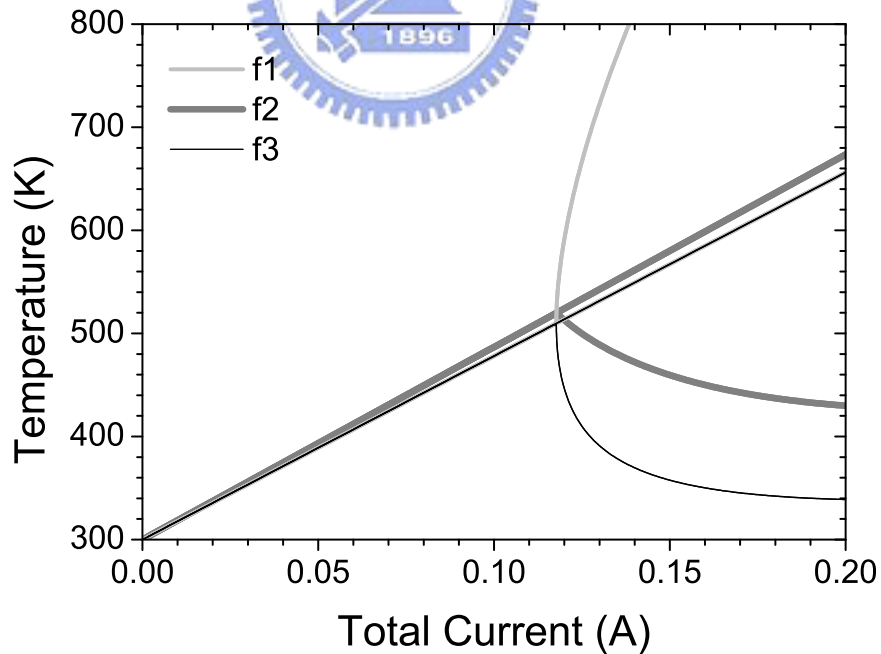
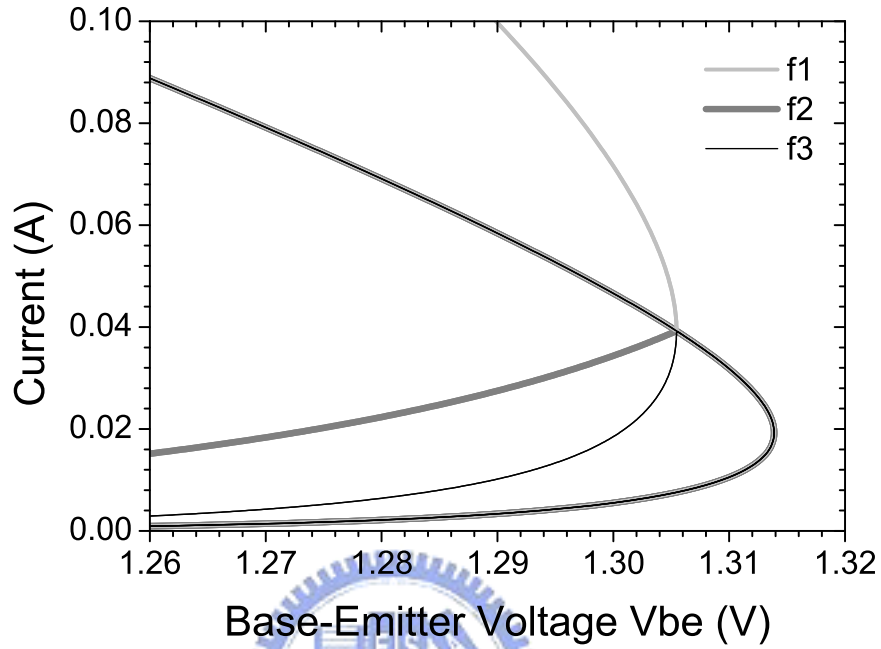


Fig. 4.4. The simulation results of a 3f 3x40 s40 HBT with $R_{E_{13}} = 4 \Omega$ and $R_{E_2} = R_{E_{2,ideal}} = 4.26 \Omega$. (a) $I_C - V_{BE}$ curves and (b) the finger temperature as a function of the total current. f2 is the center finger. f1 and f3 are the side fingers.

4.1 Ideal Emitter Ballasting Resistance Distribution: Nonuniform Ballasting Resistors

give unstable results after the current exceeds certain value. There are two intersection points corresponding to the onsets of two different unstable modes. The first one, **P1** in Fig. 4.2(a) which occurs at about 15.6 mA, is the onset point when the currents in all fingers start to differ. The second point, **P2** in Fig. 4.2(a) which is at about 22.7 mA, corresponds to that when I_{C_2} starts to differ from I_{C_1} and I_{C_3} but $I_{C_1} = I_{C_3}$. Although a stable solution with $I_{C_1} = I_{C_2} = I_{C_3}$ exists, it is almost impossible for a transistor to pass through the first intersection point and remains stable because that in practical situations, any small deviation from ideal will cause the device to fall into instability.

Fig. 4.3(a) and (b) shows the calculated $I_C - V_{BE}$ curves and the temperatures of the fingers of a transistor with uniform ballasting at $R_E = 3.4 \Omega$. It is worthwhile to point out that although this value is higher than the combination of $R_{E_{13}}/R_{E_{2,ideal}} = 3/3.26 \Omega$, the thermal stability, the highest current of the side fingers which is at about 14.4 mA, is worse than that shown in Fig. 4.2(a). This is different from the traditional belief that a higher emitter resistance always provides better thermal stability. The distribution of the ballasting resistance is also important. The reason that the thermal stability is improved by a proper combination of $R_{E_{13}}/R_{E_2}$ is very simple. The positive feedback values of each fingers are all different because that the coupling thermal resistances seen by each finger are all different. If we can make them very close to one another by adjusting the ballasting resistance according to the different positive feedback values for each finger, the thermal stability will be improved.

The current levels of the intersection points are affected by the value of $R_{E_{13}}$. If we increase $R_{E_{13}}$ from 3Ω to 4Ω but keep $R_{E_2} - R_{E_{13}} = \Delta R_{E_{2,ideal}} = 0.26 \Omega$, the curves become those shown in Fig. 4.4(a) and (b). The first unstable point, at about 39.2 mA, moves up and the second point is out of the simulation range. The device can go to a higher current before it becomes unstable. This is understandable that because the increased negative feedback provided by the higher emitter resistance compensates the positive feedback caused by the temperature rise, the transistor becomes more stable. We can conclude that a larger $R_{E_{13}}$ will result in a more stable device. However, if we

over design the ballasting resistance, the performance of the device will suffer. For this reason, an optimal design of R_{E13} is very important. We need to know a minimal value of R_{E13} to just make the device stable.

4.2 The Optimum Emitter Ballasting Resistance for Absolutely Thermal Stable Operation

From the simulation results presented above, we found that as R_{E13} increases, the unstable points will move up. Obviously, there exists an optimum value of R_{E13} that the unstable points move to just at the infinite current level. We will call this value as the optimum emitter ballasting resistance for absolutely thermal stable operation. In this section, we will derive an analytical formula for this optimum value. We start from taking the derivative of (4.1) and (4.2) with respect to V_{BE} and using the ideal emitter resistance distribution (4.3). Then, we obtain

$$\begin{aligned}
 I'_{C_1} &= I \frac{q}{kT_A} (1 + \phi T'_1 - R_{E13} I'_{C_1}) \\
 I'_{C_2} &= I \frac{q}{kT_A} (1 + \phi T'_2 - R_{E2,ideal} I'_{C_2}) \\
 I'_{C_3} &= I \frac{q}{kT_A} (1 + \phi T'_3 - R_{E13} I'_{C_3})
 \end{aligned} \tag{4.5}$$

and

$$\begin{aligned}
 T'_1 &= V_C (R_{th1} I'_{C_1} + R_{th2} I'_{C_2} + R_{th3} I'_{C_3}) \\
 T'_2 &= V_C (R_{th2} I'_{C_1} + R_{th1} I'_{C_2} + R_{th2} I'_{C_3}) \\
 T'_3 &= V_C (R_{th3} I'_{C_1} + R_{th2} I'_{C_2} + R_{th1} I'_{C_3}).
 \end{aligned} \tag{4.6}$$

We first substitute $I'_{C_1} = I'_{C_2} = I'_{C_3} = I'$ into (4.5) and (4.6), and combine them to obtain

$$I' = I \frac{q}{kT_A} [1 + (R_{th1}^* + R_{th2}^* + R_{th3}^* - R_{E13}) I']. \tag{4.7}$$

4.2 The Optimum Emitter Ballasting Resistance for Absolutely Thermal Stable Operation

This equation can be used to calculate the bend-over current, I_{bend} , which is the point that the $I_C - V_{BE}$ curve starts to bend-over. This point, which is traditionally considered as the onset point for the device to become unstable [32], can be easily found from (4.7) by requiring $I' = dI/dV_{BE} = \infty$. After this manipulation, the current at the bend-over point is

$$I_{bend} = \frac{kT_A/q}{R_{th1}^* + R_{th2}^* + R_{th3}^* - R_{E13}}. \quad (4.8)$$

This equation simply gives us the maximum current a device can operate at constant base-emitter voltage operation. If the voltage drive exceeds the voltage V_{bend} corresponding to I_{bend} , the device will be burned out because that there is no solution for the voltage exceeding V_{bend} . This kind of failure is also called second breakdown. It is the reason why the bend-over point is traditionally considered as the unstable point. But if we use a base current drive instead of a base voltage drive, this bend-over point can be passed and is not an unstable point anymore. The unstable point is actually the point that all finger currents diverge.

Next step, we will derive the relations of the unstable point current and use them to find out the optimum value of the emitter ballasting resistance. By combining (4.5) and (4.6), we get the following equation in matrix notation as

$$\begin{pmatrix} R_{th1}^* - R_{E13} - \lambda & R_{th2}^* & R_{th3}^* \\ R_{th2}^* & R_{th1}^* - R_{E2,ideal} - \lambda & R_{th2}^* \\ R_{th3}^* & R_{th2}^* & R_{th1}^* - R_{E13} - \lambda \end{pmatrix} \begin{pmatrix} I'_{C1} \\ I'_{C2} \\ I'_{C3} \end{pmatrix} = \begin{pmatrix} -1 \\ -1 \\ -1 \end{pmatrix} \quad (4.9)$$

where

$$\lambda = \frac{kT_A}{q} \frac{1}{I}.$$

As shown in Fig. 4.2(a), the unstable points can be viewed as the intercept point of two $I_C - V_{BE}$ curves which are both the solutions of (4.1). The slopes of the $I_C - V_{BE}$ curves at the unstable points are not unique because that they are both the solutions of

4.2 The Optimum Emitter Ballasting Resistance for Absolutely Thermal Stable Operation

two curves with different slopes at these points. We can use this requirement in (4.9) to solve for λ . The requirement demands

$$\begin{vmatrix} R_{th1}^* - R_{E13} - \lambda & R_{th2}^* & R_{th3}^* \\ R_{th2}^* & R_{th1}^* - R_{E2,ideal} - \lambda & R_{th2}^* \\ R_{th3}^* & R_{th2}^* & R_{th1}^* - R_{E13} - \lambda \end{vmatrix} = 0 \quad (4.10)$$

This is an eigenvalue problem and the solutions give conditions for the unstable points. The eigenvalues and the eigenvectors are

$$\begin{aligned} \text{eigenvalue : } \lambda_1 &= R_{th1}^* + R_{th2}^* + R_{th3}^* - R_{E13} \\ \text{eigenvector : } I'_{C1} &= I'_{C2} = I'_{C3} \\ \Rightarrow I_{C\lambda1} &= \frac{kT_A/q}{R_{th1}^* + R_{th2}^* + R_{th3}^* - R_{E13}} \end{aligned} \quad (4.11)$$

$$\begin{aligned} \text{eigenvalue : } \lambda_2 &= R_{th1}^* - R_{th3}^* - R_{E13} \\ \text{eigenvector : } I'_{C1} &= -I_{C3}, \quad I'_{C2} = 0 \\ \Rightarrow I_{C\lambda2} &= \frac{kT_A/q}{R_{th1}^* - R_{th3}^* - R_{E13}} \end{aligned} \quad (4.12)$$

$$\begin{aligned} \text{eigenvalue : } \lambda_3 &= R_{th1}^* - R_{th2}^* - R_{E2,ideal} \\ \text{eigenvector : } I'_{C1} &= I'_{C3}, \quad I'_{C2} = -2I'_{C1} \\ \Rightarrow I_{C\lambda3} &= \frac{kT_A/q}{R_{th1}^* - R_{th2}^* - R_{E2,ideal}}. \end{aligned} \quad (4.13)$$

One should note that the lowest unstable current solution is $I_{C\lambda1} = I_{bend}$ and the corresponding eigenvector is $I'_{C1} = I'_{C2} = I'_{C3}$. Since the slopes are the same, the currents of all fingers will keep the same after this point. This is simply the bend-over point, not really an unstable point. The other two solutions give the real unstable points where the slopes of the $I_C - V_{BE}$ curves of different fingers are different and the currents of the fingers start to deviate from one another. One can find that the three solutions given above

4.2 The Optimum Emitter Ballasting Resistance for Absolutely Thermal Stable Operation

have the sequence $I_{C_{\lambda_1}} < I_{C_{\lambda_2}} < I_{C_{\lambda_3}}$. At the first real unstable point, which happens at $I_{C_{\lambda_2}}$, the I_C-V_{BE} curves of the side fingers have opposite slopes and the center finger has zero slope. It means that the currents of the two side fingers start to deviate from each other at this point and the current of the center finger reaches its maximum value if the unstable operation occurs. The currents of the three fingers are all different after this point. One of the side fingers, not the center one, will become the hottest and the other will become the coldest one. At the second unstable point, which occurs at $I_{C_{\lambda_3}}$, the I_C-V_{BE} curves of the side fingers have the same slopes while the center finger has opposite slope to those of the side fingers. In other words, at this point the current of the center finger starts to deviate from that of the side fingers, which have the same current. At this point, there can be two unstable modes. In one mode, the center finger becomes hot and the side fingers become cold, and in the other mode, the center finger becomes cold and the side fingers become hot.

We would like to point out that the lowest unstable current, $I_{C_{\lambda_2}}$, is actually higher than the bend-over current of the I_C-V_{BE} curves. Therefore, even the I_C-V_{BE} curve of the transistor bends over into the negative resistance region, the device stays stable until $I_{C_{\lambda_2}}$ is reached. Before this point, the currents of all the fingers are the same and there is no solution allowed for different I_{C_1} , I_{C_2} and I_{C_3} . Substituting the parameters used in Fig. 4.2 into (4.11)-(4.13), we obtain $I_{C_{\lambda_1}} = 11.0$ mA, $I_{C_{\lambda_2}} = 15.6$ mA, and $I_{C_{\lambda_3}} = 22.7$ mA corresponding to P0, P1, and P2 marked in Fig. 4.2(a). And substituting the parameters used in Fig. 4.4 into (4.11)-(4.13), we obtain $I_{C_{\lambda_1}} = 19.3$ mA, $I_{C_{\lambda_2}} = 39.2$ mA, and $I_{C_{\lambda_3}} = 186.5$ mA. We will call $I_{C_{\lambda_i}}$ as the eigen-current. It can be found that as $R_{E_{13}}$ increasing the current levels of the unstable points $I_{C_{\lambda}}$ s increase very fast. We can expect that there is a finite value of $R_{E_{13}}$ that can push the unstable current levels to infinity.

Examining (4.11)-(4.13), we can see that if the denominators go to zero, there are

4.2 The Optimum Emitter Ballasting Resistance for Absolutely Thermal Stable Operation

three relationships giving conditions for $I_{C\lambda_1}$, $I_{C\lambda_2}$ and $I_{C\lambda_3}$ to go to infinity. They are

$$R_{E_{13,no-bend}} = R_{th1}^* + R_{th2}^* + R_{th3}^* \quad (4.14)$$

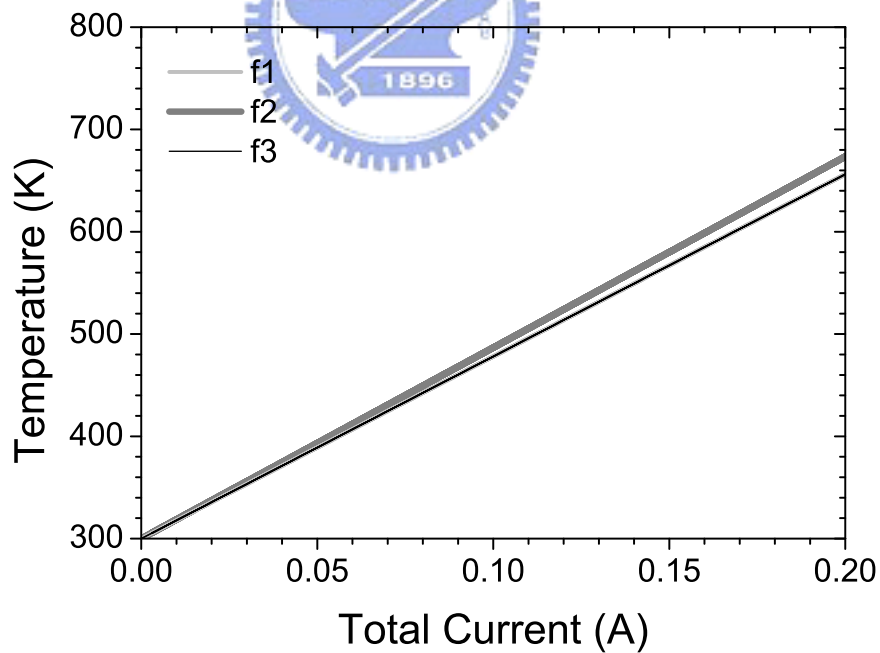
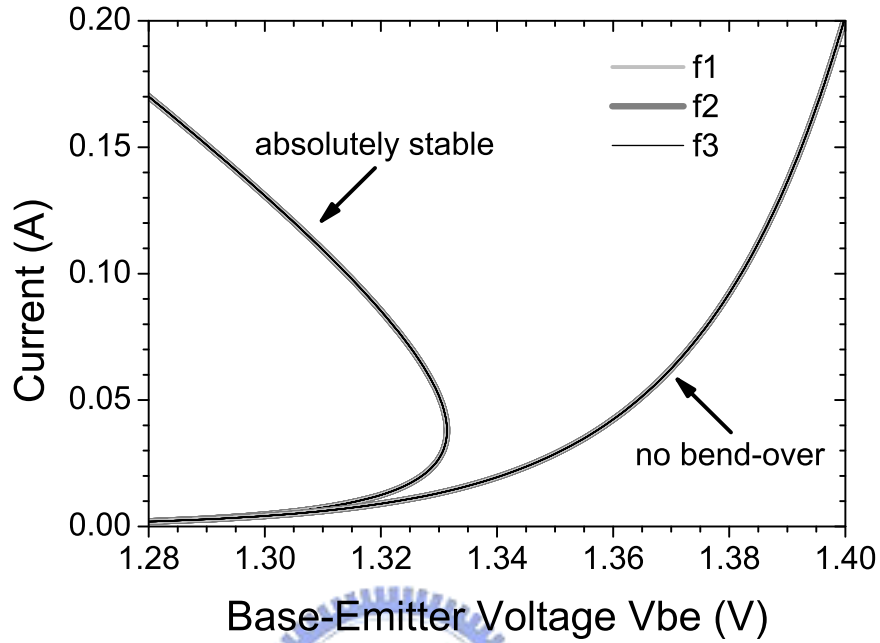
$$R_{E_{13,opt}} = R_{th1}^* - R_{th3}^* \quad (4.15)$$

$$\begin{aligned} R_{E_{13,opt2}} &= R_{th1}^* - R_{th2}^* - \Delta R_{E_{2,ideal}} \\ &= R_{th1}^* - 2R_{th2}^* + R_{th3}^*. \end{aligned} \quad (4.16)$$

Equation (4.14) is the conventional absolutely stable condition. At this condition, the bend-over point goes to infinity and the I_C-V_{BE} curve never bends over. But as mentioned above, it is more appropriate to consider (4.15) as the absolutely stable condition if the ideal emitter ballasting resistance distribution of (4.3) is satisfied. At this condition the currents of all the fingers are identical in the whole operation voltage and current range. In other words, the device will never become unstable even though the bend-over happens. The condition of (4.16) only lets the second unstable point to go to infinity and is not enough to stabilize the device.

For this 3f 3x40 s40 HBT considered above, the absolutely stable condition of the emitter resistance is $R_{E_{13,opt}} = 4.66 \Omega$ and $R_{E_{2,ideal}} = 4.92 \Omega$. The no bend-over condition, however, has $R_{E_{2,no-bend}} = 5.34 \Omega$ and $R_{E_{2,ideal}} = 5.60 \Omega$. Fig. 4.5(a) and (b) shows the I_C-V_{BE} curve and the temperature of each finger in the absolutely stable condition and the no bend-over condition. The center finger has a slightly higher temperature than the side fingers but the currents of all fingers never differ. As a result of identical currents, the temperature curves of the absolutely stable and no bend-over conditions overlap. In fact, the no bend-over condition should have higher finger temperature. It is because that the dissipated power of this condition is higher due to the higher base-emitter voltage. But the power contribution of the base-emitter voltage is minor and can be neglected as had discussed in Section 3.2. Therefore, the resultant temperature difference is not important. Although all the I_C-V_{BE} curves have negative resistance as long as $R_{E_{13,opt}}$ is smaller than $R_{E_{2,no-bend}}$, the equations do not allow solutions with

4.2 The Optimum Emitter Ballasting Resistance for Absolutely Thermal Stable Operation



(b)

Fig. 4.5. The simulation results of a 3f 3x40 s40 HBT with the absolutely stable condition, $R_{E_{13}} = R_{E_{13,opt}} = 4.66 \Omega$ and $R_{E_2} = R_{E_2,ideal} = 4.92 \Omega$, and with the no bend-over condition, $R_{E_{13}} = R_{E_{13,no-bend}} = 5.34 \Omega$ and $R_{E_2} = R_{E_2,ideal} = 5.60 \Omega$. (a) $I_C - V_{BE}$ curves and (b) the finger temperature as a function of the total current. The temperature curves of these two conditions are identical. f2 is the center finger. f1 and f3 are the side fingers.

4.2 The Optimum Emitter Ballasting Resistance for Absolutely Thermal Stable Operation

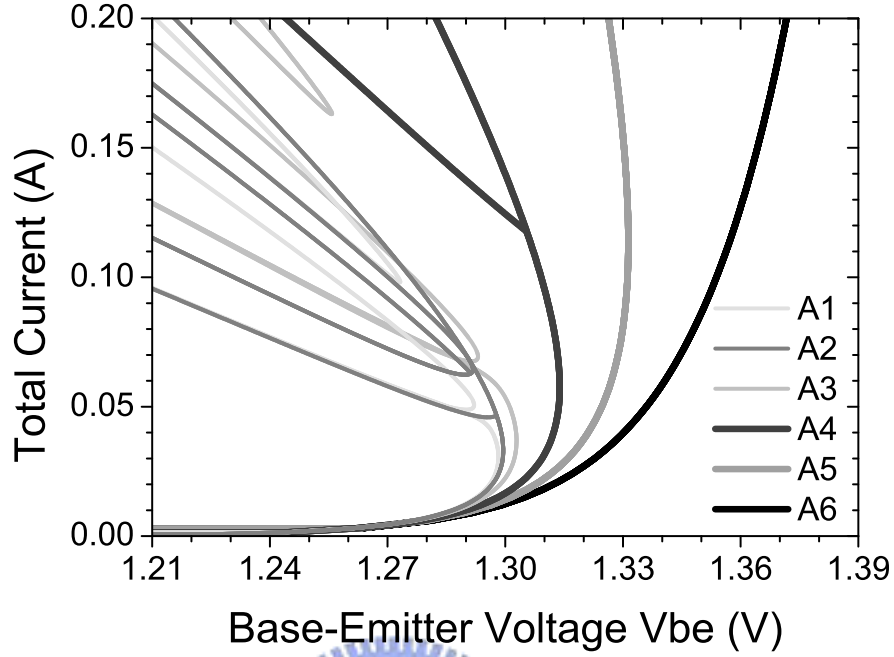


Fig. 4.6. The simulation results of the total current versus V_{BE} curves collected from Fig. 4.1-Fig. 4.5 for the 3f 3x40 s40 HBT. A1-A6 correspond to the curves of the simulation conditions of $R_E = 3 \Omega$, $R_{E_{13}}/R_{E_{2,ideal}} = 3/3.26 \Omega$, $R_E = 3.4 \Omega$, $R_{E_{13}}/R_{E_2} = 4/4.26 \Omega$, $R_{E_{13,opt}}/R_{E_{2,ideal}} = 4.66/4.92 \Omega$, and $R_{E_{13,no-bend}}/R_{E_{2,ideal}} = 5.34/5.60 \Omega$ respectively.

different current in the fingers. Consequently, even the I_C-V_{BE} curve turns over, the transistor is stable because the currents in all the fingers are identical.

Fig. 4.6 shows the simulated total current versus base-emitter voltage curves collected from Fig. 4.1-Fig. 4.5. It can be found that when the unstable point is reached, the total current with the ideal emitter resistance distribution (4.3) will have a sharp transition to the collapse solution that all finger currents diverged. On the contrary, the total current with the uniform emitter resistance distribution has a smooth shape in the full measurement range. Although we had concluded in Section 4.1 that the stability with $R_{E_{13}}/R_{E_{2,ideal}} = 3/3.26 \Omega$ as in Fig. 4.2 is better than $R_E = 3.4 \Omega$ as in Fig. 4.3, the total current with $R_E = 3.4 \Omega$ is higher than $R_{E_{13}}/R_{E_{2,ideal}} = 3/3.26 \Omega$. It is due to the center finger current of the $R_E = 3.4 \Omega$ case is higher than the $R_{E_{13}}/R_{E_{2,ideal}} = 3/3.26 \Omega$ case. However, the uniformity of the $R_E = 3.4 \Omega$ case is much worse than the $R_{E_{13}}/R_{E_{2,ideal}} = 3/3.26 \Omega$ case because that both case have similar side finger current

levels. The non-uniformity will cause the temperature of the center finger to increase more faster and be burned easily. This is unwanted for thermally stable consideration.

4.3 N-Finger Transistors: The General Case

Similarly, we can extend the above discussion of the three-finger case to the N-finger case. First, we label these fingers from left to right as shown in Fig. 2.1 which is a 3-finger example. And then, we can rewrite the N current variables and the N temperature rising variables of all fingers as one current vector \mathbf{I} and one temperature vector \mathbf{T} , respectively, as

$$\mathbf{I} = (I_{C_1} \ I_{C_2} \ I_{C_3} \ \cdots \ I_N)^T \quad (4.17)$$

$$\mathbf{T} = (T_1 \ T_2 \ T_3 \ \cdots \ T_N)^T. \quad (4.18)$$

The emitter resistances of the finger are written as a diagonal matrix \mathbf{R}_E , which is

$$\begin{aligned} \mathbf{R}_E &= \text{diag}(R_{E_1} \ R_{E_2} \ R_{E_3} \ \cdots \ R_{E_N}) \\ &= \begin{pmatrix} R_{E_1} & 0 & 0 & \cdots & \cdots & 0 \\ 0 & R_{E_2} & 0 & & & \vdots \\ 0 & 0 & R_{E_3} & & & \vdots \\ \vdots & & & \ddots & & \vdots \\ \vdots & & & & R_{E_{N-1}} & 0 \\ 0 & \cdots & \cdots & \cdots & 0 & R_{E_N} \end{pmatrix} \end{aligned} \quad (4.19)$$

where $\text{diag}(v)$ means a diagonal matrix with vector v as its diagonal elements. We can

also define the thermal resistance matrix \mathbf{R}_{th} as

$$\mathbf{R}_{th} = \begin{pmatrix} R_{th_{11}} & R_{th_{12}} & R_{th_{13}} & \cdots & R_{th_{1N}} \\ R_{th_{21}} & R_{th_{22}} & R_{th_{23}} & \cdots & R_{th_{2N}} \\ R_{th_{31}} & R_{th_{32}} & R_{th_{33}} & \cdots & R_{th_{3N}} \\ \vdots & \vdots & \vdots & \ddots & \vdots \\ R_{th_{N1}} & R_{th_{N2}} & R_{th_{N3}} & \cdots & R_{th_{NN}} \end{pmatrix}. \quad (4.20)$$

Here, $R_{th_{nn}}$ is the thermal resistance of the n -th finger and $R_{th_{nm}}$ is the coupling thermal resistance between the n -th and the m -th fingers. Then, the coupled I_C-V_{BE} equations for an N-identical-finger transistor with self-heating become

$$\mathbf{I} = I_O \exp \left\{ \frac{q}{kT_A} \left[V_{BE} + \phi (\mathbf{T} - T_A) - \mathbf{R}_E \mathbf{I} \right] \right\} \quad (4.21)$$

$$\mathbf{T} = T_A + V_C \mathbf{R}_{th} \mathbf{I}. \quad (4.22)$$

Following the same procedure as the three-finger case, the ideal emitter ballasting resistance distribution of N-fingers can be obtained as

$$\begin{aligned} \mathbf{R}_{E_{ideal}} &= \left(R_{E_1} \ R_{E_2} \ R_{E_3} \ \cdots \ R_{E_N} \right)^T \\ &= R_{E_1} + \sum_{n=1}^N \left[\begin{pmatrix} R_{th_{1n}}^* \\ R_{th_{2n}}^* \\ R_{th_{3n}}^* \\ \vdots \\ R_{th_{Nn}}^* \end{pmatrix} - R_{th_{1n}}^* \right] \\ &= R_{E_1} + \Delta \mathbf{R}_{E_{ideal}}. \end{aligned} \quad (4.23)$$

4.3 N-Finger Transistors: The General Case

Here, $R_{th_{mn}}^*$ is the effective thermal resistance defined as $R_{th_{mn}}^* = \phi V_C R_{th_{mn}}$, $\mathbf{R}_{E_{ideal}}$ is the ideal emitter ballasting resistance distribution vector and $\Delta \mathbf{R}_{E_{ideal}}$ is the emitter resistance difference vector. After taking the derivative of (4.21) and (4.22) with respect to V_{BE} and utilizing the relation of the ideal emitter resistance distribution (4.23), the bend-over current can be obtained by requiring $dI/dV_{BE} = \infty$ as

$$I_{bend} = \frac{kT_A/q}{\sum_{n=1}^N R_{th_{1n}}^* - R_{E1}}. \quad (4.24)$$

It can be found that the no bend-over condition, $I_{bend} = \infty$, is satisfied by using an emitter resistance to just cancel the total effective thermal resistance. This requirement is an over design of the thermal stability. As we will see, a smaller emitter resistance is sufficient to stabilize the device.

Similar to the three-finger case equation (4.10), by differentiating (4.21) and (4.22) with respect to V_{BE} and combining these two sets of derivative equations, the eigenvalue equation for the N-finger case is

$$\det [\mathbf{R}_{th}^* - \text{diag}(\mathbf{R}_{E_{ideal}}) - \lambda \mathbf{I}] = 0 \quad (4.25)$$

where λ has the same meaning as that defined in (4.9), \mathbf{I} is the identity matrix, \mathbf{R}_{th}^* is the effective thermal resistance defined as $\mathbf{R}_{th}^* = \phi V_C \mathbf{R}_{th}$, and $\det(\mathbf{A})$ is the determinant of matrix \mathbf{A} . From (4.25), we can obtain N solutions for λ . One is the bend-over solution and the other $N - 1$ solutions are the unstable points. Because only the real positive solutions have physical meanings, the number of the unstable points is less than or equal to $N - 1$. Using a five-identical-finger transistor as an example and assuming the same chip dimension, finger size and finger spacing as before, we can see that the $I_C - V_{BE}$ curves and the temperature distribution curves shown in Fig. 4.7(a) and (b) have four unstable points as marked by P1 to P4 under the ideal emitter ballasting resistance distribution $R_{E_{2/3/4}} = R_{E_{ideal}} = 3.37/3.45/3.37 \Omega$ and $R_{E_{15}} = 3 \Omega$ despite

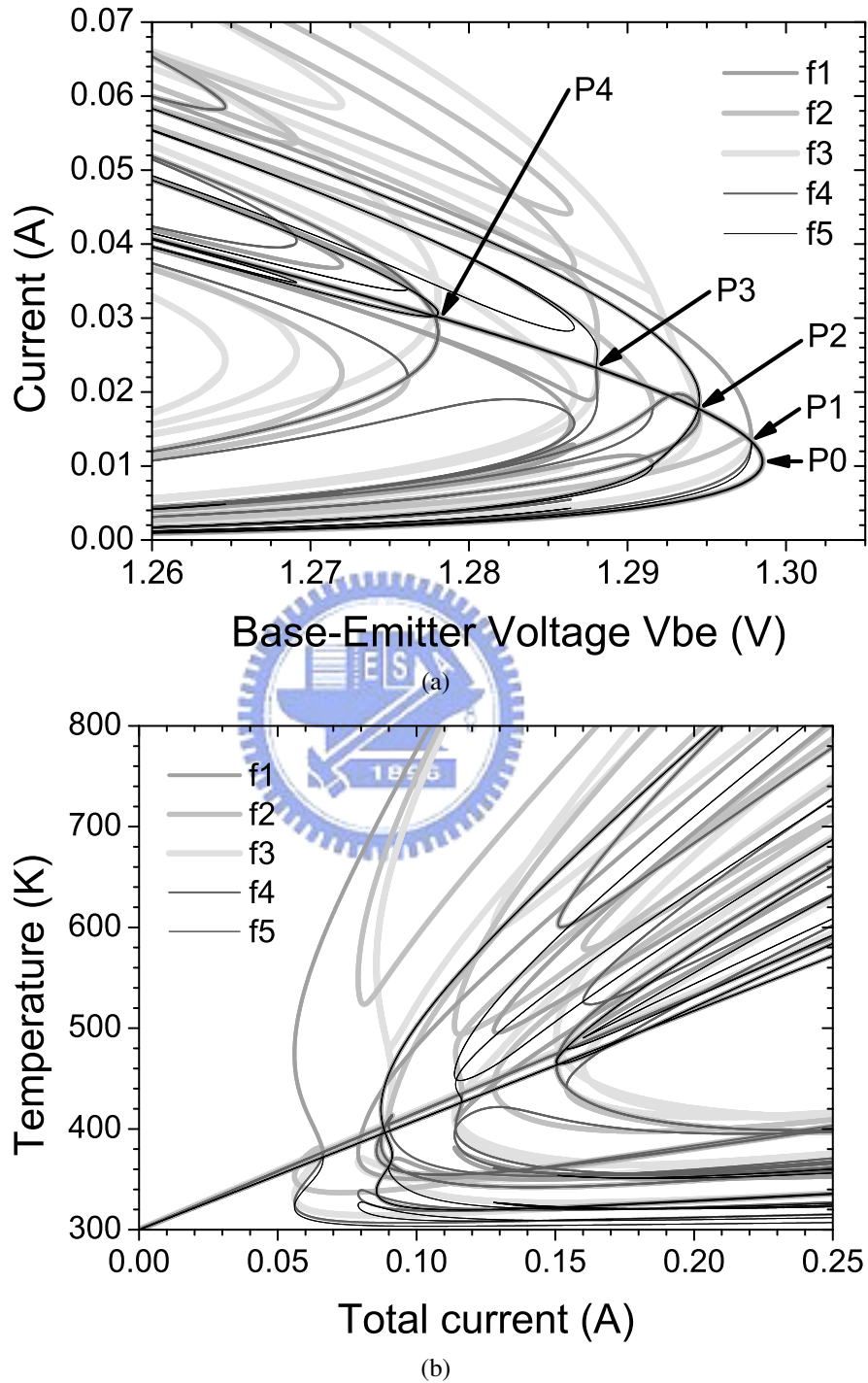


Fig. 4.7. The simulation results of a 5f 3x40 s40 HBT with $R_{E_{15}} = 3 \Omega$ and $R_{E_{2/3/4}} = R_{E_{ideal}} = 3.37/3.45/3.37 \Omega$. (a) $I_C - V_{BE}$ curves and (b) the finger temperature as a function of the total current. P1-P4 mark the four unstable points. f3 is the center finger, f1 and f5 are the outer fingers, and f2 and f4 are the side fingers beside the center finger.

of the complex structure of the solutions. It is consistent with the theoretical prediction that there are $5 - 1 = 4$ unstable points. The corresponding eigen-currents are marked from P0 to P4 in the figure as $I_{C_{\lambda_1}} = 10.6$ mA, $I_{C_{\lambda_2}} = 13.3$ mA, $I_{C_{\lambda_3}} = 17.7$ mA, $I_{C_{\lambda_4}} = 23.3$ mA, and $I_{C_{\lambda_5}} = 30.3$ mA.

If we substitute (4.23) into (4.25) and express the resultant equation by the emitter resistance difference vector $\Delta \mathbf{R}_{E_{ideal}}$, then by requiring $\lambda = 0$, equivalent to $I \rightarrow \infty$, as the unstable points go to infinity, (4.25) becomes

$$\det [\mathbf{R}_{th}^* - \text{diag}(\Delta \mathbf{R}_{E_{ideal}}) - R_{E_1} \mathbf{I}] = 0. \quad (4.26)$$

This is the equation of the absolutely stable condition. The value of the optimum emitter ballasting resistance can be obtained by solving the eigenvalue equation of (4.26). There are N solutions of R_{E_1} . The largest real positive solution corresponds to the no-bend-over condition, $R_{E_{1,no-bend}}$, and the second largest one, $R_{E_{1,opt}}$, is the absolutely stable condition, at which the first unstable point goes to infinity. For the five-finger case as shown in Fig. 4.7(a) and (b), the no-bend-over requirement is $R_{E_{1,no-bend}} = 5.43 \Omega$ and the absolutely stable requirement is $R_{E_{1,opt}} = 4.95 \Omega$. From now on, we have established a design procedure to determine the ideal values of the emitter ballasting resistance for N-finger transistors. The procedure is summarized as follows:

- 1) Once the thermal resistance matrix \mathbf{R}_{th} in (4.20) is determined by measurement using test structures or by a three-dimensional simulation, the ideal emitter ballasting resistance distribution can be obtained by (4.23). Only when this distribution is satisfied, the currents of all fingers will be exactly identical.
- 2) Then, by solving the eigenvalue equation of (4.26), the optimum value of the emitter ballasting resistance $R_{E_{1,opt}}$ for absolutely stable condition is determined by choosing the second largest real positive solution. This value is the smallest resistance needed for the absolute stable operation. There is no need for the transistor to have a higher R_{E_1} . The over design will degrade the device performance.

However, if R_{E1} is insufficient, the first unstable point will not go to infinity, unstable operation may occur.

4.4 The Effect of Finger Separation

The finger separation used in the previous example, a large value of $40 \mu\text{m}$, is specially chosen to demonstrate all of the unstable points inside a readable simulation range. But this large separation is not commonly used in real device. A reasonable value of finger separation is about $15 \mu\text{m}$ which includes, for example, $3 \mu\text{m}$ contact width for one emitter and one collector, $1.5 \mu\text{m}$ base contact width for two bases, $1 \mu\text{m}$ emitter ledge width for two sides of the emitter, and $2 \mu\text{m}$ base-collector contact spacing of two sides of the base pedestal. The corresponds coupling thermal resistances are $R_{th1} = 800 \text{ }^\circ\text{C/W}$, $R_{th2} = 185.8 \text{ }^\circ\text{C/W}$, $R_{th3} = 94.4 \text{ }^\circ\text{C/W}$, $R_{th4} = 57.3 \text{ }^\circ\text{C/W}$, and $R_{th5} = 38.0 \text{ }^\circ\text{C/W}$ computed by the effective thermal conductivity $k_{th,eff} = 0.4124 \text{ W/cm-}^\circ\text{C}$ as discussed in Section 4.1. Other parameters use the same value as the previous sections.

We firstly use these parameters to simulate the case of $R_E = 3 \Omega$ as shown in Fig. 4.8(a) and (b). It can be found that the highest current of the side fingers is about 15.0 mA which is higher than the $40 \mu\text{m}$ separation case. It means that the thermal stability is better as the finger separation becomes smaller. The temperature distribution curves can also reveal this feature. The temperature of the center finger for the $15 \mu\text{m}$ separation case is only higher before unstable point. After unstable point, the temperature increases slower than the $40 \mu\text{m}$ separation case that results in a more uniform temperature distribution. This thermal stability enhancement feature is more obvious in the next example.

In Fig. 4.8(a) and (b), we use the ideal emitter ballasting resistance $R_{E2,ideal} = 3.55 \Omega$ or $\Delta R_{E2,ideal} = 0.55 \Omega$ to calculate the $I_C - V_{BE}$ curves. The eigen-currents are $I_{C\lambda1} = 7.4 \text{ mA}$, $I_{C\lambda2} = 21.0 \text{ mA}$, and $I_{C\lambda3} = 188.3 \text{ mA}$. It can be found that the first unstable

4.4 The Effect of Finger Separation

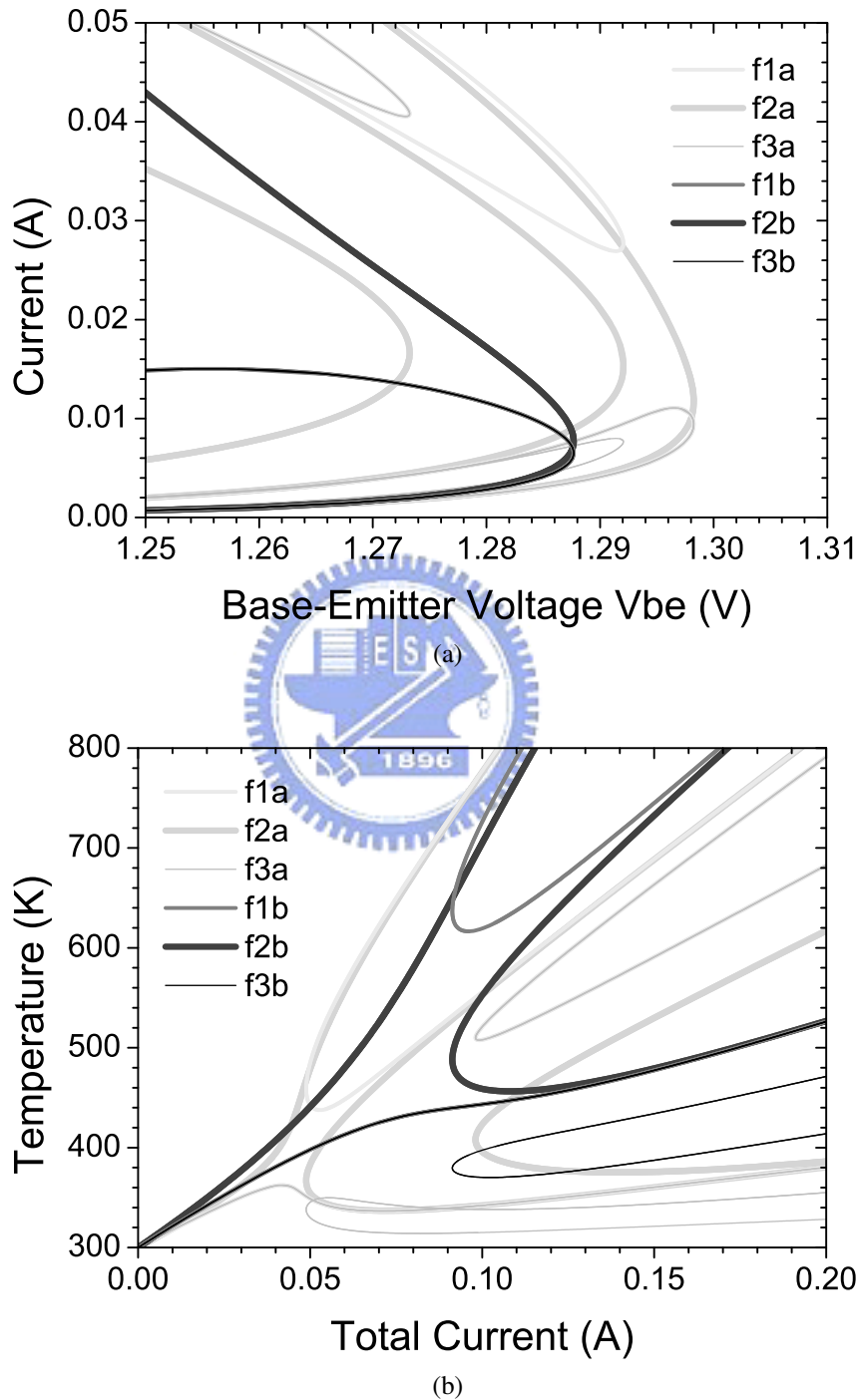


Fig. 4.8. The simulation results of a 3f 3x40 s15 HBT with $R_{E13} = R_{E2} = 3 \Omega$ compared with the results of the 3f 3x40 s40 HBT in Fig. 4.1. (a) $I_C - V_{BE}$ curves and (b) the finger temperature as a function of the total current. f2 is the center finger. f1 and f3 are the side fingers. The letter a indicates the results of a 3f 3x40 s40 HBT. The letter b indicates the results of a 3f 3x40 s15 HBT.

4.4 The Effect of Finger Separation

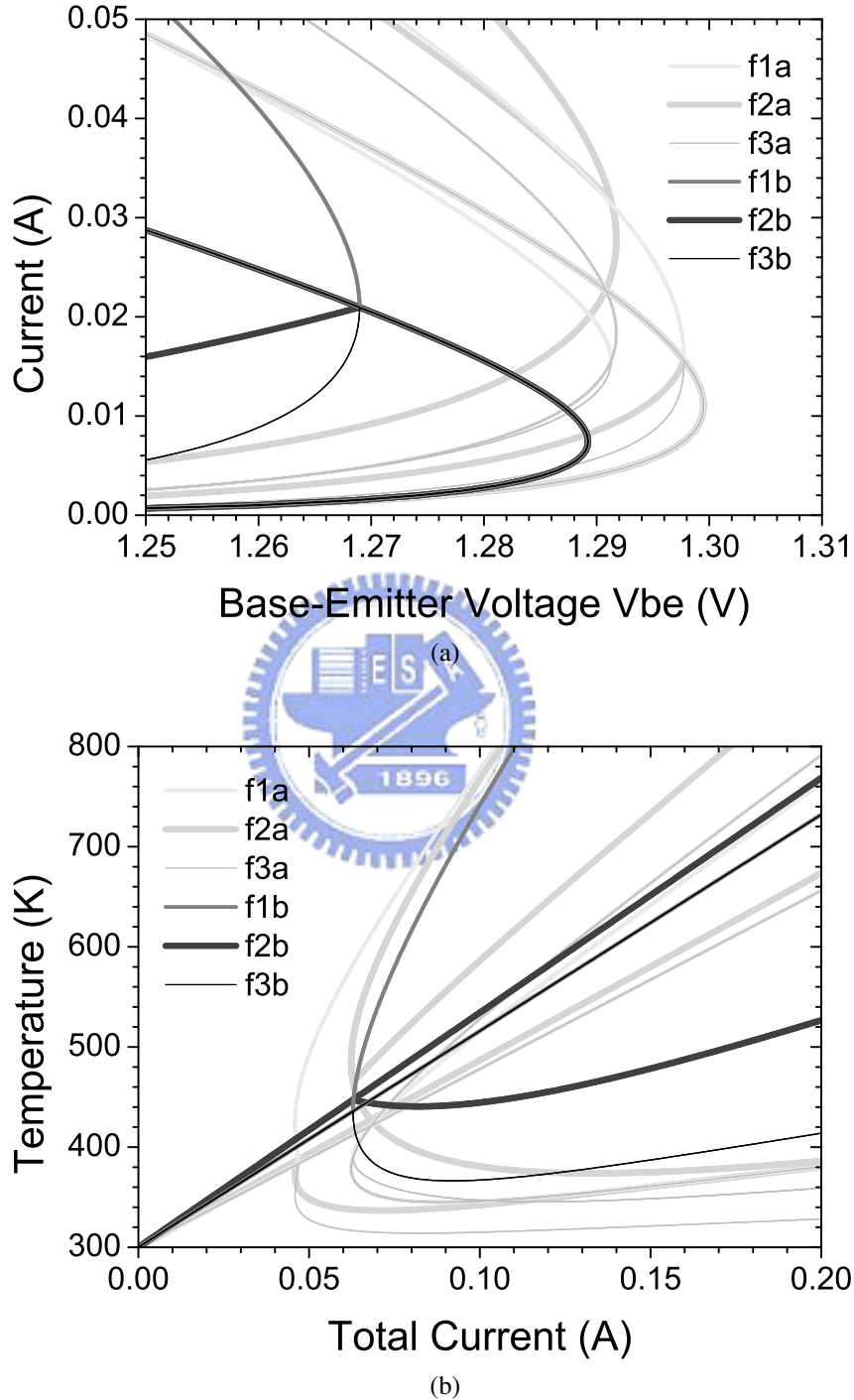


Fig. 4.9. The simulation results of a 3f 3x40 s15 HBT with $R_{E_{13}} = 3 \Omega$ and $R_{E_2} = R_{E_{2,ideal}} = 3.55 \Omega$ compared with the results of the 3f 3x40 s40 HBT in Fig. 4.2. (a) $I_C - V_{BE}$ curves and (b) the finger temperature as a function of the total current. P0 marks the bend-over point, P1 marks the first unstable point, and P2 marks the second unstable point. f2 is the center finger. f1 and f3 are the side fingers. The letter a indicates the results of a 3f 3x40 s40 HBT. The letter b indicates the results of a 3f 3x40 s15 HBT.

4.4 The Effect of Finger Separation

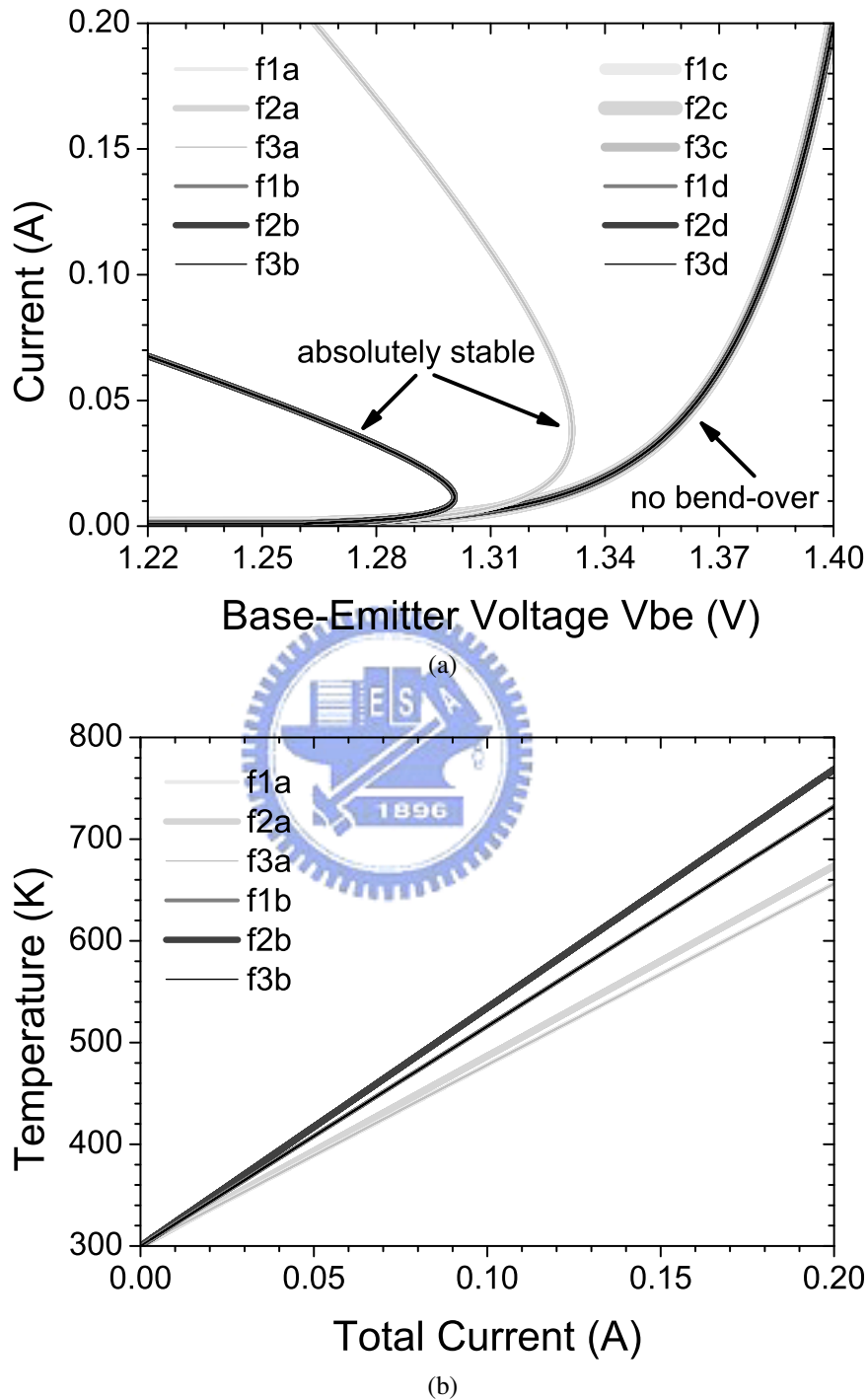


Fig. 4.10. The simulation results of a 3f 3x40 s15 HBT with the absolutely stable condition, $R_{E_{13}} = R_{E_{13,opt}} = 4.23 \Omega$ and $R_{E_2} = R_{E_2,ideal} = 4.78 \Omega$, and with the no bend-over condition, $R_{E_{13}} = R_{E_{13,no-bend}} = 6.48 \Omega$ and $R_{E_2} = R_{E_2,ideal} = 7.03 \Omega$ compared with the results of Fig. 4.5. (a) I_C-V_{BE} curves and (b) the finger temperature as a function of the total current. The temperature curves of these two conditions are identical. f2 is the center finger. f1 and f3 are the side fingers. The letter a and c indicates the results of a 3f 3x40 s40 HBT. The letter b and d indicate the results of a 3f 3x40 s15 HBT.

4.4 The Effect of Finger Separation

point is higher than the 40 μm separation case although the bend-over point is lower. The reason can be explained by (4.11) and (4.12). Since the bend-over current level is inverse proportional to the summation of all effective thermal resistance, smaller finger separation implies larger coupling thermal resistance and results in larger summation of the effective thermal resistance and smaller bend-over current. But the unstable point is determined by the inverse of the difference of R_{th1}^* and R_{th3}^* . Larger coupling thermal resistance will result in smaller difference and larger unstable current level. Shrinking finger separation actually improves the thermal stability. The small penalty we must pay is the higher finger temperature resulted from the higher total thermal resistance.

Fig. 4.10(a) and (b) show the absolutely stable condition, $R_{E13,opt} = 4.23 \Omega$ and $R_{E2,ideal} = 4.78 \Omega$, and the no-bend-over condition, $R_{E13,no-bend} = 6.48 \Omega$ and $R_{E2,ideal} = 7.03 \Omega$. As one can expect, the value of the emitter ballasting resistance used in the 15 μm separation case for the absolutely stable condition is smaller than the 40 μm separation case as a result of better thermal stability. On the contrary, the no-bend-over condition uses larger resistance in the 15 μm separation case. Besides, for the absolutely stable condition, smaller separation will result in more serious bend-over I_C-V_{BE} curves with smaller base-emitter voltage at the bend-over point. It is a result of higher finger temperature, as shown in Fig. 4.10(b). The higher the finger temperature is, the more bending the curves will have. For the no-bend-over condition, the I_C-V_{BE} curves are overlapped in both 15 μm and 40 μm separation cases. The temperature curves for both the absolutely stable and no-bend-over conditions are also overlapped that is the same situation as Fig. 4.5.

Fig. 4.11 is the collection of the simulated total currents in Fig. 4.1 for $R_E = 3 \Omega$ and in Fig. 4.2 for $R_{E13}/R_{E2,ideal} = 3/3.26 \Omega$ conditions for the 40 μm separation case, and in Fig. 4.8 for $R_E = 3 \Omega$ and in Fig. 4.9 for $R_{E13}/R_{E2,ideal} = 3/3.55 \Omega$ conditions for the 15 μm separation case. It shows that smaller finger separation will result in smaller bend-over voltage and higher unstable current. Fig. 4.12(a) and (b) shows the I_C-V_{BE} curves and the temperature distribution curves for a five-finger device with $R_{E15} = 3 \Omega$

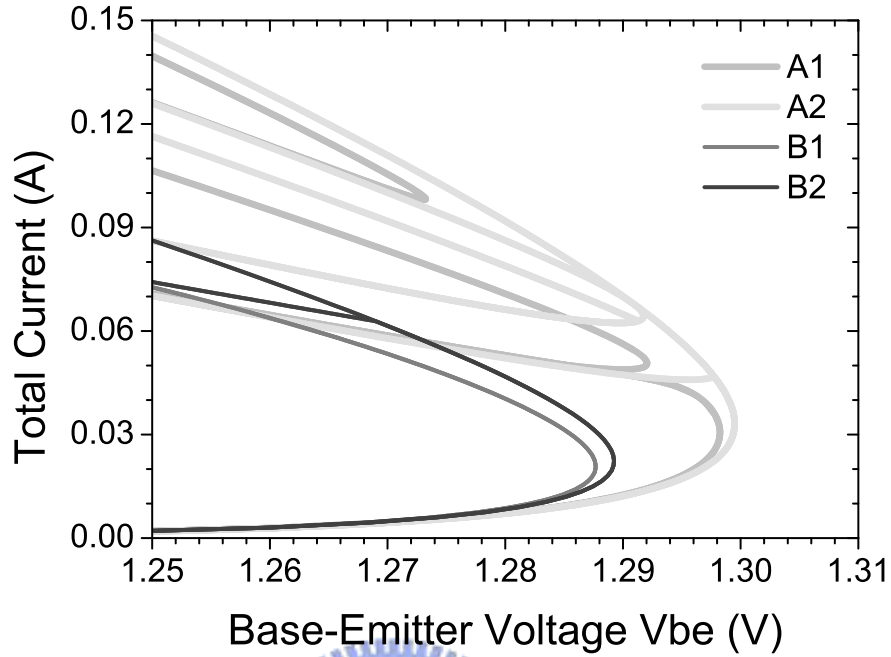


Fig. 4.11. The simulation results of the total current versus V_{BE} curves collected from Fig. 4.1-Fig. 4.2 for the 3f 3x40 s40 HBT and Fig. 4.8-Fig. 4.9 for the 3f 3x40 s15 HBT. A1 correspond to $R_E = 3 \Omega$ for a 3f 3x40 s40 HBT. A2 correspond to $R_{E13}/R_{E2,ideal} = 3/3.26 \Omega$ for a 3f 3x40 s40 HBT. B1 correspond to $R_E = 3 \Omega$ for a 3f 3x40 s15 HBT. B2 correspond to $R_{E13}/R_{E2,ideal} = 3/3.55 \Omega$ for a 3f 3x40 s15 HBT.

and $R_{E2/3/4} = R_{Eideal} = 3.37/3.45/3.37 \Omega$. In opposition to the complexity of Fig. 4.7, most unphysical solutions of the 15 μm separation case are lifted up outside of the real plane. The eigen-currents are $I_{C\lambda_1} = 6.4 \text{ mA}$, $I_{C\lambda_2} = 13.3 \text{ mA}$, $I_{C\lambda_3} = 35.7 \text{ mA}$, $I_{C\lambda_4} = -44.6 \text{ mA}$, and $I_{C\lambda_5} = -1.037 \text{ A}$. The negative eigen-currents mean that the corresponding unstable points do not exist physically. This device has only two unstable points, now, as shown in Fig. 4.12. The no-bend-over requirement is $R_{E1,no-bend} = 7.05 \Omega$ and the absolutely stable requirement is $R_{E1,opt} = 4.94 \Omega$. The same as the three-finger device, the thermal stability is also improved although the first unstable point does not change much.

4.4 The Effect of Finger Separation

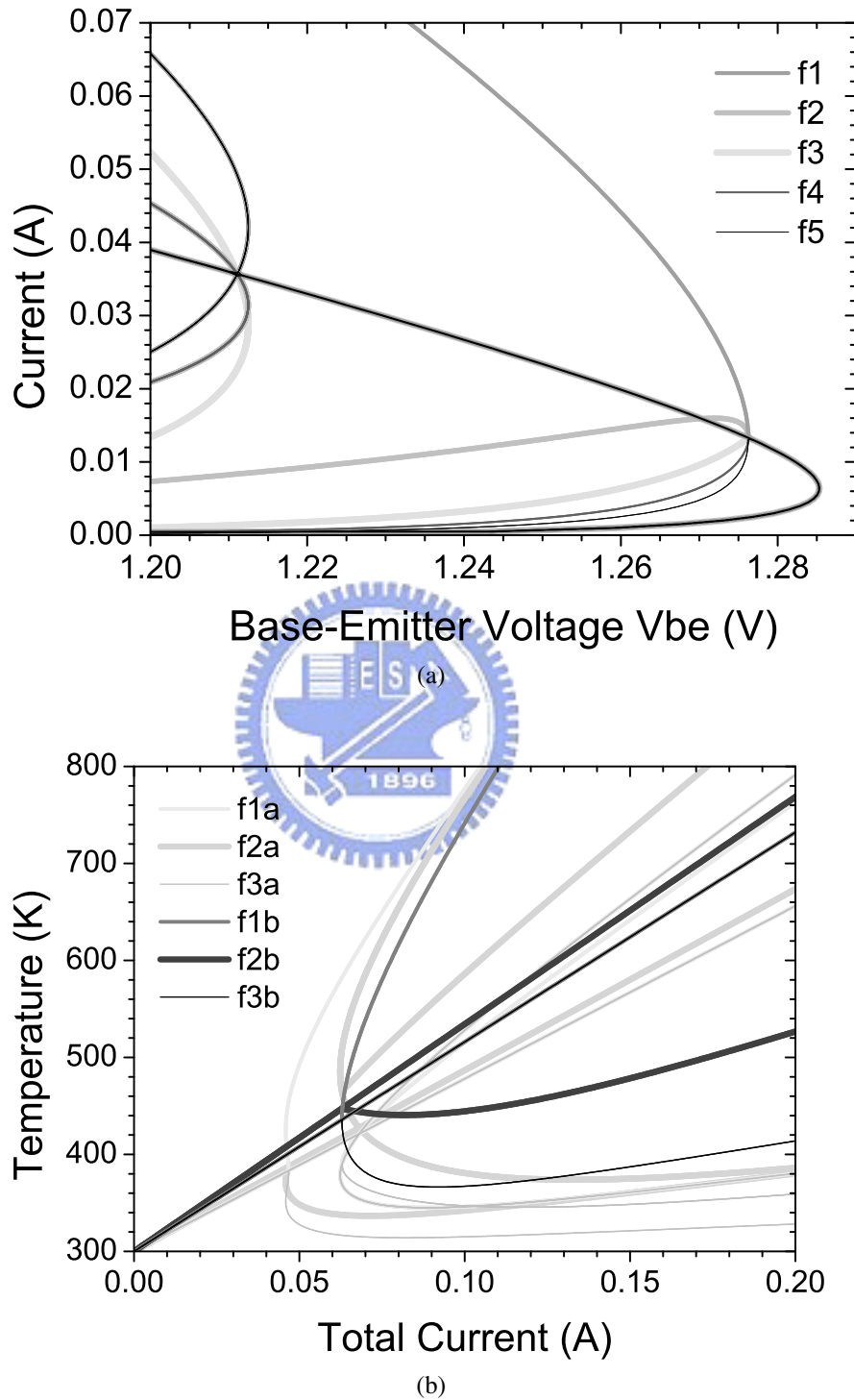
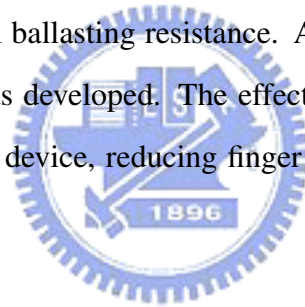


Fig. 4.12. The simulation results of a 5f 3x40 s15 HBT with $R_{E15} = 3 \Omega$ and $R_{E2/3/4} = R_{Eideal} = 3.37/3.45/3.37 \Omega$. (a) $I_C - V_{BE}$ curves and (b) the finger temperature as a function of the total current. P1-P4 mark the four unstable points. f3 is the center finger, f1 and f5 are the outer fingers, and f2 and f4 are the side fingers beside the center finger.


4.5 Summary

Multiple-finger transistors with nonuniform distribution of ballasting resistance have been analyzed by using the simple model. Analytical formulas for the best ballasting resistance distribution for optimum thermal stability operation were derived. Comparing with the conventional method of using uniform ballasting resistance, the new schemes with optimized design could result in a significant increase in the device current under stable operation. With the ideal ballasting resistance distribution, it is possible to achieve absolutely stable operation, where the device never becomes unstable, by using the optimum ballasting resistance. This optimum value could be obtained by solving an eigenvalue equation. The second largest real positive eigenvalue of this eigenvalue equation was the optimum ballasting resistance. A design procedure for the thermally stable optimum design was developed. The effect of the finger separation is also discussed. For a three-finger device, reducing finger separation will improve the thermal stability.



Chapter 5

Thermally Stable Optimum Design of Multifinger HBTs in Accurate Model



We had developed a design procedure to determine the values of the emitter ballasting resistance needed for thermal stable operation from a set of thermal-electrical feedback equations in simple model. The simple model gives us the basic concept of the thermally stable design by using the cancelation of positive and negative feedback. Based on this model, two ideas, the ideal ballasting resistance distribution and the absolutely stable condition, are derived and discussed. In this chapter, we extend our model to the accurate model and take the temperature dependence of thermal conductivity into account. A more physical model will give us a more practical result. By this manipulation, although the behavior of the I_C-V_{BE} curves are quit different from the simple model, the basic concept of the ideal ballasting resistance distribution and the absolutely stable condition are still similar and only need small modification. We could use the same derivation procedure to derive the ballasting resistance equations for the accurate model. Two practical design procedures based on uniform current and uniform temperature consideration were obtained and described [8]. The results with the temperature dependent and constant thermal conductivity were also compared.

In the calculation presented below, we use the same 3×40 InGaP/GaAs HBT on a

substrate with dimension $1000 \mu\text{m} \times 1000 \mu\text{m}$ and $100 \mu\text{m}$ thickness as mentioned in Chapter 4 to illustrate the design procedure. The parameters used in Chapter 4 combining with the parameters of the accurate model described in Chapter 3 and the temperature dependent thermal conductivity described in Chapter 2 will be used in this chapter. We relist these parameters here for convenience. They are $I_O = 6 \times 10^{-25} \text{ A}$, $E_{g0}^* = 1.483 \text{ eV}$, $\alpha^* = 4.88 \times 10^{-4} \text{ eV/K}$, $\gamma = 4.21$, $k_{th,eff} = 0.4124 \text{ W/cm-}^\circ\text{C}$, and $b = 1.25$, $V_C = 6 \text{ V}$. The calculated coupling thermal resistances are $R_{th1} = 800 \text{ }^\circ\text{C/W}$, $R_{th2} = 66.9 \text{ }^\circ\text{C/W}$, and $R_{th3} = 23.5 \text{ }^\circ\text{C/W}$ for the $40 \mu\text{m}$ finger separation device, and $R_{th1} = 800 \text{ }^\circ\text{C/W}$, $R_{th2} = 185.8 \text{ }^\circ\text{C/W}$, and $R_{th3} = 94.4 \text{ }^\circ\text{C/W}$ for the $15 \mu\text{m}$ finger separation device.

5.1 The Accurate Model

The difference between the simple model and the accurate model is that we use the general SPICE model current equation (3.9) instead of the linearized model current equation (3.15). The accurate coupled thermal-electrical feedback equation (3.36) had been discussed in Section 3.2. Using a three-identical-finger transistor as an example, the accurate coupled current-voltage equations with self-heating are

$$\begin{aligned} V_{BE} &= E_{g0}^* - \phi_1^* T_1 + R_{E13} I_{C1} \\ V_{BE} &= E_{g0}^* - \phi_2^* T_2 + R_{E2} I_{C2} \\ V_{BE} &= E_{g0}^* - \phi_3^* T_3 + R_{E13} I_{C3} \end{aligned} \quad (5.1)$$

where

$$\begin{aligned} \phi_1^* &= \phi_1 - \frac{k}{q} \gamma = -\frac{k}{q} \left(\ln \frac{I_{C1}}{I_{S0}} - \gamma \ln \frac{T_1}{300} \right) + \alpha^* \\ \phi_2^* &= \phi_2 - \frac{k}{q} \gamma = -\frac{k}{q} \left(\ln \frac{I_{C2}}{I_{S0}} - \gamma \ln \frac{T_2}{300} \right) + \alpha^* \\ \phi_3^* &= \phi_3 - \frac{k}{q} \gamma = -\frac{k}{q} \left(\ln \frac{I_{C3}}{I_{S0}} - \gamma \ln \frac{T_3}{300} \right) + \alpha^* \end{aligned} \quad (5.2)$$

and the parameters had been defined previously. The ideality factor is set to unity for simplicity as before. I_{S0} is obtained from (3.16) as

$$I_{S0} = I_O \left(\frac{T_A}{300} \right)^{-\gamma} \exp \left[\frac{q}{kT_A} (E_{g0}^* - \alpha^* T_A) \right]. \quad (5.3)$$

For our device with $I_O = 6 \times 10^{-25}$ A, $I_{S0} = 0.494$ A. From (5.1), a relation between R_{E13} and R_{E2} can be obtained as

$$\begin{aligned} R_{E2} &= \frac{I_{C1}}{I_{C2}} R_{E13} + \frac{\phi_2^* T_2 - \phi_1^* T_1}{I_{C2}} \\ &= \frac{I_{C1}}{I_{C2}} (R_{E13} + \Delta R_{E2}^*) \end{aligned} \quad (5.4)$$

where ΔR_{E2}^* is the effective emitter resistance distribution difference and the real emitter resistance distribution difference ΔR_{E2} defines as

$$\Delta R_{E2} = R_{E2} - R_{E13}. \quad (5.5)$$

This distribution is no longer a constant but is a function of the current and the temperature of all fingers because that the thermal-electrical feedback coefficient is not a constant now. Therefore, the procedure we developed in Chapter 4 is not suitable for the accurate model. However, from (5.4), we found that there are two degrees of freedom to design our thermally stable transistors under some conditions. They are the uniform current design and the uniform temperature design that will be discussed in the following sections.

The effect of temperature dependent thermal conductivity will affect the thermal stability significantly. When the thermal conductivity is a function of temperature, the temperature of fingers will become a very nonlinear function of the dissipated power. This problem can be solved by using the Kirchoff transform through defining a linearized temperature $U(x, y, z)$ as had mentioned in Section 2.2.1. The solutions of $U(x, y, z)$

5.1 The Accurate Model

are linear functions of currents. For the three-finger case,

$$\begin{aligned}
 U_1 &= T_A + V_C(R_{th1}I_{C1} + R_{th2}I_{C2} + R_{th3}I_{C3}) \\
 U_2 &= T_A + V_C(R_{th2}I_{C1} + R_{th1}I_{C2} + R_{th2}I_{C3}) \\
 U_3 &= T_A + V_C(R_{th3}I_{C1} + R_{th2}I_{C2} + R_{th1}I_{C3}).
 \end{aligned} \tag{5.6}$$

Once the temperature dependence of the thermal conductivity is known, we can solve for the actual junction temperature $T(x, y, z)$ using (2.11) and (5.6). Here, we use the temperature dependence expression of (2.1) and parameter values of Table 2.1. By using this relation, the actual junction temperature $T(x, y, z)$ can be obtained as (3.28). For the three-finger case,

$$\begin{aligned}
 T_1 &= T_A \left[1 - \frac{b-1}{T_A} V_C(R_{th1}I_{C1} + R_{th2}I_{C2} + R_{th3}I_{C3}) \right]^{\frac{-1}{b-1}} \\
 T_2 &= T_A \left[1 - \frac{b-1}{T_A} V_C(R_{th2}I_{C1} + R_{th1}I_{C2} + R_{th2}I_{C3}) \right]^{\frac{-1}{b-1}} \\
 T_3 &= T_A \left[1 - \frac{b-1}{T_A} V_C(R_{th3}I_{C1} + R_{th2}I_{C2} + R_{th1}I_{C3}) \right]^{\frac{-1}{b-1}}.
 \end{aligned} \tag{5.7}$$

From now on, we have a very nonlinear relation between temperature and current. This relation will seriously affect the behavior of the thermal-electrical feedback equation, as we will see. Similar results of the constant thermal conductivity case can be obtained by simply setting $b = 0$ to the results of the temperature dependent thermal conductivity case. In this chapter, we will discuss both the constant thermal conductivity case and the temperature dependent thermal conductivity case.

It is interesting to point out that in the temperature dependent thermal conductivity case, the linearized temperature U has an upper limit. It is because that the junction temperature T increase faster than U and will go to infinity as U increases to a certain value. It happens when the second term in the bracket of (5.7) is equal to unity. And as a result, the currents of the fingers also have a theoretical upper limit and the hottest

5.1 The Accurate Model

finger, the center finger under normal operation, decides the limit. By setting all currents the same, i.e. $I_{C_1} = I_{C_2} = I_{C_3} = I_C$, the maximum current level $I_{C_{\max}}$ is

$$I_{C_{\max}} = \frac{T_A}{(b-1)V_C(R_{th_1} + 2R_{th_2})} \quad (5.8)$$

Substituting the parameters, we have $I_{C_{\max}} = 171$ mA for the 3f 3x40 s15 HBT and $I_{C_{\max}} = 214$ mA for the 3f 3x40 s40 HBT. For the N-finger case, the upper limit becomes

$$I_{C_{\max}} = \frac{T_A}{(b-1)V_C \left[\max_{i \in \{1,2,3,\dots,N\}} \left(\sum_{j=1}^N R_{th_{ij}} \right) \right]} \quad (5.9)$$

where $R_{th_{ij}}$ is the thermal resistance matrix element. Because of the existence of this upper limit, setting the current to infinity when deriving the absolutely stable condition in Section 4.2 is not valid. Even so, the basic idea of these equations is still correct. All the change we need to do, instead of setting the current to infinity, is setting the current to a specific current level as we will do in Section 5.2.

Following the similar steps in Section 4.2, we derive the eigenvalue equations of the ballasting resistance for the accurate model. Firstly, from (5.2), the derivatives of (5.2) with respect to V_{BE} are

$$\begin{aligned} \phi_1^{*'} &= -\frac{k}{q} \left(\frac{I'_{C_1}}{I_{C_1}} - \gamma \frac{T'_1}{T_1} \right) \\ \phi_2^{*'} &= -\frac{k}{q} \left(\frac{I'_{C_2}}{I_{C_2}} - \gamma \frac{T'_2}{T_2} \right) \\ \phi_3^{*'} &= -\frac{k}{q} \left(\frac{I'_{C_3}}{I_{C_3}} - \gamma \frac{T'_3}{T_3} \right). \end{aligned} \quad (5.10)$$

Then, the derivatives of (5.1) with respect to V_{BE} are obtained as

$$\begin{aligned} 1 &= -\phi_1 T'_1 + \left(\frac{k}{q} \frac{T_1}{I_{C_1}} + R_{E_{13}} \right) I'_{C_1} \\ 1 &= -\phi_2 T'_2 + \left(\frac{k}{q} \frac{T_2}{I_{C_2}} + R_{E_2} \right) I'_{C_2} \\ 1 &= -\phi_3 T'_3 + \left(\frac{k}{q} \frac{T_3}{I_{C_3}} + R_{E_{13}} \right) I'_{C_3}. \end{aligned} \quad (5.11)$$

5.1 The Accurate Model

where ϕ_i is defined in (3.21) and (3.23). We consider the temperature dependent thermal conductivity case here. The results of the constant thermal conductivity case can be easily obtained from the temperature dependent thermal conductivity case. Because of the temperature dependence of the thermal conductivity, the derivatives of the finger temperatures with respect to the base-emitter voltage become

$$\begin{aligned} T_1' &= V_C (R_{th1} I'_{C_1} + R_{th2} I'_{C_2} + R_{th3} I'_{C_3}) \left(\frac{T_1}{T_A} \right)^b \\ T_2' &= V_C (R_{th2} I'_{C_1} + R_{th1} I'_{C_2} + R_{th2} I'_{C_3}) \left(\frac{T_2}{T_A} \right)^b \\ T_3' &= V_C (R_{th3} I'_{C_1} + R_{th2} I'_{C_2} + R_{th1} I'_{C_3}) \left(\frac{T_3}{T_A} \right)^b. \end{aligned} \quad (5.12)$$

Combining (5.11) with (5.12) and using the relation of the emitter resistance (5.4) and the definition of the effective thermal resistance (4.4), $R_{thi}^* = \phi V_C R_{thi}$, the derivatives of the current-voltage equations with respect to V_{BE} (5.1) become

$$\begin{pmatrix} \Lambda_1 - R_{E13} & \theta_1 R_{th2}^* & \theta_1 R_{th3}^* \\ \theta_2 R_{th2}^* & \Lambda_2 - \frac{1}{r}(R_{E13} + \Delta R_{E2}^*) & \theta_2 R_{th2}^* \\ \theta_3 R_{th3}^* & \theta_3 R_{th2}^* & \Lambda_3 - R_{E13} \end{pmatrix} \begin{pmatrix} I'_{C_1} \\ I'_{C_2} \\ I'_{C_3} \end{pmatrix} = \begin{pmatrix} -1 \\ -1 \\ -1 \end{pmatrix} \quad (5.13)$$

where

$$\begin{aligned} \theta_1 &= \frac{\phi_1}{\phi} \left(\frac{T_1}{T_A} \right)^b & \lambda_1 &= \frac{kT_1}{q} \frac{1}{I_{C_1}} & \Lambda_1 &= \theta_1 R_{th1}^* - \lambda_1 \\ \theta_2 &= \frac{\phi_2}{\phi} \left(\frac{T_2}{T_A} \right)^b & \lambda_2 &= \frac{kT_2}{q} \frac{1}{I_{C_2}} & \Lambda_2 &= \theta_2 R_{th1}^* - \lambda_2 \\ \theta_3 &= \frac{\phi_3}{\phi} \left(\frac{T_3}{T_A} \right)^b & \lambda_3 &= \frac{kT_3}{q} \frac{1}{I_{C_3}} & \Lambda_3 &= \theta_3 R_{th1}^* - \lambda_3 \end{aligned}$$

and

$$r = \frac{I_{C_2}}{I_{C_1}}.$$

ϕ is an arbitrary constant that we choose to be equal to 1 mV/°C as before. We can multiply the second equation of (5.13) by r to eliminate the prefatory term of R_{E13} in

the equation. And then the resultant equation is

$$\begin{pmatrix} \Lambda_1 - R_{E13} & \theta_1 R_{th2}^* & \theta_1 R_{th3}^* \\ r\theta_2 R_{th2}^* & r\Lambda_2 - R_{E13} - \Delta R_{E2}^* & r\theta_2 R_{th2}^* \\ \theta_3 R_{th3}^* & \theta_3 R_{th2}^* & \Lambda_3 - R_{E13} \end{pmatrix} \begin{pmatrix} I'_{C1} \\ I'_{C2} \\ I'_{C3} \end{pmatrix} = \begin{pmatrix} -1 \\ -r \\ -1 \end{pmatrix}. \quad (5.14)$$

We found that the eigenvalue equation can be derived by the requirement of un-unique slopes of the $I_C - V_{BE}$ curves at the unstable points as

$$\begin{vmatrix} \theta_1 R_{th1}^* - \lambda_1 - R_{E13} & \theta_1 R_{th2}^* & \theta_1 R_{th3}^* \\ r\theta_2 R_{th2}^* & r\theta_2 R_{th1}^* - r\lambda_2 - R_{E13} - \Delta R_{E2}^* & r\theta_2 R_{th2}^* \\ \theta_3 R_{th3}^* & \theta_3 R_{th2}^* & \theta_3 R_{th1}^* - \lambda_3 - R_{E13} \end{vmatrix} = 0 \quad (5.15)$$

Once a specified current or a specified temperature is given, consequently the emitter ballasting resistance distribution $R_{E2} = R_{E13} + \Delta R_{E2}$ is known. Then, the value of R_{E13} needed for thermal stable operation in the specified current or temperature range can be calculated by (5.15). The eigenvalue equation (5.15) is a general equation that can be used to calculate the value of R_{E13} needed.

5.2 The Uniform Current Design

It is because that the ballasting resistance distribution (5.4) is a function of the current and the temperature of all fingers, unlike Chapter 4 the ideal ballasting resistance distribution and the absolutely stable optimum ballasting resistance do not exist. To search for the solutions of all finger currents identical is impossible. Of course, a larger ballasting resistance will result in a more stable device. But larger ballasting resistance will degrade the device performance, such as gain and cutoff frequency, seriously. A minimum value of ballasting resistance is more preferred. To compromise the device

stability and the device performance, we still want to know an optimum ballasting resistance to suffice our requirement. One way we can do is to imitate the procedure of Chapter 4 to solve the ballasting resistance needed for stable operation under a specific current level, $I_{C_{SI}}$, by setting $I_{C_1} = I_{C_2} = I_{C_3} = I_{C_{SI}}$. This modification is so-called the uniform current design since we assume that the currents of all fingers are identical. The reason we can do this is based on the assumption that although the finger currents will not be the same in the whole current range, we still can find an optimum value of ballasting resistance to make the current-voltage curves intercept at the specified current level and make sure that this specified current level is the first unstable point. Increasing the ballasting resistance can push up the current level of this first unstable point.. We will develop a procedure to find a combination of R_{E_2} and $R_{E_{13}}$ to guarantee the first unstable point is at the specified current level.

Once $I_{C_{SI}}$ is given, we can determine the junction temperature $T_{1_{SI}}$, $T_{2_{SI}}$, and $T_{3_{SI}}$ for each finger from (5.7) as

$$\begin{aligned}
 T_{1_{SI}} &= T_A \left[1 - \frac{b-1}{T_A} V_C (R_{th1} + R_{th2} + R_{th3}) I_{C_{SI}} \right]^{\frac{-1}{b-1}} \\
 T_{2_{SI}} &= T_A \left[1 - \frac{b-1}{T_A} V_C (R_{th2} + R_{th1} + R_{th2}) I_{C_{SI}} \right]^{\frac{-1}{b-1}} \\
 T_{3_{SI}} &= T_A \left[1 - \frac{b-1}{T_A} V_C (R_{th3} + R_{th2} + R_{th1}) I_{C_{SI}} \right]^{\frac{-1}{b-1}}
 \end{aligned} \tag{5.16}$$

and $\phi_{1_{SI}}$, $\phi_{2_{SI}}$, and $\phi_{3_{SI}}$ are obtained by substituting $I_{C_{SI}}$ and (5.16) into (5.2) as

$$\begin{aligned}
 \phi_{1_{SI}} &= -\frac{k}{q} \left(\ln \frac{I_{C_{SI}}}{I_{S0}} - \gamma \ln \frac{T_{1_{SI}}}{300} - \gamma \right) + \alpha^* \\
 \phi_{2_{SI}} &= -\frac{k}{q} \left(\ln \frac{I_{C_{SI}}}{I_{S0}} - \gamma \ln \frac{T_{2_{SI}}}{300} - \gamma \right) + \alpha^* \\
 \phi_{3_{SI}} &= -\frac{k}{q} \left(\ln \frac{I_{C_{SI}}}{I_{S0}} - \gamma \ln \frac{T_{3_{SI}}}{300} - \gamma \right) + \alpha^*.
 \end{aligned} \tag{5.17}$$

Fig. 5.1 and Fig. 5.2 show the curves of $T_{2_{SI}}$ and $\phi_{2_{SI}}$ for our devices. A reasonable $I_{C_{SI}}$ is determined by the highest junction temperature that is $T_{2_{SI}}$ in the three finger case.

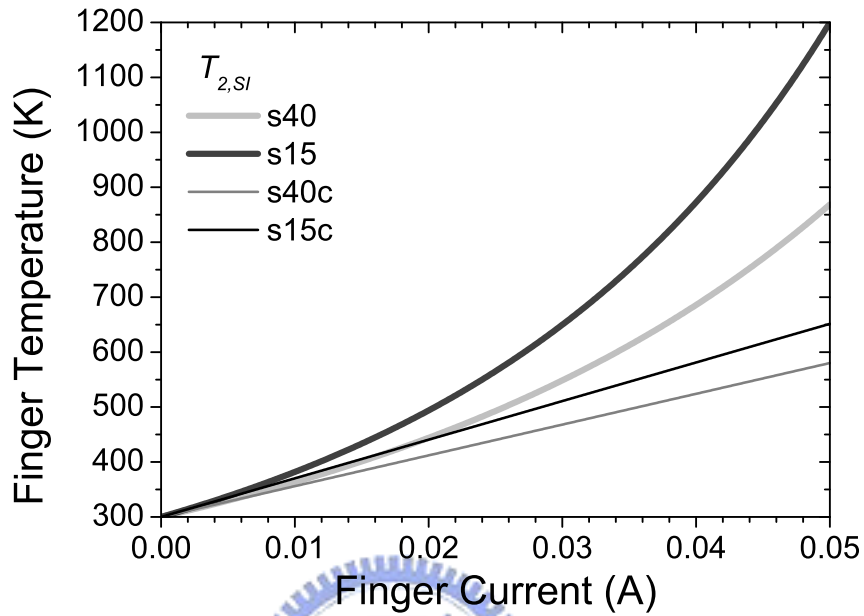


Fig. 5.1. The simulation result of $T_{2,SI}$ as a function of $I_{C_{SI}}$ for a 3f 3x40 s40 and a 3f 3x40 s15 HBT with temperature dependent and constant thermal conductivity. s40 means the 3f 3x40 s40 device. s15 means the 3f 3x40 s15 device. The letter c indicates the results with constant thermal conductivity.

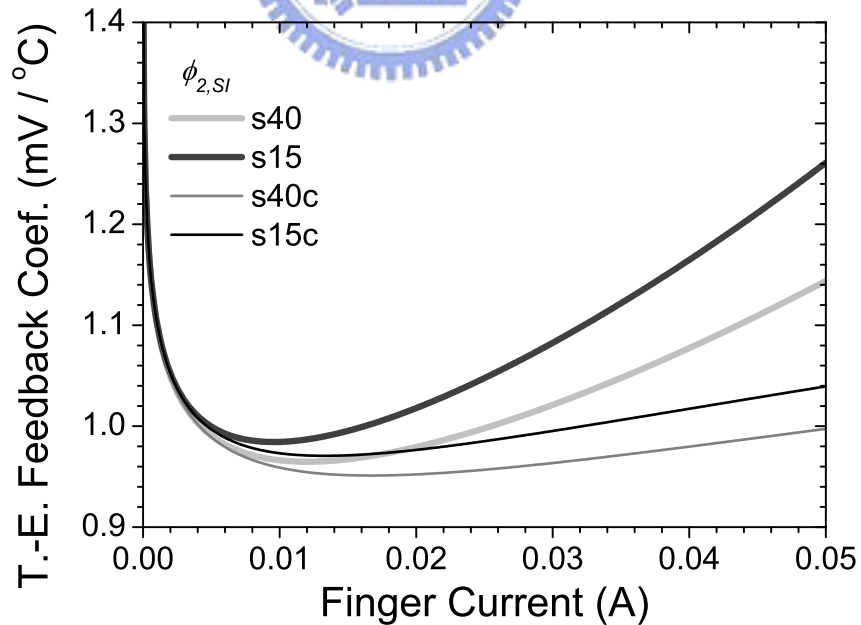


Fig. 5.2. The simulation result of $\phi_{2,SI}$ as a function of $I_{C_{SI}}$ for a 3f 3x40 s40 and a 3f 3x40 s15 HBT with temperature dependent and constant thermal conductivity. s40 means the 3f 3x40 s40 device. s15 means the 3f 3x40 s15 device. The letter c indicates the results with constant thermal conductivity.

We can see that the current level cannot exceed 20.5 mA for the 3f 3x40 s15 HBT and 25.7 mA for the 3f 3x40 s40 HBT with temperature dependent thermal conductivity and 28.5 mA for the 3f 3x40 s15 HBT and 35.7 mA for the 3f 3x40 s40 HBT with constant thermal conductivity if the junction temperatures need to be kept below 500 K. The temperature curves of the temperature dependent thermal conductivity case increase much faster than the linear curves of the constant thermal conductivity case. And smaller finger separation will result in both higher temperature and thermal-electrical feedback coefficient despite the thermal conductivity model. The thermal-electrical feedback coefficient of the constant thermal conductivity case for the current level larger than 2 mA is quit constant and close to 1 mV/°C as we used in Chapter 4.

The emitter ballasting resistance distribution $R_{E_2,SI}$ and the distribution difference $\Delta R_{E_2,SI}$ for the specified current level can be determined from (5.4) as

$$\begin{aligned}
 R_{E_2,SI} &= R_{E_{13}} + \frac{\phi_{2SI}^* T_{2SI} - \phi_{1SI}^* T_{1SI}}{I_{C_{SI}}} \\
 &= R_{E_{13}} + \Delta R_{E_2,SI}
 \end{aligned} \tag{5.18}$$

This distribution is no longer a constant but is a function of the current of fingers. Fig. 5.3 shows the simulated results of $\Delta R_{E_2,SI}$ versus the current per finger. Despite the low current region, as the specified current increases we need a higher $\Delta R_{E_2,SI}$ to guarantee identical currents in all fingers for the temperature dependent thermal conductivity case. For the constant thermal conductivity case, the increase of $\Delta R_{E_2,SI}$ is not so apparent. It is quit constant in the current range larger than 2 mA. For the temperature dependent thermal conductivity case, the increase of $\Delta R_{E_2,SI}$ for the small finger separation case is faster than the large separation because of the nonlinear behavior of the finger temperature. Besides, since it is analogous to (4.3) that the difference between the coupling thermal resistance R_{th_2} and R_{th_3} becomes larger, smaller finger separation will result in larger $\Delta R_{E_2,SI}$.

After the finger temperatures $T_{1SI} - T_{3SI}$, the thermal-electrical feedback coefficients

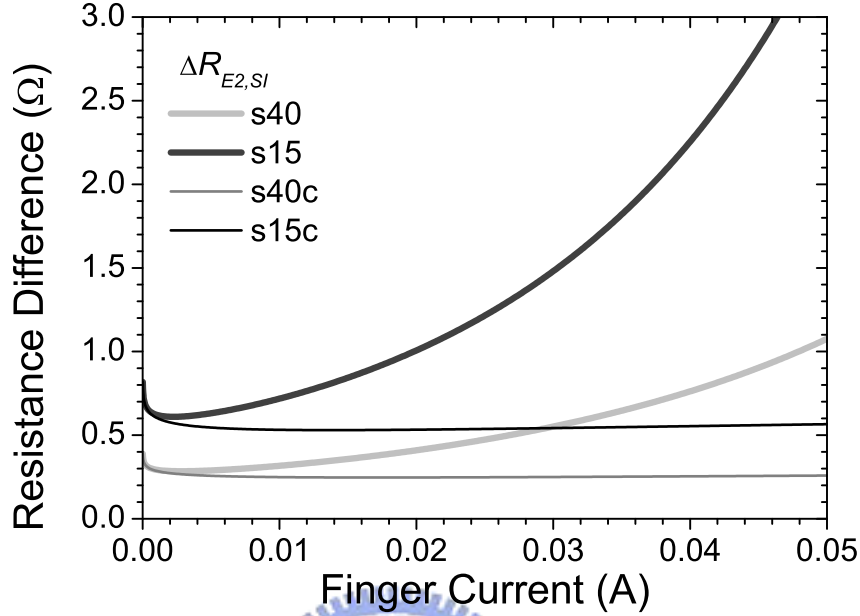


Fig. 5.3. The simulation result of $\Delta R_{E2,SI}$ as a function of $I_{C_{SI}}$ for a 3f 3x40 s40 and a 3f 3x40 s15 HBT with temperature dependent and constant thermal conductivity. s40 means the 3f 3x40 s40 device. s15 means the 3f 3x40 s15 device. The letter C indicates the results with constant thermal conductivity.

$\phi_{1_{SI}} - \phi_{3_{SI}}$, and the emitter ballasting resistance distribution $\Delta R_{E2,SI}$ under the specified current level are known, the eigenvalue equation for the uniform current design can be obtained by substituting (5.16)-(5.18) into (5.15) as

$$\begin{vmatrix} \theta_{1_{SI}} R_{th1}^* - \lambda_{1_{SI}} - R_{E13} & \theta_{1_{SI}} R_{th2}^* & \theta_{1_{SI}} R_{th3}^* \\ \theta_{2_{SI}} R_{th2}^* & \theta_{2_{SI}} R_{th1}^* - \lambda_{2_{SI}} - R_{E13} & \theta_{2_{SI}} R_{th2}^* \\ \theta_{3_{SI}} R_{th3}^* & \theta_{3_{SI}} R_{th2}^* & \theta_{3_{SI}} R_{th1}^* - \lambda_{3_{SI}} - R_{E13} \end{vmatrix} = 0 \quad (5.19)$$

where

$$\begin{aligned} \theta_{1_{SI}} &= \frac{\phi_{1_{SI}}}{\phi} \left(\frac{T_{1_{SI}}}{T_A} \right)^b & \lambda_{1_{SI}} &= \frac{kT_{1_{SI}}}{q} \frac{1}{I_{C_{SI}}} \\ \theta_{2_{SI}} &= \frac{\phi_{2_{SI}}}{\phi} \left(\frac{T_{2_{SI}}}{T_A} \right)^b & \lambda_{2_{SI}} &= \frac{kT_{2_{SI}}}{q} \frac{1}{I_{C_{SI}}} + \Delta R_{E2,SI} \\ \theta_{3_{SI}} &= \frac{\phi_{3_{SI}}}{\phi} \left(\frac{T_{3_{SI}}}{T_A} \right)^b & \lambda_{3_{SI}} &= \frac{kT_{3_{SI}}}{q} \frac{1}{I_{C_{SI}}}. \end{aligned}$$

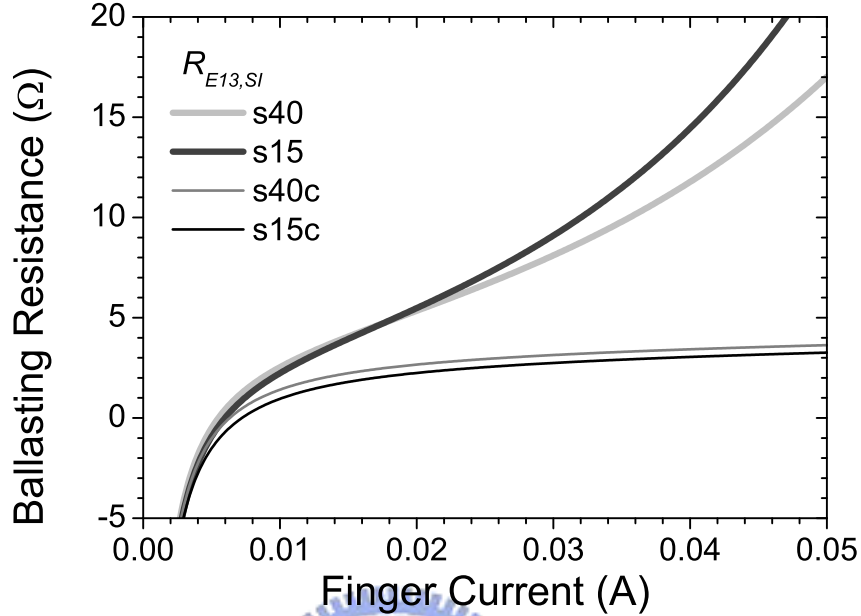


Fig. 5.4. The simulation result of $R_{E_{13,SI}}$ as a function of $I_{C_{SI}}$ for a 3f 3x40 s40 and a 3f 3x40 s15 HBT with temperature dependent and constant thermal conductivity. s40 means the 3f 3x40 s40 device. s15 means the 3f 3x40 s15 device. The letter c indicates the results with constant thermal conductivity.

There are three solutions for $R_{E_{13}}$ the same as the discussion of Section 4.2. The largest solution is the no-bend-over condition and the second is the solution for the uniform current design. The calculated second largest solution of $R_{E_{13}}$, namely $R_{E_{13,SI}}$, as a function of the specified finger current is shown in Fig. 5.4. We can find that $R_{E_{13,SI}}$ is negative if $I_{C_{SI}}$ is below 6.0 mA for the 3f 3x40 s15 HBT and 5.5 mA for the 3f 3x40 s40 HBT with temperature dependent thermal conductivity, and 7.2 mA for the 3f 3x40 s15 HBT and 6.3 mA for the 3f 3x40 s40 HBT with constant thermal conductivity. The negative $R_{E_{13,SI}}$ means that the transistor is unconditional stable below these specified current levels correspondingly. Similar to Fig. 5.3, $R_{E_{13,SI}}$ is quit constant in the current range larger than 10 mA for the constant thermal conductivity case. For the temperature dependent thermal conductivity case, $R_{E_{13,SI}}$ increases fast as the specified current increases and the increase is faster for the smaller finger separation case because of the temperature nonlinearity. But smaller finger separation will result in smaller $R_{E_{13,SI}}$ for

the constant thermal conductivity case and low current region of the temperature dependent thermal conductivity case. It can be explained by the analogous equation of the simple model (4.15) that the smaller $R_{E_{13,SI}}$ is due to the shrinkage of the difference between R_{th_1} and R_{th_3} as the finger separation decreasing. However, for the temperature dependent thermal conductivity case, as the current becomes large enough, $R_{E_{13,SI}}$ with smaller separation will surpass larger separation one due to the faster increase speed.

5.2.1 With Temperature Dependent Thermal Conductivity

We first use the same condition as Fig. 4.1 and Fig. 4.8 to set $R_E = 3 \Omega$ for all fingers. The simulated I_C-V_{BE} and finger temperature curves are shown in Fig. 5.5(a) and (b). Because of the nonlinearity of the coupled I_C-V_{BE} equations, there are many possible solutions existed mathematically in the I_C-V_{BE} plane. However, only four sets of them are physically reasonable. There are also only three sets of solutions shown in Fig. 5.5 including $I_{C_2} > I_{C_1} = I_{C_3}$, $I_{C_1} > I_{C_2} > I_{C_3}$, and $I_{C_1} = I_{C_3} > I_{C_2}$ similar to Fig. 4.1. The highest current of the side fingers when the device is powered up from zero bias, represented by the solution $I_{C_2} > I_{C_1} = I_{C_3}$, is about 8.3 mA. This value is lower than that shown in Fig. 4.8(a) for the same device. It is mainly due to the nonlinearity of the temperature function. The temperature dependent thermal conductivity will result in a more serious thermal unstable effect and lower unstable point current level.

If we set $I_{C_{SI}} = 24$ mA, which corresponds to the collector current density of 20 kA/cm², we can use (5.18) to determine $\Delta R_{E_{2,SI}} = 1.17 \Omega$. By keeping $R_{E_{13}} = 3 \Omega$ and $R_{E_2} = R_{E_{13}} + \Delta R_{E_{2,SI}} = 4.17 \Omega$, the I_C-V_{BE} and the finger temperature curves are shown in Fig. 5.6(a) and (b). We found that the currents of all fingers are not the same in the entire simulation range. It is very different from the simple model example shown in Fig. 4.2(a). The unstable point current level is at about 12 mA for the side fingers. It is lower than we expect because that $R_{E_{13}}$ is not optimized. Since $\Delta R_{E_{2,SI}}$ is computed from $I_{C_{SI}} = 24$ mA, R_{E_2} is too large for the unstable current 12 mA. And as a result, the current and temperature of the center finger are lower than the side fingers

and the temperature distribution of all fingers is more uniform.

And then, we increase $R_{E_{13}}$ to 5Ω and keep $\Delta R_{E_2} = \Delta R_{E_{2,SI}} = 1.17 \Omega$, i.e. $R_{E_2} = 6.17 \Omega$. The I_C-V_{BE} and the finger temperature curves are shown in Fig. 5.7(a) and (b) compared with the curves of Fig. 5.6. The unstable point current level is at about 19 mA for the side fingers, hither than the $R_{E_{13}} = 3 \Omega$ case. Although the current of the center finger is still lower than the side fingers, its temperature is higher, now. It means that the over-compensation of ΔR_{E_2} is improved since the difference between $R_{E_{13}}$ and $R_{E_{13,SI}}$ becomes smaller. From the fact that the unstable point current is increased by increasing $R_{E_{13}}$, we can expect that there is an optimal value of $R_{E_{13}}$ which can push up the unstable point to our specified current level as we had derived.

Now, we can obtain $R_{E_{13,SI}} = 6.79 \Omega$ by substituting $I_{C_{SI}} = 24$ mA into (5.19). The I_C-V_{BE} and the finger temperature curves are shown in Fig. 5.8(a) and (b) with $R_{E_{13,SI}} = 6.79 \Omega$ and $R_{E_{2,SI}} = 7.96 \Omega$. Before the unstable point is reached, the currents of all fingers are roughly equal but not exactly the same in contrast to Fig. 4.2(a). It is mainly because of the current and temperature dependent nature of (5.17) and (5.18). Therefore, the ballasting resistance difference of the center finger cannot cancel completely the excess thermal coupling resistance between the side fingers and the center finger in all current range. We can find that the unstable point, marked by an arrow in Fig. 5.8(a), is just at 24 mA for all fingers as we specified. At this current level, the highest finger temperature is near but below 550 K that is still in a reasonable range. When the unstable point is reached, there are two unstable modes. One is that the center finger starts to dominate most of the finger current. The other is that one of the side fingers dominates. It seems like the two unstable points shown in Fig. 4.2(a) by using the simple model merge together. In other words, every finger has the opportunity to become the hottest finger. This is quit different from the traditional brief that the center finger is always the hottest finger.

For comparison, Fig. 5.9(a) and (b) show the I_C-V_{BE} and finger temperature curves with $R_{E_{13,SI}} = 12.02 \Omega$ and $\Delta R_{E_{2,SI}} = 1.90 \Omega$ as $I_{C_{SI}} = 36$ mA, which corresponds

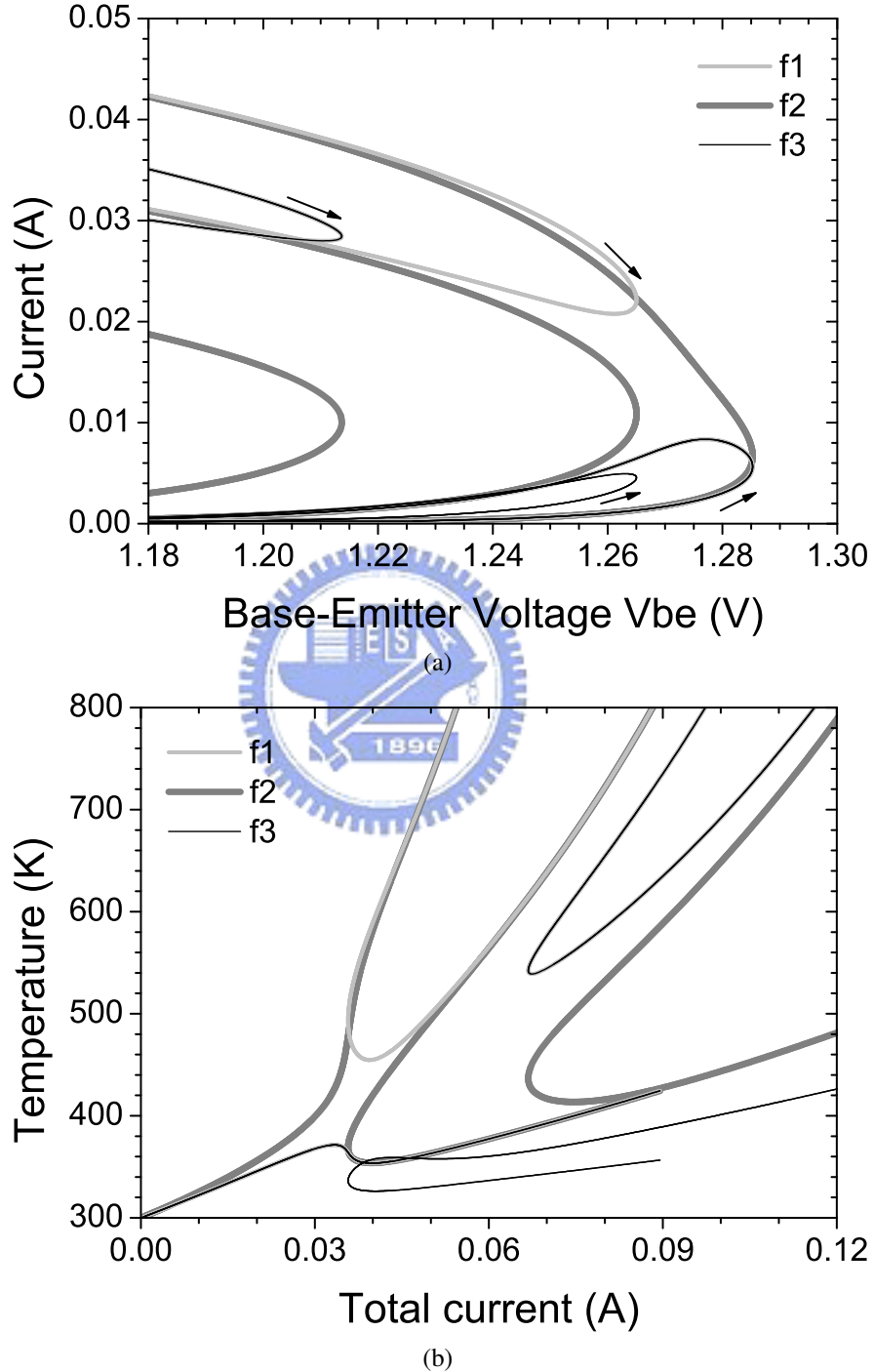


Fig. 5.5. The simulation results of a 3f 3x40 s15 HBT with $R_{E_{13}} = R_{E_2} = 3 \Omega$ in the accurate model with temperature dependent thermal conductivity. (a) $I_C - V_{BE}$ curves and (b) the finger temperature as a function of the total current. f2 is the center finger. f1 and f3 are the side fingers.

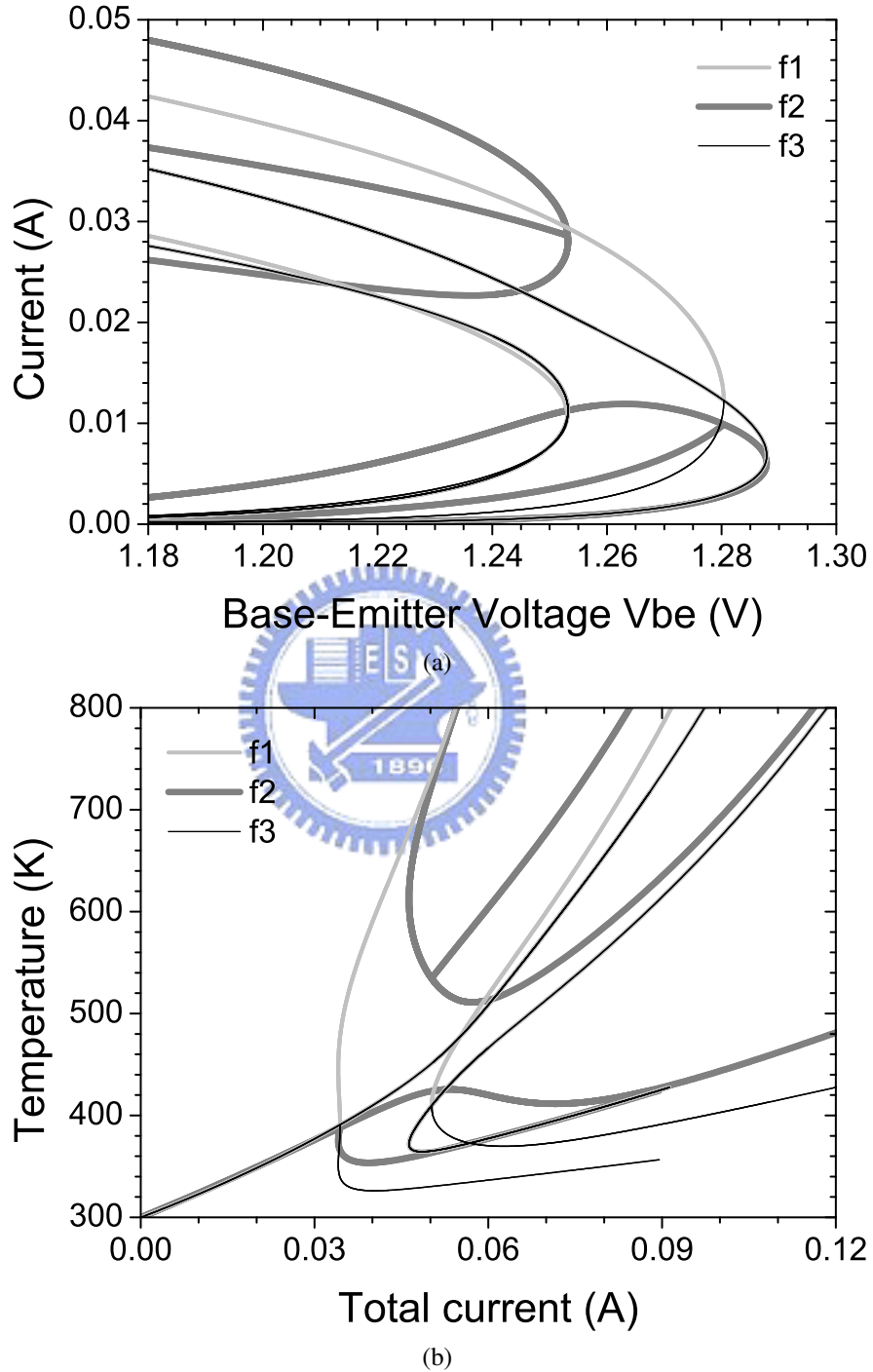


Fig. 5.6. The simulation results of a 3f 3x40 s15 HBT with $R_{E_{13}} = 3 \Omega$ and $R_{E_2} = R_{E_{13}} + \Delta R_{E_2,SI} = 4.17 \Omega$ as $I_{C_{SI}} = 24 \text{ mA}$ in the accurate model with temperature dependent thermal conductivity. (a) I_C - V_{BE} curves and (b) the finger temperature as a function of the total current. f2 is the center finger. f1 and f3 are the side fingers.

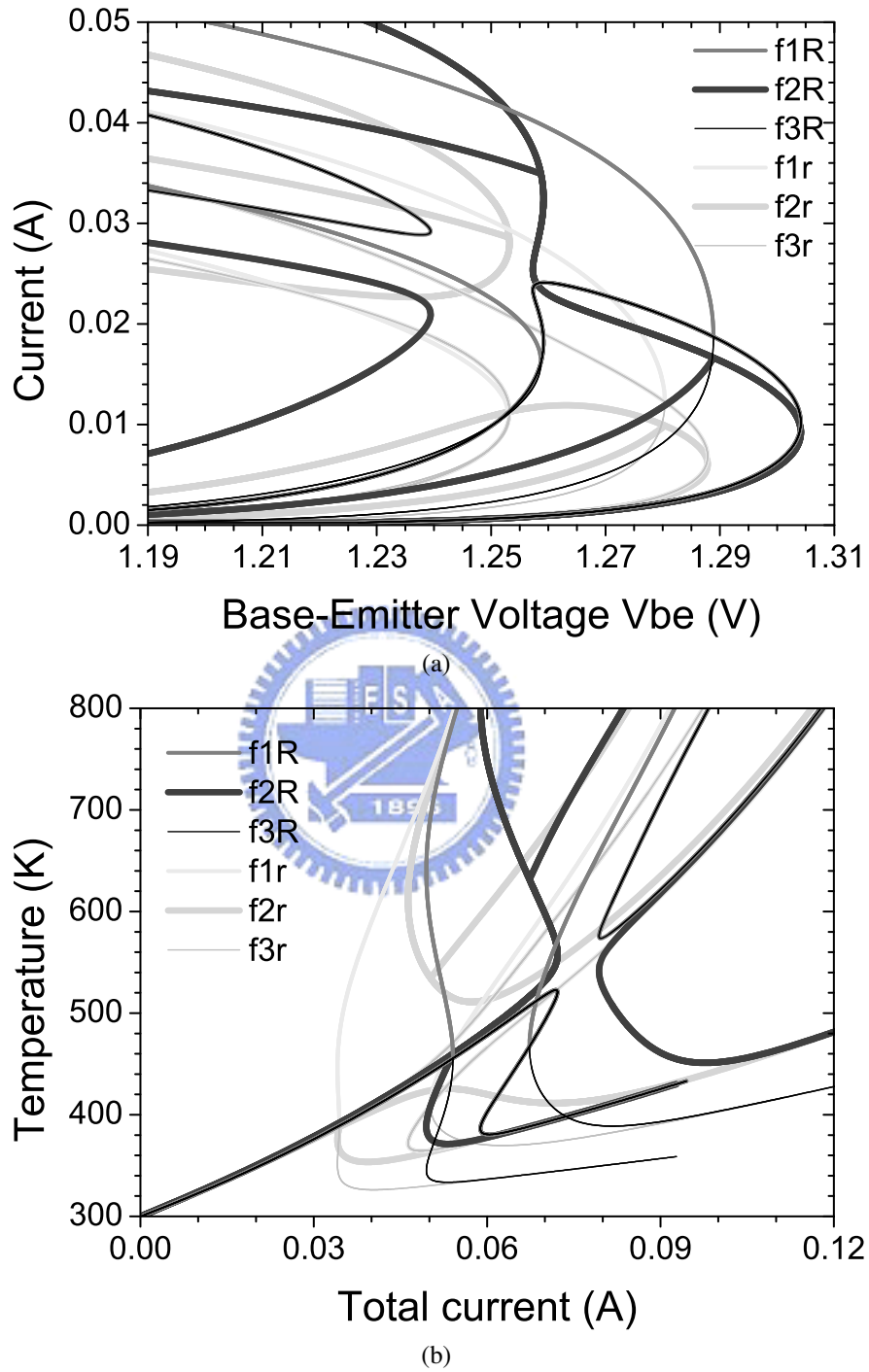


Fig. 5.7. The simulation results of a 3f 3x40 s15 HBT with $R_{E_{13}} = 5 \Omega$ and $R_{E_2} = R_{E_{13}} + \Delta R_{E_2,SI} = 6.17 \Omega$ as $I_{C_{SI}} = 24 \text{ mA}$ in the accurate model with temperature dependent thermal conductivity compared with the results of $R_{E_{13}} = 3 \Omega$ and $R_{E_2} = 4.17 \Omega$ in Fig. 5.6. (a) $I_C - V_{BE}$ curves and (b) the finger temperature as a function of the total current. f2 is the center finger. f1 and f3 are the side fingers. The letter R indicates the results of $R_{E_{13}} = 5 \Omega$ case. The letter r indicates the results of $R_{E_{13}} = 3 \Omega$ case.

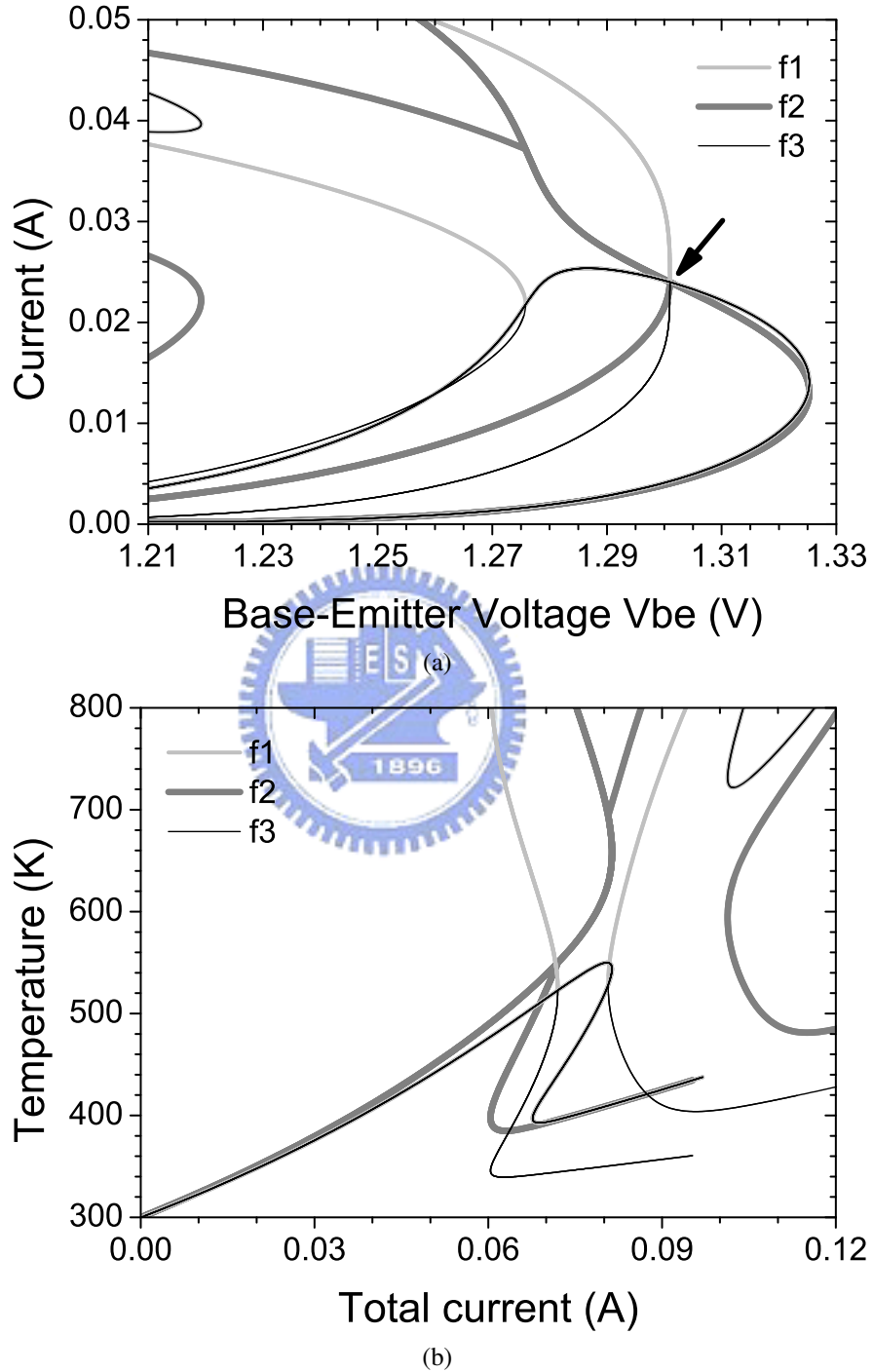


Fig. 5.8. The simulation results of a 3f 3x40 s15 HBT with $R_{E_{13}} = R_{E_{13,SI}} = 6.79 \Omega$ and $R_{E_2} = R_{E_{2,SI}} = 7.96 \Omega$ as $I_{C_{SI}} = 24 \text{ mA}$ in the accurate model with temperature dependent thermal conductivity. (a) $I_C - V_{BE}$ curves and (b) the finger temperature as a function of the total current. The arrow marks the unstable point. f2 is the center finger. f1 and f3 are the side fingers.

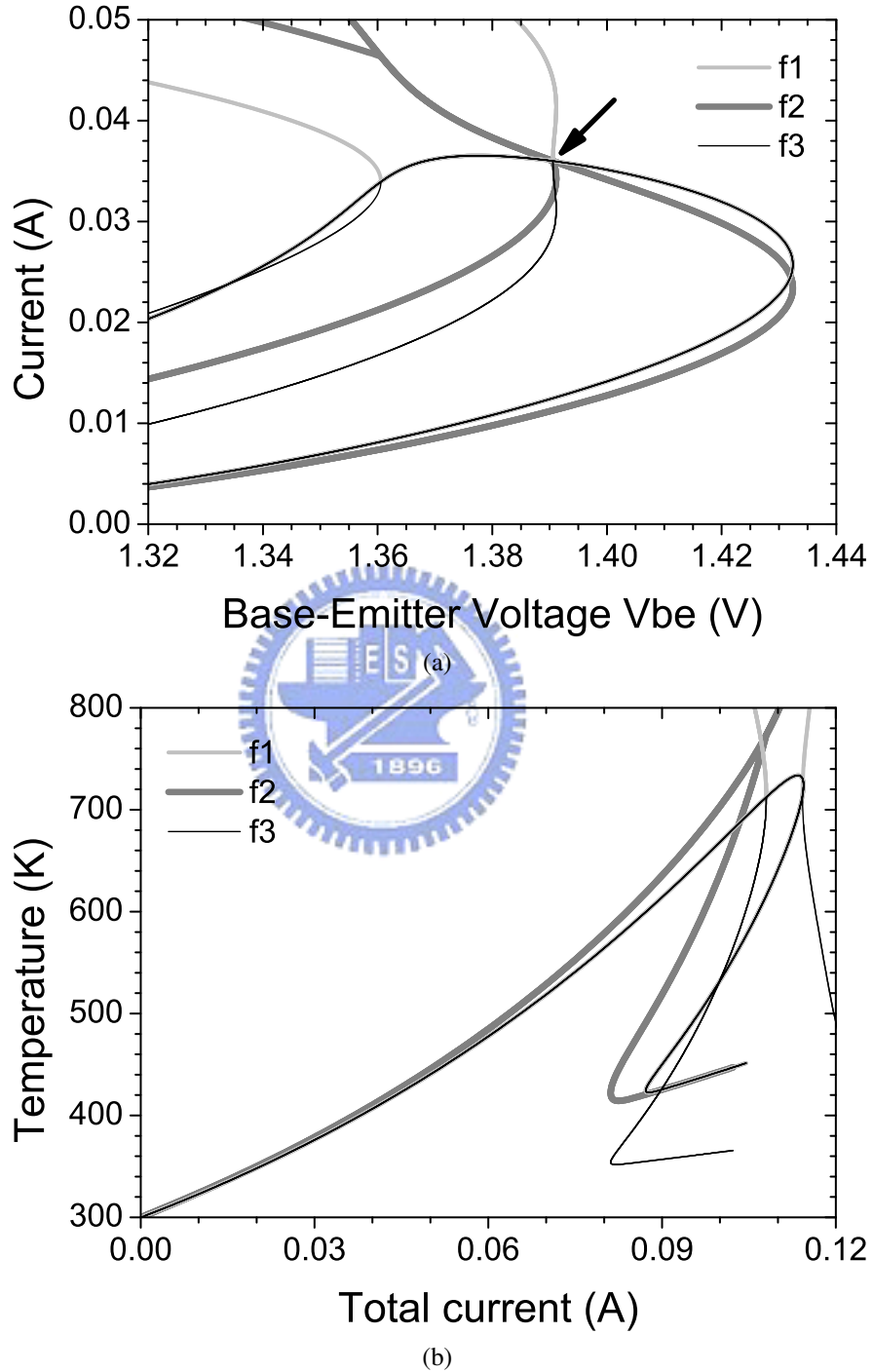


Fig. 5.9. The simulation results of a 3f 3x40 s15 HBT with $R_{E_{13}} = R_{E_{13,SI}} = 12.02 \Omega$ and $R_{E_2} = R_{E_{2,SI}} = 13.92 \Omega$ as $I_{C_{SI}} = 36 \text{ mA}$ in the accurate model with temperature dependent thermal conductivity. (a) $I_C - V_{BE}$ curves and (b) the finger temperature as a function of the total current. The arrow marks the unstable point. f2 is the center finger. f1 and f3 are the side fingers.

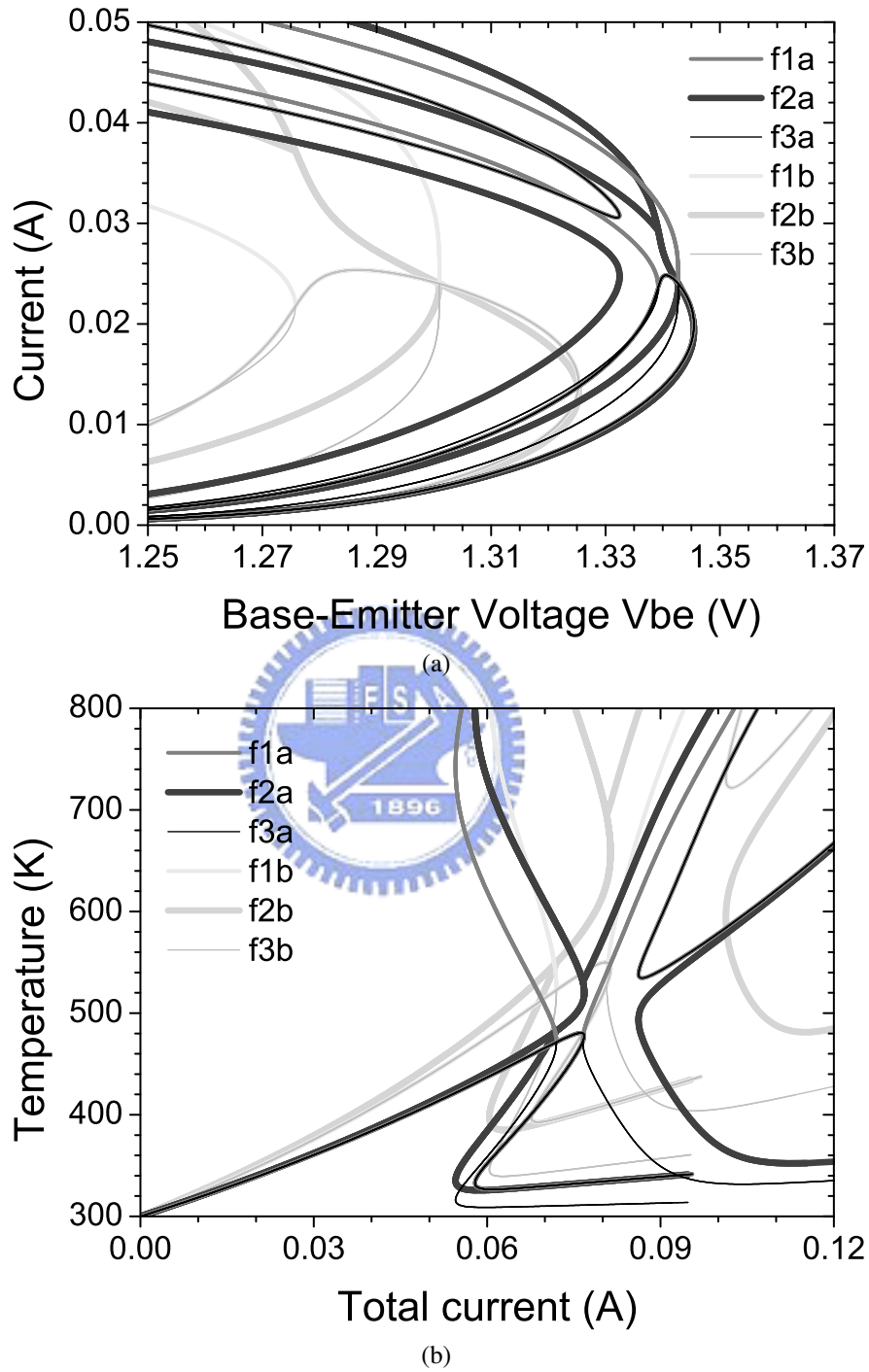


Fig. 5.10. The simulation results of a 3f 3x40 s40 HBT with $R_{E_{13}} = R_{E_{13,SI}} = 6.38 \Omega$ and $R_{E_2} = R_{E_{2,SI}} = 6.84 \Omega$ as $I_{C_{SI}} = 24 \text{ mA}$ in the accurate model with temperature dependent thermal conductivity compared with the results of the 3f 3x40 s15 HBT in Fig. 5.8. (a) $I_C - V_{BE}$ curves and (b) the finger temperature as a function of the total current. f2 is the center finger. f1 and f3 are the side fingers. The letter a indicates the results of a 3f 3x40 s40 HBT. The letter b indicates the results of a 3f 3x40 s15 HBT.

to the collector current density of 30 kA/cm^2 . It can be found that the unstable point, marked by an arrow in Fig. 5.9(a), is just at the specified 36 mA for all fingers similar to the 24 mA case. Although the current can be stable before 36 mA is reached, the temperature of the hottest finger exceeds 770 K at this high current level. It is not reasonable to operate a device at such a high temperature because of the device operation or reliability considerations. Therefore, a reasonable stable current level must be specified under an acceptable finger temperature when we use the uniform current design.

Last, Fig. 5.10(a) and (b) show the I_C-V_{BE} and finger temperature curves with $R_{E_{13,SI}} = 6.38 \Omega$ and $\Delta R_{E_{2,SI}} = 0.46 \Omega$ as $I_{C_{SI}} = 24 \text{ mA}$ for the $40 \mu\text{m}$ finger separation device. The curves of Fig. 5.8 for the $15 \mu\text{m}$ finger separation device are also shown for reference. Because of the smaller coupling effect, the I_C-V_{BE} curves of the smaller separation device are more concentrated. The temperatures of all fingers are also smaller and more uniform. The highest finger temperature exceeds 480 K . All of the above features are similar to the simple model case discussed in Section 4.4.

5.2.2 With Constant Thermal Conductivity

Without the temperature dependence, a constant thermal conductivity will result in a less nonlinear behavior of devices. We first use the same condition as Fig. 5.5 to set $R_E = 3 \Omega$ for all fingers. The simulated I_C-V_{BE} and finger temperature curves are shown in Fig. 5.11(a) and (b). And the curves of Fig. 5.5 are also shown for reference. There are also three sets of solutions but out of the range displayed in the figures. Only parts of the second set of the solutions are shown in Fig. 5.11(b). The highest current of the side fingers is about 28.0 mA . This value is about 3.5 times larger than that shown in Fig. 5.5(a) for the same device. It is a good evidence for the fact that the device nonlinearity is mainly due to the temperature dependence of the thermal conductivity.

By substituting $I_{C_{SI}} = 24 \text{ mA}$ corresponding to the collector current density of 20 kA/cm^2 into (5.18), we obtain $\Delta R_{E_{2,SI}} = 0.54 \Omega$. The I_C-V_{BE} and the finger temperature curves are shown in Fig. 5.12(a) and (b) with $R_{E_{13}} = 3 \Omega$ and $R_{E_2} =$

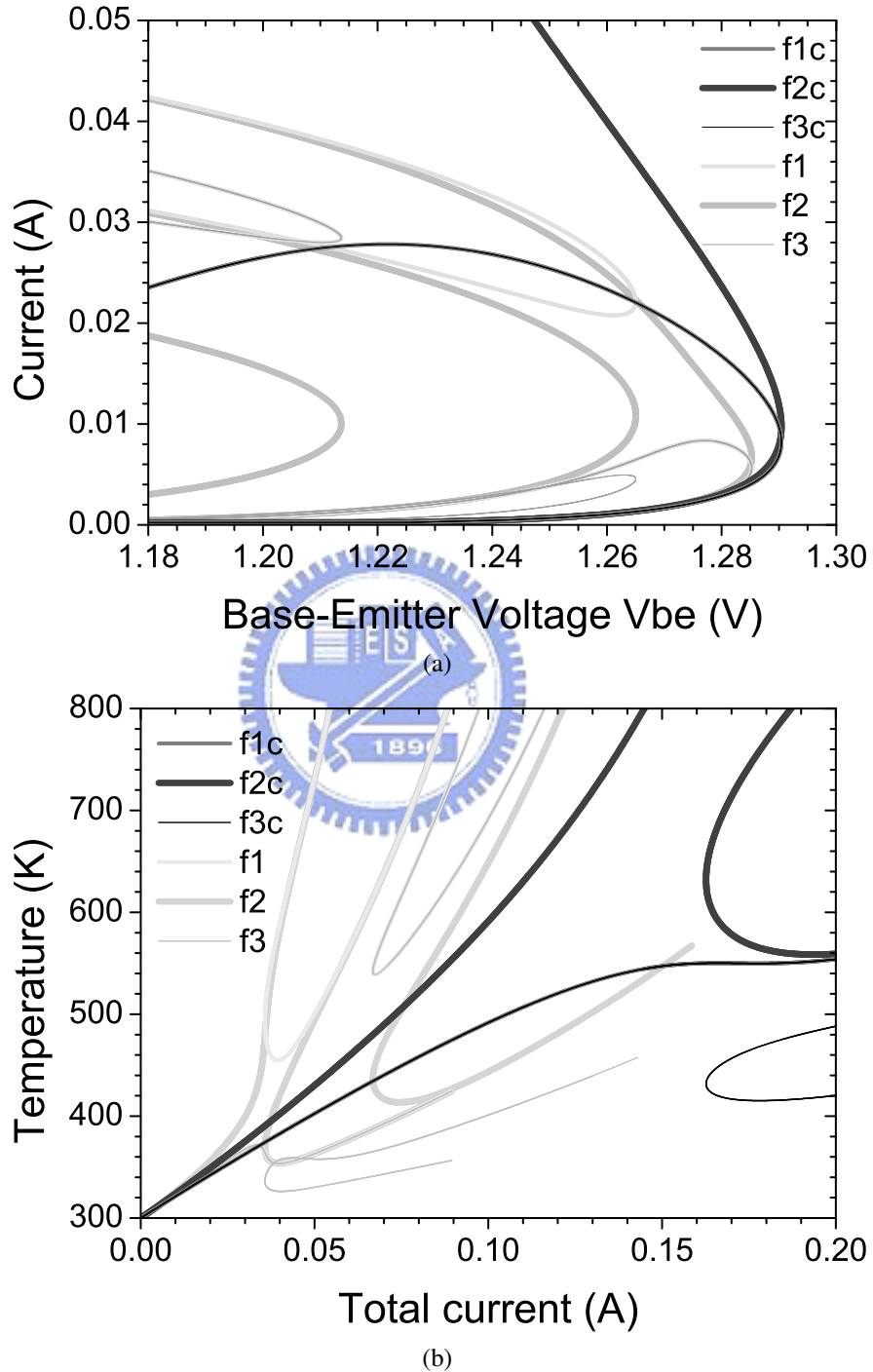


Fig. 5.11. The simulation results of a 3f 3x40 s15 HBT with $R_{E_{13}} = R_{E_2} = 3 \Omega$ in the accurate model with constant thermal conductivity. (a) $I_C - V_{BE}$ curves and (b) the finger temperature as a function of the total current. f2 is the center finger. f1 and f3 are the side fingers.

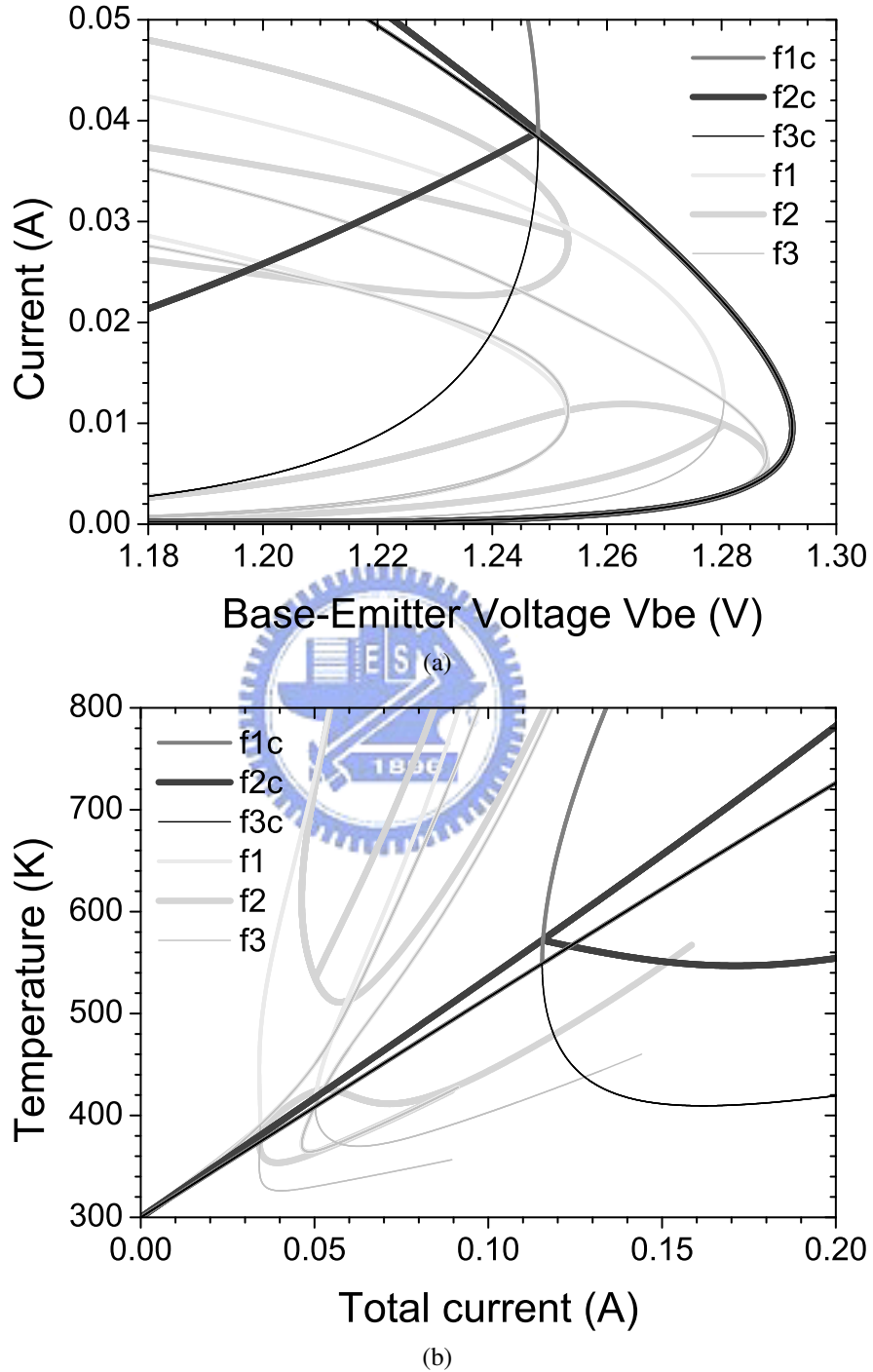


Fig. 5.12. The simulation results of a 3f 3x40 s15 HBT with $R_{E_{13}} = 3 \Omega$ and $R_{E_2} = R_{E_{13}} + \Delta R_{E_2,SI} = 3.54 \Omega$ as $I_{CS1} = 24 \text{ mA}$ in the accurate model with constant thermal conductivity. (a) $I_C - V_{BE}$ curves and (b) the finger temperature as a function of the total current. f2 is the center finger. f1 and f3 are the side fingers.

$R_{E_{13}} + \Delta R_{E_{2,SI}} = 3.54 \Omega$. The curves of Fig. 5.6 are also shown for reference. We found that the currents of all fingers are nearly below the unstable current level. It is different from the curves shown in Fig. 5.6(a) but similar to Fig. 4.2(a). The unstable point current level is at about 39 mA for the center finger. It is higher than the value we wanted because that $R_{E_{13}}$ is too large for the unstable current 24 mA. If we still want to obtain the original current level, $R_{E_{13}}$ must be reduced.

If we set $I_{C_{SI}} = 24$ mA and use (5.18) and (5.19) to determine $R_{E_{2,SI}}$ and $R_{E_{13,SI}}$, the $I_C - V_{BE}$ and the finger temperature curves are shown in Fig. 5.13(a) and (b) with $R_{E_{13,SI}} = 2.48 \Omega$ and $R_{E_{2,SI}} = 3.02 \Omega$. Before the unstable point is reached, the currents of all fingers are almost equal with small deviation. It is different from the curves shown in Fig. 5.8(a) because of the smaller temperature nonlinearity. But it is still not the same as Fig. 4.2(a) because of the current and temperature dependent nature of (5.17) and (5.18). We can find that the unstable point, as marked by an arrow in Fig. 5.13(a), is just at 24 mA as we specified. At this current level, the temperature is near but below 470 K. When the unstable point is reached, there are two unstable modes as in Fig. 5.8. The other features of Fig. 5.13 are nearly the same as Fig. 5.8 and had been discussed in Section 5.2.1 except the less nonlinear coupling effect for the constant thermal conductivity case.

Fig. 5.14(a) and (b) show the $I_C - V_{BE}$ and finger temperature curves for $I_{C_{SI}} = 36$ mA, which corresponds to the collector current density of 30 kA/cm². With this current level, $R_{E_{13,SI}} = 2.94 \Omega$ and $\Delta R_{E_{2,SI}} = 0.55 \Omega$. The unstable point, marked by an arrow in Fig. 5.9(a), is just at the specified 36 mA as before. The highest finger temperature is about 550 K at the unstable current level. It is much lower than the results of Fig. 5.9. It is also a result of the difference between these two temperature models of the thermal conductivity.

Then, Fig. 5.15(a) and (b) show the $I_C - V_{BE}$ and finger temperature curves with $R_{E_{13,SI}} = 2.89 \Omega$ and $\Delta R_{E_{2,SI}} = 0.25 \Omega$ as $I_{C_{SI}} = 24$ mA for the 40 μm finger separation device. The curves of Fig. 5.13 for the 15 μm finger separation device are

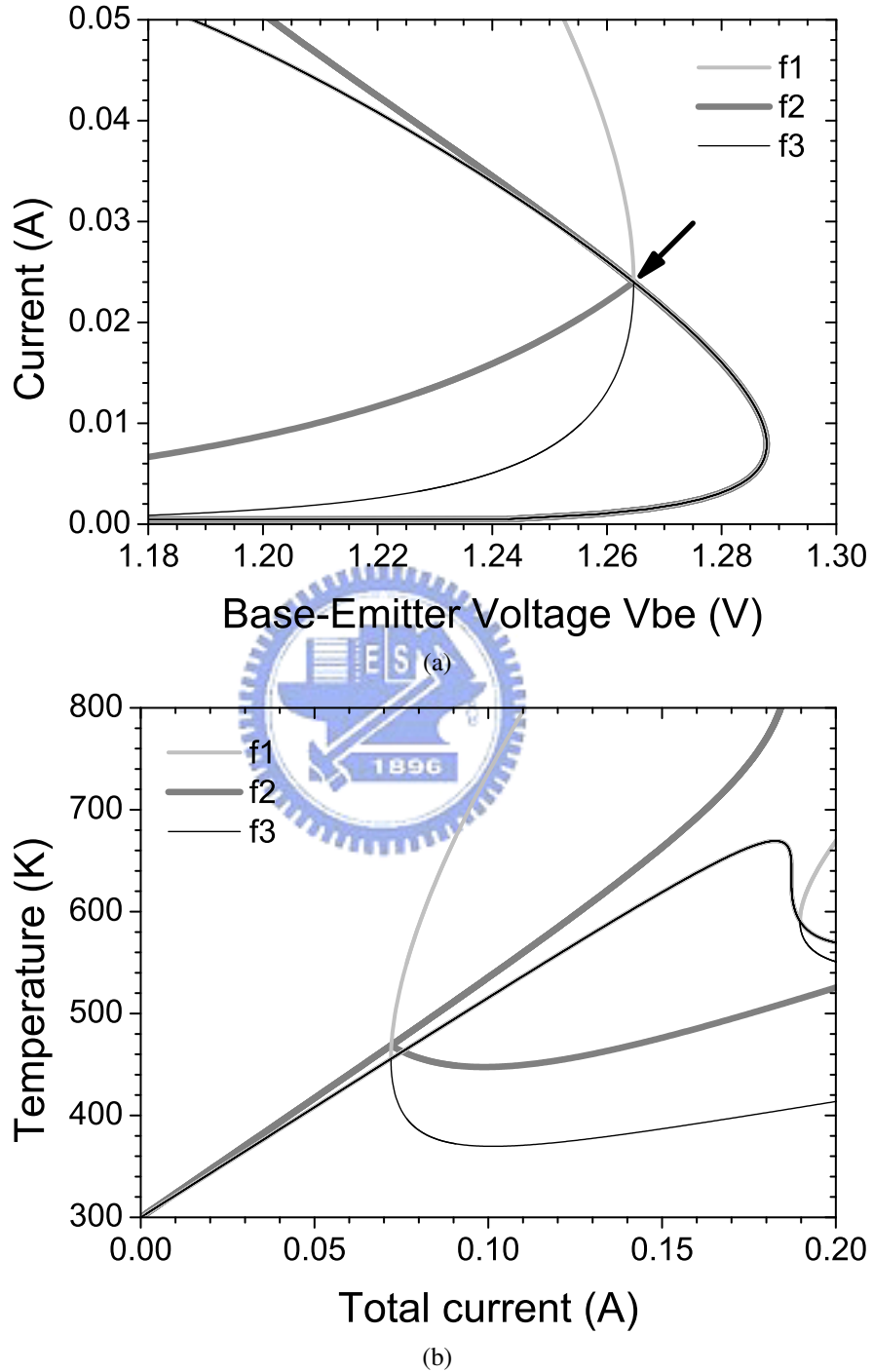


Fig. 5.13. The simulation results of a 3f 3x40 s15 HBT with $R_{E_{13}} = R_{E_{13,SI}} = 2.48 \Omega$ and $R_{E_2} = R_{E_{2,SI}} = 3.02 \Omega$ as $I_{C_{SI}} = 24$ mA in the accurate model with constant thermal conductivity. (a) $I_C - V_{BE}$ curves and (b) the finger temperature as a function of the total current. The arrow marks the unstable point. f2 is the center finger. f1 and f3 are the side fingers.

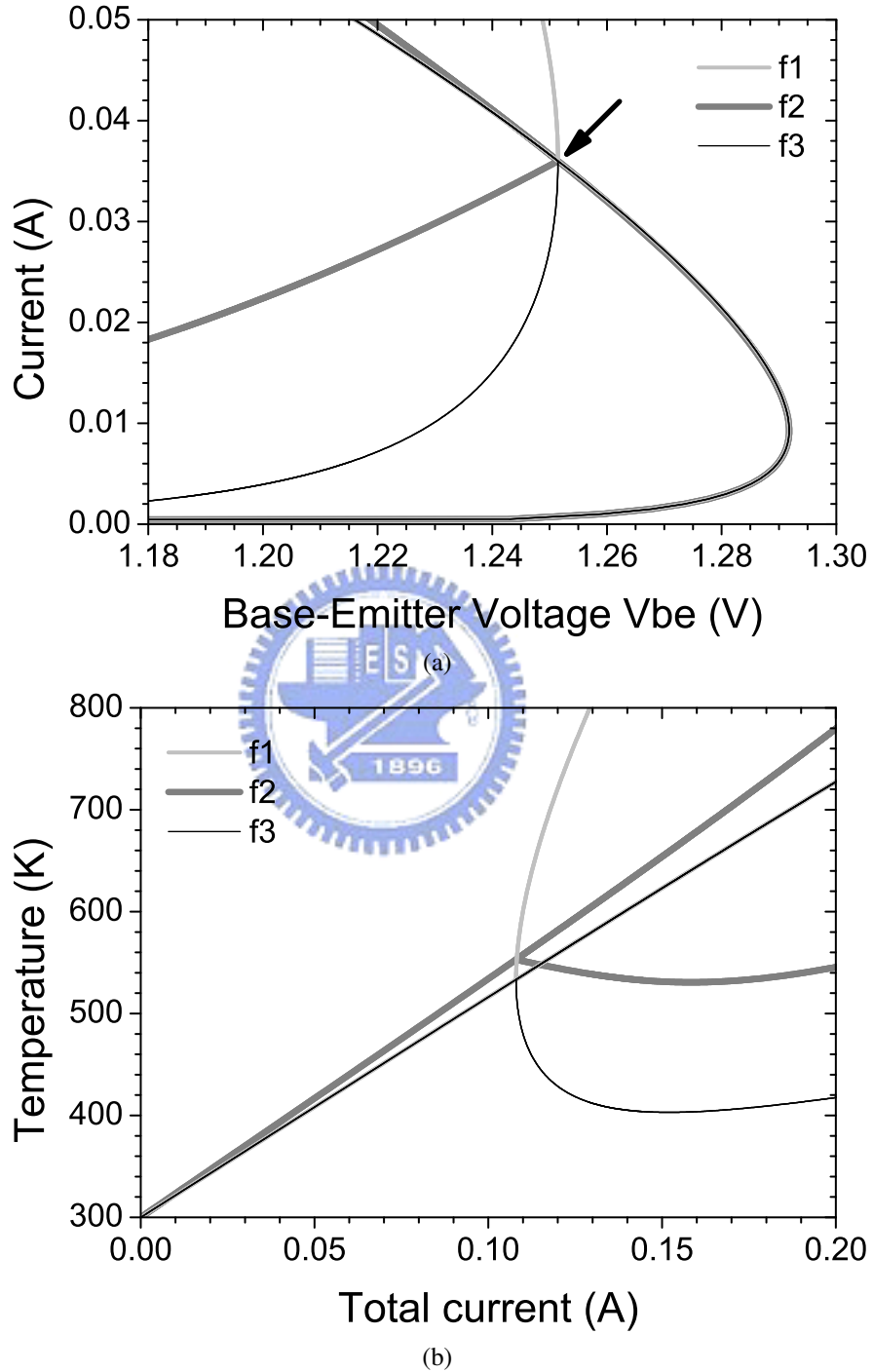


Fig. 5.14. The simulation results of a 3f 3x40 s15 HBT with $R_{E_{13}} = R_{E_{13,SI}} = 2.94 \Omega$ and $R_{E_2} = R_{E_{2,SI}} = 3.49 \Omega$ as $I_{C_{SI}} = 36$ mA in the accurate model with constant thermal conductivity. (a) $I_C - V_{BE}$ curves and (b) the finger temperature as a function of the total current. The arrow marks the unstable point. f2 is the center finger. f1 and f3 are the side fingers.

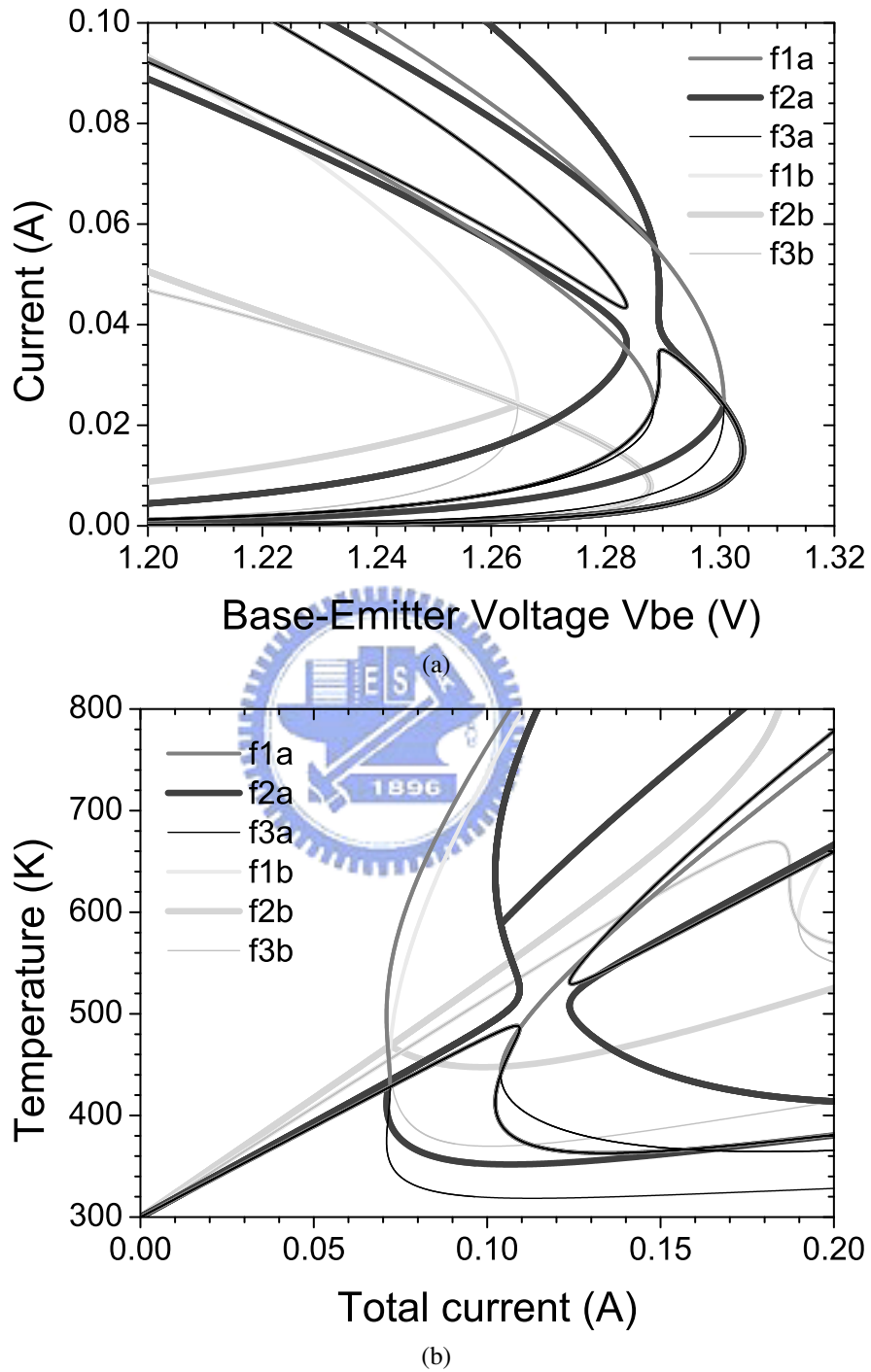


Fig. 5.15. The simulation results of a 3f 3x40 s40 HBT with $R_{E13} = R_{E13,SI} = 2.89 \Omega$ and $R_{E2} = R_{E2,SI} = 3.14 \Omega$ as $I_{C,SI} = 24 \text{ mA}$ in the accurate model with constant thermal conductivity compared with the results of the 3f 3x40 s15 HBT in Fig. 5.13. (a) $I_C - V_{BE}$ curves and (b) the finger temperature as a function of the total current. f2 is the center finger. f1 and f3 are the side fingers. The letter a indicates the results of a 3f 3x40 s40 HBT. The letter b indicates the results of a 3f 3x40 s15 HBT.

also shown for reference. Because of the smaller coupling effect as discussed in Section 5.2.1, the I_C-V_{BE} curves are more concentrated and the finger temperature are also smaller and more uniform.

5.3 The Uniform Temperature Design

Besides uniform current distribution, we can also require the temperature of all fingers identical. As shown in Fig. 5.8(b) and Fig. 5.9(b), the center finger will be hotter than the side fingers when approaching to the unstable point under the uniform current requirement at this point. If we increase the value of the ballasting resistance of the center finger, the current and temperature of this finger will decrease. There will be a certain value for the ballasting resistance of the center finger that will result in identical temperature of all fingers. Because the temperature difference is small, the increment of the ballasting resistance is minor. We can expect that the behavior of the curves will not change too much under the uniform temperature design. But we still need a procedure to decide the distribution of the ballasting resistance under temperature consideration. We will call this procedure as the uniform temperature design. Similar to Section 5.2, we will solve the ballasting resistance needed for stable operation under a specific finger temperature, T_{ST} , by setting $T_1 = T_2 = T_3 = T_{ST}$.

First, we rewrite (5.6) as

$$\begin{aligned}
 I_{C_1} &= A_{t_1}(U_1 - T_A) + A_{c_1}(U_2 - T_A) + A_{c_2}(U_3 - T_A) \\
 I_{C_2} &= A_{c_1}(U_1 - T_A) + A_{t_2}(U_2 - T_A) + A_{c_1}(U_3 - T_A) \\
 I_{C_3} &= A_{c_2}(U_1 - T_A) + A_{c_1}(U_2 - T_A) + A_{t_1}(U_3 - T_A)
 \end{aligned} \tag{5.20}$$

where

$$\begin{pmatrix} A_{t_1} \\ A_{t_2} \\ A_{c_1} \\ A_{c_2} \end{pmatrix} = \frac{1}{V_C (R_{th_1} - R_{th_3}) (R_{th_1}^2 + R_{th_1} R_{th_3} - 2R_{th_2}^2)} \begin{pmatrix} R_{th_1}^2 - R_{th_2}^2 \\ R_{th_1}^2 - R_{th_3}^2 \\ R_{th_2} R_{th_3} - R_{th_1} R_{th_2} \\ R_{th_2}^2 - R_{th_1} R_{th_3} \end{pmatrix}$$

According to (5.7), it will also result in $U_1 = U_2 = U_3 = U_{ST}$ by setting the temperature of all fingers identical, i.e. $T_1 = T_2 = T_3 = T_{ST}$. We can get the following relation of U_{ST} and T_{ST} from (5.7) and (5.6) as

$$U_{ST} - T_A = \frac{T_A}{b-1} \left[1 - \left(\frac{T_{ST}}{T_A} \right)^{-(b-1)} \right]. \quad (5.21)$$

Then, (5.20) becomes

$$\begin{aligned} I_{C_{1,ST}} &= (A_{t_1} + A_{c_1} + A_{c_2}) \frac{T_A}{b-1} \left[1 - \left(\frac{T_{ST}}{T_A} \right)^{-(b-1)} \right] \\ I_{C_{2,ST}} &= (A_{c_1} + A_{t_2} + A_{c_1}) \frac{T_A}{b-1} \left[1 - \left(\frac{T_{ST}}{T_A} \right)^{-(b-1)} \right] \\ I_{C_{3,ST}} &= (A_{c_2} + A_{c_1} + A_{t_1}) \frac{T_A}{b-1} \left[1 - \left(\frac{T_{ST}}{T_A} \right)^{-(b-1)} \right]. \end{aligned} \quad (5.22)$$

and ϕ_{1ST} , ϕ_{2ST} , and ϕ_{3ST} are obtained by substituting T_{ST} and (5.22) into (5.2) as

$$\begin{aligned} \phi_{1ST} &= -\frac{k}{q} \left(\ln \frac{I_{C_{1,ST}}}{I_{S0}} - \gamma \ln \frac{T_{ST}}{300} - \gamma \right) + \alpha^* \\ \phi_{2ST} &= -\frac{k}{q} \left(\ln \frac{I_{C_{2,ST}}}{I_{S0}} - \gamma \ln \frac{T_{ST}}{300} - \gamma \right) + \alpha^* \\ \phi_{3ST} &= -\frac{k}{q} \left(\ln \frac{I_{C_{3,ST}}}{I_{S0}} - \gamma \ln \frac{T_{ST}}{300} - \gamma \right) + \alpha^*. \end{aligned} \quad (5.23)$$

The specification of the upper temperature limit of fingers by the uniform temperature

5.3 The Uniform Temperature Design

design is more directly in the physical sense than the uniform current design. It is not like the uniform current design that need to compute the reasonable $T_{2_{SI}}$ from $I_{C_{SI}}$. The finger current level is also constrained by the upper limit of the finger temperature. In the uniform current design, we have the possibility to specify the current level too high and kill the device. In uniform temperature design, it will not happen. Fig. 5.16 and Fig. 5.17 show the curves of $I_{2_{ST}}$ and $\phi_{2_{ST}}$ for our devices. We can see that the current level cannot exceed 19.4 mA for the 3f 3x40 s15 HBT and 25.5 mA for the 3f 3x40 s40 HBT with temperature dependent thermal conductivity and 27.0 mA for the 3f 3x40 s15 HBT and 35.4 mA for the 3f 3x40 s40 HBT with constant thermal conductivity if the junction temperatures need to be kept below 500 K. The other properties of the temperature curves and the thermal-electrical feedback coefficient are similar to the uniform current design and had been discussed in Section 5.2.

By substituting (5.22) and (5.23) into (5.4), the emitter ballasting resistance distribution $R_{E_{2,ST}}$ and the effective distribution difference $\Delta R_{E_{2,ST}}^*$ for the specified current level can be determined as

$$\begin{aligned}
 R_{E_{2,ST}} &= \frac{I_{C_{1,ST}}}{I_{C_{2,ST}}} \left[R_{E_{13}} + \frac{(\phi_{2_{ST}} - \phi_{1_{ST}})T_{ST}}{I_{C_{1,ST}}} \right] \\
 &= \frac{I_{C_{1,ST}}}{I_{C_{2,ST}}} (R_{E_{13}} + \Delta R_{E_{2,ST}}^*) \\
 &= \frac{A_{t_1} + A_{c_1} + A_{c_2}}{A_{t_2} + 2A_{c_1}} R_{E_{13}} + \frac{(\phi_{2_{ST}} - \phi_{1_{ST}})T_{ST}}{(A_{t_2} + 2A_{c_1})(U_{ST} - T_A)}
 \end{aligned} \tag{5.24}$$

and the real emitter resistance distribution difference is

$$\Delta R_{E_{2,ST}} = R_{E_{2,ST}} - R_{E_{13}}.$$

Similar to (5.18), this distribution is temperature and current dependent. But different from (5.18), the distribution difference is a function of $R_{E_{13}}$. It is the reason that we need to define the effective distribution difference $\Delta R_{E_{2,ST}}^*$ to obtain a $R_{E_{13}}$ independent distribution difference. The independence of the distribution difference is necessary when

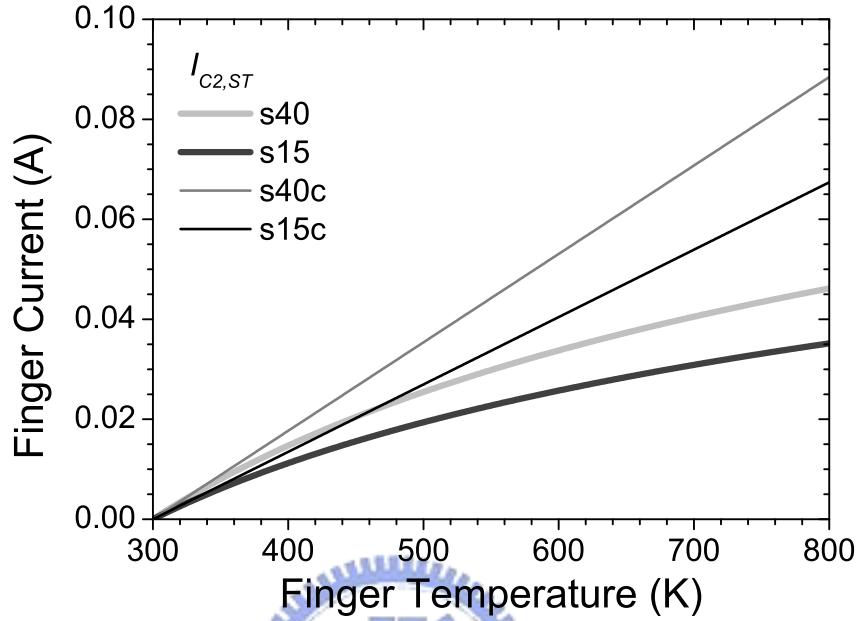


Fig. 5.16. The simulation results of $I_{C_{2,ST}}$ as a function of T_{ST} for a 3f 3x40 s40 and a 3f 3x40 s15 HBT with temperature dependent and constant thermal conductivity. s40 means the 3f 3x40 s40 device. s15 means the 3f 3x40 s15 device. The letter c indicates the results with constant thermal conductivity.

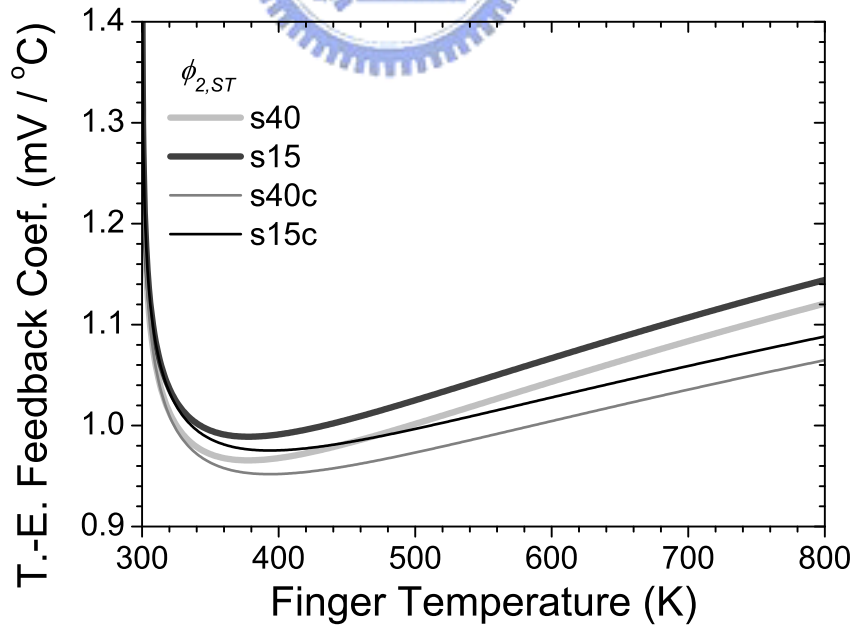


Fig. 5.17. The simulation results of $\phi_{2,ST}$ as a function of T_{ST} for a 3f 3x40 s40 and a 3f 3x40 s15 HBT with temperature dependent and constant thermal conductivity. s40 means the 3f 3x40 s40 device. s15 means the 3f 3x40 s15 device. The letter c indicates the results with constant thermal conductivity.

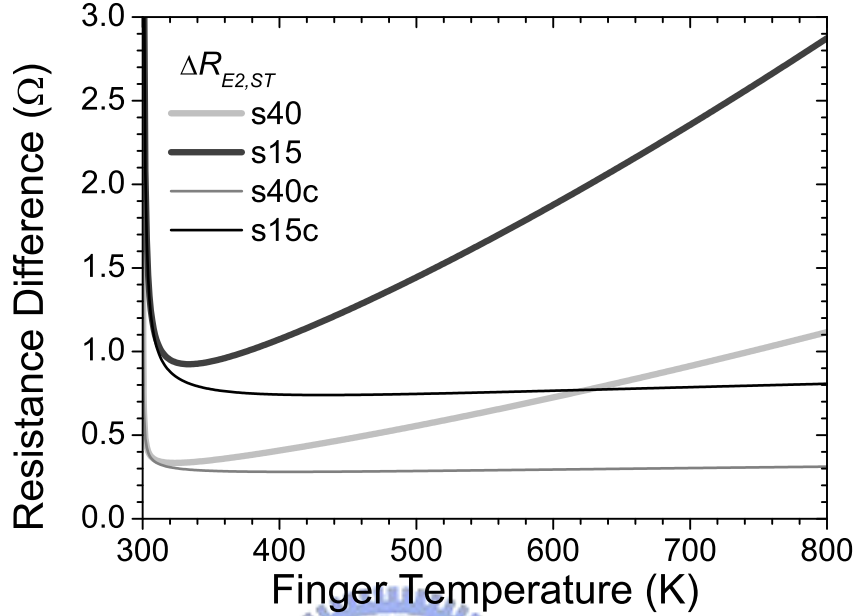


Fig. 5.18. The simulation results of $\Delta R_{E2,ST}$ as a function of T_{ST} for a 3f 3x40 s40 and a 3f 3x40 s15 HBT with temperature dependent and constant thermal conductivity. s40 means the 3f 3x40 s40 device. s15 means the 3f 3x40 s15 device. The letter C indicates the results with constant thermal conductivity.

we derive the eigenvalue equation of R_{E13} of the uniform temperature design. Fig. 5.18 shows the simulated results of $\Delta R_{E2,ST}$ versus the specified finger temperature. It is the real ballasting resistance used in device unlike $\Delta R_{E2,ST}^*$. For this reason, we do not concern the value of $\Delta R_{E2,ST}^*$ which is only used temporarily for solving R_{E13} . Despite the temperature close to ambient temperature, as the specified temperature increases we need a higher $\Delta R_{E2,ST}$ to guarantee identical temperature in all fingers for the temperature dependent thermal conductivity case. For constant thermal conductivity case, the increase of $\Delta R_{E2,ST}$ is not so apparent. It is quit constant in the temperature range larger than 320 K. For temperature dependent thermal conductivity case, the increase of $\Delta R_{E2,ST}$ for the small finger separation case is faster than the large separation because of the nonlinear behavior of the finger temperature. Besides, since it is analogous to (4.3) that the difference between the coupling thermal resistance R_{th2} and R_{th3} becomes larger, smaller finger separation will result in larger $\Delta R_{E2,ST}$.

After the finger currents $I_{C1,ST} - I_{C2,ST}$, the thermal-electrical feedback coefficients

5.3 The Uniform Temperature Design

$\phi_{1ST} - \phi_{3ST}$, and the emitter ballasting resistance distribution difference $\Delta R_{E2,ST}^*$ under the specified finger temperature are known, the eigenvalue equation for the uniform temperature design can be obtained by substituting (5.22)-(5.24) into (5.15) as

$$\begin{vmatrix} \theta_{1ST} R_{th1}^* - \lambda_{1ST} - R_{E13} & \theta_{1ST} R_{th2}^* & \theta_{1ST} R_{th3}^* \\ r_{ST} \theta_{2ST} R_{th2}^* & r_{ST} \theta_{2ST} R_{th1}^* - \lambda_{2ST} - R_{E13} & r_{ST} \theta_{2ST} R_{th2}^* \\ \theta_{3ST} R_{th3}^* & \theta_{3ST} R_{th2}^* & \theta_{3ST} R_{th1}^* - \lambda_{3ST} - R_{E13} \end{vmatrix} = 0 \quad (5.25)$$

where

$$\begin{aligned} \theta_{1ST} &= \frac{\phi_{1ST}}{\phi} \left(\frac{T_{ST}}{T_A} \right)^b & \lambda_{1ST} &= \frac{kT_{ST}}{q} \frac{1}{I_{C1,ST}} \\ \theta_{2ST} &= \frac{\phi_{2ST}}{\phi} \left(\frac{T_{ST}}{T_A} \right)^b & \lambda_{2ST} &= \frac{kT_{ST}}{q} \frac{1}{I_{C2,ST}} r_{ST} + \Delta R_{E2,ST}^* \\ \theta_{3ST} &= \frac{\phi_{3ST}}{\phi} \left(\frac{T_{ST}}{T_A} \right)^b & \lambda_{3ST} &= \frac{kT_{ST}}{q} \frac{1}{I_{C3,ST}} \end{aligned}$$

and

$$r_{ST} = \frac{I_{C2,ST}}{I_{C1,ST}}.$$

There are also three solutions for R_{E13} the same as the discussion of Section 5.2. The largest solution is the no-bend-over condition and the second is the solution for the uniform temperature design. The calculated second largest solution of R_{E13} , namely $R_{E13,ST}$, as a function of the specified finger temperature is shown in Fig. 5.19. We can find that $R_{E13,ST}$ is negative if I_{CST} is below 340 K for the 3f 3x40 s15 HBT and 330 K for the 3f 3x40 s40 HBT with temperature dependent thermal conductivity and 345 K for the 3f 3x40 s15 HBT and 335 K for the 3f 3x40 s40 HBT with constant thermal conductivity. The negative $R_{E13,ST}$ means that the transistor is unconditional stable below these finger temperatures correspondingly. $R_{E13,ST}$ is quit constant for the constant thermal conductivity case and increases almost linearly as the specified finger temperature increases for the temperature dependent thermal conductivity case in the temperature

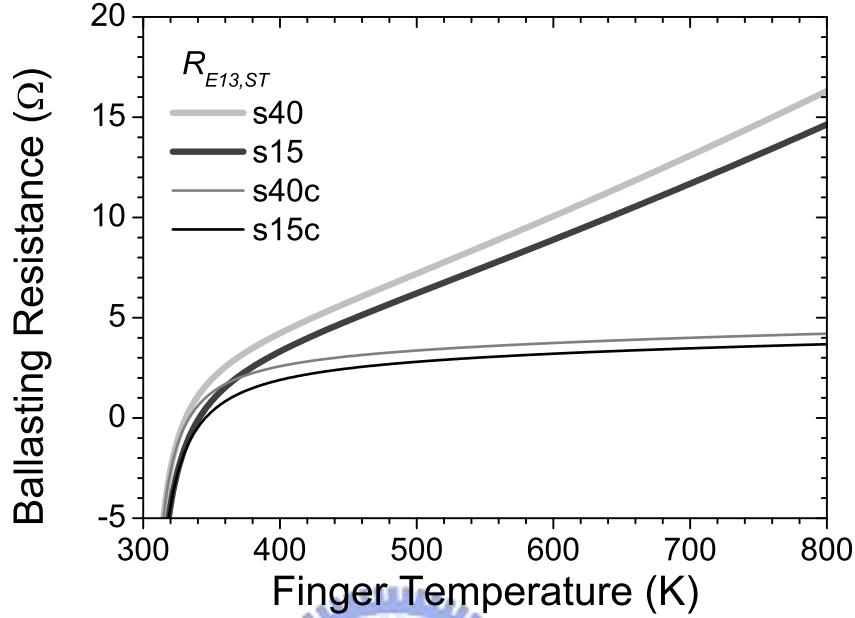


Fig. 5.19. The simulation results of $R_{E13,ST}$ as a function of T_{ST} for a 3f 3x40 s40 and a 3f 3x40 s15 HBT with temperature dependent and constant thermal conductivity. s40 means the 3f 3x40 s40 device. s15 means the 3f 3x40 s15 device. The letter c indicates the results with constant thermal conductivity.

range larger than 400 K.

5.3.1 With Temperature Dependent Thermal Conductivity

If we set $T_{ST} = 470$ K, we can compute that $R_{E13,ST} = 5.41 \Omega$ and $\Delta R_{E2,ST} = 1.32 \Omega$ for a 3f 3x40 s15 HBT. The $I_C - V_{BE}$ and finger temperature curves are shown in Fig. 5.20(a) and (b). Below the specified temperature, the temperatures of all fingers are almost the same. We can find that the unstable point, as marked by an arrow in Fig. 5.20(b), is just at 470 K as we specified. At this specified temperature, the total current of the unstable point is 58 mA. Before the unstable point is reached, the current of the center finger is always smaller than the side finger. Small current will result in small self-heating. It is the reason that uniform finger temperature can be obtained.

Fig. 5.21(a) and (b) show the results under $T_{ST} = 550$ K with $R_{E13,ST} = 7.55 \Omega$ and $\Delta R_{E2,ST} = 1.65 \Omega$ for comparison. The simulated curves under these two specified

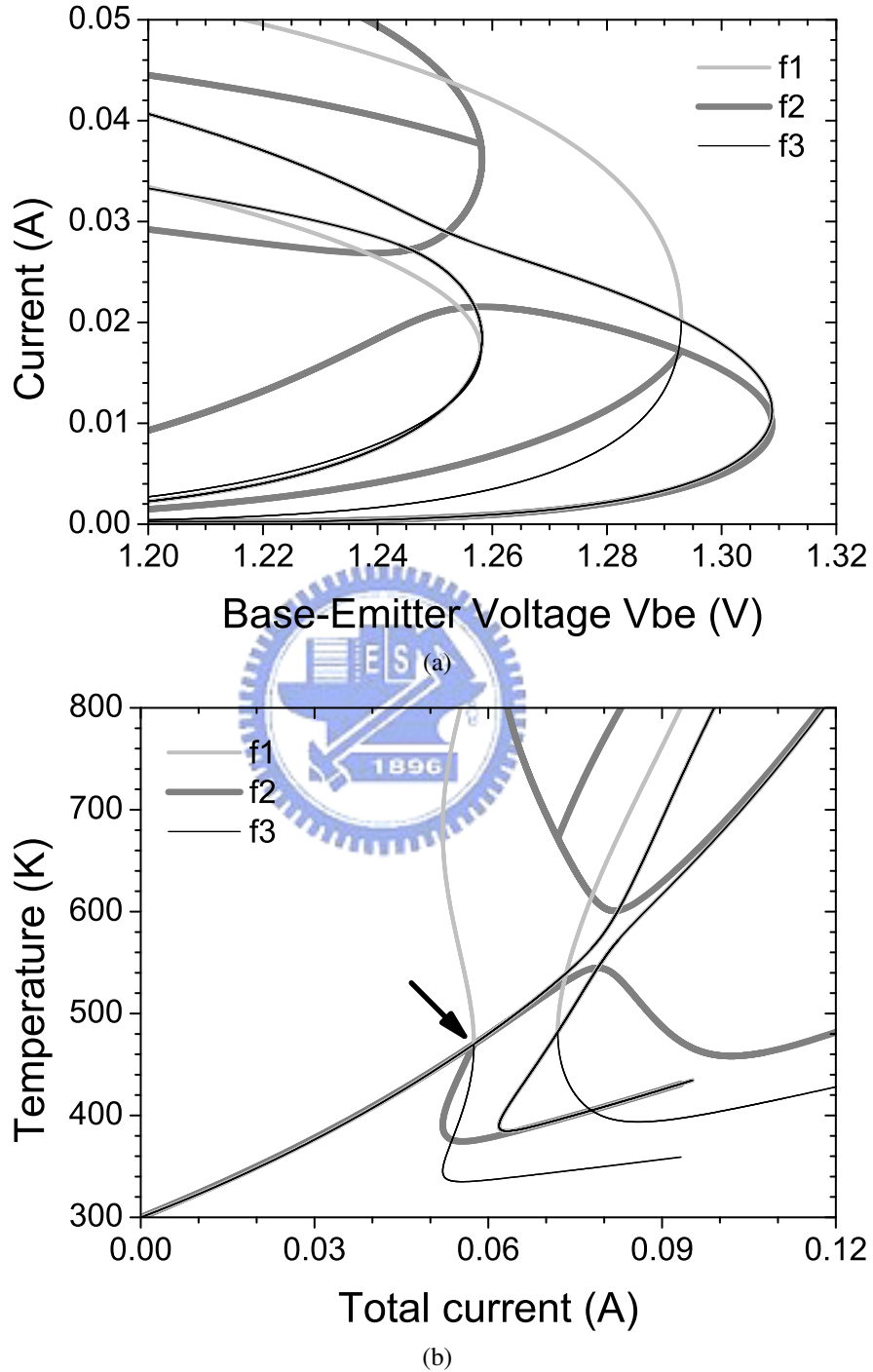


Fig. 5.20. The simulation results of a 3f 3x40 s15 HBT with $R_{E_{13}} = R_{E_{13,ST}} = 5.41 \Omega$ and $R_{E_2} = R_{E_{2,ST}} = 6.73 \Omega$ as $T_{ST} = 470 \text{ K}$ in the accurate model with temperature dependent thermal conductivity. (a) $I_C - V_{BE}$ curves and (b) the finger temperature as a function of the total current. The arrow marks the unstable point. f2 is the center finger. f1 and f3 are the side fingers.

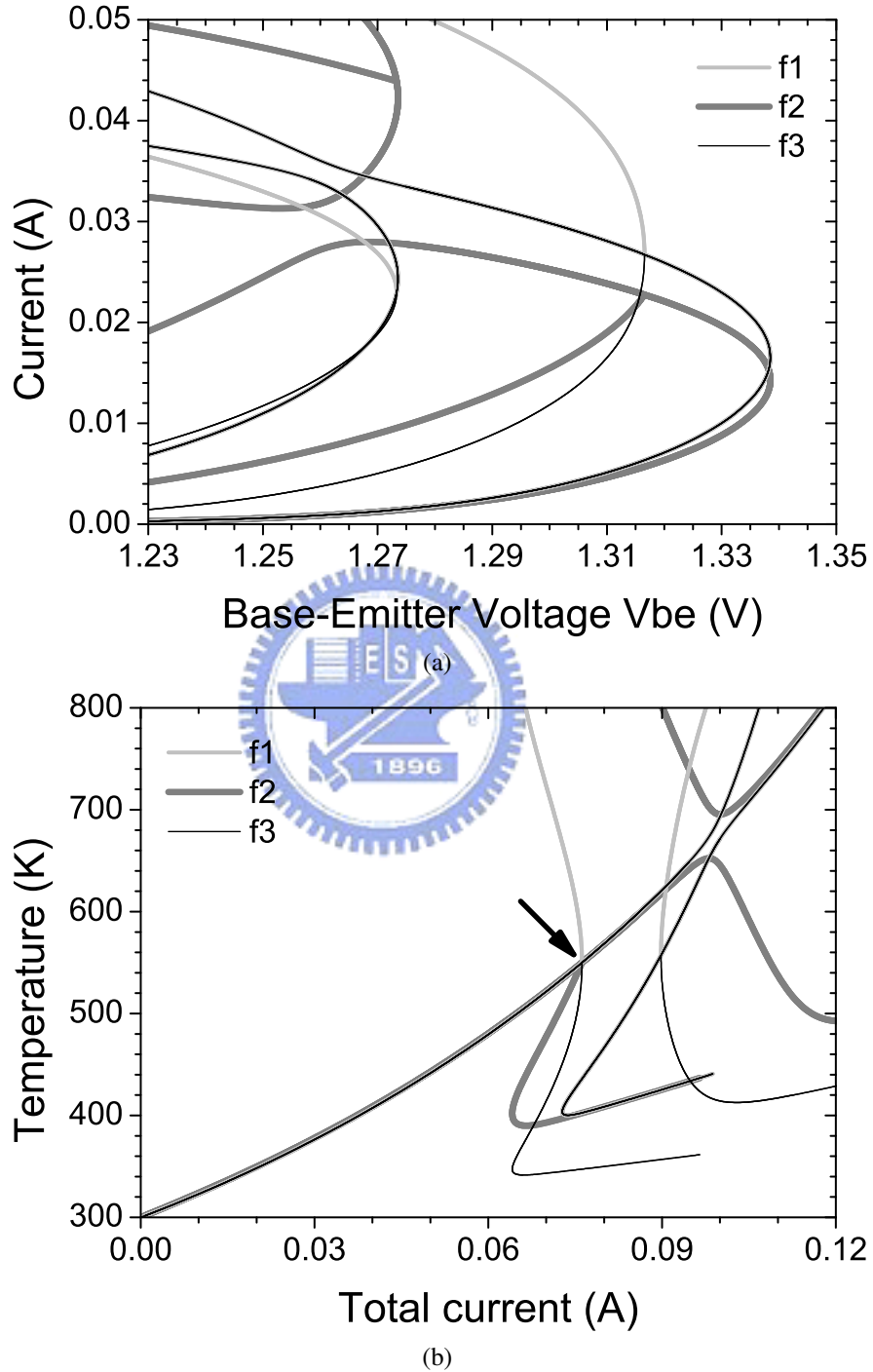


Fig. 5.21. The simulation results of a 3f 3x40 s15 HBT with $R_{E_{13}} = R_{E_{13,ST}} = 7.55 \Omega$ and $R_{E_2} = R_{E_{2,ST}} = 9.20 \Omega$ as $T_{ST} = 550 \text{ K}$ in the accurate model with temperature dependent thermal conductivity. (a) $I_C - V_{BE}$ curves and (b) the finger temperature as a function of the total current. The arrow marks the unstable point. f2 is the center finger. f1 and f3 are the side fingers.

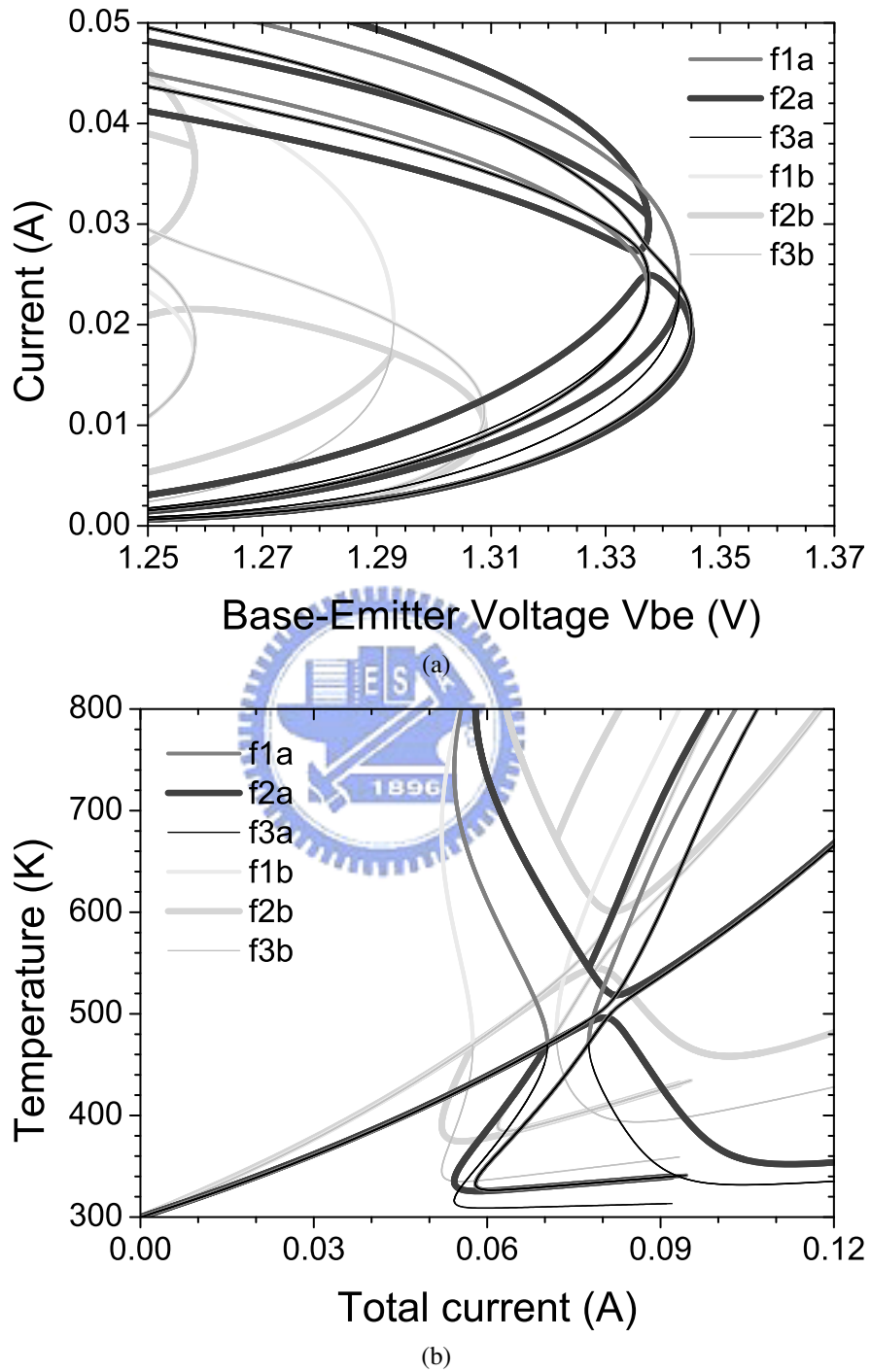


Fig. 5.22. The simulation results of a 3f 3x40 s40 HBT with $R_{E13} = R_{E13,ST} = 6.35 \Omega$ and $R_{E2} = R_{E2,ST} = 6.86 \Omega$ as $T_{ST} = 470 \text{ K}$ in the accurate model with temperature dependent thermal conductivity compared with the results of the 3f 3x40 s15 HBT in Fig. 5.20. (a) $I_C - V_{BE}$ curves and (b) the finger temperature as a function of the total current. f1 and f3 are the side fingers. The letter a indicates the results of a 3f 3x40 s40 HBT. The letter b indicates the results of a 3f 3x40 s15 HBT.

temperatures are similar. The total current of the unstable point under $T_{ST} = 550$ K is 76 mA as marked by an arrow in Fig. 5.21(b). By comparing to 72 mA of $I_{CSI} = 24$ mA for the uniform current case in Fig. 5.8 whose maximum finger temperature is also 550 K, the total current under uniform temperature consideration is larger than that under uniform current consideration. Although the total current is about 6 % larger, the total ballasting resistance is about 13 % larger for the uniform temperature design, i.e. 24.3 Ω versus 21.5 Ω . It seems that the uniform current design is better in the consideration of efficient ballasting resistance usage. However, since the uniform temperature method have the advantage of identical finger temperature, we think these two designs are both useful.

Fig. 5.25(a) and (b) show the I_C-V_{BE} and finger temperature curves for a 3f 3x40 s40 HBT under $T_{ST} = 470$ K with $R_{E_{13,ST}} = 6.35 \Omega$ and $\Delta R_{E_{2,ST}} = 0.51 \Omega$. The curves of Fig. 5.20 for the 3f 3x40 s15 HBT under the same specified temperature are also shown for comparison. As the finger separation increases, the total current of the unstable point increases from 58 mA to 71 mA and the bend-over current increases from 32 mA to 59 mA under the same $T_{ST} = 470$ K. It is a result of smaller coupling thermal resistance. Because of the smaller coupling effect, the I_C-V_{BE} curves of the smaller separation device are more concentrated and the unstable point moves to higher current level.

5.3.2 With Constant Thermal Conductivity

If we set $T_{ST} = 470$ K, we can compute that $R_{E_{13,ST}} = 2.62 \Omega$ and $\Delta R_{E_{2,ST}} = 0.74 \Omega$ for a 3f 3x40 s15 HBT. The I_C-V_{BE} and finger temperature curves are shown in Fig. 5.23(a) and (b). Below the specified temperature, the temperatures of all fingers are almost the same. We can find that the unstable point, marked by an arrow in Fig. 5.23(a), is just at 470 K as we specified. At this specified temperature, the total current of the unstable point is 77 mA comparing to 72 mA of $I_{CSI} = 24$ mA for the uniform current case in Fig. 5.13 whose maximum finger temperature is also 470 K. Although the total

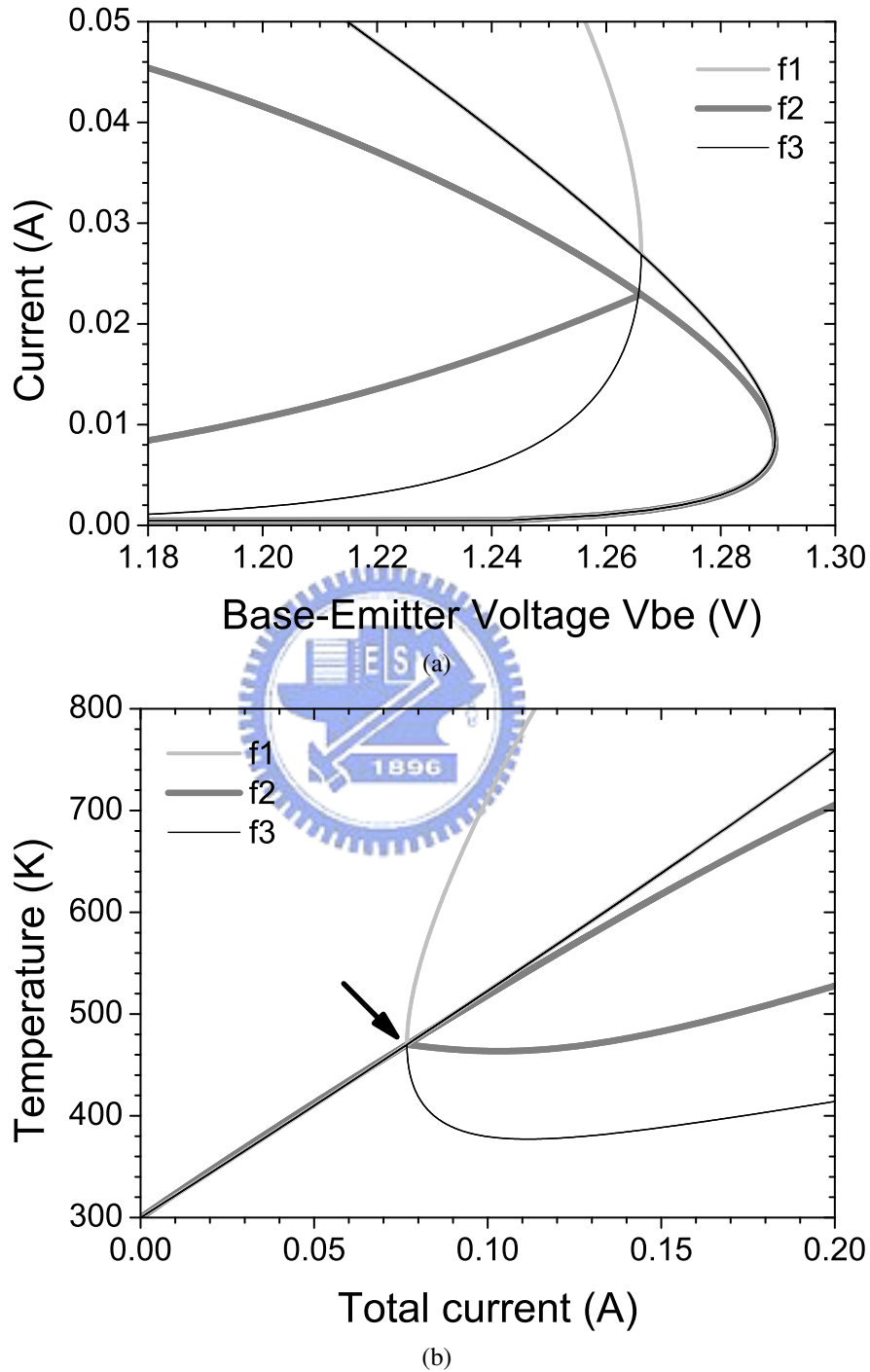


Fig. 5.23. The simulation results of a 3f 3x40 s15 HBT with $R_{E_{13}} = R_{E_{13,ST}} = 2.62 \Omega$ and $R_{E_2} = R_{E_{2,ST}} = 3.36 \Omega$ as $T_{ST} = 470$ K in the accurate model with constant thermal conductivity. (a) $I_C - V_{BE}$ curves and (b) the finger temperature as a function of the total current. The arrow marks the unstable point. f2 is the center finger. f1 and f3 are the side fingers.

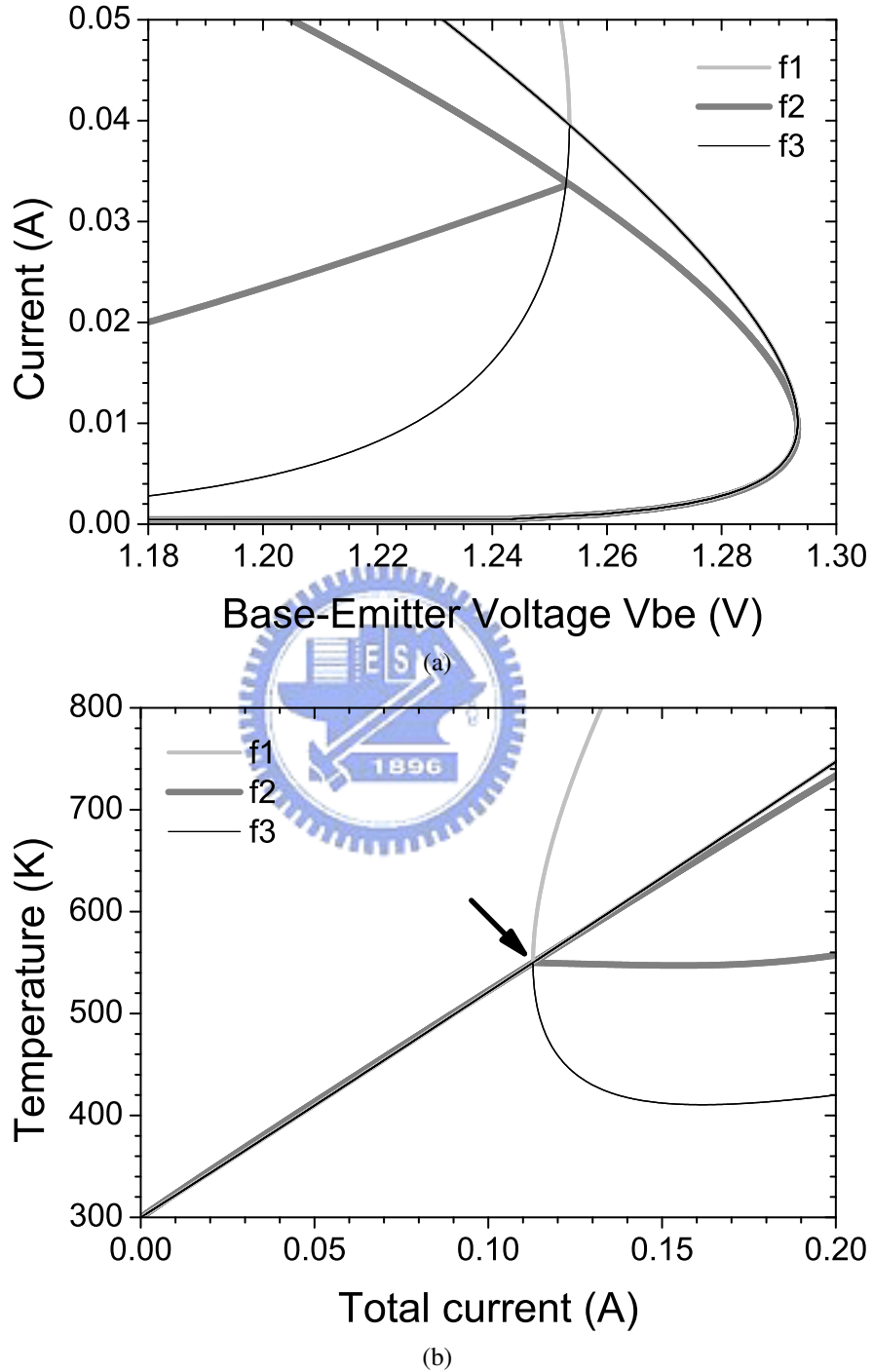


Fig. 5.24. The simulation results of a 3f 3x40 s15 HBT with $R_{E_{13}} = R_{E_{13,ST}} = 3.03 \Omega$ and $R_{E_2} = R_{E_{2,ST}} = 3.78 \Omega$ as $T_{ST} = 550 \text{ K}$ in the accurate model with constant thermal conductivity. (a) $I_C - V_{BE}$ curves and (b) the finger temperature as a function of the total current. The arrow marks the unstable point. f2 is the center finger. f1 and f3 are the side fingers.

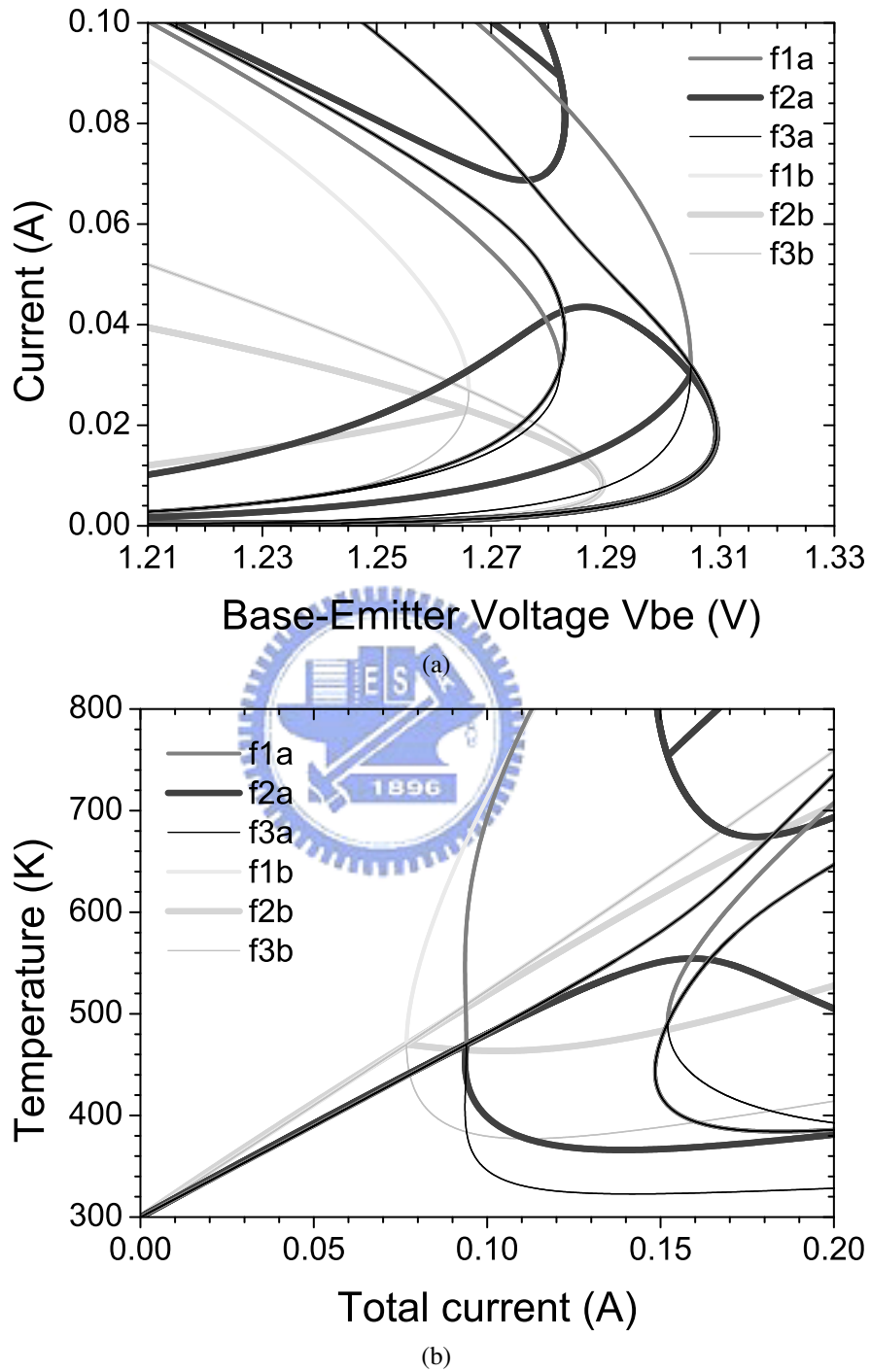


Fig. 5.25. The simulation results of a 3f 3x40 s40 HBT with $R_{E_{13}} = R_{E_{13,ST}} = 3.20 \Omega$ and $R_{E_2} = R_{E_{2,ST}} = 3.49 \Omega$ as $T_{ST} = 470 \text{ K}$ in the accurate model with constant thermal conductivity compared with the results of the 3f 3x40 s15 HBT in Fig. 5.23. (a) $I_C - V_{BE}$ curves and (b) the finger temperature as a function of the total current. f1 and f3 are the side fingers. The letter a indicates the results of a 3f 3x40 s40 HBT. The letter b indicates the results of a 3f 3x40 s15 HBT.

current is about 7 % larger, the total ballasting resistance is about 8 % larger for the uniform temperature design, i.e. 8.6Ω versus 8.0Ω . Contrary to the temperature dependent thermal conductivity case, the percentages of the increase of these two parameters are very close. It is a result of lower finger temperature and less temperature nonlinearity. In this constant thermal conductivity case, these two designs are both useful and have their own advantages.

Fig. 5.24(a) and (b) show the results under $T_{ST} = 550 \text{ K}$ with $R_{E_{13,ST}} = 3.03 \Omega$ and $\Delta R_{E_{2,ST}} = 0.76 \Omega$ for comparison. The simulated curves under these two specified temperatures are similar. The total current of the unstable point under $T_{ST} = 550 \text{ K}$ is 113 mA as marked by an arrow. As one can expect, the linear temperature model will result in a higher unstable current level under the same specified temperature.

Fig. 5.25(a) and (b) show the $I_C - V_{BE}$ and finger temperature curves for a 3f 3x40 s40 HBT under $T_{ST} = 470 \text{ K}$ with $R_{E_{13,ST}} = 3.20 \Omega$ and $\Delta R_{E_{2,ST}} = 0.28 \Omega$. The curves in Fig. 5.23 for the 3f 3x40 s15 HBT under the same specified temperature are also shown for reference. As the finger separation increases, the current level of the unstable point increases from 77 mA to 94 mA and the bend-over current increases from 25 mA to 56 mA under the same $T_{ST} = 470 \text{ K}$.

5.4 The General N-Finger Case

Base on the discussions of Section 5.2 and Section 5.3, we extend the 3-finger results to the N-finger case. Unlike Section 4.3 having only one procedure, there are two designs procedures, the uniform current design and the uniform temperature design, for the accurate model. The design procedures of these two designs will be given separately in this section. A 10-finger transistor with each finger area fixed at $100 \mu\text{m}^2$ will be analyzed as an example to illustrate the dependence of the ballasting resistance upon the finger width and the finger separation for these two designs respectively. Because that

the finger area is fixed, the finger length is determined by the finger width. The ballasting resistance will be calculated under the specified current or the specified temperature as the previous sections.

5.4.1 The Uniform Current Design

We list the formulas of the general N-finger case as follows. All variables will use the index **SI** to indicate that they are obtained under the specified finger current. Once $I_{C_{SI}}$ is given, we know that

$$\mathbf{T}_{SI} = T_A \left[1 - \frac{b-1}{T_A} V_C \mathbf{R}_{th} \mathbf{I}_{C_{SI}} \right]^{\frac{-1}{b-1}} \quad (5.26)$$

and

$$\Phi_{SI} = -\frac{k}{q} \left(\ln \frac{I_{C_{SI}}}{I_{S0}} - \gamma \ln \frac{\mathbf{T}_{SI}}{300} - \gamma \right) + \alpha^* \quad (5.27)$$

$$\Phi_{SI}^* = -\frac{k}{q} \left(\ln \frac{I_{C_{SI}}}{I_{S0}} - \gamma \ln \frac{\mathbf{T}_{SI}}{300} \right) + \alpha^* \quad (5.28)$$

where $\mathbf{I}_{C_{SI}}$ is the current vector that satisfies $I_{C_1} = I_{C_2} = I_{C_3} = \dots = I_N = I_{C_{SI}}$, \mathbf{T}_{SI} is the junction temperature vector, Φ_{SI} is the thermal-electrical feedback coefficient vector, and Φ_{SI}^* is the effective thermal-electrical feedback coefficient vector. All variables use the index **SI** to indicate that they are obtained under the specified current level. \mathbf{R}_{th} is the thermal resistance matrix as before. The ideal emitter ballasting resistance distribution, (5.18), becomes

$$\begin{aligned} \mathbf{R}_{ESI} &= R_{E1} + \frac{\Phi_{SI}^* \cdot \mathbf{T}_{SI} - \phi_{1SI}^* T_1}{I_{C_{SI}}} \\ &= R_{E1} + \Delta \mathbf{R}_{ESI} \end{aligned} \quad (5.29)$$

where \mathbf{R}_{ESI} is the ideal emitter ballasting resistance distribution vector and $\Delta \mathbf{R}_{ESI}$ is the emitter resistance difference vector under $I_{C_{SI}}$. Then, the eigenvalue equation (5.19)

becomes

$$\det [\text{diag}(\Theta_{SI})\mathbf{R}_{th}^* - \text{diag}(\Lambda_{SI}) - R_{E1}\mathbf{I}] = 0 \quad (5.30)$$

where

$$\Theta_{SI} = \frac{\Phi_{SI}}{\phi} \cdot \left(\frac{T_{SI}}{T_A} \right)^b \quad \Lambda_{SI} = \frac{kT_{SI}}{q} \frac{1}{I_{CSI}} + \Delta\mathbf{R}_{ESI}$$

$\det(\mathbf{A})$ is the determinant of matrix \mathbf{A} , $\text{diag}(\mathbf{v})$ means a diagonal matrix with vector \mathbf{v} as its diagonal elements, and \mathbf{I} is the identity matrix. Now, we have a modified version for the design procedure of the ballasting resistance for an N-finger transistor when the temperature dependent thermal conductivity is considered. We conclude as follows.

- 1) The thermal resistance matrix \mathbf{R}_{th} is determined by measurement using test structures or by a three-dimensional simulation.
- 2) We specify the highest current level I_{CSI} from device operation or reliability considerations and solve for the corresponding specific junction temperature T_{ST} from (5.26). The junction temperature T_{ST} must keep below a reasonable value.
- 3) The thermal-electrical feedback coefficient vector Φ_{ST} and Φ_{ST}^* can be obtained from (5.27) and (5.28) correspondingly.
- 4) The ideal emitter ballasting resistance distribution under I_{CSI} can be obtained by (5.29). Even when this distribution is satisfied, the currents of all fingers will not be exactly identical because of the temperature dependence nature of the ideal distribution in (5.29).
- 5) Then, by solving the eigenvalue equation of (5.30), the second largest real positive solution is the optimum value of the emitter ballasting resistance $R_{E1,SI}$ for stable operation up until I_{CSI} is reached. This value is the smallest resistance needed for the stable operation.

We use the above procedure to analyze a 10-finger transistor with the finger area fixed at $100 \mu\text{m}^2$. The fingers are assumed to be identical and equal spaced. The parameters needed are assumed to be the same as used in Section 5.2 and Section 5.3 except I_O which is scaled by the finger area from $I_O = 6 \times 10^{-25}$ A for a 3×40 HBT

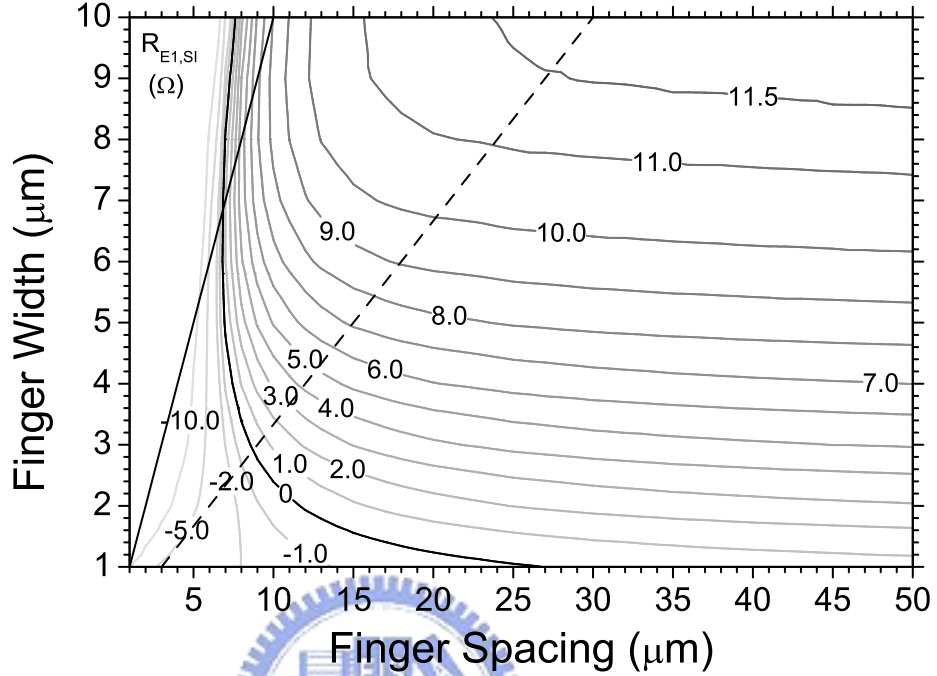


Fig. 5.26. The contour plot of the optimum ballasting resistance $R_{E1,SI}$ of a 10-finger device varied with the finger width w and the finger separation s for the specified current $I_{CS1} = 20$ mA and the finger area fixed at $100 \mu\text{m}^2$. The black straight line is the function of $s = w$. The black dash line is the function of $s = 3w$.

to $I_O = 5 \times 10^{-25}$ A for a $100 \mu\text{m}^2$ device. Fig. 5.26 shows the optimum ballasting resistance $R_{E1,SI}$ as a function of the finger width w and the finger separation s for the specified current $I_{CS1} = 20$ mA. The coupling thermal resistance matrix is calculated by using (2.21) for every (s, w) points. The specified current I_{CS1} is selected as the current density equal to $20 \text{ kA}/\text{cm}^2$. There are two black straight lines, the solid line and the dash line. The data on the left side of the solid line are un-physical because $s < w$ means the fingers are overlapped. The dash line $s = 3w$ corresponds to the minimum separation needed in most case. The ratio of three times the finger width is a roughly estimated value. Actually, devices with smaller finger width will have larger ratio. It can be found that $R_{E1,SI}$ is mainly determined by the shape of finger or the self-thermal resistance if the finger separation is larger than the dash line. Fig. 5.27(a) and (b) show the ballasting resistance distribution difference of finger 2, $\Delta R_{E2,SI}$, and

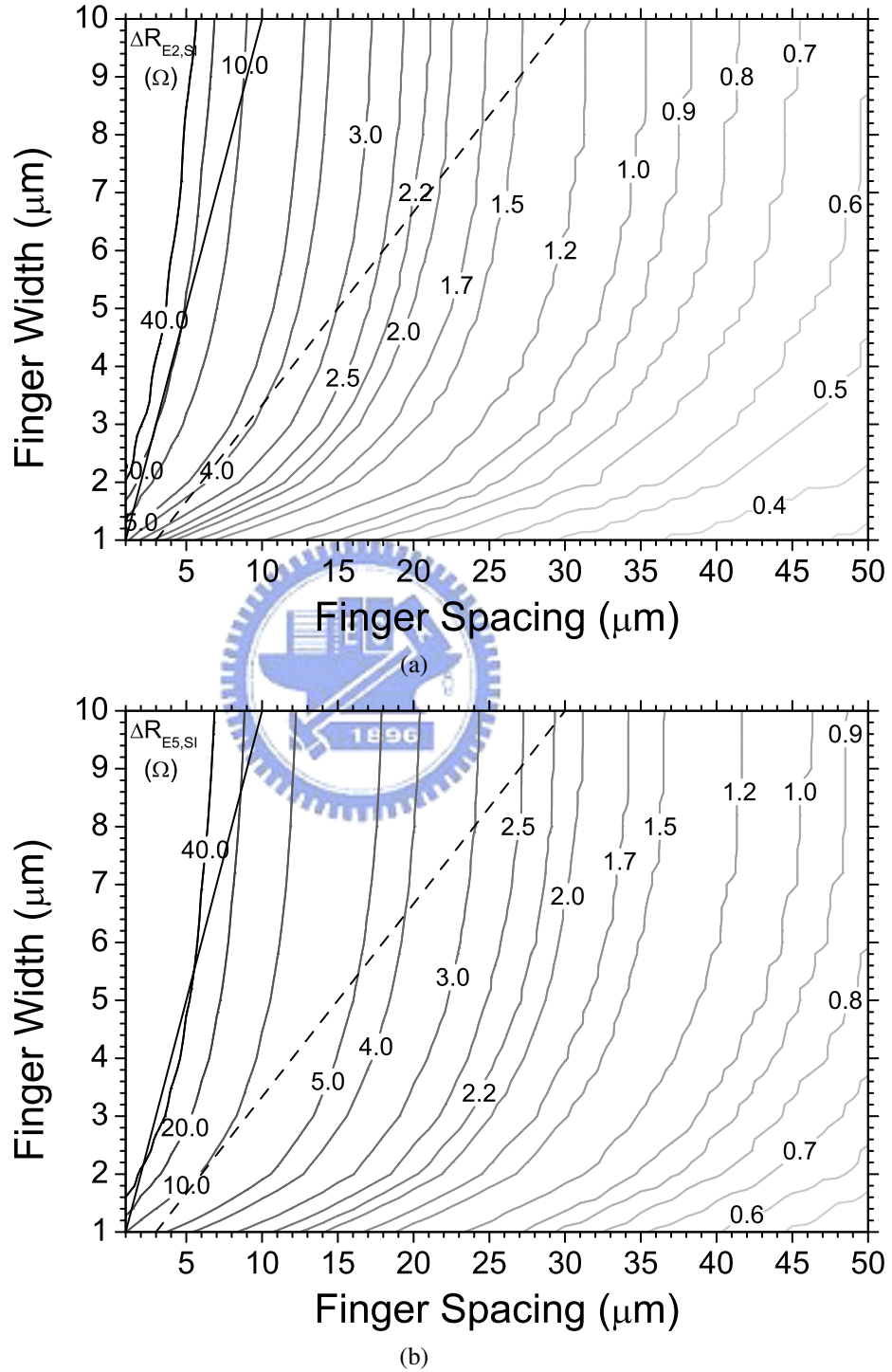


Fig. 5.27. The contour plot of the optimum resistance distribution difference of finger 2, $\Delta R_{E2,S1}$, and finger 5, $\Delta R_{E5,S1}$, of a 10-finger device varied with the finger width w and the finger separation s for the specified current $I_{CS1} = 20$ mA and the finger area fixed at $100 \mu\text{m}^2$. (a) $\Delta R_{E2,S1}$ and (b) $\Delta R_{E5,S1}$. The black straight line is the function of $s = w$. The black dash line is the function of $s = 3w$.

finger 5, $\Delta R_{E_5,SI}$. Contrary to $R_{E_1,SI}$, $\Delta R_{E_2,SI}$ and $\Delta R_{E_5,SI}$ are mainly determined by the finger separation. The fact that the difference of finger 5, the center finger, is larger than finger 2, the side finger results in the contours of Fig. 5.27(b) look like the contours of Fig. 5.27(a) with a right shift.

5.4.2 The Uniform Temperature Design

Finally, we derive the formulas of the general N-finger case as follows. All variables will use the index ST to indicate that they are obtained under the specified finger temperature. The definitions of the used variables are analogical to Section 5.4.1. Once T_{ST} is given, the specified current vector $\mathbf{I}_{C_{ST}}$ is obtained from (5.22) as

$$\mathbf{I}_{C_{ST}} = \mathbf{A} \frac{T_A}{b-1} \left[1 - \left(\frac{T_{ST}}{T_A} \right)^{-(b-1)} \right] \quad (5.31)$$

where

$$\mathbf{A} = (V_C \mathbf{R}_{th})^{-1}.$$

From (3.13), the thermal-electrical feedback coefficient vector and its effective version are

$$\Phi_{ST} = -\frac{k}{q} \left(\ln \frac{\mathbf{I}_{C_{ST}}}{I_{S0}} - \gamma \ln \frac{T_{ST}}{300} - \gamma \right) + \alpha^* \quad (5.32)$$

$$\Phi_{ST}^* = -\frac{k}{q} \left(\ln \frac{\mathbf{I}_{C_{ST}}}{I_{S0}} - \gamma \ln \frac{T_{ST}}{300} \right) + \alpha^*. \quad (5.33)$$

Then, the ideal emitter ballasting resistance distribution (5.24) becomes

$$\begin{aligned} \mathbf{R}_{E_{ST}} &= \frac{1}{\mathbf{r}_{ST}} \left[R_{E1} + \frac{(\Phi_{ST}^* - \phi_{1,ST}^*) T_{ST}}{I_{C_{1,ST}}} \right] \\ &= \frac{1}{\mathbf{r}_{ST}} (R_{E1} + \Delta \mathbf{R}_{E_{ST}}) \end{aligned} \quad (5.34)$$

5.4 The General N-Finger Case

where

$$\mathbf{r}_{ST} = \frac{\mathbf{I}_{CST}}{I_{C1,ST}} \quad \frac{1}{\mathbf{r}_{ST}} = [\text{diag}(\mathbf{r}_{ST})]^{-1}.$$

Following the procedure as before, we obtained the eigenvalue equation (5.25) as

$$\det [\text{diag}(\mathbf{r}_{ST} \cdot \Theta_{ST}) \mathbf{R}_{th}^* - \text{diag}(\Lambda_{ST}) - R_{E1} \mathbf{I}] = 0 \quad (5.35)$$

where

$$\Theta_{ST} = \frac{\Phi_{ST}}{\phi} \cdot \left(\frac{T_{ST}}{T_A} \right)^b \quad \Lambda_{ST} = \frac{kT_{ST}}{q} \frac{\mathbf{r}_{ST}}{\mathbf{I}_{CST}} + \Delta \mathbf{R}_{EST}$$

and

$$\frac{\mathbf{r}_{ST}}{\mathbf{I}_{CST}} = \text{diag}(\mathbf{r}_{ST}) [\text{diag}(\mathbf{I}_{CST})]^{-1}.$$

The optimum value of the emitter ballasting resistance $R_{E1,ST}$ for stable operation up to T_{ST} can be solved by (5.35). The design procedure of the ballasting resistance for an N-finger transistor with temperature dependent thermal conductivity under uniform temperature consideration is similar to that of Section 5.2. We list it as follows:

- 1) The thermal resistance matrix \mathbf{R}_{th} is determined by measurement using test structures or by a three-dimensional simulation.
- 2) We specify the highest junction temperature T_{ST} from device operation or reliability consideration and solve the corresponding specific current level \mathbf{I}_{CST} from (5.31).
- 3) The thermal-electrical feedback coefficient vector Φ_{ST} and Φ_{ST}^* can be obtained from (5.32) and (5.33) correspondingly.
- 4) The ideal emitter ballasting resistance distribution under T_{ST} can be obtained from (5.34).
- 5) Then, by solving the eigenvalue equation of (5.35), the second largest real positive solution is the optimum value of the emitter ballasting resistance $R_{E1,ST}$ for stable operation up until T_{ST} is reached. This value is the smallest resistance needed for the stable operation.

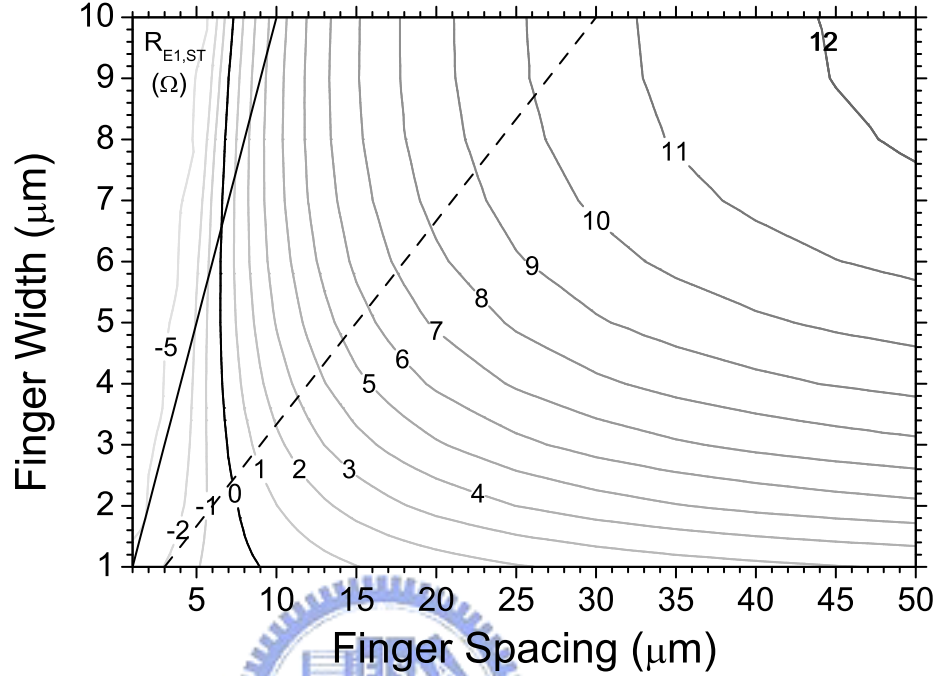


Fig. 5.28. The contour plot of the optimum ballasting resistance $R_{E1,ST}$ of a 10-finger device varied with the finger width w and the finger separation s for the specified current $T_{ST} = 550$ K and the finger area fixed at $100 \mu\text{m}^2$. The black straight line is the function of $s = w$. The black dash line is the function of $s = 3w$.

Analogous to Section 5.4.1, we use the above procedure to analyze a 10-finger transistor with the finger area fixed at $100 \mu\text{m}^2$. The fingers are assumed to be identical and equal spaced. The parameters needed are discussed in Section 5.4.1. Fig. 5.28 shows the optimum ballasting resistance $R_{E1,ST}$ as a function of the finger width w and the finger separation s for the specified temperature $T_{ST} = 550$ K. The coupling thermal resistance matrix is calculated by the same method as Section 5.4.1. The specified temperature T_{ST} is selected from the value used in Section 5.3. The meanings of the solid line and the dash line are discussed in Section 5.4.1. It is different from Fig. 5.26 that although $R_{E1,ST}$ is mainly determined by the shape of finger or the self-thermal resistance, it is more seriously affected by the finger separation. The curves at large separation are not so flat as Fig. 5.26. It is because the finger separation will affect the uniformity of

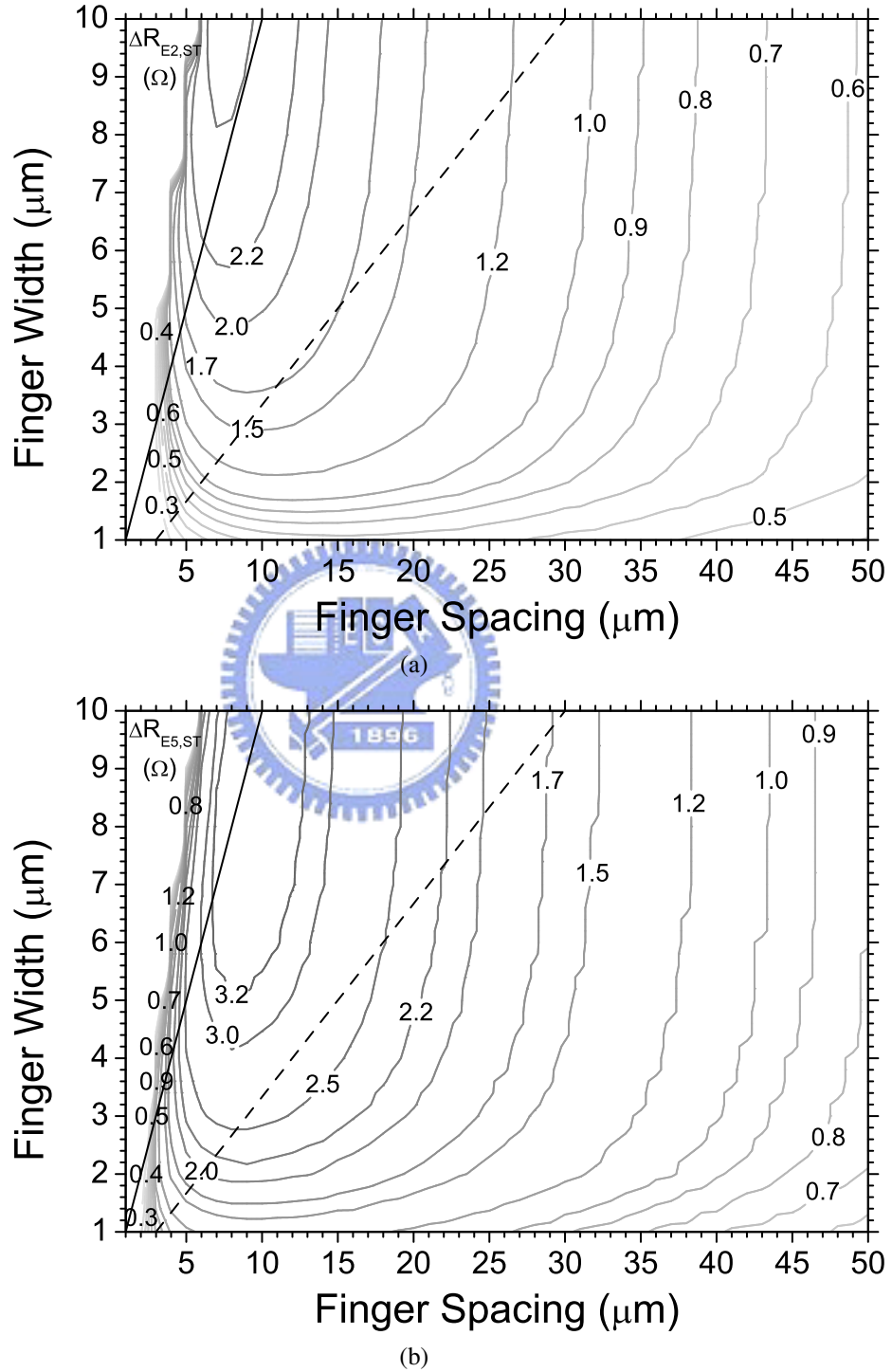


Fig. 5.29. The contour plot of the optimum resistance distribution difference of finger 2, $\Delta R_{E_{2,ST}}$, and finger 5, $\Delta R_{E_{5,ST}}$, of a 10-finger device varied with the finger width w and the finger separation s for the specified current $T_{ST} = 550$ K and the finger area fixed at $100 \mu\text{m}^2$. (a) $\Delta R_{E_{2,ST}}$ and (b) $\Delta R_{E_{5,ST}}$. The black straight line is the function of $s = w$. The black dash line is the function of $s = 3w$.

the temperature distribution. Fig. 5.29(a) and (b) show the ballasting resistance distribution difference of finger 2, $\Delta R_{E_2,ST}$, and finger 5, $\Delta R_{E_5,ST}$. Contrary to Fig. 5.27, $\Delta R_{E_2,ST}$ and $\Delta R_{E_5,ST}$ have flat portions at small finger width region. In this region, the resistance distribution does not change much and the most change is on $R_{E_1,ST}$. The contours of Fig. 5.29(b) also look like the contours of Fig. 5.29(a) with a right shift similar to Fig. 5.27.

5.5 Summary

We extended our works on the multiple-finger transistor thermal stability from the simple thermal-electrical feedback equations to the accurate model equations and taking the temperature dependence of the thermal conductivity into account. Transistors with 3-fingers have been analyzed. Two design flows, uniform current design and uniform temperature design, of the best ballasting resistance distribution of a N-finger transistor for optimum thermal stability operation were developed. Using these design flows, we can design the best ballasting resistance needed for thermally stable operation under the specified current level or junction temperature. A 10-finger device with $100 \mu\text{m}^2$ finger area for each finger was analyzed. The best ballasting resistance distribution of this device was evaluated as a function of finger width and finger separation.

Chapter 6

Conclusion

The primary goal of this work was to develop an optimum design procedure of multi-finger transistors for thermally stable operation. This procedure was used to find two ballasting resistance values, the ideal resistance distribution difference and the optimum resistance. The practical value of the ballasting resistance was the sum of these two values. The ideal resistance distribution difference was used to ensure that the currents or the temperatures of all fingers were identical. The optimum resistance was used to push the unstable current or temperature to the desired value. Comparing to conventional method of using uniform ballasting resistance, the new schemes with optimized design could result in a significant increase in the device current under stable operation.

6.1 Summary

The values of the thermal conductivity and its temperature dependence of GaAs and InGaP in literature had been reviewed. The effect of temperature dependent thermal conductivity on the heat flow equation and the thermal resistance was also explained. Theoretical calculation of the thermal resistance was shown and the properties of the thermal resistance dependent on device geometry were discussed. A small, long and

narrow finger is better for the sake of reducing thermal resistance. Thinning the substrate is not an effective way to reduce thermal resistance. Two methods of DC measurement were investigated and the conclusion is that Bovolon's method is preferred.

The coupled current-voltage equations were derived and discussed. A linearized temperature dependent band-gap energy expression is used to simplify the definition of the thermal-electrical feedback coefficient and the coupled I_C-V_{BE} equations. The goal function is defined and used to solve the thermal coupling problems. There are three models that need to be solved, including the simple model, the accurate model with constant thermal conductivity, and the accurate model with temperature dependent thermal conductivity. The procedure utilized to solve the coupled I_C-V_{BE} equations by using the Newton-Raphson method was developed.

Multiple-finger transistors with nonuniform distribution of ballasting resistance have been analyzed by using the simple model. Analytical formulas for the best ballasting resistance distribution for optimum thermal stability operation were derived. With the ideal ballasting resistance distribution, it is possible to achieve absolutely stable operation by using the optimum ballasting resistance. This optimum value could be obtained by solving an eigenvalue equation. The second largest real positive eigenvalue of this eigenvalue equation was the optimum ballasting resistance. A design procedure for the thermally stable optimum design was developed.

We extended our works on the multiple-finger transistor thermal stability from the simple thermal-electrical feedback equations to the accurate model equations and taking the temperature dependence of the thermal conductivity into account. Two design flows, uniform current design and uniform temperature design, of the best ballasting resistance distribution of a N-finger transistor for optimum thermal stability operation were developed. Using these design flows, we could design the best ballasting resistance needed for thermally stable operation under the specified current level or junction temperature.

6.2 Future Work

Three future works are suggested. First, the implementation of the procedure of the thermally stable optimum design to the real devices is the most important future work to be done. The power amplifier modules with the thermally optimum designed ballasting resistors are very useful for the application of the output stage of wireless systems. Second, in addition to the thermal stability, the effects of the nonuniform ballasting resistors on the RF performance and linearity of devices still need to be investigated. The performance of thermal optimum designed devices should be better than the traditional design because of the uniformity of the currents and temperatures of fingers. Last, besides emitter ballasting, base ballasting is another method to stabilize the transistors. The use of base ballasting needs to incorporate the more complex model of the current gain. The analysis of the thermal stability by using the full SPICE model equations is worth doing for base ballasting.



References

- [1] B. Bayraktaroglu and J. A. Higgins, "HBTs for microwave power applications," in *Current Trends in Heterojunction Bipolar Transistors*, M. F. Chang, Ed. Singapore: World Scientific, 1996.
- [2] R. H. Winkler, "Thermal properties of high-power transistors," *IEEE Trans. Electron Devices*, vol. ED-14, no. 5, pp. 260-264, May 1967.
- [3] J. A. Higgins, "Thermal properties of power HBTs," *IEEE Trans. Electron Devices*, vol. 40, pp. 2171-2177, Dec. 1993.
- [4] W. Liu, S. Nelson, D. Hill, and A. Khatibzadeh, "Current gain collapse in microwave multi-finger heterojunction bipolar transistors," *IEEE Trans. Electron Devices*, vol. 40, pp. 1917-1927, Nov. 1993.
- [5] L. L. Liou, B. Bayraktaroglu, and C. I. Huang, "Thermal stability analysis of multiple emitter finger microwave AlGaAs/GaAs heterojunction bipolar transistors," in *IEEE MTT-S Microwave Symp. Tech. Dig.*, 1993, pp. 281-284.
- [6] The MathWorks Inc., MATLAB® – The Language of Technical Computing. Available: <http://www.mathworks.com/>
- [7] C. H. Liao, C. P. Lee, N. L. Wang, and B. Lin, "Optimum design for a thermally stable multifinger power transistor," *IEEE Trans. Electron Devices*, vol. 49, pp. 902-908, May 2002.

References

- [8] C. H. Liao and C. P. Lee, "Optimum design for a thermally stable multifinger power transistor with temperature-dependent thermal conductivity," *IEEE Trans. Electron Devices*, vol. 49, pp. 909-915, May 2002.
- [9] R. Anholt, *Electrical and thermal characterization of MESFETs, HEMTs, and HBTs*, Boston: Artech House, 1995, pp. 62.
- [10] L. L. Liou, J. L. Ebel, and C. I. Huang, "Thermal effects on the characteristics of AlGaAs/GaAs heterojunction bipolar transistors using two-dimensional numerical simulation," *IEEE Trans. Electron Devices*, vol. 40, pp. 35-43, Jan. 1993.
- [11] V. Palankovski, R. Schultheis, and S. Selberherr, "Simulation of power heterojunction bipolar transistors on gallium arsenide," *IEEE Trans. Electron Devices*, vol. 48, pp. 1264-1269, June 2001.
- [12] C. J. Glassbrenner and G. A. Slack, "Thermal Conductivity of Silicon and Germanium from 3K to the Melting Point," *Phys. Rev.*, vol. 134, pp. A1058-A1069, May 1964.
- [13] M. G. Holland, "Phonon scattering in semiconductors from thermal conductivity studies," *Phys. Rev.*, vol. 134, pp. A471-A480, Apr. 1964.
- [14] A. Amith, I. Kudman, and E. F. Steigmeier, "Electron and phonon scattering in GaAs at high temperatures," *Phys. Rev.*, vol. 138, pp. A1270-A1276, May 1965.
- [15] P. D. Maycock, "Thermal conductivity of silicon, germanium, III-V compounds and III-V alloys," *Solid-State Electron.*, vol. 10, pp. 161-168, Sep. 1962.
- [16] J. Blanc, R. H. Bube, and L. R. Weisberg, "Evidence for the Existence of High Concentrations of Lattice Defects in GaAs," *Phys. Rev. Lett.*, vol. 9, pp. 252-254, Apr. 1964.
- [17] S. Adachi, "Lattice thermal resistivity of III-V compound alloys," *J. Appl. Phys.*, vol. 54, pp. 1844-1848, Apr. 1983.

References

- [18] W. B. Joyce, "Thermal resistance of heat sinks with temperature-dependent conductivity," *Solid-State Electron.*, vol. 18, pp. 321-322, Apr. 1975.
- [19] G. B. Gao, M. Z. Wang, X. Gui, and H. Morkoc, "Thermal design studies of high-power heterojunction bipolar transistors," *IEEE Trans. Electron Devices*, vol. 36, no. 5, pp. 854-863, May 1989.
- [20] W. Liu and B. Bayraktaroglu, "Theoretical calculations of temperature and current profiles in multi-finger heterojunction bipolar transistors," *Solid-State Electron.*, vol. 36, pp. 125-132, Feb. 1993.
- [21] W. Liu, *Handbook of III-V Heterojunction Bipolar Transistors*, New York: John Wiley & Sons, Inc., 1998.
- [22] N. Rinaldi, "Thermal analysis of solid-state devices and circuits: an analytical approach," *Solid-State Electron.*, vol. 44, pp. 1789-1798, Oct. 2000.
- [23] N. Rinaldi, "On the modeling of the transient thermal behavior of semiconductor devices," *IEEE Trans. Electron Devices*, vol. 48, pp. 2796-2802, Dec. 2001.
- [24] J. Scott, "Reconciliation of methods for bipolar transistor thermal resistance extraction," *IEEE ISCAS 2001*, vol. 42, pp. 465-468, 2001.
- [25] P. M. McIntosh, M. J. Staniforth, and C. M. Snowden, "Determination of HBT thermal resistance using pulsed I-V measurements," in *High Performance Electron Devices for Microwave and Optoelectronic Applications Workshop, 1996. EDMO'96*, pp. 120-125, Nov. 1996.
- [26] D. E. Dawson, A. K. Gupta, and M. L. Salib, "CW measurement of HBT thermal resistance," *IEEE Trans. Electron Devices*, vol. 39, pp. 2235-2239, Oct. 1992.
- [27] W. Liu and A. Yuksel, "Measurement of junction temperature of an Al-GaAs/GaAs heterojunction bipolar transistor operating at large power densities," *IEEE Trans. Electron Devices*, vol. 42, pp. 358-360, Feb. 1995.

References

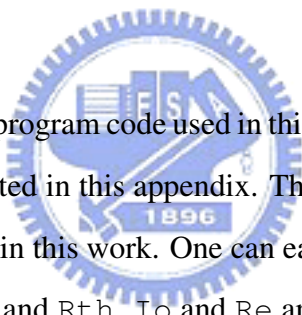
- [28] N. Bovolon, P. Baureis, J.-E. Müller, P. Zwicknagl, R. Schultheis, and E. Zanoni, "A simple method for the thermal resistance measurement of AlGaAs/GaAs heterojunction bipolar transistors," *IEEE Trans. Electron Devices*, vol. 45, pp. 1846-1848, Aug. 1998.
- [29] S. P. Marsh, "Direct extraction technique to derive the junction temperature of HBT's under high self-heating bias conditions," *IEEE Trans. Electron Devices*, vol. 47, pp. 288-291, Feb. 2000.
- [30] C. M. Wu and E. S. Yang, "Carrier transport across heterojunction interfaces," *Solid-State Electron.*, vol. 22, pp. 241-248, Mar. 1979.
- [31] E. S. Harmon, M. R. Melloch, and M. S. Lundstrom, "Effective band-gap shrinkage in GaAs," *Appl. Phys. Lett.*, vol. 64, pp. 502-504, Jan. 1994.
- [32] W. Liu, "Thermal coupling in 2-finger heterojunction bipolar transistors," *IEEE Trans. Electron Devices*, vol. 42, pp. 1033-1038, June 1995.
- [33] J. S. Blakemore, "Semiconducting and other major properties of gallium arsenide," *J. Appl. Phys.*, vol. 53, pp. R123-R181, Oct. 1982.
- [34] K. Lu and C. M. Snowden, "Analysis of thermal instability in multi-finger power AlGaAs/GaAs HBT's," *IEEE Trans. Electron Devices*, vol. 43, pp. 1799-1805, Nov. 1996.
- [35] Yu Zhu, J. K. Twynam, M. Yagura, M. Hasegawa, T. Hasegawa, Y. Eguchi, Y. Amano, E. Suematsu, K. Sakuno, N. Matsumoto, H. Sato, and N. Hashizume, "Self-heating effect compensation in HBTs and its analysis and simulation," *IEEE Trans. Electron Devices*, vol. 48, pp. 2640-2646, Nov. 2001.
- [36] G. B. Gao, H. Morkoc, and M. F. Chang, "Heterojunction bipolar transistor design for power applications," *IEEE Trans. Electron Devices*, vol. 39, pp. 1987-1997, Sept. 1992.

References

- [37] W. Liu, A. Khatibzadeh, J. Sweder, and H. Chau, "The use of base ballasting to prevent the collapse of current gain in AlGaAs/GaAs heterojunction bipolar transistors," *IEEE Trans. Electron Devices*, vol. 43, pp. 245-251, Feb. 1996.
- [38] C. W. Kim, H. Goto, and K. Honjo, "Thermal behavior depending on emitter finger and substrate configurations in power heterojunction bipolar transistors," *IEEE Trans. Electron Devices*, vol. 45, pp. 1190, June 1998.
- [39] L. L. Liou and B. Bayraktaroglu, "Thermal stability analysis of AlGaAs/GaAs heterojunction bipolar transistors with multiple emitter fingers," *IEEE Trans. Electron Devices*, vol. 41, pp. 629-636, Mar. 1994.
- [40] G. B. Gao, M. S. Unlu, H. Morkoc, and D. L. Blackburn, "Emitter ballasting resistor design for the current handling capability of AlGaAs/GaAs power heterojunction bipolar transistors," *IEEE Trans. Electron Devices*, vol. 38, no. 2, pp. 185-196, Feb. 1991.
- [41] R. P. Arnold and D. S. Zoroglu, "A quantitative study of emitter ballasting," *IEEE Trans. Electron Devices*, vol. ED-21, pp. 385-391, July 1974.
- [42] K. Fukino, "Multi-emitter power transistor having emitter region arrangement for achieving substantially uniform emitter-base junction temperatures," U.S. Patent 3 704 398, 1972.
- [43] J. G. Lee, T. K. Oh, B. Kim, and B. K. Kang, "Emitter structure of power heterojunction bipolar transistor for enhancement of thermal stability," *Solid-State Electron.*, vol. 45, pp. 27-33, Jan. 2001.

Appendix A

Program Code for Solving The Coupled $I_C - V_{BE}$ Equations



The MATLAB® [6] program code used in this work with the procedure mentioned in Section 3.3 is listed in this appendix. This program is a three-finger example as the most case simulated in this work. One can easily expand to the N-finger example by changing f_{in} , I_o , R_e , and R_{th} . I_o and R_e are N-dimension vectors and R_{th} is a $N \times N$ matrix. The simulation of a device with an arbitrary layout can be achieved by using a proper I_o and R_{th} . The problem of how to find the corresponding I_o and R_{th} is out of the scope of this program. One is required to provide I_o and R_{th} in advance when using this program.

The model flag sel is used to select the model applied in simulation. “ $sel = 1$ ” selects the simple model, “ $sel = 2$ ” selects the accurate model with the uniform current design, and “ $sel = 3$ ” selects the accurate model with the uniform temperature design. I_{si} is the specified current level for the uniform current design and T_{st} is the specified finger temperature for the uniform temperature design. One should change these parameters to conform to different problems. If a constant thermal conductivity model is needed, one can set the parameter “ $bb = 0$ ” to meet this requirement.

```

%%%%%%%%%%%%%%%%%%%%%%%%%%%%%%%%%%%%%%%%%%%%%%%%%%%%%%%%%%%%%%%%%%%%%%%%
%
%   MATLAB Program File for Solving The Coupled Current-Voltage Equations
%
%%%%%%%%%%%%%%%%%%%%%%%%%%%%%%%%%%%%%%%%%%%%%%%%%%%%%%%%%%%%%%%%%%%%%%%%
%   Copyright 2005 by Chih-Hao Liao   (liawch.ee88g@nctu.edu.tw)
%%%%%%%%%%%%%%%%%%%%%%%%%%%%%%%%%%%%%%%%%%%%%%%%%%%%%%%%%%%%%%%%%%%%%%%%

warning off;
clear;

k = 1.3806505e-23;    % Boltzmann constant [J/K].
q = 1.60217653e-19; % Elementary charge [C].
TA = 300;            % Ambient temperature [K].
bb = 1.25;           % Temperature parameter of the thermal conductivity [].
Vbe = 0;             % Base-emitter voltage [V].
phi = 0.001;        % The thermal-electrical feedback coefficient [V/K].
Vc = 6;             % Collector-emitter voltage [V].
Eg0 = 1.483;        % Energy band gap at 0 K [eV] fit from 250K to 700K.
alpha = 4.88e-4;    % Bandgap shrinkage per unit temperature rise [eV/K].
r = 4.21;           % Temperature parameter of the saturation current [].

Io1 = 6e-25;
Io2 = 6e-25;
Io3 = 6e-25;
Io = [Io1; Io2; Io3]; % Saturation current [A]

%sel = 1;           % Model flag, the simple model.
sel = 2;           % Model flag, the uniform current design.
%sel = 3;          % Model flag, the uniform temperature design.
fin = 3;           % The finger number.
dim = fin - 1;
cen = fix(fin / 2);
Vt = k * TA / q;
Iso = Io * (TA/300)^(-r) * exp((Eg0 - alpha * TA) / Vt);

```

```

ckq = k / q;
cbb1TA = (bb - 1) / TA;
clbb1 = - 1 / (bb - 1);

% The thermal resistance matrix.
%a = 1000;           % The chip dimension [um].
%c = 100;           % The chip thickness [um].
%w = 3;            % The finger width [um].
%l = 40;           % The finger length [um].
%s = 15;           % The finger separation [um].
Rth1 = 7.330925044176360e+002;
Rth2 = 1.702258367445874e+002;
Rth3 = 8.650771092852000e+001;
Rth = [ Rth1 Rth2 Rth3;
        Rth2 Rth1 Rth2;
        Rth3 Rth2 Rth1; ];
Rth = Rth * 800 / Rth1; % Normalize to the experimental data.

dIr = 0.25e-3;      % The step of reference current sweep.
Nipt = 800;        % The number of the sweep points.
Im = Nipt * dIr;   % The highest reference current.
Ii = 1e-20;        % The lowest reference current.
itmax = 5000;      % The maximum number of iteration.
n0 = 0;
If0 = zeros(fin, 1);

if sel == 1,       % For the simple model.
    A = phi * Rth * Vc; % The effective thermal resistance.
else               % For the accurate model.
    A = Rth * Vc;
end; for i = 1:fin,
    RE(i,1) = sum(A(i,:));
end;

```

```

% Emitter ballasting resistnace.
if sel == 1,    % For the simple model.
    Re1 =3;
    %Re2 = Re1;
    Re2 = Re1 + RE(2) - RE(1);
    Re3 = Re1;
    Re = [Re1; Re2; Re3];
end;
if sel == 2,    % For the uniform current design.
    Isi = 0.024;    % The specified current level.
    Tsi = TA * (1 - cbb1TA * RE * Isi) .^ clbb1;
    PsiS = -ckq * ( log(Isi / Iso(1)) - r * log(Tsi / 300) ) + alpha;
    Psi = PsiS + ckq * r;
    dRe = (PsiS .* Tsi - PsiS(1) * Tsi(1)) / Isi;
    B = diag(Psi .* (Tsi / TA) .^ bb) * A - diag(ckq * Tsi / Isi + dRe);
    Relopt = sort(eig(B));    % The optimum ballasting resistance.

    Re1 = Relopt(2);
    Re2 = Re1;
    Re3 = Re1;
    Re = [Re1; Re2; Re3];
    Re = Re + dRe;
end;
if sel == 3,    % For the uniform temperature design.
    Tst = 500;    % The specified temperature.
    D = inv(A);
    du = (1 - (Tst / 300) ^ (1 / clbb1)) / cbb1TA;
    Ist = D * du * ones(fin, 1);
    rs = Ist / Ist(1);
    PstS = -ckq * ( log(Ist / Iso(1)) - r * log(Tst / 300) ) + alpha;
    Pst = PstS + ckq * r;
    dRe = (PstS - PstS(1)) * Tst / Ist(1);
    B = diag(rs) * ( diag(Pst * (Tst / TA) ^ bb) * A;
    B = B - diag(ckq * Tst ./ Ist) ) - diag(dRe);

```

```

Relopt = sort(eig(B));      % The optimum ballasting resistance.

Rel = Relopt(2);
Re2 = Rel;
Re3 = Rel;
Re = [Rel; Re2; Re3];
Re = (Rel + dRe) ./ rs;
end;

for i = 0:(2^fin - 1), % Build up the initial guesses.
    inistr(i + 1,:) = dec2bin(i, fin);
end;

Iini = zeros(dim, 1); % Build up the current variable.
for f = 1:(cen + 1), % Select the reference finger.
    ref = f;

    for ini = 1:size(inistr, 1), % Sweep all initial guesses.
        strini = inistr(ini,:);
        if str2num(strini(ref)) == 0,
            % If the initial guess of the reference finger is low,
            % the reference current sweeps from low to high.
            strini(ref) = [];
            for i = 1:dim,
                Iini(i, 1) = (Im - Ii) * str2num(strini(i)) + Ii;
            end;
            start = 0;
            step = 1;
            stop = Nipt;
        else
            % If the initial guess of the reference finger is high,
            % the reference current sweeps from high to low.
            strini(ref) = [];
            for i = 1:dim,

```

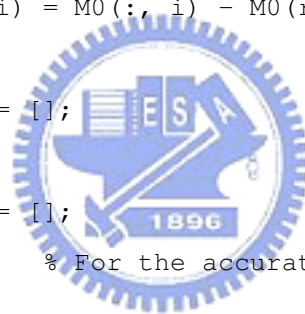
```

        Iini(i, 1) = (Im - Ii) * str2num(strini(i)) + Ii;
    end;
    start = Nipt;
    step = -1;
    stop = 0;
end;

% Build up the vectors and matrices which we need to use.
if sel == 1, % For the simple model.
    M0 = A - diag(Re);
    M = M0;
    for i = 1:fin,
        M(:, i) = M0(:, i) - M0(ref, i);
    end;
    M(ref, :) = [];
    R = M;
    R(:, ref) = [];
else % For the accurate model.
    M = A;
    M(:, ref) = [];
    R = M;
    R(ref, :) = [];
    Isi = Iso;
    Isi(ref) = [];
    Rei = Re;
    Rei(ref) = [];
end;

I = Iini;
I0 = Iini;
Irini = Ii;
nbad = 0;
for ni = start:step:stop, % Sweep the reference current.
    Ir = Irini + ni * dIr;

```



```

        if sel == 1,% For the simple model.
            logI1 = Vt * log(Ir);
            Ia = M(:,ref) * Ir;
        else          % For the accurate model.
            Ia = A(:,ref) * Ir;
            Ib = Ia(ref);
            Ia(ref) = [];
            v1 = Re(ref) * Ir;
        end;

% The main solving loop.
solved = -1; checkdIg = zeros(dim, dim); for times = 1:itmax,
    if sel == 1,      % For the simple model.
        % The goal function and the derivative matrix.
        Ig = Vt * log(I) - logI1 - R * I - Ia;
        dIg = diag(Vt ./ I) - R;
    else              % For the accurate model.
        % The finger temperature.
        Tr = TA * (1 - cbb1TA * (Ib + M(ref,:) * I)) ^ clbb1;
        if ~isreal(Tr),      % Check real number.
            solved = 0;
            break;
        end;
        Ti = TA * (1 - cbb1TA * (Ia + R * I)) .^ clbb1;
        if ~isreal(Ti),      % Check real number.
            solved = 0;
            break;
        end;
    % The thermal-electrical feedback coefficient.
    PrS = -ckq * ( log(Ir / Iso(ref)) - r * log(Tr/300) ) + alpha;
    PiS = -ckq * ( log(I / Iso(ref)) - r * log(Ti/300) ) + alpha;
    Pr = PrS + ckq * r;
    Pi = PiS + ckq * r;
end;

```

```

% The goal function and the derivative matrix.
Ig = -(PiS .* Ti - PrS * Tr) + (Rei .* I - v1);
dIg = diag(ckq * Ti ./ I + Rei) - diag(Pi .* ((Ti / TA) .^ bb)) * R;
dIg = dIg + ones(dim) * diag(Pr * ((Tr / TA) ^ bb) * M(ref,:));
end;

dI = -inv(dIg) * Ig; % The step.
I = I + dI; % The new guess.
if ~isreal(dI), % Check real number.
    solved = 0;
    break;
end;

% Convergence criteria.
if max(abs(dI ./ (I + 1e-30))) < 1e-6,
    % Compute the final current solutions.
    If(ref,1) = Ir;
    If(1:(ref - 1),1) = I(1:(ref - 1));
    If((ref + 1):fin, 1) = I(ref:end);
    if sel == 1, % For the simple model.
        Vbe = Vt * log(Ir / Io(ref)) - M0(ref,:) * If;
    else % For the accurate model.
        Tr = TA * (1 - cbb1TA * (Ib + M(ref,:) * I)) ^ c1bb1;
        PrS = -ckq * ( log(Ir / Iso(ref)) - r * log(Tr/300) ) + alpha;
        Vbe = Eg0 - PrS * Tr + Re(ref) * Ir;
    end;
    I0 = I; % Remember the last good solution.

% Eliminate unreasonable solutions.
if min(If) < 0,
    solved = 0;
    break;
end;

% Eliminate symmetric solutions.
check = ones(cen, 1);

```

```

Icheck = If;
Icheck(cen + 1) = [];
for i = 1:cen,
    if (max(Icheck) - If(i)) > 1e-4,
        check(i) = 0;
    end;
end;
if check == 0,
    solved = 0;
    break;
end;

if Vbe > 0.0, % Save the solutions we need.
    dImax = max(abs(If - If0));
    if dImax > 2e-3 & ni > 0,
        % Insert blank line to eliminate the solution discontinuity.
        n0 = n0 + 1;
        sol(:, n0) = [0; zeros(fin, 1); 0; zeros(fin, 1)];
    end;
    If0 = If;
    n0 = n0 + 1;
    % Compute the final temperature solutions.
    It = sum(If);
    if sel == 1, % For the simple model.
        T = A * If / phi + 300;
    else % For the accurate model.
        T(ref,1) = Tr;
        T(1:(ref - 1),1) = Ti(1:(ref - 1));
        T((ref + 1):fin, 1) = Ti(ref:end);
    end;
    sol(:, n0) = [Vbe; If; It; T];
end;
solved = 1;
break;

```

```

end;

% Avoid slope change sign but allow exceed slightly.
check = diag(dIg .* checkdIg);
check1 = min(check);
if check1(1) < -0.1,
    I = Iini;
    solved = 0;
    break;
end;
checkdIg = dIg;
end;%times

if times == itmax,
    'error: times exceed'
    I = Iini;
    break;
end;
if solved == 1,
    nbad = 0;
end;
if solved == 0,
    if nbad == 0,
        % Insert blank line to separate differnt solution sets.
        n0 = n0 + 1;
        sol(:, n0) = [0; zeros(fin, 1); 0; zeros(fin, 1)];
    end;
    nbad = nbad + 1;
    I = I0;
    continue;
end;
end;%ni
[f ini n0 (ni-start) str2num(inistr(ini,:)) solved]
% Insert blank line to separate differnt solution sets.

```



```
        n0 = n0 + 1;
        sol(:, n0) = [0; zeros(fin, 1); 0; zeros(fin, 1)];
    end;%ini
end;%f

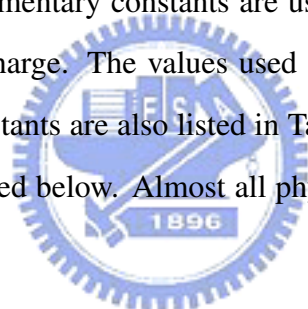
sol = sol';
save -ascii fig1.txt sol
```



Appendix B

Elementary Constants

In this work, some elementary constants are used, such as the Boltzmann constant and the elementary charge. The values used are listed in Table B.1. Some other important elementary constants are also listed in Table B.1. All values in Table B.1 are referred to the website listed below. Almost all physical constants can be found in this website.



<http://physics.nist.gov/cuu/Constants/index.html>

Quantity	Symbol	Value	Unit
Boltzmann constant	k	1.380 6505(24)e-23	[J/K]
electric constant	ϵ_0	8.854 187 817e-14	[F/cm]
electron mass	m_0	9.109 3826(16)e-31	[kg]
elementary charge	q	1.602 176 53(14)e-19	[C]
Planck constant	h	6.626 0693(11)e-34	[J-s]

Table B.1. The important elementary constants.

Vita

Name: Chih-Hao Liao, 廖志豪 .

Date of birth: October 30, 1974.

Place of birth: Taoyuan, Taiwan, R.O.C.

Educations:

National Taiwan University, Department of Physics, B.S. September, 1992 – June, 1996.

Department of Physics

National Chiao Tung University, Institute of Electronics Engineering, M.S. September, 1999 – August, 2000.

Institute of Electronics Engineering

National Chiao Tung University, Institute of Electronics Engineering, Ph.D. September, 2000 – October, 2005.

Institute of Electronics Engineering

Major: Electronics Engineering.

Title of Ph.D. dissertation:

Thermally Stable Optimum Design of Power Heterojunction Bipolar Transistors.

Publication List

- [1] C. H. Liao, C. P. Lee, N. L. Wang, and B. Lin, "Optimum design for a thermally stable multifinger power transistor," *IEEE Trans. Electron Devices*, vol. 49, pp. 902-908, May 2002.
- [2] C. H. Liao and C. P. Lee, "Optimum design for a thermally stable multifinger power transistor with temperature-dependent thermal conductivity," *IEEE Trans. Electron Devices*, vol. 49, pp. 909-915, May 2002.
- [3] Chih-Hao Liao, Chien-Wei Gwan, Chien-Ping Lee, "Extraction of temperature dependent conduction band offset in InGaP/GaAs HBT using 1-D simulation," in *International Conference on Solid State Devices and Materials, SSDM*, 2004, pp. 106-107.